DETERMINATION OF STATIC AND DYNAMIC INTERLAMINAR FRACTURE TOUGHNESS - A COMBINED EXPERIMENTAL AND FINITE ELEMENT METHOD

by

SANJAY KUMAR VERMA

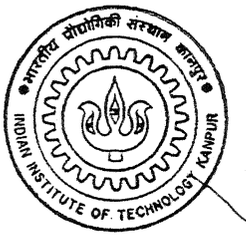

DEPARTMENT OF MECHANICAL ENGINEERING

INDIAN INSTITUTE OF TECHNOLOGY KANPUR

JUNE, 1995

DETERMINATION OF STATIC AND DYNAMIC INTERLAMINAR FRACTURE TOUGHNESS - A COMBINED EXPERIMENTAL AND FINITE ELEMENT METHOD

A Thesis Submitted
in Partial Fulfilment of the Requirements
for the Degree of

DOCTOR OF PHILOSOPHY

by

SANJAY KUMAR VERMA

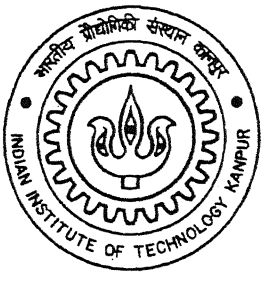

to the

DEPARTMENT OF MECHANICAL ENGINEERING
INDIAN INSTITUTE OF TECHNOLOGY KANPUR
JUNE, 1995

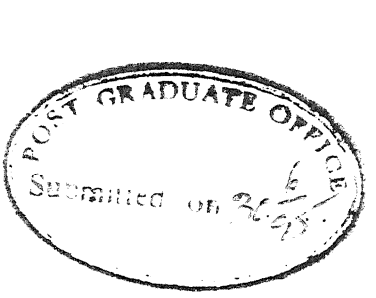

CERTIFICATE

It is certified that the work contained in the thesis entitled **"DETERMINATION OF STATIC AND DYNAMIC INTERLAMINAR FRACTURE TOUGHNESS - A COMBINED EXPERIMENTAL AND FINITE ELEMENT METHOD"**, by **Sanjay Kumar Verma**, has been carried out under our supervision and that this work has not been submitted elsewhere for a degree.

JUNE, 1995

(Prof. N.N. Kishore)
Department of Mechanical Engineering
Indian Institute of Technology, Kanpur

(Prof. Prashant Kumar)
Department of Mechanical Engineering
Indian Institute of Technology, Kanpur

Dedicated to

MY MOTHER

ACKNOWLEDGEMENTS

I wish to record my profound gratitude to Prof. Prashant Kumar and Prof. N.N. Kishore who inspired and encouraged me throughout with their invaluable guidance, constructive suggestions and detailed instructions at every stage of my research work. They have been sympathetic and affectionate in moments of despair.

I am thankful to Prof. N.G.R. Iyengar, Prof. B.D. Agarwal, Dr. R. Sethuraman and Dr. K. Ramesh for their invaluable suggestions and encouragements. I am also thankful to Prof. S.G. Dhande for his help as Head of the Department.

A special word of appreciation is due to Mr. Anurag Goel for his kind help in all the experimentation and thesis preparation works. Mr. B.D. Pandey and Mr. Ram Chandra Tiwari deserve special thanks for their help in fabrication of experimental setup.

I am grateful to Mr. D.K. Sarkar and Mr. S.L. Srivastava for their kind help in experimental work and fatherly suggestions.

It is my pleasure that I recall my association with Dr. B. Rai, Mr. K.K. Bajpai, Mr. S.C. Gupta, Mr. P.S. Chandel, Mr. D.Datta, Mr. Atul Agarwal, Mr. Ravi, Mr. S. Dhar, Mr. Mahesh, Mr. Radhay Shyam, Mr. Avinash, Mr. Trivedi and Mr. Diwakar who provided a homely atmosphere to me in the Lab.

I am thankful to Kesavan Potty P.K., Abdul Jaleel, A.K. Yadav, Ajay Ray, Loviraj, Suresh Babu, Gawhale, Sridhar who helped me in developing the experimental setup and FE code.

I express my thanks to Ashok Chaudhary, Atul Verma, Venkat Reddy, Sanat Agarwal, P.V.M. Rao for assistance in thesis preparation.

My Thanks are also due to Mr. Ved Prakash Gupta and Mr. B.K. Jain for their nice tracing works and Mr. Ravi Shanker Shukla for his excellent photography.

SYNOPSIS

Techniques are developed to determine interlaminar fracture toughness of the specimen of slender steel plates bonded together in the form of double cantilever beam (DCB). For quasistatic loading conditions and dynamic conditions, fracture toughness is evaluated through a combined experimental and finite element technique.

Quasistatic Loading Condition

The DCB specimen has been made by bonding two thin (~ 2.8 mm) strips of hardened alloy steel with epoxy. A precrack of desired length is introduced by placing a plastic sheet of BOPP (bidirectional oriented polypropylene) between the strips. The specimen was loaded in an Instron machine in tension (mode I). The load was applied under displacement controlled mode at very low pulling rate so that the crack propagation is very slow. For determining fracture toughness, K_{Ic}, of the interlaminar crack, strain is measured close to the crack tip on the side face of the DCB specimen. An optimum location and orientation of the strain gauge is determined by a finite element analysis and a relationship between the strain at this location and stress intensity factor (SIF) is obtained. Based on the finite element analysis, it was decided to bond a strain gauge on the neutral plane of upper cantilever at 45°. It was observed from FE analysis that the strain will increase slowly as the crack tip approaches this point and reaches peak value when the crack tip is 1.0 mm behind this location. Afterward the strain decreases and becomes zero as the crack tip passes the specified location.

A small strain gauge of gauge length 0.2 mm and width of 1.4 mm is chosen for experimental study. Response of the strain gauge was monitored by a strain indicator. The experimentally obtained value of K_{Ic} determined from the relationship between peak strain and SIF, has been compared with that calculated by FE method using the load corresponding peak strain. Six experiments were conducted for the crack lengths varying from 23 to 36 mm. The maximum percentage variation between FE results and

A word of thanks are also due to my friends Jawed, Koshy, Ravindra, Snehansu, K.M. Pandey, Jimmy, Salim, Delta, Dada, Baba, Pradhan, Deepak Murthy, Deepak Gupta, P Deb, Razee, Shamshi, Kapil, Alok, Baldev, Manoj Nair, K.M. Singh, Subba Rao, Chandra, Chhotu Tiwari who made my stay at IITK a pleasent memeory.

I find myself short of words to express my gratefulness to my father, brothers and sisters for their cooperations and the wishes bestowed by them.

Last but not least, I am grateful to the Aeronautics Research and Development Board (Structural Panel) for providing financial assistance.

SANJAY KUMAR VERMA

SYNOPSIS

Techniques are developed to determine interlaminar fracture toughness of the specimen of slender steel plates bonded together in the form of double cantilever beam (DCB). For quasistatic loading conditions and dynamic conditions, fracture toughness is evaluated through a combined experimental and finite element technique.

Quasistatic Loading Condition

The DCB specimen has been made by bonding two thin (~ 2.8 mm) strips of hardened alloy steel with epoxy. A precrack of desired length is introduced by placing a plastic sheet of BOPP (bidirectional oriented polypropylene) between the strips. The specimen was loaded in an Instron machine in tension (mode I). The load was applied under displacement controlled mode at very low pulling rate so that the crack propagation is very slow. For determining fracture toughness, K_{Ic}, of the interlaminar crack, strain is measured close to the crack tip on the side face of the DCB specimen. An optimum location and orientation of the strain gauge is determined by a finite element analysis and a relationship between the strain at this location and stress intensity factor (SIF) is obtained. Based on the finite element analysis, it was decided to bond a strain gauge on the neutral plane of upper cantilever at 45°. It was observed from FE analysis that the strain will increase slowly as the crack tip approaches this point and reaches peak value when the crack tip is 1.0 mm behind this location. Afterward the strain decreases and becomes zero as the crack tip passes the specified location.

A small strain gauge of gauge length 0.2 mm and width of 1.4 mm is chosen for experimental study. Response of the strain gauge was monitored by a strain indicator. The experimentally obtained value of K_{Ic} determined from the relationship between peak strain and SIF, has been compared with that calculated by FE method using the load corresponding peak strain. Six experiments were conducted for the crack lengths varying from 23 to 36 mm. The maximum percentage variation between FE results and

experimental values was found to be within 8 to 55%.

Dynamic Loading Condition

A special fixture is designed to mount the DCB specimen and apply a dynamic load. One cantilever of DCB is bonded to a rigid block and a load bar is attached to second cantilever. The load bar is impacted by a striker accelerated in an air gun. The incident and reflected pulses in the load bar are monitored by two strain gauges bonded on the load bar. These strain gauges are connected to a storage oscilloscope through a bridge circuit. The one dimensional analysis of elastic wave propagation in the load bar gives the deformation of its end face with time which is equal to the deflection of the cantilever's end. The velocity of the fast moving interlaminar crack is measured by monitoring the response of strain gauges mounted in series ahead of the crack tip on the side face of one cantilever. These strain gauges are also connected to the same storage oscilloscope through bridge circuits. The first strain gauge is bonded close to the crack tip. The peak response of the strain gauges gives the crack propagaiton history. A curve is drawn through the three data ponits at which peak strain occurs. When the curve is extrapolated to the initial crack length, it gives the initiation time. The slope of the fitted curve gives the crack velocity history.

The experimental measurements provide (i) deflection of second cantilever end (load point) with time, (ii) crack initiation time and (iii) crack propagaiton history. These experimental data are used as input to a FE code developed to find the dynamic interlaminar fracture toughness for the specimen configuration used in the experiment. The FE code calculate $\hat{J}$-integral given by Kishimota, Aoki and Sakata (1980). This is an inertia enhanced version of J-integral. The value of $\hat{J}$-integral is theoretically independent of the choice of path as shown by Dexter (1987). A modified gradual release technique similar to the techniques discussed by Nishioka and Atluri (1986) is used to model the propagation of the interlaminar crack. In the present work, the holding back force is calculated before the release of the crack tip node and this force is decreased linearly as the crack reaches the end of the next element. For different

experiments, the initiation fracture toughness and propagation fracture toughness are evaluated. At the same time the variation of propagation toughness with crack velocity is also studied.

The crack initiated in two different time zone depending on the high or low impact load. At high impact load, the initiated time was 40 to 45 μs and for low impact load, it was 105 to 112 μs. The fracture toughness in the case of static loading was found to be 12 J/m^2. In the case of dynamic loading conditions, the initiation toughness was 90 to 230 J/m^2. Then crack propagates at very high speed (100-1800 m/s). The propagaiton toughness was found to vary between 2 to 100 J/m^2. In comparison to static interlaminar toughness and initiation toughness, the propagation toughness is lower at high crack propagaiton speed. (close to Rayleigh wave).

References:

1. Kishimoto K., Aoki S. and Sakata M., 1980, On the path Independent Integral - J, Engg. Fracture Mechanics, 13, pp. 841-850.

2. Dexter R.J., 1987, Sources of Error in Finite Element Computations of the Stress Intensity Factor for Running Crack, 4th International Conference on Numerical Methods in Fracture Mechanics, eds. A.R. Luxmoore, D.R.J. Owens, Y.P.S. Rajapakse, M.F. Kannien, San Antonio, Texas, USA, pp. 153-172.

3. Nishioka T. and Atluri S.N.,1986, Computation Method in Dynamic Fracture, Chapter - 10, Computational Methods in the Mechanics of Fracture, edited by S.N. Atluri, Elsevier Science Publication.

LIST OF PUBLICATIONS

Verma S.K., Kumar Prashant, Kishore N.N. and Kesavan Potty P.K., 1995, Evaluation of Critical Interlaminar SIF of DCB Specimen, Engineering Fracture Mechanics, Vol. 50, No. 3, pp. 345-353.

Kishore N.N., Kumar Prashant and Verma S.K., 1993, Numerical Methods in Dynamic Fracture, Journal of Aeronautical Society of India, Vol. 45, No. 4, pp. 323-333.

Verma S.K, Kumar Prashant, Kishore N.N. and Gupta Lovi Raj, 1993, Determination of Critical SIF of an Interlaminar Crack in Thin Laminate - An Experimental cum Numerical Approach, Proceedings of National Seminar on Aero Structures, Edited by Prashant Kumar and N.G.R. Iyengar.

CONTENTS

LIST OF SYMBOLS

a	Crack length
a(t)	Crack length varying with time
å	Crack velocity
å(t)	Crack velocity varying with time
b	Width of the specimen
[B]	Elastic strain displacement matrix
c	Wave velocity
[D]	Elastic constitutive relation
$\{\varepsilon\}$	Strain vector
E	Young's modulus
F_{HB}	Holding back force at crack tip
G	Strain energy release rate
Γ	Contour
h	Thickness of the cantilever
$\hat{J}$	Fracture toughness
$\hat{J}_{ini}$	Initiation fracture toughness
$\hat{J}_{prop}$	Propagation fracture toughness
K	Stress intensity factor
[K]	Elastic stiffness matrix
L	Length of the specimen
[M]	Mass matrix
[N]	Shape functions
ν	Poisson's ratio
P	Applied force
S	Surface area
ρ	density
$\{\sigma\}$	Stress vector
{t}	Traction vector
T	Kinetic energy

$\{u\}$	Displacement vector
U	Strain energy
V	Volume
W_{ext}	External work done

LIST OF TABLES

LIST OF FIGURES

CHAPTER - 1

INTRODUCTION

1.1 INTRODUCTION

Laminated fibre composites are now increasingly used as structural members of aircrafts, rockets and space ships, automobiles, boats, sport articles, etc. They offer attractive properties such as lightweightness, high specific strength and stiffness and environmental stability. A laminate is commonly made from many laminae laid over each other before they are cured at high pressure and temperature. Thus, the neighbouring laminae are bonded to each other with the help of comparatively low strength matrix material. In other words, fibres of high strength and stiffness do not reinforce the laminate through the thickness direction.

When conventional metals are impacted, a small dent on the surface is generally not considered to be serious because it just workhardens the material locally. In contrast, when a foreign object impacts the surface of a component made of fibre composites, it generates high shear stresses and flexural waves causing interlaminar failure or delamination. As a result, in comparison to conventional metals, the laminates are less tough and fracture spreads to larger areas. Since the damage can spread along the interfaces between various plies not visible from outside, it may not be detected easily. Therefore, for reliability and damage tolerance considerations, interlaminar fracture toughness is of utmost importance whenever fibre composites are used in structural applications.

As stated earlier laminates fabricated by bonding thin layers, are known to be susceptible to interlaminar crack growth. In fact, the fracture toughness of interlaminar cracks in laminates of fibre reinforced plastic is found to be considerably less than that of through the thickness cracks. For example, in a typical angle ply laminate say, carbon-epoxy, the

ıl energy release rate of interlaminar crack growth is of the order of hundreds of (Davies et al., 1990), while the critical energy release rate of through the thickness is of the order of several thousands J/m^2 (Shukla et al., 1989).

ıinate shows considerable delamination damage when it is impacted by a projectile 'opped tool. Under impact loading, the cracks can propagate at high speeds :da et al., 1982). However, toughness of interlaminar crack determined under static loading condition is not very small that it would explain very high speeds of aminar crack propagation in fibre reinforced plastic (FRP) laminates with impact ;y as low as 4-10 J. Furthermore, the propagation toughness of a brittle crack is er for the cracks moving at higher speeds (Freund, 1990). This results in trophic failure of the material if, under certain circumstances, the crack starts ıgating at higher speeds. It is therefore important to characterize the interlaminar ıre toughness under dynamic crack propagation in composite laminates so as to mize its performance under impact loads.

composite laminate which is usually very thin (less than 5 mm thick) , the free ces are quite close to the crack location at interlaminar zone. Crack tip stresses are ted by the free surfaces making it difficult to determine analytical solutions. ever, the static toughness of interlaminar crack growth, in mode I and II, have been :mined experimentally in terms of the global parameter, strain energy release rate (Davies et. al.,1990). This technique does not provide displacement, strain or stress in the vicinity of the interlaminar crack tip. It is therefore felt that at first 'native methods should be developed for experimental determination of the static ture toughness of interlaminar cracks. Once experience is acquired through erimentation at quasistatic crack growth, techniques will be developed for the amic interlaminar fracture toughness.

:re exist methods to determine stress intensity factor (SIF) through strain field near slowly moving crack tip which can be measured using strain gauges bonded at a ticular location and orientation from the crack tip for the large plate. However, sed form solutions for the strain field, near the crack tip, in terms of stress intensity

factor are not available for slender laminates. Therefore, it is envisaged that a general method should be developed which would involve experimental measurements and finite element analysis to determine critical interlaminar fracture toughness for quasistatic crack growth.

It is difficult to extend the experimental technique of determining G to cases when interlaminar cracks grow at high speeds. During the dynamic crack growth, stress wave interact with local defects and a part of energy is converted into heat as well. Consequently, accurate experimental determination of various energy component is difficult. The problem is acute for interlaminar crack growth as the energy release rate is very low; only a few joules of energy can snap off the bonds between two layers in a typical specimen. Any small error in carrying out energy balance would lead to a large error in the value of critical energy release rate.

The study of dynamic fracture is complex from both experimental and numerical point of view. In experimental work, related parameters have to be measured in a very short time duration. This requires sophisticated instrumentation, precise methodology and skilled personnel. Most of the work on dynamic fracture is done through the method of caustics for large plate but this technique is not yet extended to interlaminar crack in thin sheets. In the case of numerical solution, the inertia effect and the changing boundary conditions (because new surfaces are generated), have to be accounted. This iterative process requires large amount of computation. At the same time, characterization of material properties can not be done by numerical method alone. It was felt that a combined technique should be developed which will require not too sophisticated instrumentation but will make use of some of the numerical simulation to determine dynamic interlaminar fracture toughness of materials. Therefore, in the present work, a new hybrid technique which involves both experiment and finite element method is developed to determine the interlaminar fracture toughness for cracks moving at high speeds (100-1800 m/s).

apparent stress intensity factors associated with the corresponding problem for the crack in material. Comninou (1990) has given a review of the behaviour of interface cracks between two different constituents in the context of linear elastic fracture mechanics.

Ozdil and Carlsson (1992) investigated energy release rate and stress intensity factor with finite element analysis of DCB specimen loaded in mode I. Analysis was carried out for isotropic and orthotropic materials of thin cantilevers with very thin interleaves between cantilevers. Through finite element analysis they found out the displacement field and hence strain-stress field using four noded elements. Virtual crack closure technique was adopted to calculate strain energy release rate which lead to determination of stress intensity factor. Manoharan and Sun (1990) investigate mode I, II and III strain energy release rates for a crack lying along the interface of two dissimilar anisotropic elastic solids subjected to uniform axial strain analytically and also by the finite element method. It was shown that owing to the violent oscillatory crack tip stress behaviour, the strain energy release rates for modes I, II and III do not converge to definite value. However, the total strain energy release rate is well defined.

Suo and Hutchinson (1990) considered a semi-infinite interface crack between two isotropic elastic layers under general edge loading conditions. The problem was solved analytically except for a single real scalar independent of loading, which was then extracted from the numerical solution for one particular combination. Jensen (1991) used the blister test for the measurement of interface fracture toughness for a thin film bonded to an elastic substrate. Results for the energy release rate and mixity of modes I and II for the interface crack were presented for cases where the debond had been initiated and extended several film thickness. Analytical results were given in the two extreme cases of very small film deflections (weak interfaces) and very large film deflections (tough interfaces). Numerical results were presented in the intermediate zone.

Dattaguru et al. (1994) evaluated strain energy release rate in mode I and mode II at the tip of an interface crack in a bimaterial plate under tension. They used finite element analysis and modified crack closure integral (MCCI) technique. Renard and Roudolff

(1991) studied the delamination of an infinite plate subjected to tensile stress. The stress state was studied by a numerical finite element analysis and by an analytical model based on the Love-Kirchhoff plate theory. The global strain rate and its mode I, II and III components are calculated during delamination extension. A correlation was made between these two formulation.

1.2.2 DYNAMIC CRACK PROPAGATION

Most of the work on dynamic fracture are done on large plates with a through the thickness crack; the slender plates have attracted little attention. The duration of study is limited to the period before the crack starts reflecting from free boundary and interacting with loading pulse. The important aspect of dynamic crack propagation study is the measurement of crack velocity. Takeda et al. (1982) used high speed photography to measure the interlaminar crack propagating speed in composite laminates. They observed that the interlaminar crack in composite laminates moves at 200-500 m/s, when impacted by foreign body. They also used silver coating ahead of the crack tip as propagation gauge. Cantwell et al. (1989) used the graphite gauge technique to measure crack velocity in composite laminates. In this technique, graphite layer is sprayed ahead of the crack tip and when the crack moved through this layer, change of resistance with time is monitored through oscilloscope, to get the crack velocity.

Freund (1990) observed that the crack velocity is subsonic i.e. less than shear wave speed. However, in some special cases, the crack speed was greater than the shear wave speed or even dilatational wave speed, where the loading was applied directly at the crack tip by means of a fluid under high pressure flowing into the opening crack or some other extreme conditions. The analysis for the cases when crack speed is more than shear wave speed but less than dilatational wave speed (transonic) is not very clear. Burridge (1973) showed that if a slip plane has very little resistance to fracture and if the crack rapidly accelerate upto the Rayleigh wave speed, then the observation identifies a possible mechanism by which the crack can induce secondary fracture ahead of the crack tip and thereby precipitate crack growth at a speed beyond the Rayleigh wave

speed. The mechanism was suggested by numerical results reported by Andrews (1976) on the expansion of a shear crack along a weak interface.

The different method of determining dynamic fracture toughness as suggested in literature are discussed in brief in subsequent paragraphs.

Method of Caustics

Earlier experiments to determine dynamic fracture toughness were developed through the method of caustics. It was introduced by Schardin (1959) and latter developed by Mannog (1966) and Theocaris (1970). The method of caustic is discussed in detail by Popadopoulas (1993). The basis of the method is that a light ray passing through a stressed plate is deviated from its straight path partly due to thickness variation and partly due to change in refractive index caused by stress optic effect. If the plate contains a crack, the ray are deviated from the region around the crack tip and these form a singular curved called variously "stress corona", "shadow spot" or "caustic" on a reference plane some distance away from the specimen. The size of the caustic is related to the stress intensity factor. For opaque specimens the optical shadow spot pattern is formed by reflection of the light from the polished specimen surface. The method of caustics has been applied to measurements of static as well as dynamic stress intensity factor. The method of caustics has many advantages such as simplicity of equipment and measurement, and non contact measurability. A laser caustic which combines a high speed camera with a laser beam as light source, is considered to be most powerful technique to measure dynamic stress intensity factor during fast fracture, because the laser beam, triggered with an appropriate system can be synchronised to initiation of fast fracture in an extremely short time.

Most of the work on caustic is done on large plate of polymeric material or steel with through the thickness crack. Kalthoff (1985) gave the review of the work done on dynamic fracture phenomenon. The influence of dynamic effects on test procedures for measuring the crack arrest toughness and the impact fracture toughness was presented. Ravi Chandar and Knauss (1982, 1984a, 1984b, 1984c, 1984d) have done an exhaustive

study of dynamic crack propagation phenomena using the method of caustics for Homalite-100. This included study of crack tip stress on a double cantilever beam specimen using electromagnetic stress wave generator, crack initiation and arrest, microstructural aspects, crack branching and interaction of stress waves with the crack tip.

Rosakis, Duffy and Freund (1984) performed dynamic crack propagation experiments on double cantilever beam specimen of AISI 4340 steel (229 X 76 X 12.7 mm) using wedge loading. The dynamic stress intensity factor was measured by means of optical method of caustics. The instantaneous value of dynamic SIF was obtained as a function of crack tip velocity. The crack velocity is high when the initiation stress intensity factor is more. The interaction of reflected shear and Rayleigh waves with the moving crack tip stress field was also considered.

Takashahi and Arakawa (1987) used the method of caustics with high speed photography to study velocity effect on the dynamic stress intensity factor of fast cracks in polymeric material. Specimen geometry were chosen such that both acceleration and deceleration occurs in one fracture event. The results showed that the dynamic intensity factor depends on not only on crack velocity but also on crack acceleration, and the accelerating crack has a smaller value than the decelerating crack at the same velocity.

Zehnder and Rosakis (1990) used optical method of reflected caustics combined with high speed photography to investigate the dynamic fracture initiation and propagation in 4340 steel specimen (304 X 128 X 95 mm). A three point bend specimen was loaded by a drop weight. It was shown that the dynamic fracture propagation toughness depends on crack tip velocity through a relation that is a material property. Nishioka et. al. (1991) took photographs of caustic pattern of dynamically propagating cracks in double cantilever beam specimen of an optically isotropic material, polymethyl methacrylate (PMMA). The influence of the length of DCB specimen were investigated. It was found that the longer specimens should be used to obtain conservative arrest toughness K_{Ia}.

The method of caustic has been very effectively used to study the fracture phenomena in a large plate with through the thickness crack, but it is not so far been developed for interlaminar crack in a slender sheet. This is because of the fact that the strength of the interlaminar bond is very weak and it will introduce very little strain in the bonded sheet. Also the size of the caustic will be negligibly small. Furthermore, the method of caustics may be more complex to apply to the case of dynamic interlaminar crack in slender sheet owing to the fact that the free surfaces are very close to the crack tip and influence the strain field in the vicinity of crack tip.

Experimental Works on Dynamic Fracture

The dynamic tests were conducted on notched round bar specimens loaded in tension by stress pulse using split Hopkinson bar technique by Wilson, Hawley and Duffy (1980). They conducted the fracture initiation experiments to determine the fracture toughness of an AISI 1020 hot rolled steel and cold rolled steel under quasi-static and dynamic loading conditions. In another study through a tensile split Hopkinson bar, Abdelaziz et al. (1987) proposed an experimental method for fracture characterization of solid propellants. The specimen was loaded at high strain rates. However, the critical J-integral as defined by Rice (1968) for the static case was evaluated neglecting the inertia effect of crack propagation. The split Hopkinson bar technique has not been used so far for evaluation of dynamic interlaminar fracture toughness.

Shukla (1983) made a comparison of static and dynamic energy release rate for different type of specimens material and geometries using an energy balance in the system. The experiment was conducted on specimen made of polymeric material. Rectangular double cantilever beam, modified compact tension and ring type specimens were used. The dynamic SIF was obtained by recording the isochromatic fringe pattern. A substantial amount of energy was lost away from the crack tip during a dynamic fracture event and this energy loss depends on the specimen geometry and material.

The strain gauges are also used by different researcher to evaluate the static and dynamic fracture toughness of isotropic and orthotropic materials. Shukla, Agarwal and

Nigam (1988) bonded strain gauge on one face of the specimen and employ photoelastic coatings method on the other side of the specimen to determine dynamic fracture mechanics. Experiments were conducted on steel and aluminium with face grooved SEN specimen geometries. Instantaneous stress intensity fracture factors as a function of crack lengths are obtained independently from strain gauge and photoelasticity methods, and compared. Both techniques yielded similar results.

Berger and Dally (1990a) used a series of strain gauges ahead of the crack tip at a certain predetermined location to monitor the strain and crack propagation. An overdeterministic system of equations is developed, which were solved to determine dynamic stress intensity factor. Berger, Dally and Sanford (1990b) also used strain gauges ahead of the crack tip to determine dynamic stress intensity factor associated with a propagating crack. But the crack tip position was precisely located by developing an algorithm. The method of analysis is demonstrated in dynamic experiments with a high strength 4340 alloy steel.

Wada (1992) also used strain gauge methods to analyze the dynamic initiation SIF for PMMA (polymethyl methacrylate). The analysis was carried out for plates with edge crack subjected to one point bending in a plane of plate. The FEM simulation was also done using forces measured with the strain gauge. Also, the crack initiation time is measured with the strain gauge mounted close to the crack tip. The dynamic initiation SIF is determined by adapting the crack initiation time to the simulated curve of dynamic SIF calculated by FEM. The technique is used for the large plate and the crack propagation and propagation fracture toughness was not studied.

The strain gauges are frequently used to find static and dynamic SIF in a large plate, but a similar technique is not applied to slender sheet.

A special technique to study the initiation and propagation in of crack in the steel under dynamic impact loading was developed by Ravichandran and Clifton (1989). They presented a plate impact experiment and related finite difference model to study the fracture process that occurs in sub-micron loading. A disc containing a mid-plane, pre-

fatigued, edge crack that has been propagated half way across the diameter is impacted by a thin flyer plate of same material. A compressive pulse propagates through the specimen and reflects from the rear surface as a step tensile pulse with a duration of 1 μs. The plane wave loads the crack and cause the initiation and propagation of the crack. The motion of the rear surface is monitored by using the laser interferometer system. The location of the crack front was mapped before and after the experiment using a focused ultrasonic transducer. Experiments were conducted on 4340 VAR steel at temperature ranging from room temperature to -100°C. A finite difference method was used for numerical simulation of the experiments. Crack velocities were prescribed corresponding to various fracture models.

A study on dynamic interlaminar fracture toughness of composite materials was carried out by Sun and Grady (1988). They investigated dynamic interlaminar initiation fracture toughness of graphite/epoxy by impacting a cantilever specimen with interlaminar crack at the centre, with rubber ball. The crack propagated in mode II. The contact force parameters were evaluated for rubber ball impact on different specimens. The threshold impact velocity that causes propagation of delamination crack was used in the dynamic analysis with finite element method. From the finite element solution, the time history of strain release rate was calculated. The maximum value of strain release rate was taken as critical strain energy release rate. The study is restricted to initiation toughness and no attempt was made to measure crack speed and propagation toughness. The analysis is based on evaluation of contact force during impact through an indirect procedure and several approximations.

Numerical Work on Dynamic Fracture

Though considerable amount of work have been done to study the fracture phenomena through numerical methods, only large rectangular double cantilever beam specimens were given special attention. Owen and Shantaram (1977) started the use of finite element method to study dynamic crack growth. They studied double cantilever beam specimen and pipeline problems under transient loading. Parabolic isoparametric

elements were used for discritization and explicit scheme (central difference) was employed for time integration. The crack was advanced from one node to the next node, when the stress at the gauss point nearest to the crack tip exceeded a certain value and then the damping coefficient was made zero at the released node. The crack propagation history was simulated for the given loading conditions.

Nishioka and Atluri (1982a) investigated the crack propagation and arrest in a high strength steel DCB specimen using moving singular dynamic finite element procedure. An edge crack in a rectangular DCB specimen was propagated by inserting a wedge. The results were compared with available experiment data of caustics. In another work, Nishioka and Atluri (1982b) presented the results of generation and prediction studies of dynamic crack propagation in plane stress/strain situations. The studies were conducted by using finite element method, taking into account the propagating stress singularities near the crack tip. The variation of dynamic stress intensity factor with time and the variation of dynamic fracture toughness with velocity were studied and compared with available experimental results.

Crouch and Williams (1987) used dynamic and generation mode finite element program to analyze different specimen geometries. Chiang (1990) presented a numerical procedure based on eigen functions to determine the dynamic stress intensity factor of crack moving at steady state under antiplane strain condition. An edge crack problem and a radial crack problem was solved using traction and displacement boundary conditions separately. It was shown that the dynamic effect is relatively insignificant for low crack propagation speeds provided that the specimen size is fairly large.

Aminpour and Holsapple (1991) developed a finite element procedure to provide the state of stress, displacement and stress intensity factors of a propagating crack at the interface of the two dissimilar anisotropic materials. In the finite element mesh the crack tip is embedded in a singular element. Crack propagation is accomplished by moving the crack tip inside the singular element according to a prescribed crack tip position history. A local redefinition of the finite element is required when the crack tip reaches an extreme position inside the singular element. When local redefinition of

Gudmundson (1991) worked with an elsto-dynamic moving element formulation incorporating a variable order singular element to enhance the local crack tip description. The moving mesh zone is embedded in a finite element global mesh providing a functional tool for the analysis of dynamic crack growth experiments.

Williams and Ivankovic (1991) used the spring model to determine a crack speed, crack length and loading relationship in terms of energy release rate. An essential feature of the analysis is the inclusion of contact stiffness and geometry dependent limiting speed. Yuechuan (1991) used the Gurtin variational principle to compute dynamic stress intensity factor. The differential equations thus obtained is solved by modal superposition. A centre crack in large plate subjected to uniform tension is solved and the results were compared.

Kennedy and Kim (1993) incorporated micropolar elasticity theory into a plane strain finite element formulation to analyze the dynamic response of the crack. Two cases were considered; a stationary crack subjected to dynamic load and a crack propagating under constant load. Material with strong micropolar properties were found to have significantly lower dynamic energy release rates than their classic material counterparts. Wang and Williams (1994) investigated high speed crack growth in a thin double cantilever beam specimen using finite element method. The strain release rate obtained by FEM was compared with the quasi-static solution based on beam theory, for various loading conditions. The cantilever end was loaded under an initial step displacement of 1 mm and then pulled further with a constant velocity. The crack was propagated at assumed speed by gradual node release technique. Strong dynamic effects were observed because of wave reflections within finite specimen size. The faster the crack speed, the more kinetic energy was radiated and the bigger the drop in G obtained.

Most of the numerical works is limited to large plates with edge/central cracks or three point bend specimens. The reflection and interaction of the waves from the free boundary were avoided by limiting the duration of study.

1.3 LAYOUT OF THE THESIS

Chapter 2 discusses the combined experimental and finite element method to determine static stress intensity factor of double cantilever beam specimen under quasistatic loading conditions. The DCB specimen was made by bonding two slender sheet of hardened steel of 2.8 mm thickness. This chapter has three major sections; first section gives finite element analysis, second section deals with experimental technique and results are presented in third section.

Chapter 3 discusses the technique to evaluate initiation and propagation fracture toughnesses under impact loading through a hybrid technique involving experimental results and finite element analysis. This chapter also has three major sections; the finite element analysis, crack propagation model and analysis of the specimen is presented in first section, second section is devoted to experimental technique and results are presented and discussed in third section.

The conclusions and scope for further work is outlined in Chapter 4.

CHAPTER - 2

QUASI STATIC CRACK PROPAGATION

This chapter describes the analysis of interlaminar crack propagation under quasi static conditions. It is a combined (hybrid) method of finite element analysis and experimental measurements; the section 2.1 gives a brief description of FEM, the section 2.2 to discuss the experimental details and the section 2.3 presents the results.

2.1 FINITE ELEMENT ANALYSIS OF CRACK GROWTH

Finite element analysis has been carried out to determine the strain field near the crack tip in the double cantilever beam specimen with slender cantilevers. One of the goals of this study is to identify the optimum location for a strain gauge near the crack tip which leads to the determination of stress intensity factor accurately.

2.1.1 SPECIMEN GEOMETRY AND MATERIAL

The DCB specimen under investigation is made by joining two thin strips of hardened alloy steel with epoxy (Fig. 2.1). The thickness of the epoxy bond is very small (less than 0.03mm) and is considered to be a line in the finite element formulation. However, it is to be noted that the fracture behaviour of the specimen will mostly be determined by the bond strength. The material used for the specimen is hardened 40Ni2Cr1Mo28 (EN-24). Hardening increases the yield stress value thereby decreasing the size of the plastic zone around the crack tip. The plastic zone can be estimated by Irwin's formula (Broek, 1989)

$$r_p = K^2 / \pi\sigma_{ys} \qquad (2.1)$$

where r_p is plastic zone size, K is stress intensity factor and σ_{ys} is yield stress. In the present case, specimen has a Rockwell hardness of 33 on the C-scale and a yield stress of approximately 1000 MPa. In order to estimate the size of the plastic zone, K_{Ic} of the DCB specimen was determined by preliminary experiments through G_{Ic} and then using the relation for plain strain

$$K_{Ic} = \frac{\sqrt{G_{Ic}E}}{(1-\nu^2)} \qquad (2.2)$$

For a K_{Ic} value of 1.5 MPa$\sqrt{m}$, the plastic zone size is less than 0.0007mm which is small enough to be neglected and the cantilever can be considered to be elastic.

2.1.2 FORMULATION

In this two dimensional finite element analysis, the standard displacement based stiffness formulation is used (Cook et al., 1989). The technique is widely used and for the sake of completeness, it is briefly explained in appendix-A.

2.1.3 MESH GENERATION

A suitable mesh of eight noded isoparametric is generated by a preprocessor program as shown in Fig. 2.2 and 2.3. Near the crack tip, mesh is kept fine and it is made coarse away from the crack tip where stress gradients are expected to be small. The size of the elements which lie near the crack tip is 0.5 mm and the coarse elements have a size of 11 mm. Figure 2.2 shows the complete mesh used and Fig. 2.3 shows the details near the crack tip including the collapsed elements at the crack tip. At the crack tip three nodes are collapsed to model quarter point elements to simulate the square root singularity of the stresses which is explained in the next section. A mesh having 364 elements and 1384 nodes was used.

2.1.4 QUARTER POINT FORMULATION

The behaviour of quarter point element is explained below. The derivation is for 1-D and can be extended to higher dimensions (Barsom, 1976).

An element can display a square root singularity in stress or strain by suitably defining its geometry. Consider for example the three noded bar element as shown in Fig. 2.4(a). The displacement u at any point is given as

$$u = N_1 u_1 + N_2 u_2 + N_3 u_3 \qquad (2.3)$$

and the coordinate x at any point is

$$x = N_1 x_1 + N_2 x_2 + N_3 x_3 \qquad (2.4)$$

where N_i are the shape functions defined as

$$\begin{aligned} N_1 &= \frac{1}{2}\xi(\xi-1) \\ N_2 &= (1-\xi^2) \\ N_3 &= \frac{1}{2}\xi(1+\xi) \end{aligned} \qquad (2.5)$$

Substituting in Eq. 2.4,

$$x = \frac{\xi}{2}(\xi-1)x_1 + (1-\xi^2)x_2 + \frac{\xi}{2}(1+\xi)x_3 \qquad (2.6)$$

If the middle node is shifted to a point which is at a distance rL from node 1 (Fig. 2.4 b), it can be shown that for the stress to be singular at node 1 for r = ¼ and the nature of singularity is a square root. Coordinates of three nodes are (Fig. 2.4 b)
$x_1 = 0$, $x_2 = rL$, $x_3 = L$
Then Eq. 2.6 becomes,

$$x = \frac{L}{2}[2r - 2r\xi^2 + \xi + \xi^2] \qquad (2.7)$$

Now differentiating displacement u with respect to x,

$$\frac{\partial u}{\partial x} = \frac{\partial u}{\partial \xi}\frac{\partial \xi}{\partial x} = \left[\frac{\partial u}{\partial \xi}\right][J]^{-1} \qquad (2.8)$$

where [J] denotes the Jacobian given by

$$J = \frac{\partial x}{\partial \xi} = \frac{L}{2}[-4r\xi + 1 + 2\xi] \qquad (2.9)$$

Substituting in Eq. 2.8,

$$\frac{\partial u}{\partial x} = \frac{\partial u}{\partial \xi}\left[\frac{L}{2}(-4r\xi + 1 + 2\xi)\right]^{-1} \qquad (2.10)$$

At node 1, $\xi = -1$ and $x = 0$. Therefore,

$$\frac{\partial u}{\partial x}\Big|_{\substack{\xi=-1 \\ x=0}} = \frac{\partial u}{\partial \xi}\left[\frac{L}{2}(4r + 1 - 2)\right]^{-1} = \frac{\partial u}{\partial \xi}\left[\frac{L}{2}(4r - 1)\right]^{-1}$$

for $\frac{\partial u}{\partial x}\Big|_{\xi=-1} \to \infty$

$$\frac{L}{2}(4r - 1) = 0 \Rightarrow r = \frac{1}{4} \qquad (2.11)$$

Substituting r=¼ in Eq. 2.7,

$$x = \frac{L}{4}(1 + \xi)^2$$

or,

$$(1 + \xi) = \sqrt{\frac{4x}{L}} \qquad (2.12)$$

Substituting r=¼, in Eq. 2.9

$$J = \frac{\partial x}{\partial \xi} = \frac{L}{2}(1 + \xi)$$

Eliminating ξ using Eq. 2.12, one obtains,

$$J^{-1} = \frac{1}{L}\sqrt{\frac{L}{x}} \qquad (2.13)$$

Using equations 2.5, 2.12 and 2.13 in 2.10, one obtains

$$\frac{\partial u}{\partial x} = \left[\left(\frac{2}{L} - \frac{3}{2L}\sqrt{\frac{L}{x}}\right)u_1 - \left(\frac{4}{L} - \frac{2}{L}\sqrt{\frac{L}{x}}\right)u_2 + \left(\frac{2}{L} - \frac{1}{2L}\sqrt{\frac{L}{x}}\right)u_3\right] = f\left(\frac{1}{\sqrt{x}}\right)$$

which means stress is inversely proportional to square root of the distance from the node.

2.1.5 CALCULATION OF STRESS INTENSITY FACTOR

The stress intensity factor can be determined using the displacement of the relevant nodes of the quarter point collapsed element (Fig. 2.5) around the crack tip as follows (Cook et al., 1989)

$$K_I = \frac{2G}{(Q+1)}\sqrt{\frac{\pi}{2l}}\left[(4V_{B2} - V_{C2}) - (4V_{B1} - V_{C1})\right] \qquad (2.14)$$

where Q = 3-4ν (plane strain)

ν = Possion's Ratio

G = Shear Modulus

u = x-displacement at the node point and

v = y-displacement at the node point

2.1.6 TEST PROBLEMS

The programme has been validated using following known problems.

1. Large plate with a centre crack
2. Large plate with an edge crack

Large Plate with a Centre Crack

The problem of large plate with centre crack under uniformally distributed load is solved for stresses and stress intensity factor in Mode I. Figure 2.6 shows the geometry of the specimen and mesh details are shown in the Fig. 2.7. The stress intensity factor determined by FEM is 3.57 MPa$\sqrt{m}$ compared to a value of 3.76 MPa$\sqrt{m}$ from the theoretical formula

$$K = \sqrt{\sec\frac{\pi a}{w}}\ \sigma\sqrt{\pi a} \qquad (2.15)$$

The numerical result is within 5% of theoretical result. The stress field obtained from FEM solution is found to be in good agreement with analytical results.

Large Plate with an Edge Crack

The stress intensity factor K_I and stresses for an edge crack shown in the Fig. 2.8 in opening mode are determined. The mesh used for the purpose is shown in the Fig. 2.9.

The value of K_I, obtained as 0.32 MPa$\sqrt{m}$ from finite element calculations, is within 3 % of the value 0.33 MPa$\sqrt{m}$ calculated using the equation $K = 1.12\,\sigma\sqrt{\pi a}$. The stress field is thus found to be in good agreement with analytical results.

2.1.7 RESULTS OF DCB SPECIMEN WITH THIN CANTILEVERS

A DCB specimen of the geometry shown in Fig. 2.1 is analyzed for stresses and SIF. The finite element mesh used is shown in Fig. 2.2 and 2.3. The value of stress intensity factor is obtained as 1.6 MPa$\sqrt{m}$ from finite element analysis for a load of P = 60N applied at the cantilever ends.

For validation purpose, K_I is compared with the value of SIF determined through the equation

$$K_I = \frac{2\sqrt{3}\,P\,a}{h^{\frac{3}{2}} B(1-\nu^2)} \qquad (2.16)$$

where P is load applied at the cantilever end, a is the crack length, h is the thickness of each cantilever and B is the width of the cantilever. This method is referred to as 'K_I through G_I approach' because the expression of Eq. 2.16 is determined by finding G_I first and then evaluating K_I using the relation (2.2). The derivation of Eq. 2.16 is presented in Appendix-B. This analysis provides K_I for a known load at the cantilever ends, crack length and specimen dimensions. However, it does not give any information of strain field near the crack tip. Obtaining closed form solution for strain field is difficult as the free surfaces are very close to the crack tip and influence the stress/strain field significantly in the vicinity of crack tip. Because the smallest available strain gauges are of dimensions (0.2 mm x 1.4 mm), they cannot be bonded closer than 1.5 mm to the crack tip. Determination of strain field in a DCB specimen with cantilevers of thickness less than 3 mm, it is necessary to make use of finite element analysis.

In the derivation of Eq. 2.16 (Appendix-B), the cantilevers have been considered to deform under flexure only and the shear strain energy and the strain energy in the bulk material beyond the crack tip do not effect the evaluation of the compliance. This

assumption of neglecting these strain energies is reasonable as the cantilevers are thin and flexural energy is the one which is significant.

The value of K_I from Eq. 2.16 is obtained as 1.89 MPa$\sqrt{m}$ for load P = 60 N. This differs from the result of finite element analysis by 18 %. The finite element analysis has been carried out for different loads and crack lengths and the results are presented in Table 2.1. The difference between the values obtained through the two methods is consistent. The finite element results are preferred as it models the specimen more accurately and is free from assumptions made in the 'G_I approach'.

Table 2.1 Comparison between K_I obtained by FE analysis and K_I calculated through Eq. 2.16.

sl. No.	Load (N)	Crack Length (mm)	K_I through G_I approach MPa$\sqrt{m}$	K_I from F.E.Analysis MPa$\sqrt{m}$	Diff. %
1	58	36.0	2.29	1.89	-18
2	50	36.0	1.98	1.63	-18
3	56	36.0	2.21	1.82	-18
4	70	35.0	2.77	2.29	-17
5	82	30.0	2.71	2.18	-19
6	81	23.0	1.93	1.76	-14

Strain Field

The resulting displacement field is post processed to obtain the strain field around crack tip in the specimen and strain contours are plotted (Ramesh, 1991). Finite element analysis determines the strains reasonably accurate at Gauss Points in each element. These strains are then linearly extrapolated to find strains at the nodes (Cook et al., 1989)

$$\begin{Bmatrix} \varepsilon_A \\ \varepsilon_B \\ \varepsilon_C \\ \varepsilon_D \end{Bmatrix} = \frac{1}{2} \begin{bmatrix} 1+\frac{\sqrt{3}}{2} & -0.5 & 1-\frac{\sqrt{3}}{2} & -0.5 \\ -0.5 & 1+\frac{\sqrt{3}}{2} & -0.5 & 1-\frac{\sqrt{3}}{2} \\ 1-\frac{\sqrt{3}}{2} & -0.5 & 1+\frac{\sqrt{3}}{2} & -0.5 \\ -0.5 & 1-\frac{\sqrt{3}}{2} & -0.5 & 1+\frac{\sqrt{3}}{2} \end{bmatrix} \begin{Bmatrix} \varepsilon_1 \\ \varepsilon_2 \\ \varepsilon_3 \\ \varepsilon_4 \end{Bmatrix} \qquad (2.17)$$

where ε_A, ε_B, ε_C, ε_D and ε_1, ε_2, ε_3, ε_4 represents a strain component ε_x, ε_y and γ_{xy} at node point and Gauss point location respectively (Fig. 2.10). In a 2-point integration, ρ is $1/\sqrt{3}$. The principal strains and their orientations are then determined at each node. The orientations of the principal strains are calculated by solving for eigen vectors of the strain matrix corresponding to eigen values ε_1 and ε_2.

The strain fields for the upper cantilever are given in Fig. 2.11 to 2.13 for 37 mm crack length and 60 N load at the cantilever ends. Fig. 2.11 gives the strains along the y-axis and the Fig. 2.12 shows the strains along X-axis. As expected it can be seen that the strain values are high near the crack tip. The principal strains and its orientation are also plotted which is shown in Fig. 2.13(a) and 2.13(b) respectively.

2.1.8 OPTIMUM LOCATION AND ORIENTATION FOR STRAIN GAUGE

Location of the strain gauge (0.2 mm gauge length and 1.4 mm width) which is to be bonded on the side face of the cantilever beam is selected on the basis of the following criteria :

(a) Strain due to flexure should becomes zero (or small) once the crack passes ahead of the strain gauge. This makes it possible to separate the effect of crack tip strain from

the flexural strain. This condition can be met by fixing the strain gauge on the neutral axis (mid plane) of the upper cantilever.

(b) The orientation of the strain gauge be such that it provides maximum strain.

The variation of principal strain and its orientation on the mid plane of the DCB specimen in front of the crack tip are shown in Fig. 2.14. It is quite evident from this figure that the principal strain is maximum at a distance of nearly 1 mm ahead of the crack tip and the orientation of principal strain at this point is 48° from the mid plane. It should be noted here that ahead of the crack tip, the strains are caused mainly due to the crack tip singularity, while behind the crack tip the strains are developed primarily due to flexure in the cantilever

For the sake of convenience in conducting the experiments, the strain gauge was bonded at an angle of 45° from centre line. Strain gauge readings for several crack lengths along 45° direction and at the midplane of the upper cantilever are shown in the Fig. 2.15. The maximum strain in each case occurs at a distance of 1 mm from the crack tip. The strain field is shown in Fig. 2.16 along with the strain gauge. Because the strain gauges have a finite size, the measured strain would be the average of strain over the area of the strain gauge. The average strain from the FEM solution is determined using the value at 9 points on the centre line.

2.1.9 SIF FROM MEASURED STRAIN

It can be observed from Fig. 2.14, the crack tip at the peak value of the strain will be 1 mm behind the strain gauge. Based on the FEM results a relationship is developed between the peak strain value and stress intensity factor (K_I). Since the material is assumed to remain elastic under the test load, the measured peak strain, ε_{pk}, and SIF of the interlaminar crack are proportional to the load, P, expressed as

$$K_I = M\,\varepsilon_{pk} \qquad (2.18)$$

$$K_I = B\,P \qquad (2.19)$$

where M and B are proportionality constants. Figure 2.17 shows the variation of M and B with the crack length for the geometry of the specimen considered in the study. For the case of a growing crack at low speeds K_I approaches K_{Ic}. A typical relationship between K_{Ic} and ε_{pk}, for a crack length of 37 mm, is

$$K_{Ic} = 0.0242\ \varepsilon_{pk} \qquad (2.20)$$

where K_I is in MPa$\sqrt{m}$ and ε_{pk} is in micro strain. Through this relationship, the measured peak strain provides the critical stress intensity factor of the interlaminar crack. Similarly, a typical relationship between load and the K_I for a crack length of 37 mm is

$$K_I = 0.0326\ P \qquad (2.21)$$

where K_I is in MPa$\sqrt{m}$.

2.2 EXPERIMENTAL DETAILS

2.2.1 INTRODUCTION

This section deals with experimental details including design and preparation of specimen, equipments used, parameters controlled and measurements made during the quasi-static experiment. The experiment is conducted under controlled displacement condition so as to obtain a quasi-static crack growth.

2.2.2 SPECIMEN GEOMETRY, MATERIAL AND SPECIMEN HOLDER

Geometry

The DCB specimen used has two thin metal strips joined together with epoxy. The crack length is varied between 23 and 36 mm and the thickness of the cantilevers is 2.8 mm each. Figure 2.18 provides information on the specimen and specimen holder.

Material

The material used is hardened alloy steel, 40Ni2Cr1Mo28 (British EN24, US 4340), which has a high yield stress value after hardening. Hardening is done by keeping the metal at 830° - 850° C for one hour and then quenching in oil. This is followed by annealing to relieve the residual stresses. In annealing, the metal is heated to about 310° C for a period of nearly 20 minutes accompanied by furnace cooling. The hardness of the strips is then checked. In the present case the average hardness of the strips on C-scale is 33 which corresponds a yield stress of nearly 1000 MPa. Each strip was ground flat and polished with alumina powder.

Bonding

The faces of the metal strips to be bonded are etched to give better interfacial bonding. The etching was done by dilute nitric acid. For bonding, epoxy LY 556 and hardener HY 1907IN in the ratio 100:85 by weight are used. To this mixture, accelerator DY 062 also is added at the rate of 1.5 ml per 100 gm of epoxy. The resin, the hardener and the accelerator are supplied by Ciba-Geigy Limited, Bombay. The sides of the specimen are covered with a layer of wax to prevent them from getting coated with epoxy and the faces to be bonded are cleaned with pure acetone. The epoxy mixture is then spread on the faces that are to be bonded. The two strips are then put together and pressed in a specially built fixture made of two stiff steel plates (each 25mm thick) with ground flat faces (Fig. 2.19). The locating pins to properly hold the specimen are shown in Fig. 2.20. Between the strips and the flats of the fixture, a sheet of BOPP (biaxially

oriented polyproplyne) was placed on each side that works as a release film.

Provisions are made in the fixtures for keeping the two strips in position while curing. The base plate of the fixture has three cylindrical stops and four adjustable buttons (Fig. 2.20). Both the thin strips are butted against the cylindrical stops and kept in place with the adjustable buttons. Each adjustable button has slot of 4 x 7 mm so that they can be tightened to the base at a desired location. Also, these buttons have different heights so as to hold each strip in its place.

The fixture along with the specimen is placed between two platens of a hydraulic press. The platens are heated through inbuilt heaters and the temperature of the specimen is monitored by placing a chromel-alumel thermocouple. The temperature of the specimen is maintained at 130°C under 1.2 MPa pressure for one hour. It is then allowed to cool under the same pressure to room temperature.

Precrack

While bonding the strips, a precrack of desired length is introduced by placing a plastic sheet of BOPP (biaxially oriented poly-propylene) so that the strips are not bonded there. In the present study, several crack length of 23.5 and 36.5 mm are used.

Crack Sharpening

The pre-crack introduced in the DCB specimen by placing a BOPP sheet needs further preparation before the specimen is loaded. The tip of the pre-crack is not very sharp due to the BOPP sheet's finite thickness. Therefore the pre-crack should be grown further by a few millimetres to sharpen the crack. Furthermore, although the BOPP sheet does not bond well to the steel faces, it does stick weakly to the steel faces at many points. The cantilevers of the DCB are therefore pulled to snap off these weak sticking. A fixture is designed to sharpen the crack. It consists of three plates. The specimen is clamped between two 20 mm thick plates. The inner faces of the thick plates are ground flat so as to have uniform pressure on the specimen. Before the plates

are tightened between the two jaws of a vice, the specimen and both the plates are placed on their side faces over the third plate of the fixture whose top surface is also grounded flat. This ensures that the edges of the thick plates are parallel to the crack front. The specimen is placed between thick plates in such a way that the tip of the pre-crack is projected out by 2-3 mm beyond the edges of the plates. The specimen between the thick plates is pressed properly between the jaws of a vice (Fig. 2.21). Before opening the crack of the DCB specimen with a wedge (sharp chisel), a layer of white ink is applied at the side faces of specimen and allowed to dry. First a shaving blade and then a sharp chisel is cautiously and gently pressed to open the crack. The dry white ink cracks with opening of the pre-crack of the specimen and thus gives the location of the tip of the sharpened crack.

Hinges

Hinges have been designed and fabricated for applying load to the cantilever ends (Fig. 2.22). For fixing the hinges, two tapped holes have been provided at the ends of the cantilevers. Each hinge consists of a bracket, a support and a pin all made of steel. The bracket is fixed to the cantilever with the help of two high strength capscrews. The support is inserted into the bracket and the pin is used to join the two. The 10 mm diameter pin makes the hinge strong and stiff. All the holes of the hinges and the diameter of the pin are made with close tolerances. The end of the support is cylindrical of diameter 12mm, made to fit the inside loading fixture of the tension machine, INSTRON 1195. The hinge so designed is moment free while load is applied. Further, it keeps the load line always vertical.

2.2.3 PRELIMINARY EXPERIMENTS TO ESTIMATE K_{Ic}

A preliminary experimental study was conducted to get information about the expected K_{Ic} and the order of the maximum load when the DCB specimen is pulled in the Instron machine. This is done by first finding G_{Ic} through the standard technique of

successive growth of crack (Narayanan, 1988) and then estimating K_{Ic} by using the well known Eq. 2.2.

2.2.4 EXPERIMENTAL DETERMINATION OF K_{Ic}

The major objective is to correlate strain measurements in the vicinity of the crack tip (through a strain gauge) with stress intensity factor of a DCB specimen that is made of thin cantilevers. The loads are applied in displacement control mode with a very slow cross head speed. This work is expected to pave way for a more widespread use of strain gauges in this field. It is hoped that this procedure could be extended to dynamic problems also.

The strain gauges used in these experiments have been supplied by Tokyo Sokki Kenkyujo Co.,Ltd.,Japan. They have a gauge length of 0.2 mm and a gauge width of 1.4 mm. The base of the strain gauge is rectangular with dimensions 3.5 mm X 2.5 mm. Its resistance is 120 ± 0.3 Ω and gauge factor, 2.07. Figure 2.23 shows the details of the strain gauge. The accuracy of the strain gauge of 0.2 mm gauge length has been checked by bonding the strain gauge to a long cantilever and measuring the bending strain caused by dead weights. The error in measurements was found to be within 5%.

Extreme care is taken in fixing the strain gauges as it has a very small area for bonding. Epoxy LY 556 and hardener HY 951 are used in bonding. They are mixed well in the ratio 10:1 by weight. The ambient temperature is kept around 55 to 60° C for about 24 hours to help curing. Localized pressure is applied while the curing takes place.

Positioning of the strain gauge is done with the help of a fixture made out of self sticking paper. It provides two sides as reference for fixing the strain gauge (Fig. 2.24). A corner of the strain gauge is cut as shown in Fig. 2.24 so that the strain gauge base does not extend beyond the crack plane. The accuracy of the fixture is checked from the observations made under travelling microscope. It is found that the centre of the strain

gauge is bonded very near to the required point, the error being less than 0.1mm. The strain gauge output is measured using strain indicator (Model P-350A, Measurement Group). The crack velocity being very small the strain indicator can be conveniently used. The strain indicator has a least count of 1 micro strain and hence provides reasonably accurate observations. The measurement is made continually at regular intervals of time. The experiment is conducted on INSTRON, model 1195. This is a highly flexible machine and can be used for testing materials in tension, compression, flexure and torsion. Its chart recorder system records the displacement against load at the cantilever ends accurately.

Procedure

The specimen is mounted on the INSTRON machine and the trailing end of the specimen is suspended by a thread and a small counterweight to keep the axis of the specimen horizontal. It is a pulley like arrangement so that the specimen as a whole can move up and down but remains always horizontal. The specimen is loaded in displacement controlled mode and the cross head speed is fixed at 0.1 mm/minute. From the preliminary experiments it was observed that the crack velocity remains quite low under such a displacement rate. Since the maximum load during the initial experiments was in the range of 50 - 75 N, the full scale load on the machine is kept 100 N. The chart speed for recording the graph displacement versus load is maintained at a convenient value of 10 mm/minute. In this machine, the upper jaw is fixed and the lower jaw moves down thus applying the load. Once the experiment is started and the load reaches around half the expected maximum load, recording of the strain indicator readings is started. Once the crack has moved well past the strain gauge, the specimen is unloaded and the readings are also noted during unloading. The entire experiment lasts for approximately 20 minutes.

Data analysis

The experiments were conducted with the strain gauge fixed at a distance of about 5 to 8 mm beyond the tip of the precrack. From the FE analysis, it is estimated that the

maximum value of strain recorded will be when the crack tip is 1.0 mm away from the strain gauge. Hence, the crack length corresponding to the peak obtained in the strain plots can be deduced. It was found that for a crack length of 30 mm and load of the order of 60 N, the maximum strain expected is around 140 micro according to FE prediction. The graphs and other results of the experiments are shown in subsequent pages.

2.3 RESULTS AND DISCUSSION

For comparison purposes, K_{Ic} is determined by two methods. In the first method, K_{Ic} comes out as a closed form solution described in section 2.1.7and in Appendix B and is called 'K_I through G_I approach' in this study. The second method finds K_{Ic} directly through the finite element scheme developed in section 2.1.9. Here it may be noted that the value obtained by finite element analysis is preferred to the one obtained through G approach as explained in Sec. 2.1.7.

2.3.1 EXPERIMENTAL RESULTS

A total of six experiments were conducted in this study. The crack length for each experiment is shown in column I of Table 2.2. In each experiment, Load vs. Crack Opening Displacement (COD) and Strain vs. COD are recorded. The COD is directly recorded by the strip chart recorder.

The chart speed and crosshead speed have been maintained at 10 mm/minute and 0.1mm/minute respectively. Hence 10 mm movement of the chart corresponds to a COD of 0.1 mm. The chart recorder plots the COD against the load applied. The strains measured through a strain indicator are then plotted on the same graph. For explaining the results of the experiment, the observations of the Exp. No. 1 are considered. Figure 2.25 shows two curves for experimental results. It is found that the observed peak strain is 138 μm/m. Substituting this value of ε_{pk} in Eq. 2.18, the value

of K is obtained as 1.55 MPa$\sqrt{m}$. This is referred to as experimental K_{Ic} in column V of Table 2.2.

Table 2.2 Experimentally observed peak strain and associated K_{Ic} and its comparison with K_{Ic} obtained through G_{Ic} approach and K_{Ic} obtained numerically.

I	II	III	IV	V	VI	VII	VIII
Exp. No.	Crack Length (mm)	Load (N)	Exp. Peak Strain X 10^{-6}	K_{Ic} Exp. MPa$\sqrt{m}$	K_{Ic} Num. MPa$\sqrt{m}$	K_{Ic} by G_I MPa$\sqrt{m}$	Diff. (V-VI)/V %
1	36.0	58	138	1.55	1.89	2.29	- 18
2	36.0	50	66	0.74	1.63	1.98	- 55
3	36.0	56	90	1.01	1.82	2.21	- 45
4	35.0	70	147	1.65	2.29	2.77	- 28
5	30.0	82	120	1.37	2.18	2.71	- 37
6	23.0	81	134	1.61	1.76	1.93	- 08

The load corresponding to the peak strain can also be read from the same figure as 58 N. Also, in this particular experiment, the strain gauge was at a distance of 38 mm from the hinges (load points). As discussed in Sec. 2.1.8,the crack length corresponding to the peak is 36.0 mm. Now, for these values, the K_{Ic} value is predicted as 2.29 Mpa$\sqrt{m}$ through G_I approach using Eq. 2.16 (column VII)

Similarly FE value of K_{Ic} can also be calculated from the known load at the cantilever ends (58 N for Expt. 1) corresponding to the peak value of the strain. Using Eq. 2.20, K_{Ic} is determined as 1.89 Mpa$\sqrt{m}$. The FE value is 18 % less than the experimental K_{Ic}.

Figures 2.26 through 2.30 show the graphs for the other five experiments conducted. In

each experiment, measured strain increases as the crack tip approaches the strain gauge, reaching a sharp and distinct peak. The results are tabulated in Table 2.2.

Table 2.2 shows that K_{Ic} of numerical simulation is consistently lower than K_{Ic} of 'G_I approach'. This difference is expected as explained in Sec. 2.1.7. However the results of FE simulation is regarded to be more accurate as explained in Sec. 2.1.7. Therefore the experimentally recorded K_{Ic} is compared with K_{Ic} obtained through numerical simulation and the percentage difference is given in Col. VIII. The difference between the two values varying between 8 to 55 %.

It is expected that the strain gauge reading would be zero after the crack has passed the gauge since the location of the strain gauge is such that the bending strains are zero. Instead it is seen that the strain reading assumes another level and remains there even after unloading. The difference varies considerably from one experiment to another. The specimen was checked for flatness after the two cantilevers were bonded. Formation of a slight curvature during the bonding of the two cantilevers together could not be avoided. Because of this curvature prestresses were developed in the specimen. As the strain gauge was glued to the prestressed DCB assembly, it did not show any strain until the crack passes through the strain gauge and prestressing is relieved.

2.3.2 REFINEMENT

The inconsistency in the value of the critical stress intensity factor measured experimentally is partly due to the fact that during bonding the cantilevers were found to have a curvature, though small, in spite of pre and post bonding precautions. This curvature causes a residual strain in the DCB specimen apart from the strains produced by the delamination crack, leading to variation in experimental values of observed SIF. It was therefore proposed to bond two strain gauges (Fig. 2.31) at symmetrical location on both the cantilevers to cancel the effect of the curvature. Gupta (1992) did experiments with two strain gauges, wherein the percentage variation in the experimental and numerical values came down to 19 %.

2.4 CLOSURE

The aim of the chapter was to determine the stress intensity factor by measuring strain near crack tip through strain gauges in a double cantilever specimen with thin cantilevers. A finite element software has been developed for estimating the strain field which has been used in selecting an optimum location and orientation for fixing small strain gauges.

The DCB specimen was made by bonding two thin strips of hardened alloy steel with epoxy. While bonding, a precrack of desired length was introduced by keeping a BOPP sheet between the strips. The strain gauge of gauge length 0.2 mm was bonded to the side face of the specimen at 45^{o} with the help of a special fixture.

The specimen was loaded in mode I in an INSTRON machine. The experiment was conducted quasi-statically under controlled displacement conditions. The measured peak strain has given the value of critical stress intensity factor through the relationship between strain and SIF which is obtained through the FE analysis. This experimentally obtained value of K_{Ic} has been compared with the finite element prediction calculated using the load corresponding to the instant at which strain reaches the peak value. It was observed that the technique, which involved both finite element analysis and experimentations to evaluate critical stress intensity factor on interlaminar crack growth of a DCB specimen worked well.

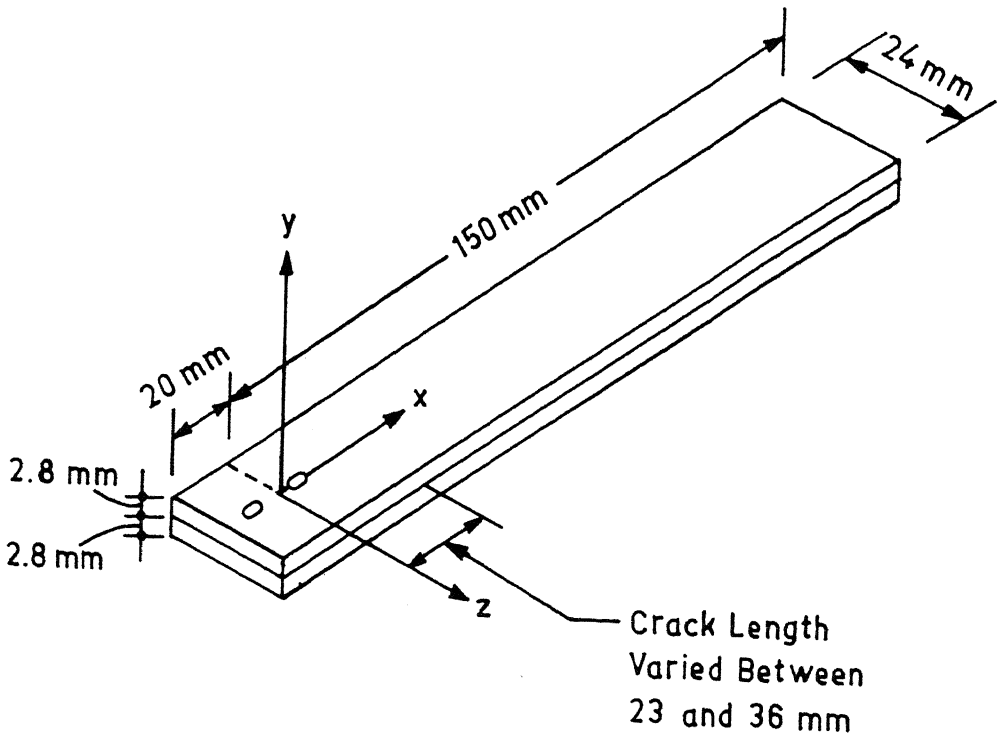

Fig. 2.1 DCB specimen

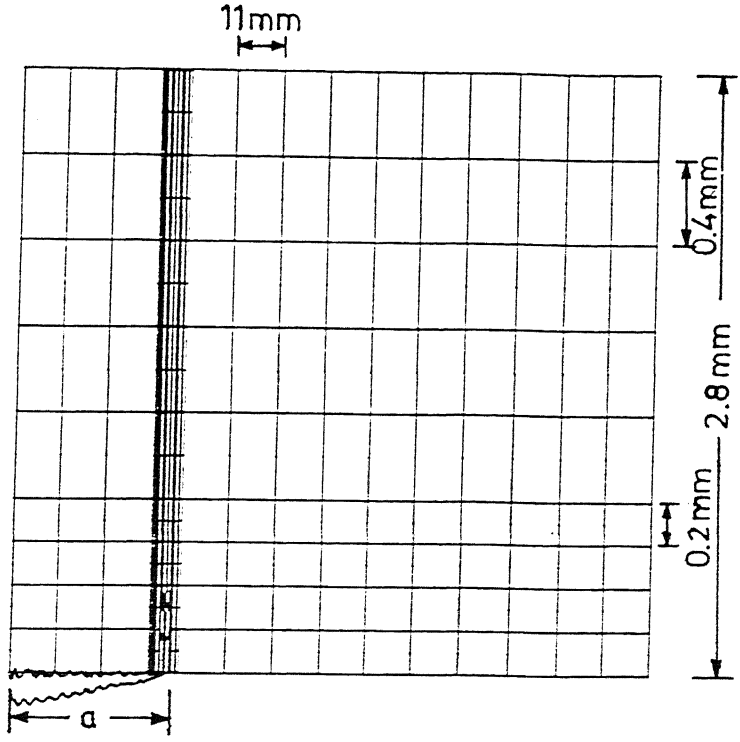

Fig. 2.2 Mesh for DCB specimen

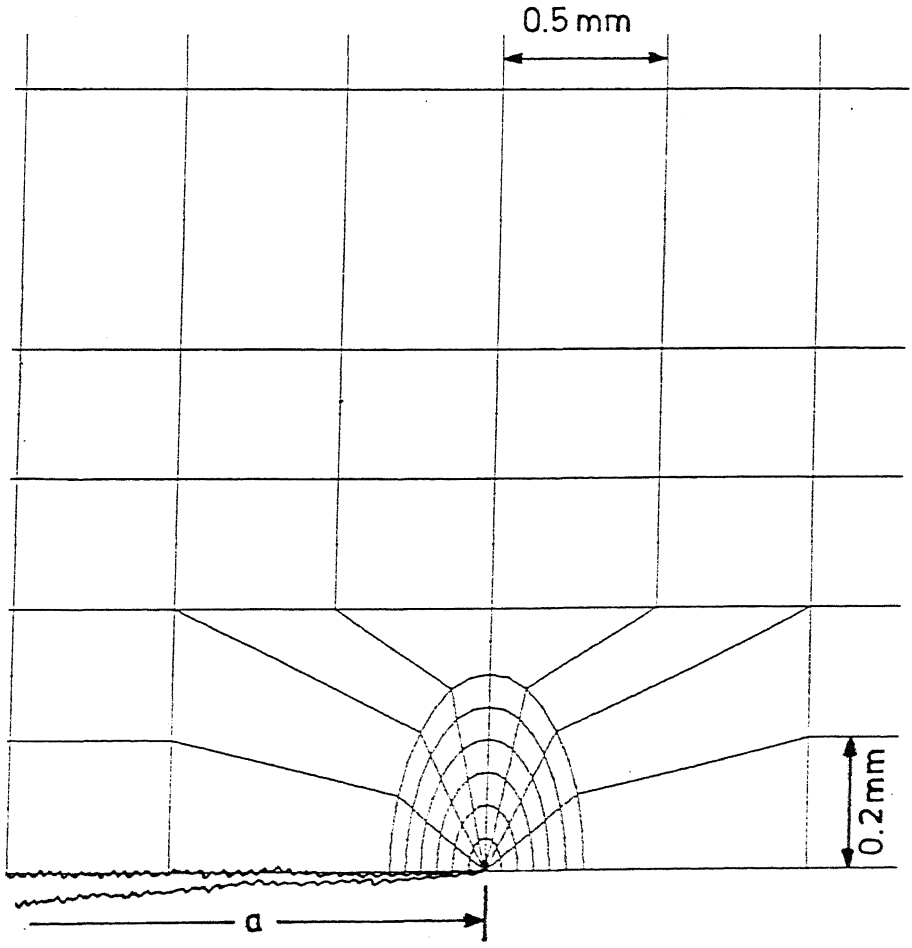

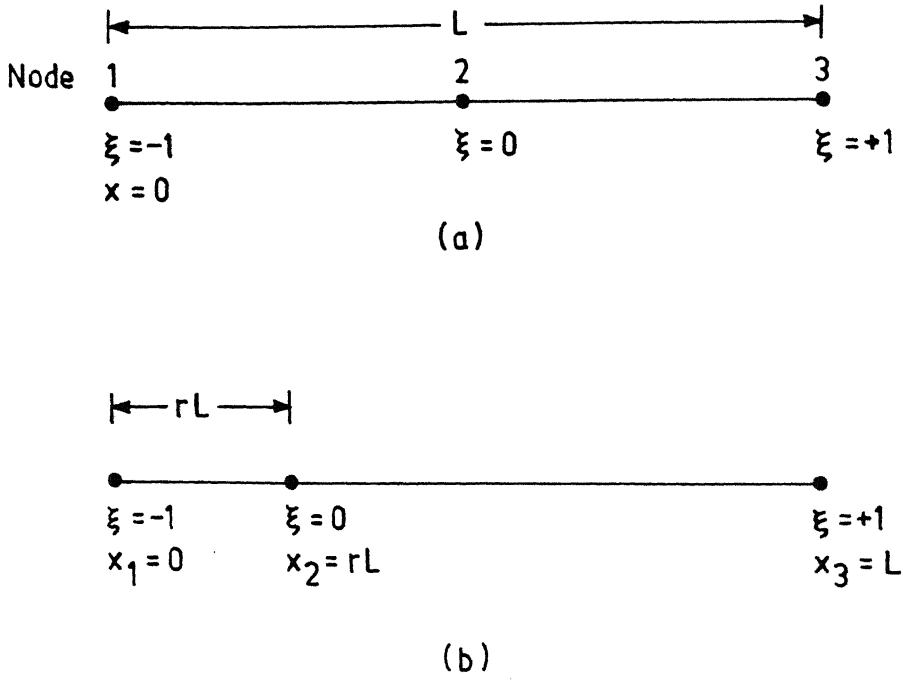

Fig. 2.4(a) Three noded bar element

Fig. 2.4(b) Three noded bar element with shifted mid node

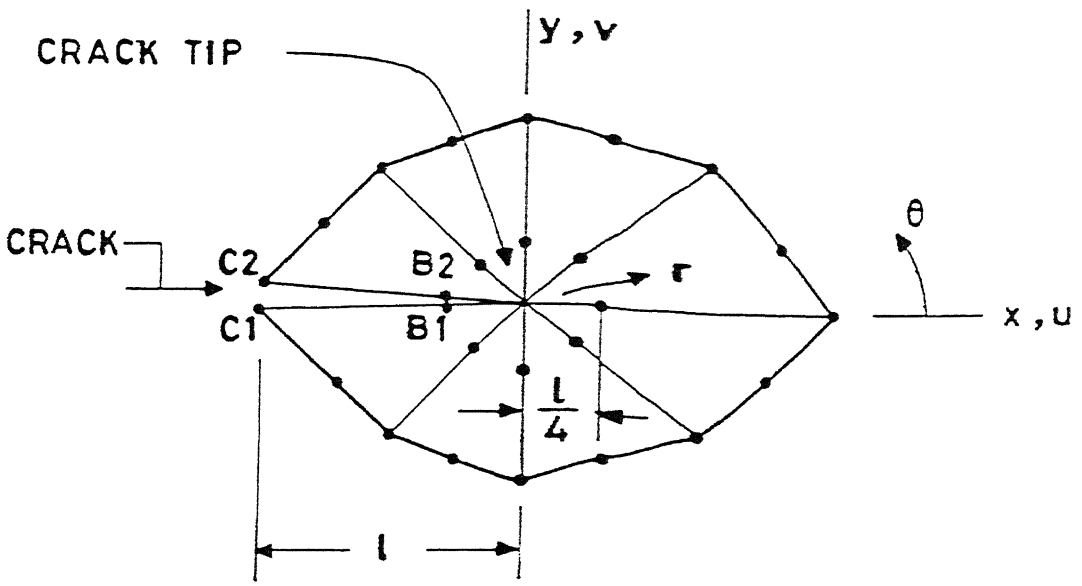

Fig. 2.5 Quarter point collapsed element at the crack tip

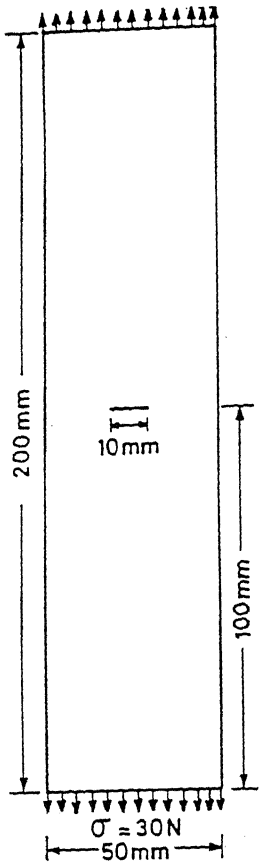

Fig. 2.6 Test problem of centre crack

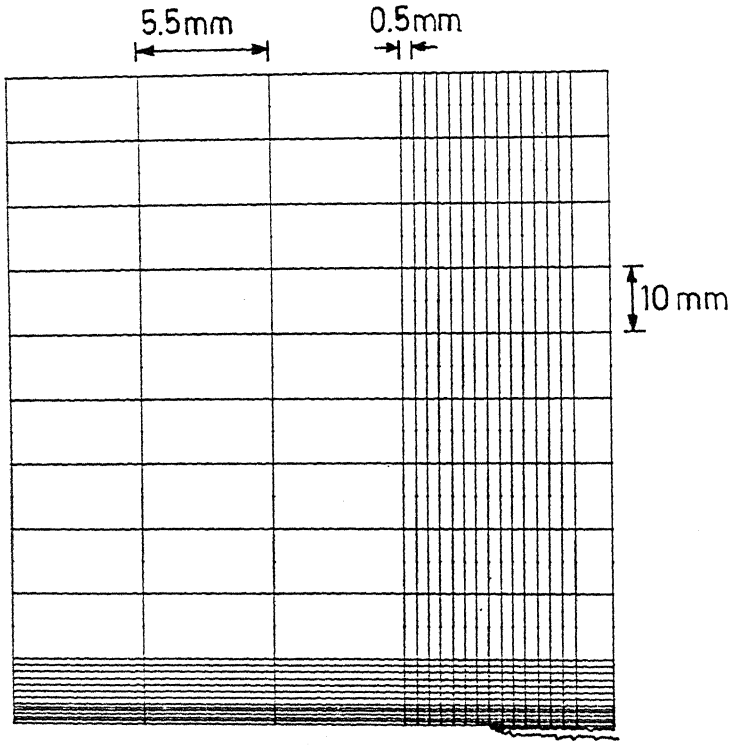

Fig. 2.7 Mesh for centre crack problem

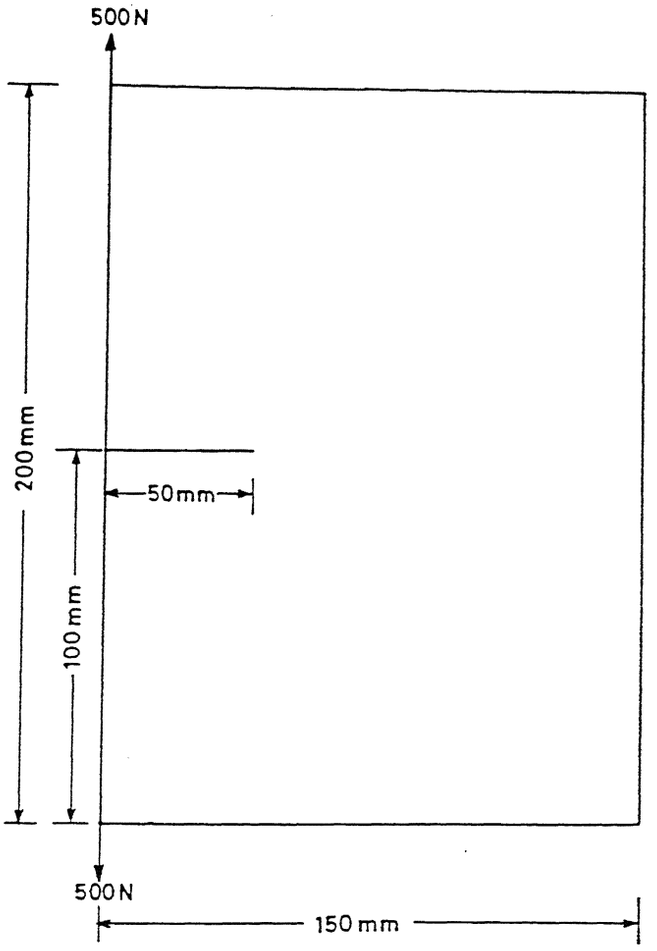

Fig. 2.8 Test problem of edge crack

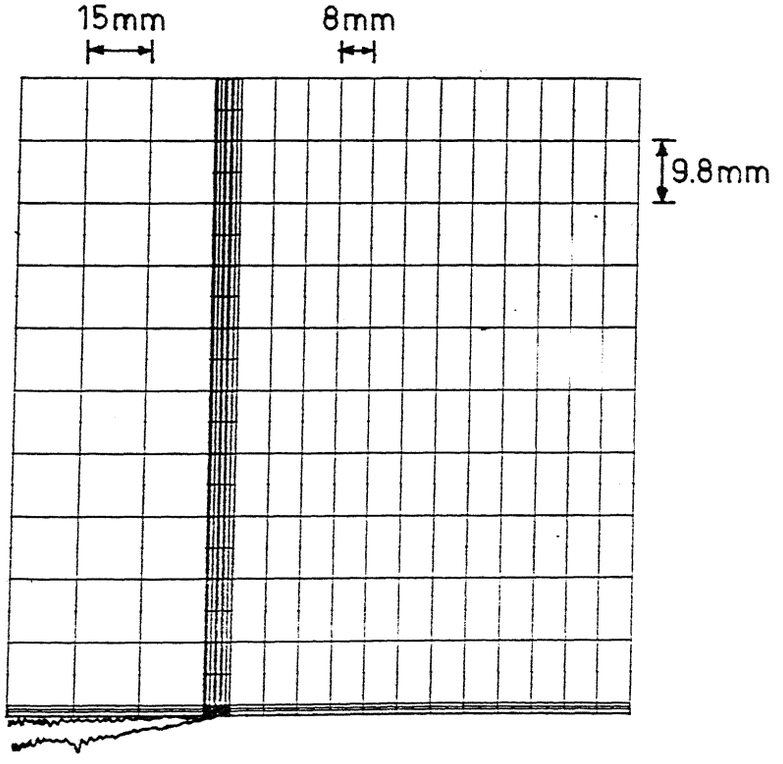

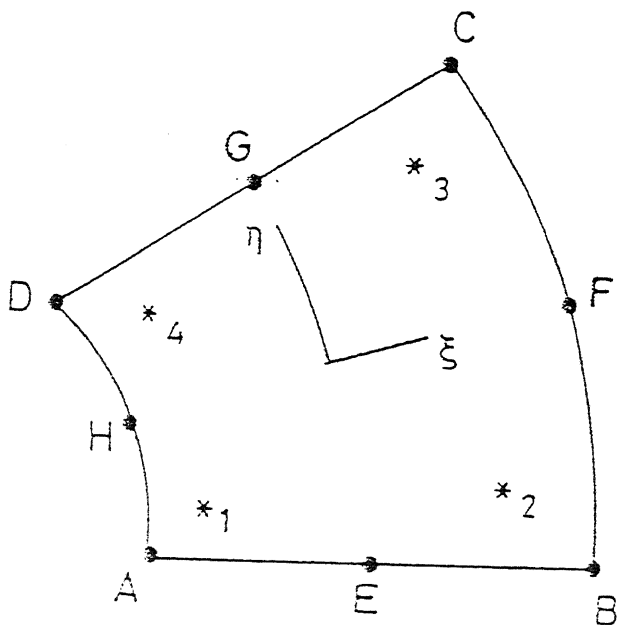

Fig. 2.10 Element to explain extrapolation of stress

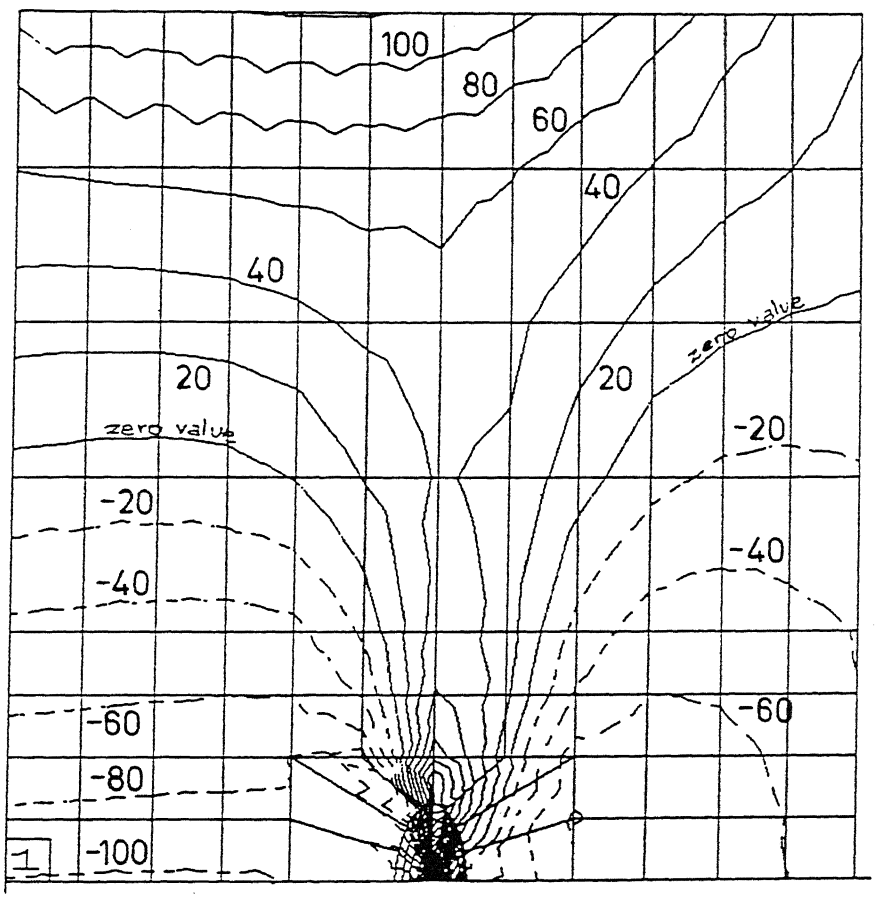

Fig. 2.11 ε_{yy} around crack tip of DCB specimen

(strain in μm/m)

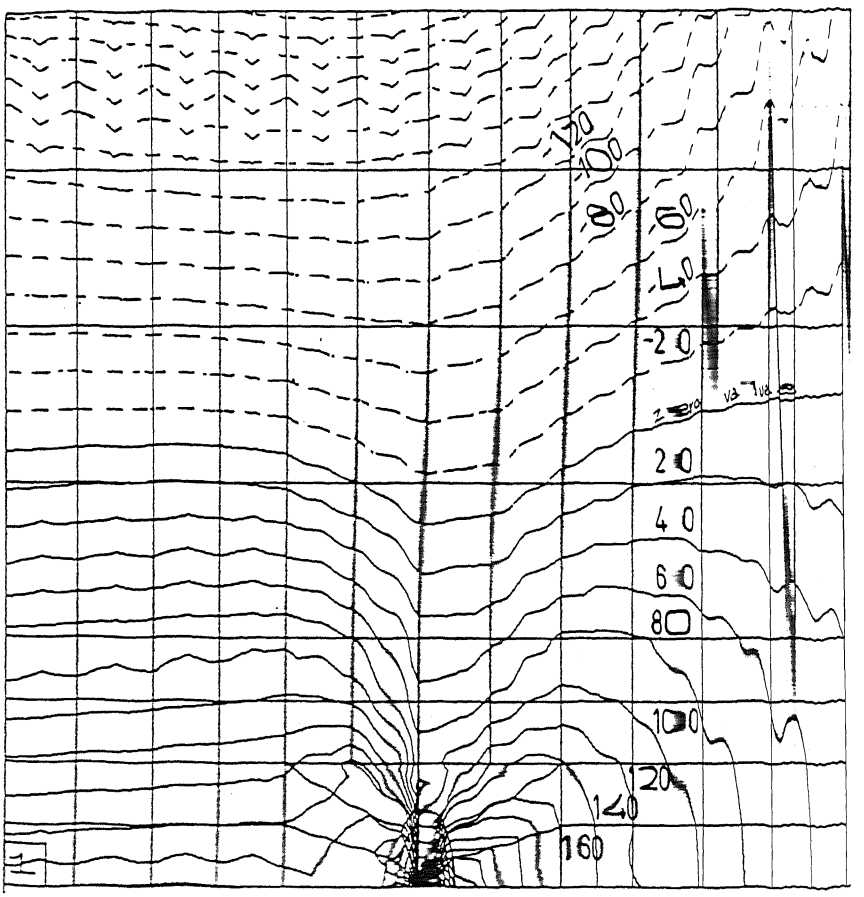

Fig. 2. 12 ε_{xx} around crack tip of DCB specimen

(strain in μm/m)

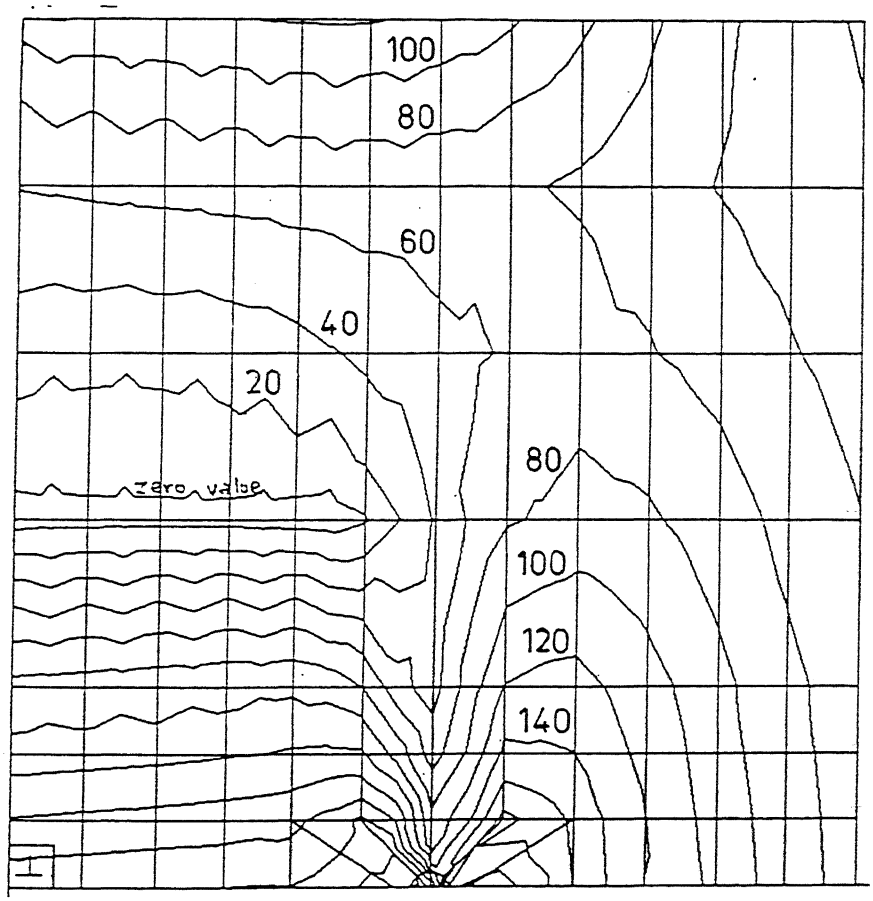

Fig. 2.13(a) Principal strain around crack tip of DCB specimen

(strain in μm/m)

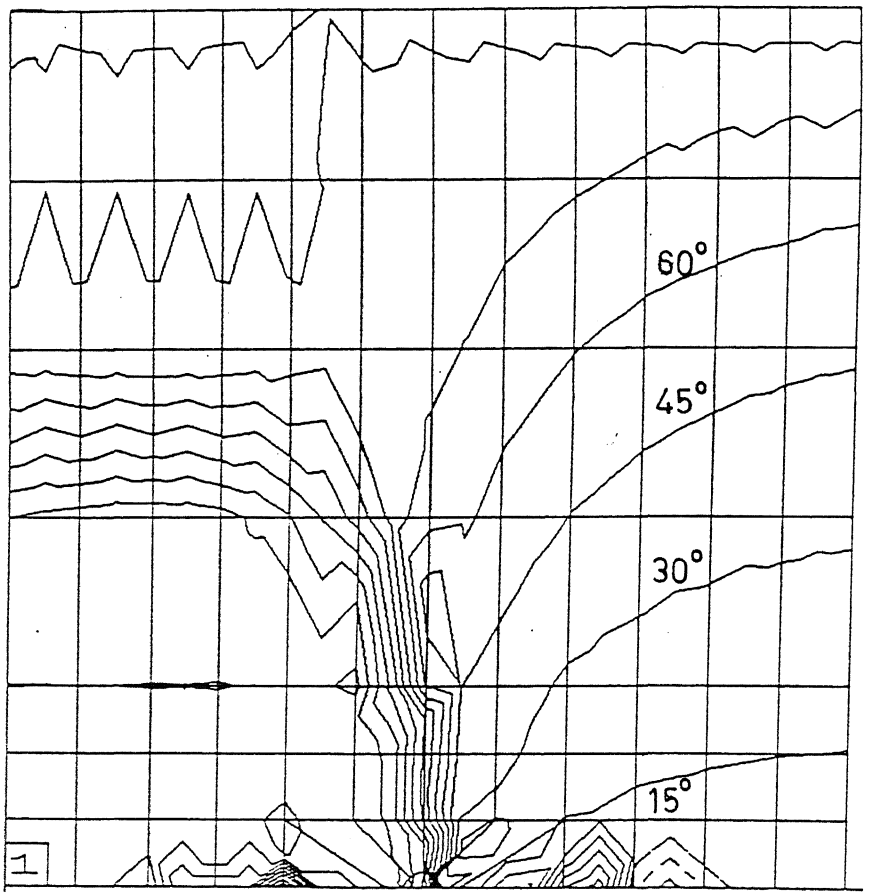

Fig. 2.13(b) Orientation of principal strain around crack tip of DCB specimen

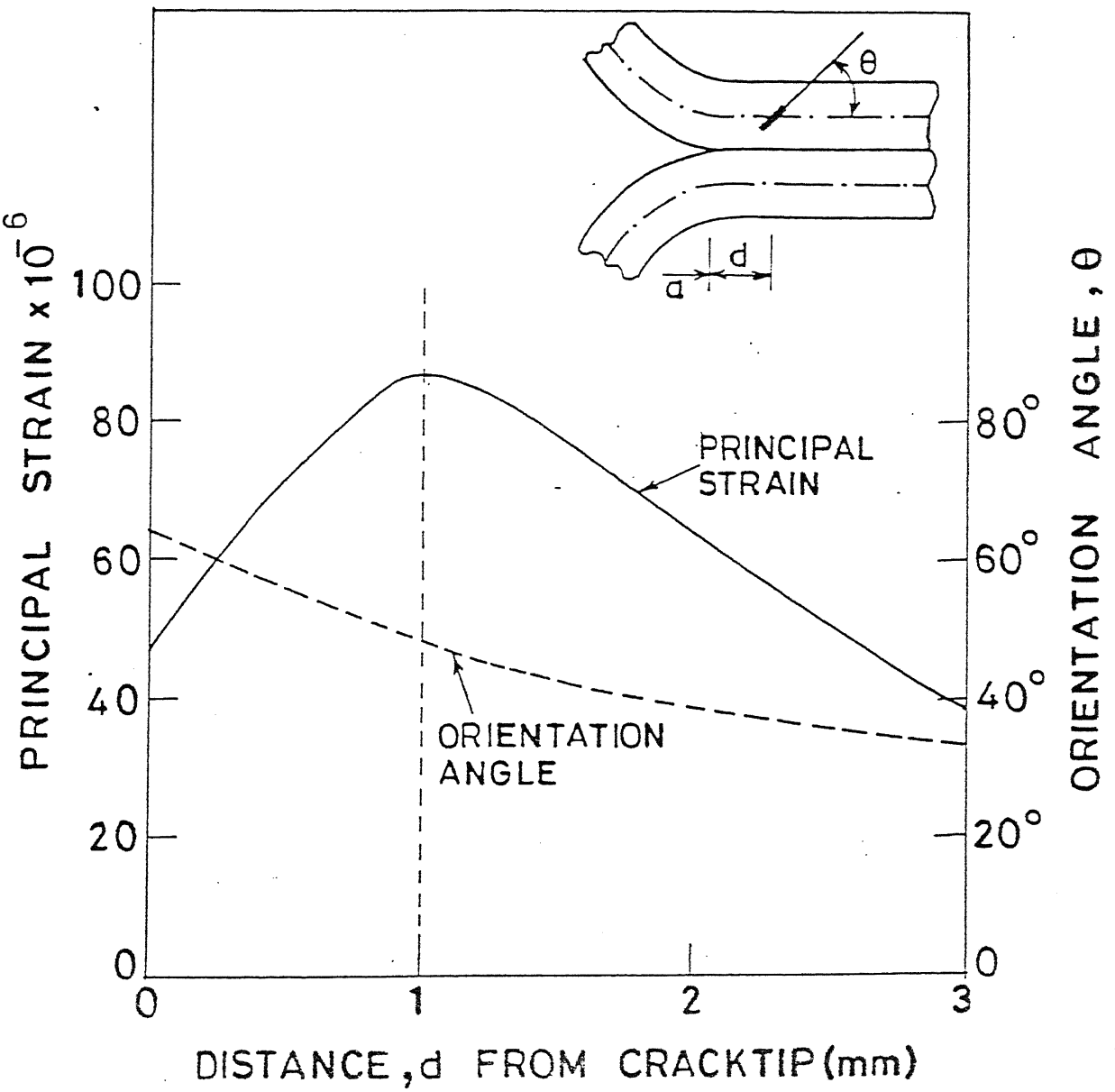

Fig. 2.14 Principal strain and its orientation in front of the crack tip at the mid plane of the upper cantilever for the crack length of 31 mm

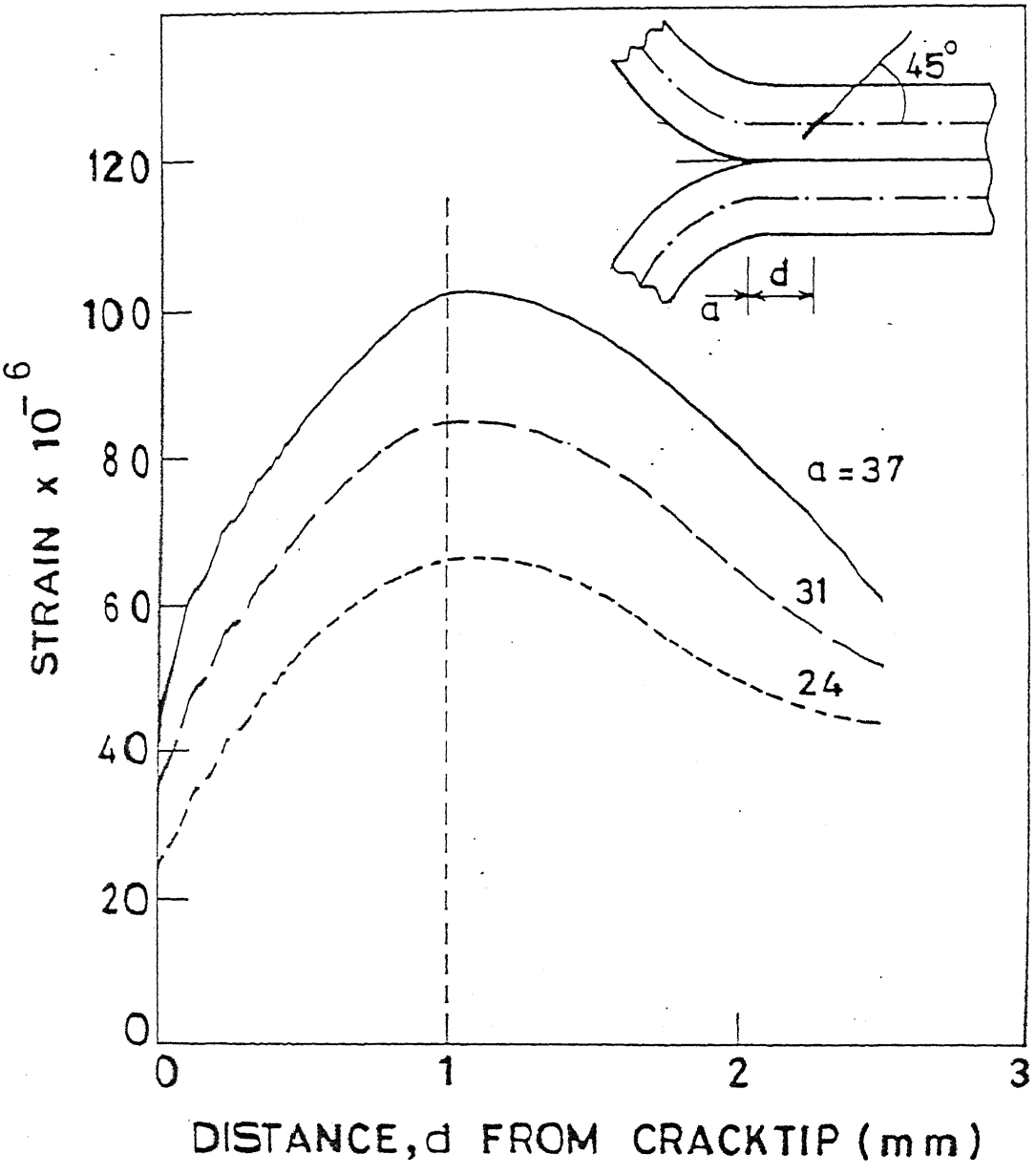

Fig. 2.15 Strain at 45° direction from x-axis in front of the crack tip and at mid plane of upper cantilever of DCB specimen for different crack lengths

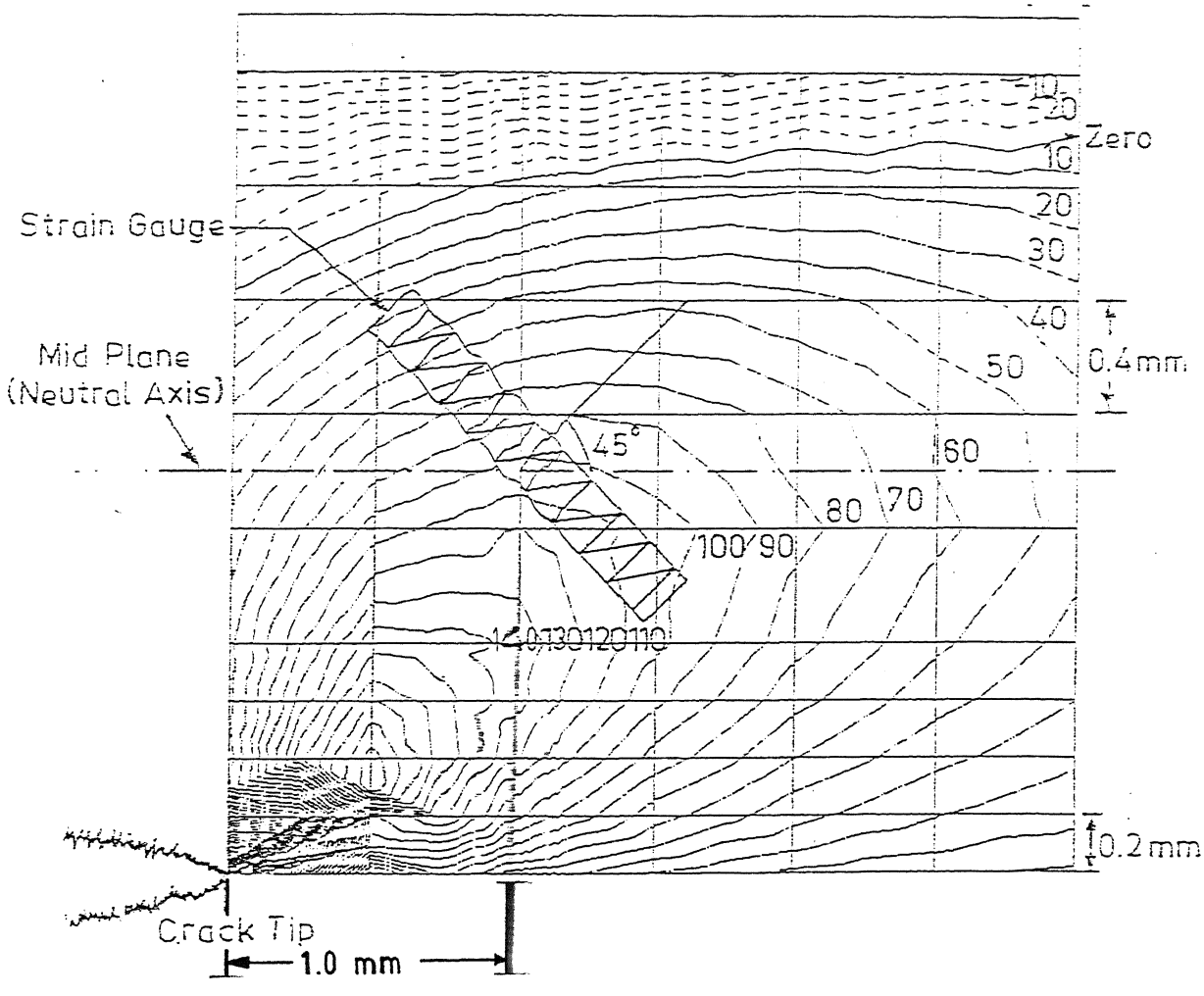

Fig. 2.16 Strain field in front of the crack tip and strain gauge (strain in μm/m)

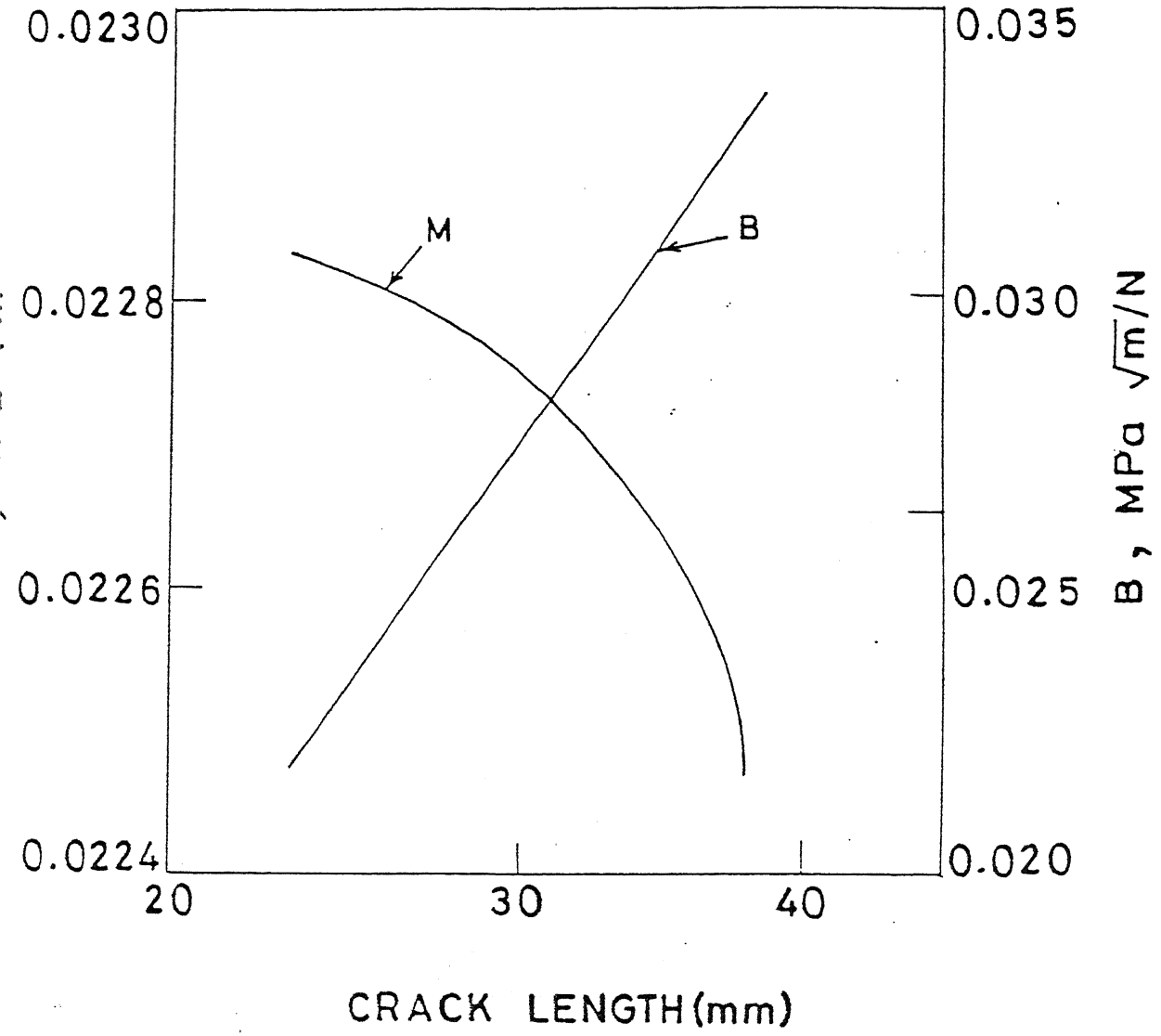

Fig. 2.17 Variation of M and B with crack length

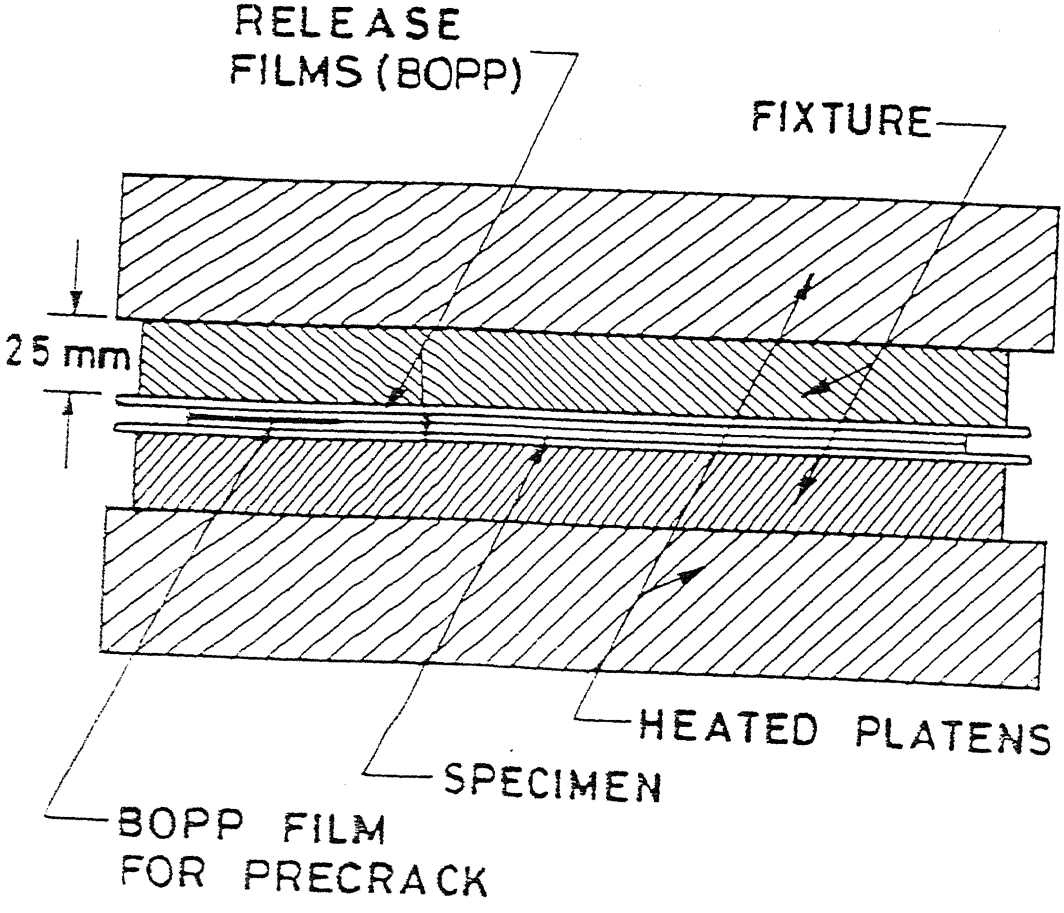

Fig. 2.19 Pressing of two cantilevers of DCB specimen for bonding them with epoxy at high temperature and pressure with a precrack

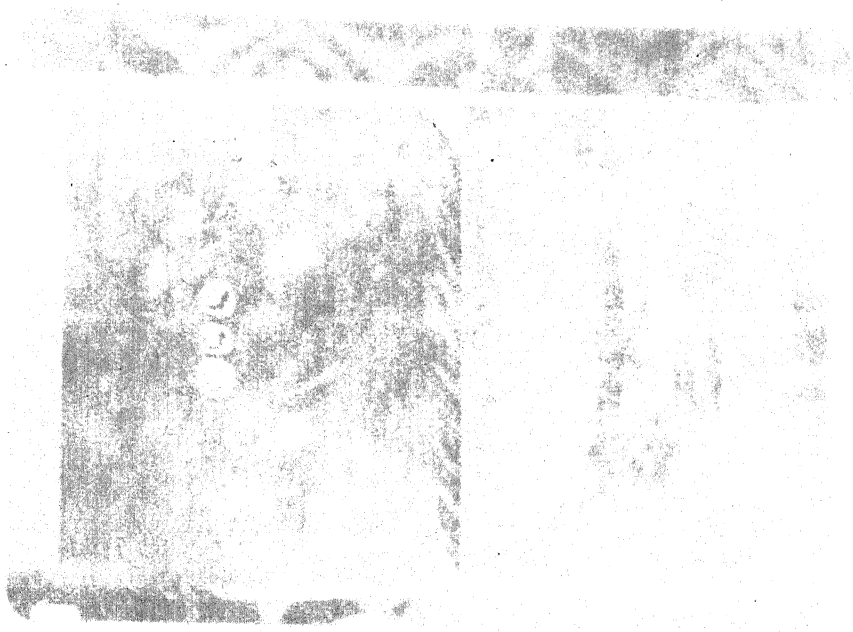

Fig. 2.20 Photograph showing both the plates of bond fixture. The base plate has three cylindrical stops and four adjustable buttons

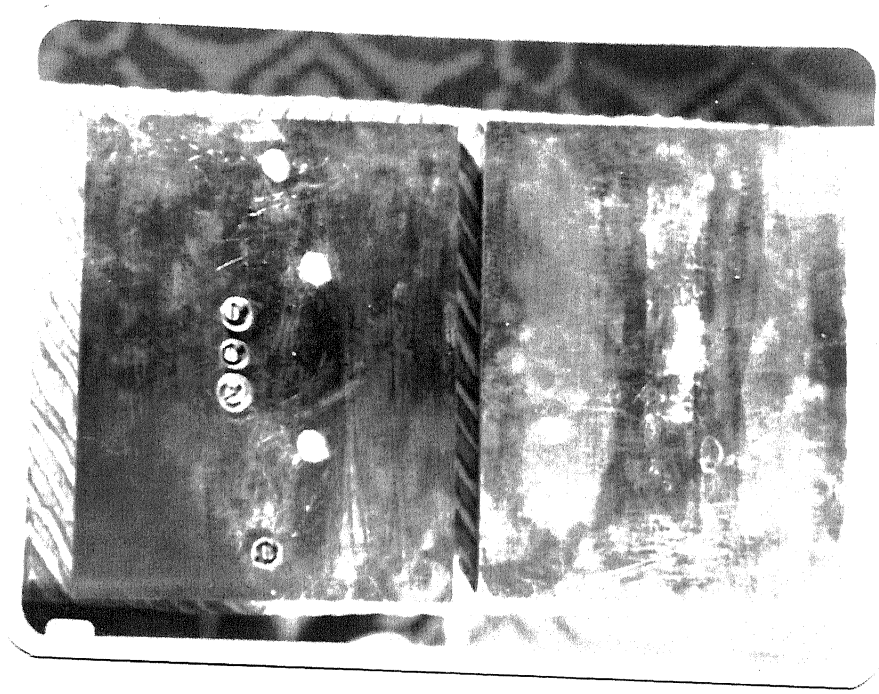

Fig. 2.20 Photograph showing both the plates of bond fixture. The base plate has three cylindrical stops and four adjustable buttons

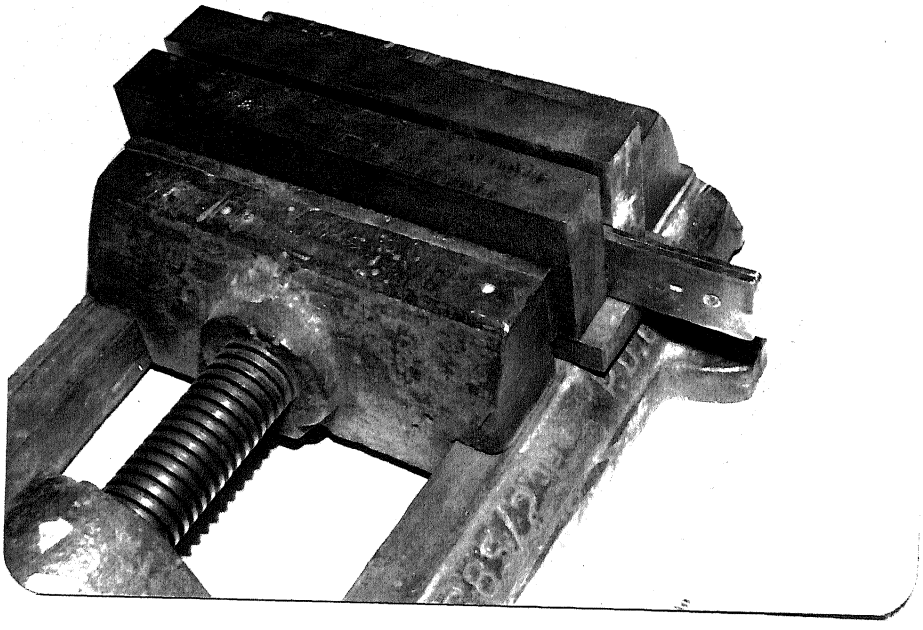

Fig. 2.21 Photograph of crack sharpening fixture

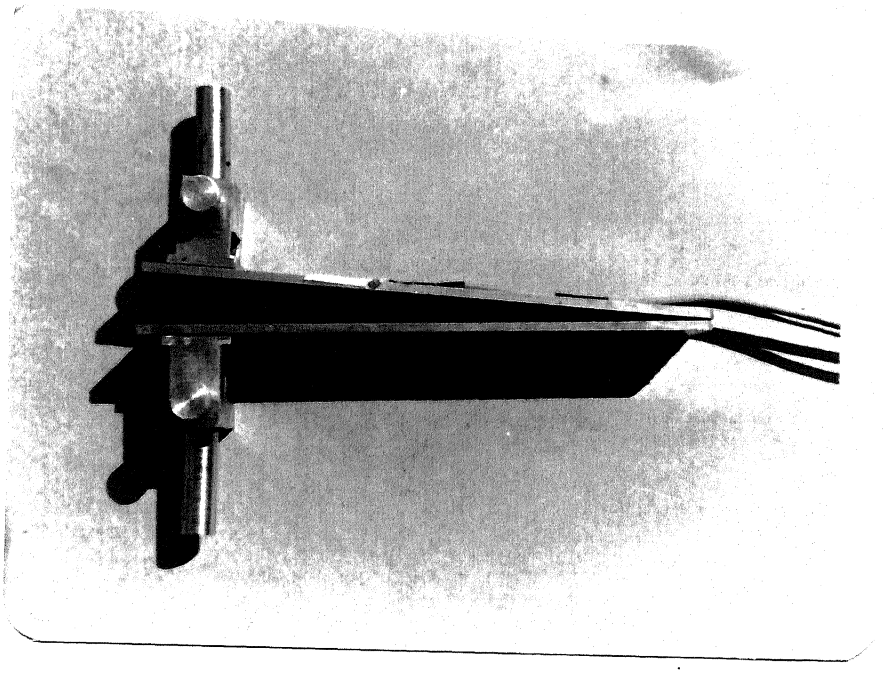

Fig. 2.22(a) Overall view of the DCB specimen hinges and strain gauge

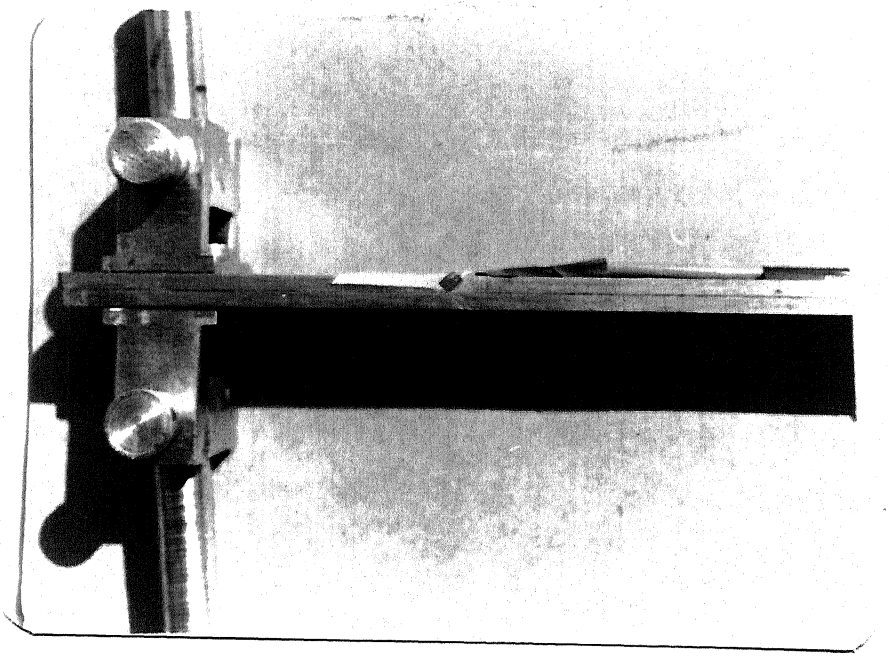

Fig. 2.22(b) Near view of strain gauge and hinges

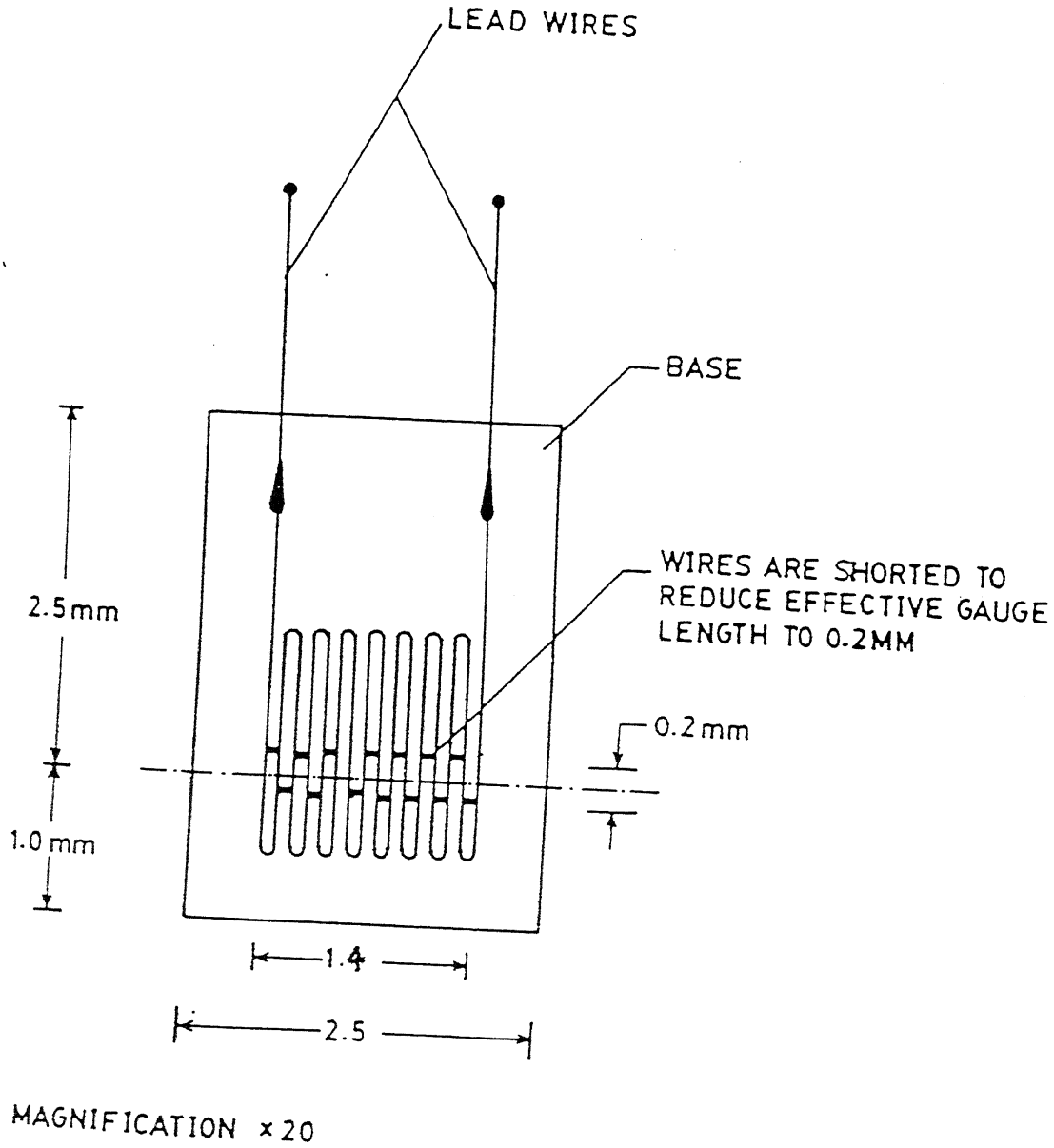

Fig. 2.23 Schematic diagram of strain gauge

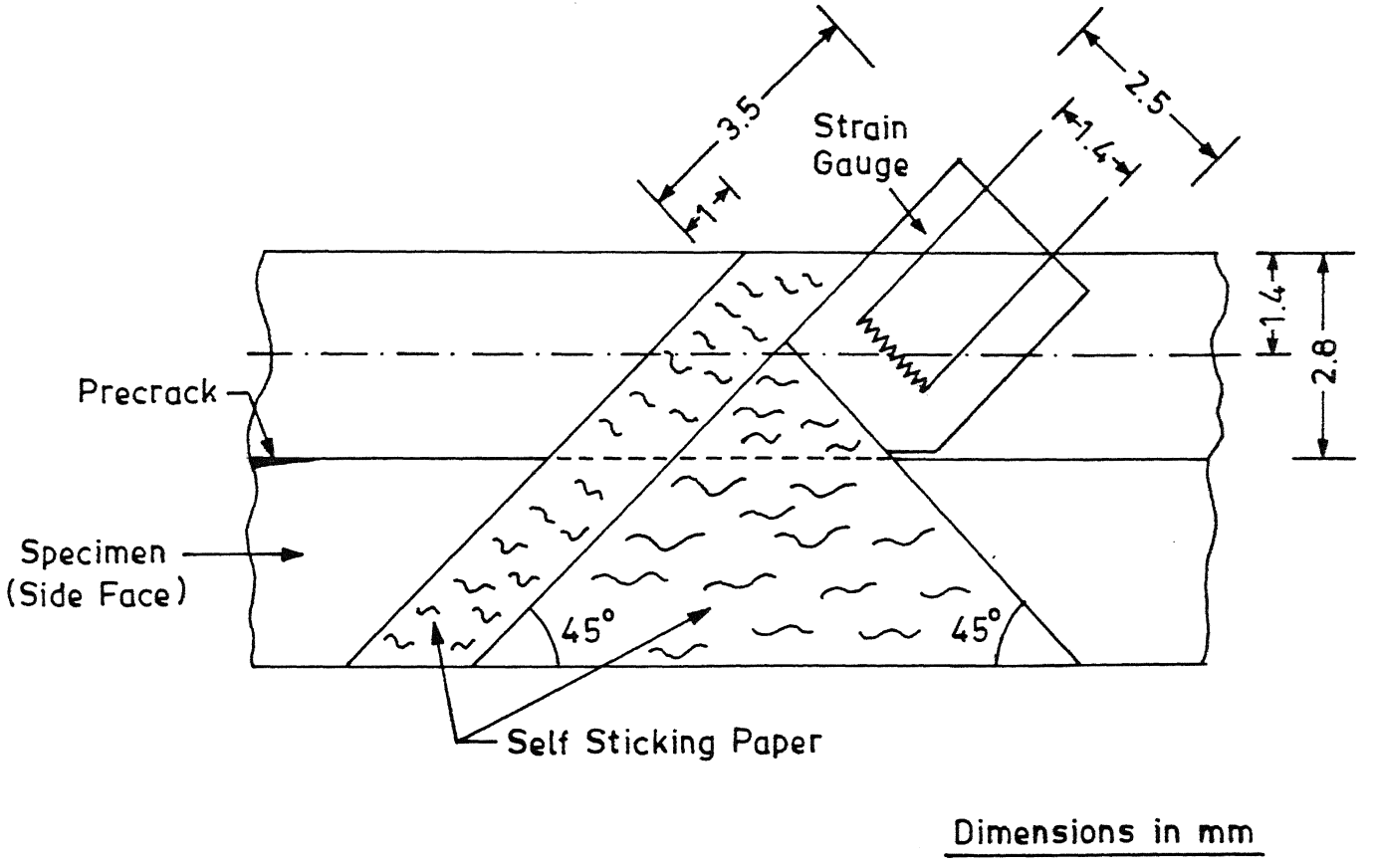

Fig. 2.24 Fixture of self sticking paper to locate the strain gauge

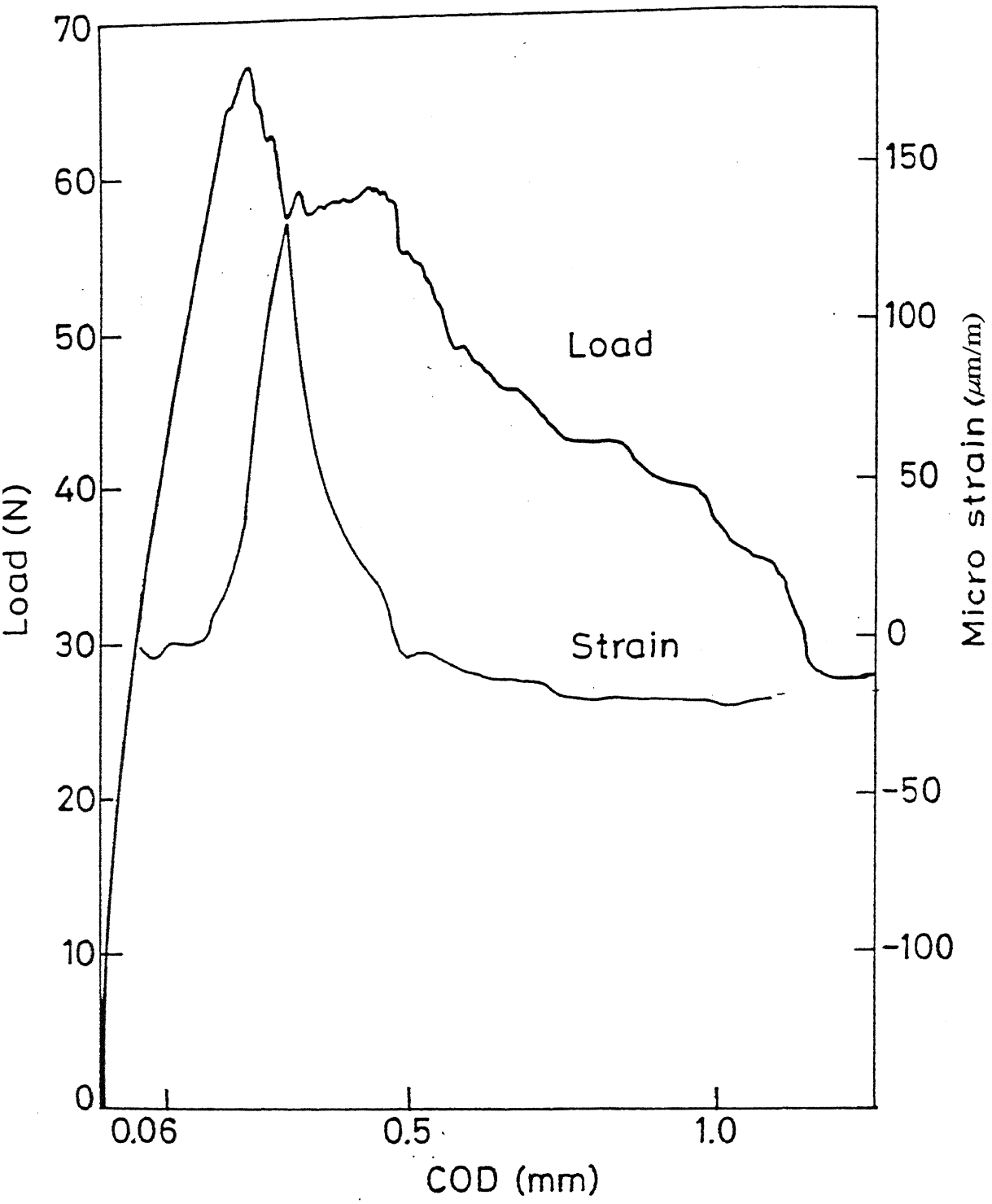

Fig. 2.25 Experimental record of strain and load for Expt. 1

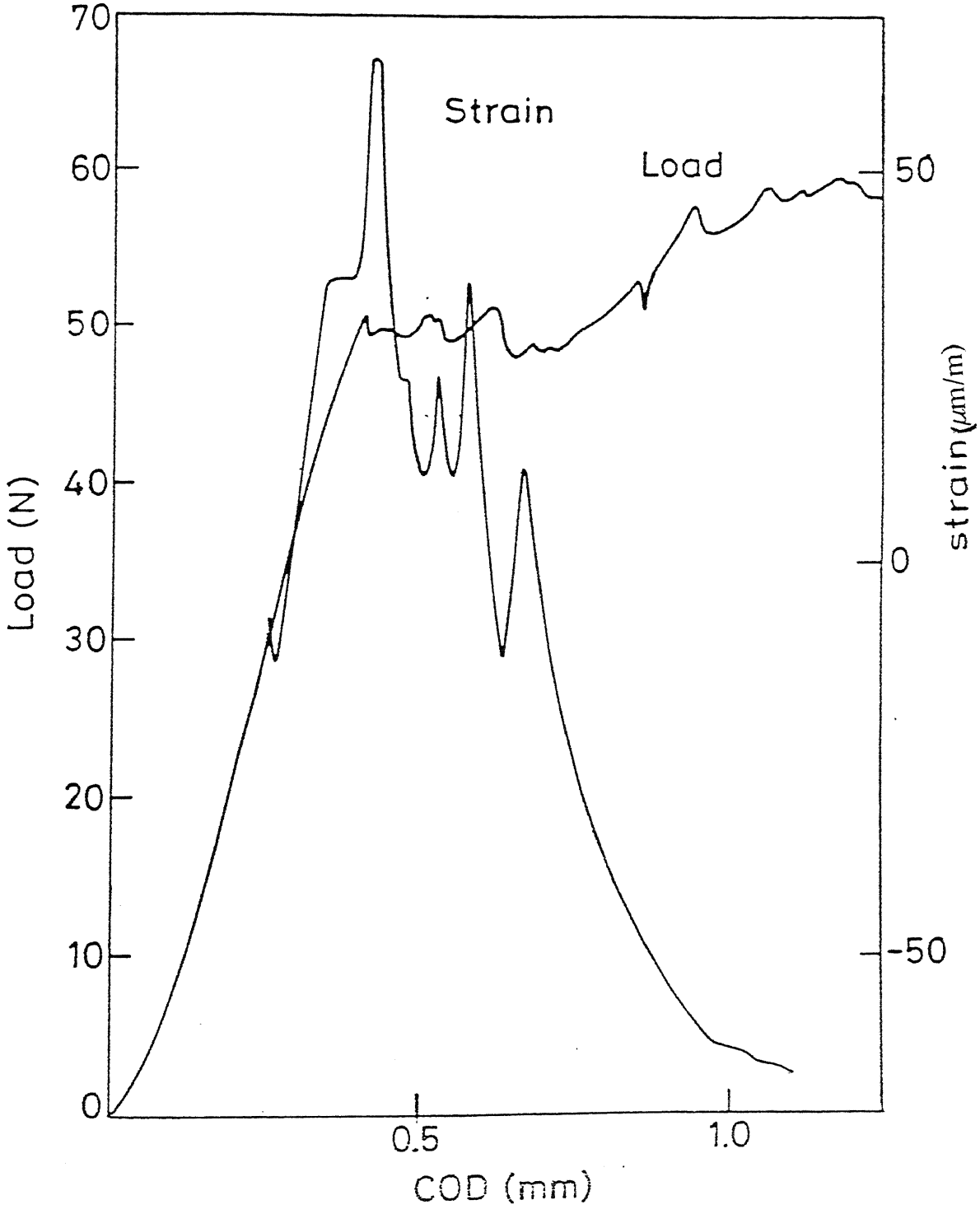

Fig. 2.26 Experimental record of strain and load for Expt. 2

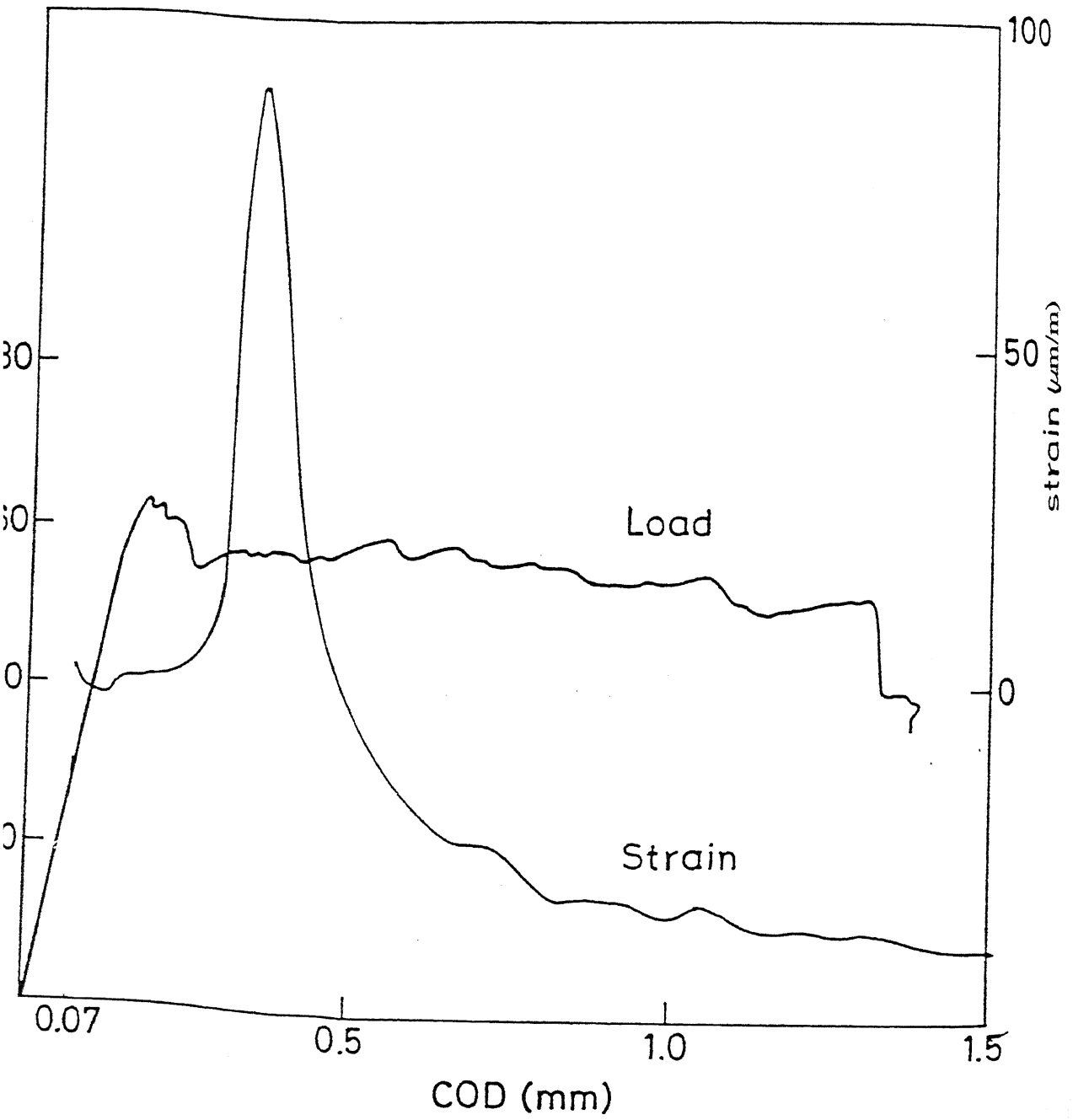

Fig. 2.27 Experimental record of strain and load for Expt. 3

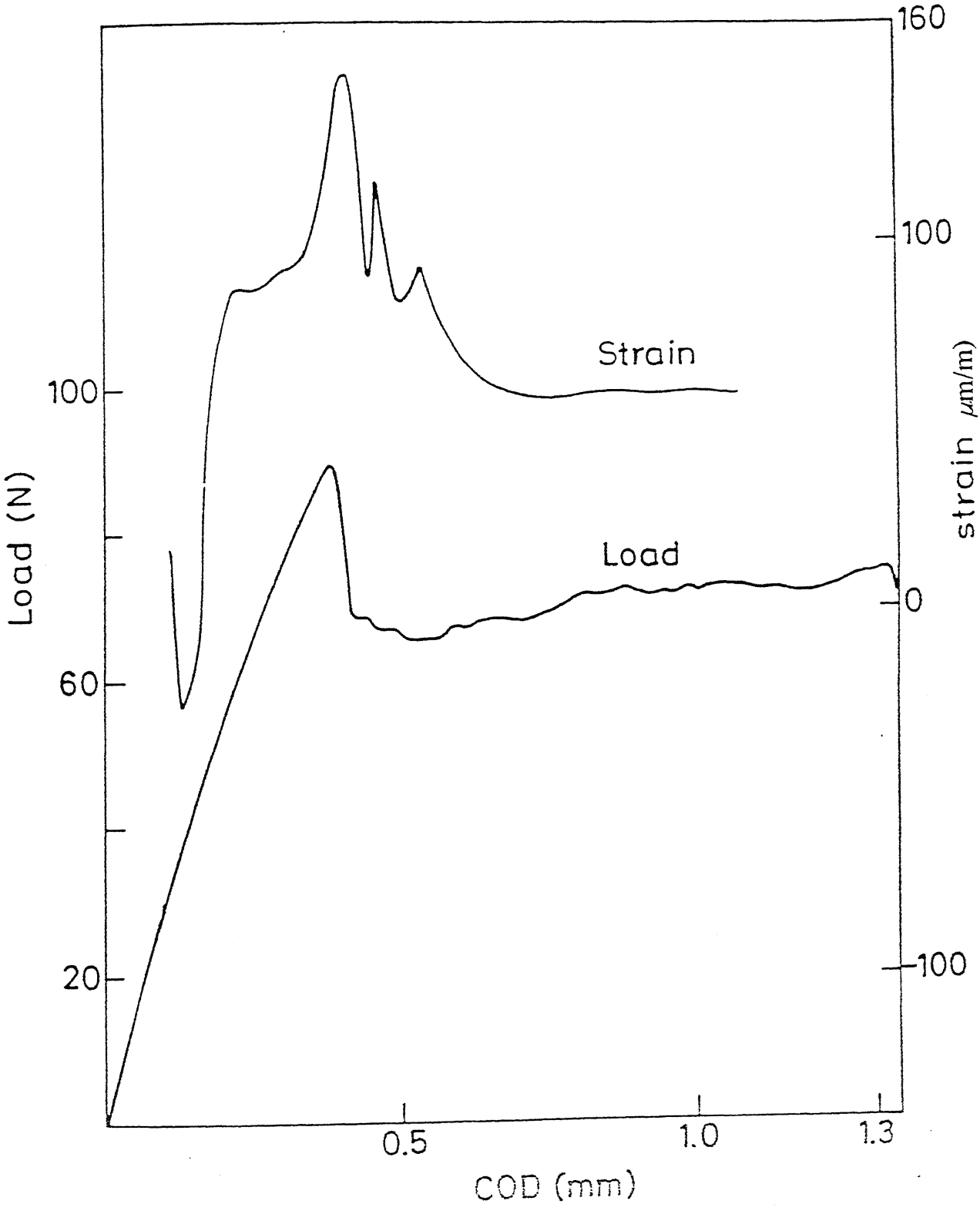

Fig. 2.28 Experimental record of strain and load for Expt. 4

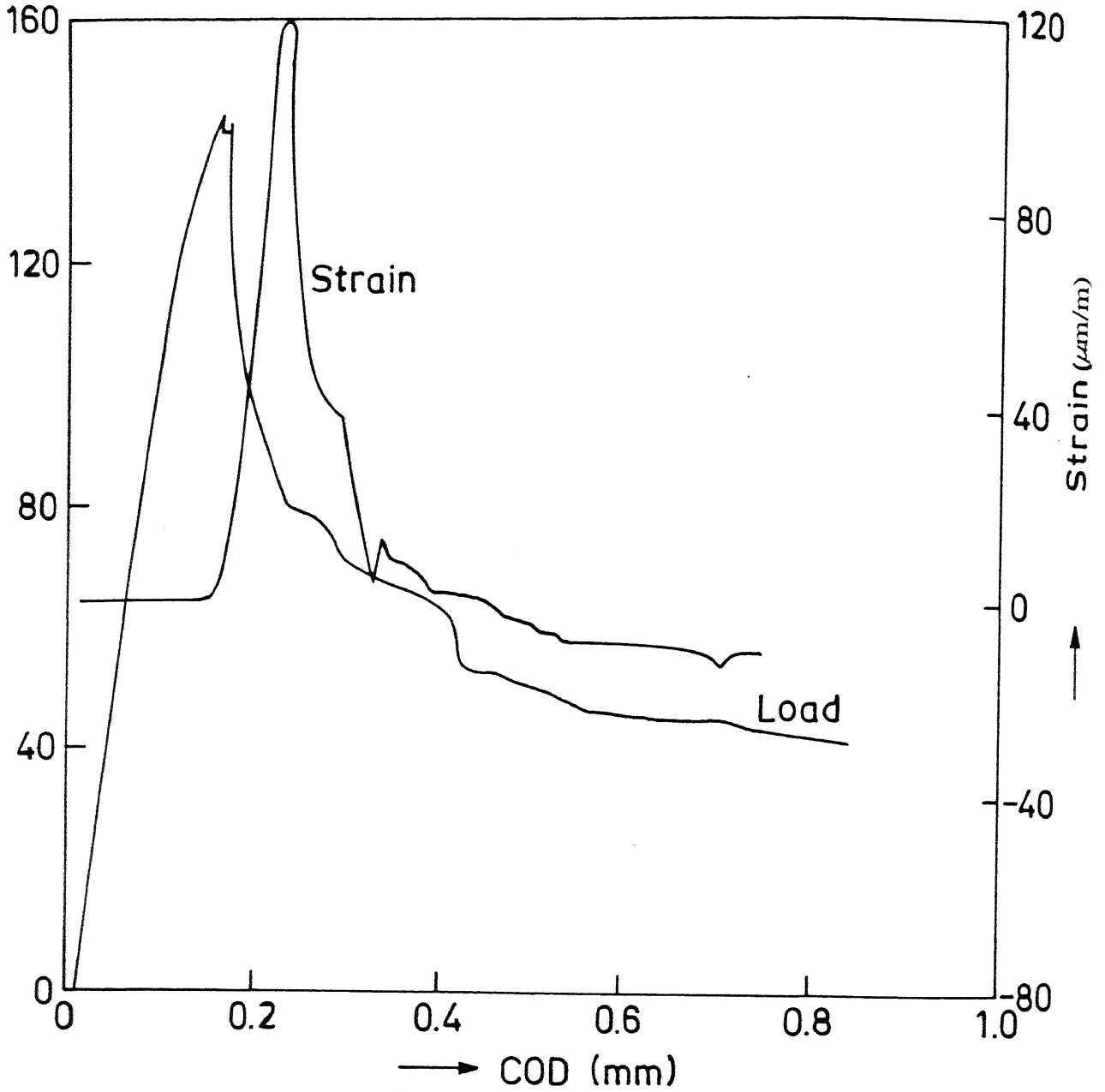

Fig. 2.29 Experimental record of strain and load for Expt. 5

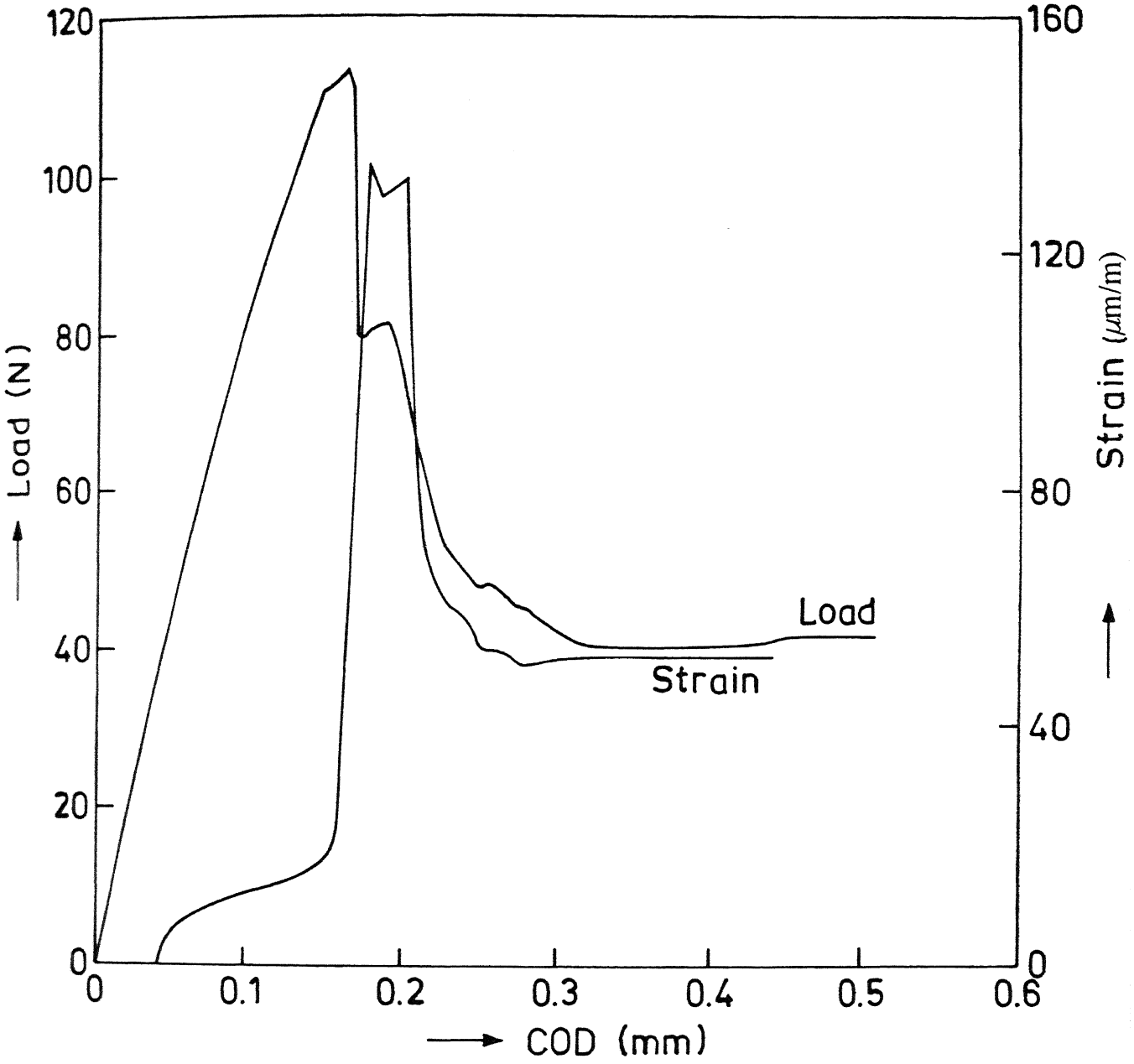

Fig. 2.30 Experimental record of strain and load for Expt. 6

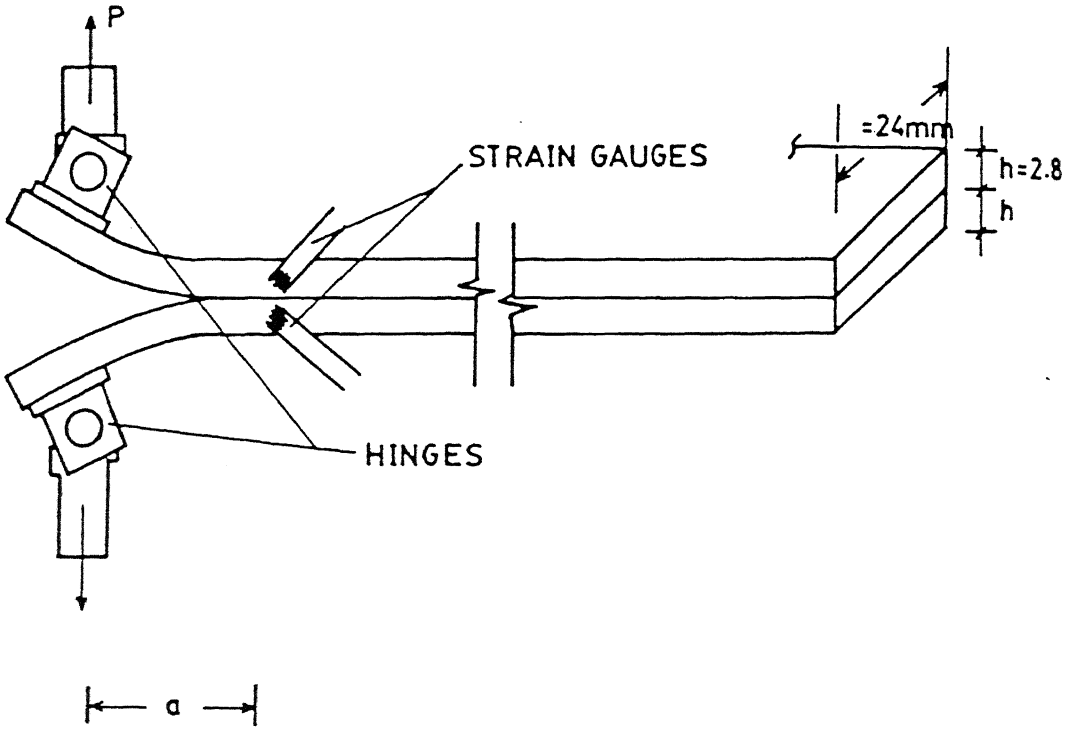

Fig. 2.31 DCB specimen two strain gauges

CHAPTER - 3

DYNAMIC CRACK PROPAGATION

3.1 INTRODUCTION

Dynamic fracture mechanics is a subfield of fracture mechanics concerned with fracture phenomena in which the role of materials inertia becomes significant. The inertia effect may arise due to two reasons (i) rapidly applied load on a cracked solid and (ii) rapid crack propagation. In the first case the influence of the load is transferred to the crack by stress waves through the material. In the second case the material particles on the two crack faces displace with respect to each other, as the crack advances. The inertia effect, in the first case, is considered significant when the time taken to load the specimen to maximum value is small as compared to the time required for a characteristic stress wave of the material travel a characteristic dimension of the body. In the second case, the inertia effect should be accounted for whenever the crack velocity is a significant fraction of the characteristic velocity (e.g. Rayleigh wave velocity). Dynamic fracture phenomena has several important features. As the boundaries of the body changes with time, mathematical models are more complex than those of static case. From experimental point of view, parameters are transient and for a short period and measurements have to be made at high speed and accurately. Crack tip parameters require modified definition. The crack propagation criterion known for quasi static loading is no longer valid and a new criterion for the dynamic crack propagation has to be defined. In the static case the crack propagates when the fracture toughness exceeds a certain critical value, whereas in the dynamic case there is no well defined criterion for crack initiation and propagation. Studies of dynamic crack propagation require both loading and measuring techniques which are not readily achievable with commercially available facilities. Moreover, the requisite experimental apparatus is complex and its development constitutes usually a heavy investment of time before the experiment can begin.

Therefore, in the present work a combined experimental and finite element method is envisaged to determine the interlaminar dynamic fracture toughness of double cantilever beam (DCB) specimen. The experimental technique uses some concepts of split Hopkinson bar. One cantilever of the DCB specimen is glued to a rigid support whereas the other is attached to the load bar. The load bar is impacted by a striker accelerated in the barrel of an air-gun. Strain gauges are mounted ahead of the crack tip on one side face of the cantilever to find the crack propagation velocity. The experimental measurements gives the profile of the displacement applied at the cantilever end, the time of initiation of crack propagation and crack propagation history. These data are latter used in a finite element code to simulate the dynamic fracture behaviour of the DCB specimen. The FE analysis of the time varying stress field of dynamic fracture is more involved than that of static fracture. Besides requiring fine mesh and special singular elements at the crack tip to model the crack tip singularity, the analysis be capable of modelling the crack extension. The finite element analysis gives the details of initiation and propagation fracture toughnesses.

3.2 FINITE ELEMENT ANALYSIS

3.2.1 FORMULATION

The system of finite element equations governing the linear dynamic response of an elastic body is given in the matrix form as

$$[M]\ \{\ddot{U}\} + [C]\ \{\dot{U}\} + [K]\ \{U\} = \{R\} \qquad (3.1)$$

where [M], [C] and [K] are the mass, damping and stiffness matrices respectively and R is the external load vector; and U, $\dot{U}$, $\ddot{U}$ are displacement, velocity and acceleration vectors of finite element assemblage respectively.
It may be noted, in the Eq. 3.1.

$$[M] = \sum [M]^e$$
$$[K] = \sum [K]^e$$
$$[R] = \sum [R]^e$$

where mass, stiffness and traction matrices of individual elements are given by

$$[M]^e = \int_V \rho \ [N]^T \ [N] \ dV$$

$$[K]^e = \int_V \rho \ [B]^T \ [D] \ [B] \ dV$$

$$\{R\}^e = \int_S [N] \ \{t\} \ dS$$

where N is shape function, B is derivative of shape functions, D is elastic constitutive relation matrix and t is traction vector.

In the present analysis the damping is neglected and hence the governing equation of dynamic response reduces to

$$[M] \ \{U\} + [K] \ \{U\} = \{R\} \qquad (3.2)$$

The equation (3.2) can be solved either by time integration or by mode superposition, of which the former is preferred in the wave propagation problem of present kind. In this integration scheme, there are many different methods, which can be classified as "explicit" or "implicit". Relative advantages and disadvantages of each method are given in detail in Bathe (1990). In the present work Newmark integration method for time variable is used. The details of the Newmark method are given in Bathe (1990). The choice of time step Δt for time integration is important for an accurate solution. An optimum choice of time step is $\Delta t = d/C_d$ in which d is the smallest mesh size and C_d is dilatation wave velocity.

3.2.2 MODELLING OF CRACK PROPAGATION

As the crack propagation velocity is lower than the wave velocities, in general, the crack tip occupies positions in between the nodes at various time step of the numerical integration (time marching). Thus, if a simple node-shifting procedure is used, then the crack tip either stay at one node or jump from one node to next node in time Δt in the computational simulation. When the crack tip movement is irregular, serious violations of the kinematics and traction conditions ahead of the actual crack tip will result. Also sudden increase of crack length by the release of constraints on displacement induces spurious high frequency oscillations in the finite element solutions. To overcome such difficulties, several algorithm have been suggested in literature to release the node gradually, over a period of time. Suppose that the actual crack tip is located at C in between the finite element nodes B and D as shown in the Fig. 3.1. The lengths of segment BC and BD are b and d respectively. The holding back force, F, at node B is gradually reduced to zero as the crack tip reaches the node D. The various scheme available to decrease the force to zero are as follows :

(i) Malluck and King (1978) suggested the release rate based on constant stress intensity factor; that is,

$$\frac{F}{F_0} = (1 - b/d)^{1/2} \qquad (3.3)$$

where F_o is the original reaction force when the crack tip was located at node B.
(ii) Rydhom et al. (1978) suggested the release rate based on constant energy release rate.

$$\frac{F}{F_0} = (1 - b/d)^{3/2} \qquad (3.4)$$

(iii) Kobayasi et al. (1978) suggested the linear release rate based on no physical argument other than pure intuition.

$$\frac{F}{F_0} = (1 - b/d) \qquad (3.5)$$

In the present work to have a more gradual and smooth propagation of crack a modified method has been used. The holding back force at the crack tip B is linearly decreased to zero when the crack reaches the end of the next element. Thus, when the crack tip goes beyond node B then

$$\frac{F_B}{F_{HB}} = \left(1 - \frac{b}{d+d_1}\right) \qquad (3.6)$$

where F_{HB} is reaction at node B, when the node was closed; b is the crack extension and d, d_1 are the element lengths as shown in the Fig. 3.1. And when the crack moves beyond node D to a point D_1

$$\frac{F_B}{F_{HB}} = \left(1 - \frac{d+b_2}{d+d_1}\right) \qquad (3.7)$$

$$\frac{F_D}{F_{HD}} = \left(1 - \frac{b_2}{d_1+d_2}\right) \qquad (3.8)$$

where F_{HD} is the reaction at node D, when the nodes was closed; b, b_2 are the crack extension and d, d_1, d_2 are the element lengths as shown in the Fig. 3.1.

3.2.3 PATH INDEPENDENT INTEGRAL

Under appropriate assumptions of material homogeneity, the strength of the crack tip field is governed by an integral evaluated over a path that is far removed from the crack tip. Since the stress and displacement data are evaluated away from the crack tip, these values are relatively insensitive to the finer details of modelling of crack tip region. J-integral is used for computing elsto-static fracture in mode I. Also the far field integral

can be calculated with reasonable accuracy using relatively coarse finite element models of the structure. A similar "path independent integral" can be used in elsto-dynamic crack propagation. This involves domain integral also owing to material inertia. Atluri (1982) and Nishioka and Atluri (1983) have undertaken the study of various path independent integrals, of relevance in the analysis of growth initiation and propagation of cracks in elastic or inelastic materials under quasi static or dynamic conditions.

$\hat{J}$-Integral

In the present work $\hat{J}_k$ given by Kishimoto, Aoki and Sakata (1980) is used. $\hat{J}_k$ is defined as follows

$$\hat{J}_k = \lim_{\varepsilon \to 0} \int_{\Gamma_\varepsilon} [W n_k - T u_{i,k}] \, dS \qquad (3.9)$$

$$\hat{J}_k = \lim_{\varepsilon \to 0} \int_{\Gamma + \Gamma_c} [W n_k - t_i u_{i,k}] dS + \int_{V - V_\varepsilon} \rho \ddot{u} u_{i,k} dV \qquad (3.10)$$

where W and T are strain energy density and kinetic energy density respectively; n_k are direction cosines of unit outward normal, t_i are the surface traction and the definition of the paths Γ_ε, Γ, Γ_c and the volume V, V_ε are shown in Fig. 3.2.

$$\hat{J} = \hat{J}_1 = \lim_{\varepsilon \to 0} \int_{\Gamma + \Gamma_c} [W n_1 - t_i u_{i,1}] dS + \int_{V - V_\varepsilon} \rho \ddot{u} u_{i,1} dV \qquad (3.11)$$

For the case of plane strain, neglecting a speed dependent correction very close to unity for the range of crack speeds of interest, the relation between the $\hat{J}$ and the dynamic SIF (K_d) is given by Dexter (1987)

$$K_d = \left(\frac{E \hat{J}}{1 - \nu^2} \right)^{1/2} \qquad (3.12)$$

The value of $\hat{J}$ is independent of the choice of Γ only under stringent ideal conditions, for example, steady state crack growth. In many cases, though these conditions are obviously not met the path independence of $\hat{J}$-Integral can still be established within certain allowances for error. The path was held stationary as the crack tip is extended in a self similar manner.

3.2.4 TEST PROBLEMS

Large Plate with Centre Crack Subjected to Dynamic Load without Crack Propagation

To validate the FE computer code, a rectangular plate with centre crack, subjected to uniform far field step load (Fig. 3.3) is presented by Parton and Boriskovsky (1989) was studied. The $\hat{J}$-Integral was calculated taking an arbitrary contour and using the Eq. 3.11 and the SIF is evaluated using the Eq. 3.12. Fig.3.3 gives the comparison of present result and that of Parton and Boriskovsky (1989).

Effect of the singular Element

Above mentioned problem is also studied for the effect of singular elements (quarter point collapsed element, discussed in section 2.1.4)at the crack tip. Fig.3.4compares the result obtained for the $\hat{J}$-integral with and without singular elements around the crack tip. The value of $\hat{J}$-Integral are almost same in both the cases because the paths are taken away from the crack tip which are not much affected by singularity at the crack tip. Therefore, in the present study, singular elements were not used around the crack tip.

Three Point Bend Specimen Subjected to Impact Loading

A 3-point bend specimen subjected to impact loading is studied (Fig. 3.5). In the problem, by Nishioka and Atluri (1986), the impact load point of the specimen moves with a velocity of 6.88 m/s. The crack starts propagating after 95 μs and with a velocity of 375 m/s. An arbitrary path away from the crack tip is chosen so that the same path can be used even when the crack propagates. The SIF is then calculated using Eq. 3.12. The comparison of the results shown in the Fig.3.6 are in good agreement.

Thin DCB Specimen

A thin DCB specimen with 1.6 mm thick cantilever was given an initial displacement of 1 mm and then cantilever ends were pulled at constant rate (Wang and William, 1994). The specimen dimension and material properties are given in Fig. 3.7. The initial crack length was 4 mm and the crack was propagating as $1.118\sqrt{t}$. The $\hat{J}/\hat{J}_{ST}$ of present study was compared with G/G_{ST} of Wang and William (1994) and shown in Fig. 3.7. Although there are differences in finite element analysis procedure, such as type of element (8 node/3 node), mass distribution (consistent mass/ lumped mass); the results are in good agreement.

3.2.5 ANALYSIS OF DCB SPECIMEN

The various aspects of DCB specimen used in the present study is investigated. 2-D analysis of the side face of the DCB specimen was carried out.

Mesh Generation

A computer code is developed to generate mesh for the DCB specimen. Since the specimen is loaded in bending, C_1-continuous elements are required. As discussed by Seron et al. (1990) the higher order elements are not used for dynamic problem. Therefore four noded isoparametric element are used. To take into consideration effect

of bending well, very fine mesh is used. At the same time, to avoid nonuniformity in mass distribution which leads to reflection of waves, uniform mesh throughout the specimen is generated. As shown in the Fig. 3.8, uniform mesh of four noded isoparametric element of the size 0.4 X 0.28 mm is generated.

Analysis of Full/half DCB Specimen

In the experimental study, one of the cantilever is bonded to a rigid block and the other cantilever is loaded. It is verified that the cantilever fixed to the rigid block does not experience much strain, and hence while calculating $\hat{J}$-integral, the contribution of the path in bonded cantilever will be much less as compared to other cantilever. Therefore the DCB specimen is studied for two different configuration:

(i) Full DCB specimen with nodes on the upper cantilever fixed (figure 3.9(a)).

(ii) Only the load end cantilever, the Y-displacement on the interface node fixed (figure 3.9(b)).

The $\hat{J}$ integral is calculated for both the configuration and the result is shown in the Fig. 3.10. It can be seen from this figure that the there is not much difference in $\hat{J}$-integral for both configuration. Hence to avoid unnecessary computation, only half of the DCB specimen is analyzed.

Effect of Time Step

As discussed by Bathe (1990), the time step to satisfy the stability criterion is given by

$$\Delta t \leq \frac{h}{C_m} \qquad (3.13)$$

where h is the minimum spatial resolution and C_m is the maximum propagation velocity, i.e., that of dilatation wave velocity for isotropic solid.

From the point of view of time integration, the different time frequencies which are

present in the wave will be modelled using different numbers of time steps. Hence, the FE modelling act as a low pass filter, since low frequencies (wavelength large compared to mesh size) propagate correctly, whereas high frequency (wavelength small compared to mesh size) do not propagate well.

The $\hat{J}$-integral is calculated for DCB specimen under same loading condition, but for different time steps. The variation of $\hat{J}$-integral (when the crack is not propagating) for different time steps is shown in the Fig. 3.11. It can be seen that the $\hat{J}$-integral does not change till the time step is increased upto 0.2 μs, whereas the required time step as per Eq. 3.13 is only 0.08 μs. Thus, to save computation time, it was decided to use the time step of 0.2 μs.

Effect of Path in Calculating $\hat{J}$-Integral

The different contours used to evaluate $\hat{J}$-integral is shown in the Fig. 3.12 for the DCB specimen under same loading condition. The variation of $\hat{J}$-integral (without propagating the crack) for different paths are shown in the Fig. 3.13. It can be observed that the $\hat{J}$-integral is nearly same for all the paths, hence the $\hat{J}$-integral is path independent.

Effect of Crack Length

The $\hat{J}$-integral (without crack propagation) is calculated for different crack lengths. The variation of $\hat{J}$-integral for different crack lengths is shown in the Fig. 3.14 under same loading condition. It can be observed that for smaller crack length the $\hat{J}$-integral starts early, as expected, but rises to a lower value compared with longer crack length.

3.3 EXPERIMENTAL TECHNIQUE

Experiments were conducted to get the crack propagation history, initiation time and load/displacement profile under impact load on DCB specimen. This section deals with experimental details of specimen preparation, experimental setup, experimental

measurements and data processing.

In this technique a stress pulse is generated in a cylindrical load bar (Fig. 3.15) by impacting it with a striker accelerated in an air-gun. This load bar applies load to one cantilever of the DCB specimen whereas the other cantilever is bonded to a very high inertia solid block. Two strain gauges at symmetrically opposite locations are mounted in the longitudinal direction on the surface of load bar. These strain gauges record the incident and reflected pulse in the load bar. Strain gauges are also bonded ahead of the crack tip on the side face of the loaded cantilever to determine crack velocity history.

3.3.1 SPECIMEN PREPARATION

Specimen

Each cantilever of the DCB is 2.8 mm thick and 24mm wide. The cantilevers are bonded together by epoxy with an offset of 20 mm (Fig.3.16) so that the rear cantilever can be impacted by the load bar. The material of the specimen and other details are already discussed in Sec 2.1.1. The photograph of the specimen is shown in Fig. 3.17.

Bonding of Cantilevers

The faces of the metal strips to be bonded are etched to obtain better adhesive bonding. The etching is done by dilute nitric acid. For bonding, epoxy LY556 and hardener HT976 are mixed in the ratio of 100:35 and 2% accelerator XY 73 is also added. The resin, the hardener and the accelerator are supplied by Hindustan Ciba-Geigy Limited, Bombay. During bonding, the faces to be bonded are cleaned with AR grade acetone and all other faces are covered with a layer of wax to prevent them from getting coated with epoxy. The mixture is then applied to the cleaned faces of the DCB specimen. Two strips are then put together with an offset of 20 mm and pressed in specially built fixture made of two steel plates (each 25 mm thick) with ground flat faces (Fig. 3.18). Between the strips and the flats of the fixture plate a sheet of BOPP film is placed on

each side to work as a release film. The BOPP films are very thin, nearly 20 μm. Provisions are made in the fixture for keeping the two strips in position while curing. The base plate of the fixture has four cylindrical stops and two adjustable buttons. Two cylindrical stops are placed at a distance of 190 mm from each other. This is done to allow for an off set of 20 mm. Each cantilever of the specimen is butted against three of the four stops and kept in place with the help of adjustable buttons. Both the adjustable buttons have a slot of 4X7 mm , so that they can be tightened to the base at the desired location. Also, they are of different heights so as to hold lower and upper cantilever separately. This enables to hold cantilever securely even if there is slight difference in the width of the cantilevers. The fixture along with the specimen is placed between two plates of a hydraulic press. The plates are heated by inbuilt heating platens and the temperature of the specimen is monitored by placing a chromel-alumel thermo-couple between the plates. The specimen is kept at 140° C for four hours under a pressure of 0.5 MPa. It is then cooled to room temperature at the same pressure.

Crack Sharpening

The pre-crack introduced in the DCB specimen by placing a BOPP sheet needs further preparation before the specimen is impacted. The crack sharpening procedure is similar to one used in the case of static loading conditions discussed in sec. 2.2.2.

Bonding of the Strain Gauges

Three strain gauges are bonded on the side face of the loaded cantilever after polishing the face. The details of bonding is given is Sec. 2.2.4. The strain gauges details are also described in this section. The distance between the strain gauges is nearly 5 mm. The first strain gauge is bonded close to the crack tip so that the time of initiation of the crack is obtained accurately.

3.3.2 OVERALL EXPERIMENTAL SETUP

Figure 3.15 shows the schematic diagram and Fig. 3.19 the photograph of the complete experimental setup which includes specimen, load bar, striker, bridge circuit and the oscilloscope. A phonographic needle is used to trigger the oscilloscope after the striker, shot by the air gun, hits the load bar. The oscilloscope records the strain pulses in the load bar and specimen, picked by strain gauges, through the bridge circuits. The specimen is held in its position by gluing the front cantilever of the DCB specimen to a rigid mass. The load bar is screwed to the rear cantilever. When the striker, from the air gun, hits the load bar a stress pulse is generated. This pulse is partly transmitted to the cantilever, thus dynamically loading the specimen.

Fixture for Holding the Specimen

One cantilever of the DCB specimen is glued to a block of mild steel (50 X 50 X 150 mm) which acts as a rigid mass (figure 3.15). The block is placed on a base plate and after aligning the specimen to the load bar the block is firmly clamped to the base plate with the help of C-clamp.

Striker and the Load Bar

Applying a dynamic load pulse to the DCB specimen include an air gun and a load bar. The load bar is properly aligned with the centre-line of the barrel of the air gun. When the striker, from the air gun, impacts the load bar, a longitudinal compressive stress pulse is generated in the load bar. As this compressive stress pulse reaches the specimen end of the load bar, part of it is transmitted to the specimen and remaining is reflected back as a tensile pulse. Two strain gauges bonded at diametrically opposite locations on the load bar (Fig. 3.18) connected in a bridge circuit pick up these stress pulses and are recorded in a storage oscilloscope. The oscilloscope is triggered by a phonographic needle, kept in contact with the surface of the load bar, with the help of a rubber band.

3.3.3 STRESS PULSES

A typical record of the incident and reflected pulses in the load bar is shown in the Fig. 3.20. From this experimental record the load pulse imparted to the specimen can be obtained using one dimensional wave propagation theory. Figure 3.21 shows the time distance (t-x) diagram for propagation of stress pulse in the load bar. When the striker bar impacts the load bar, the compressive incident pulse propagates towards the DCB specimen and is recorded at the location 1. The reflected tensile pulse is recorded at the same location but at a different time and is depicted by point 3 in the t-x diagram. The aim is to express stress σ_2 in terms of experimentally recorded σ_1 and σ_3. One dimensional wave equation along the characteristic with the acoustic impedance, ρc, is expressed as

$d\sigma - \rho c dv = 0$ (Along +ve characteristic)

$d\sigma + \rho c dv = 0$ (Along -ve characteristic)

Using above equations the relation along characteristic 1-2 simplifies

$$\sigma_2 - \rho C v_2 = \sigma_1 - \rho C v_1 \qquad (3.14)$$

Along the characteristic 1-1'

$$\sigma_1 + \rho C v_1 = \sigma_{1'} + \rho C v_{1'} \qquad (3.15)$$

But $\sigma_{1'} = 0$ and $v_{1'} = 0$ because the load bar is initially at rest and stress waves never reaches at point 1'. Then the above equation gives

$$\sigma_1 = -\rho C v_1 \qquad (3.16)$$

Using Eq. 3.14 and Eq. 3.16

$$\sigma_2 - \rho C v_2 = 2\sigma_1 \qquad (3.17)$$

Relations along characteristics 2-3 and 3-4 are

$$\sigma_2 + \rho C v_2 = \sigma_3 + \rho C v_3 \qquad (3.18)$$

$$\sigma_3 - \rho C v_3 = \sigma_4 - \rho C v_4 \qquad (3.19)$$

$\sigma_4 = 0$ and $v_4 = 0$ at point 4, because the striker and the load bar are of same material and diameter and the striker comes to rest. The above two equations yield

$$\sigma_2 + \rho C v_2 = 2\sigma_3 \qquad (3.20)$$

Eq. 3.17 and Eq. 3.20 give

$$\sigma_2 = \sigma_1 + \sigma_3 \qquad (3.21)$$

and

$$v_2 = (\sigma_3 - \sigma_1)/\rho C \qquad (3.22)$$

Note that σ_2 in Eq. 3.21 gives the stress pulse imparted to the specimen and v_2 the particle velocity in the load bar. Since σ_1 is compressive and σ_3 is tensile in nature, the pulse transmitted to the specimen is actually the difference in magnitude of incident and reflected pulse. Thus the particle velocity of the cantilever end can be found by taking sum of the absolute value of incident and reflected pulse.

3.3.4 DETAILS OF BRIDGE CIRCUIT

The bridge circuit converts the change in resistance of the strain gauges bonded to the load bar into a potential difference. This potential difference is in turn, recorded on the oscilloscope. Fig. 3.22 shows the configuration of the bridge circuit used in this study. R_1, R_2, R_3 and R_4 are four strain gauges each having a resistance value of $120 \pm 0.3\,\Omega$. R_1 and R_3 represent the strain gauges bonded to the load bar. R_2 and R_4 are the dummy gauges. These dummy strain gauges are bonded on a steel plate which acts as a heat sink to the heat generated in the strain gauge when current flows through it. The bridge circuit is balanced to give zero voltage output for no change in resistance of the active strain gauges. This is done by connecting a $1.0\,\Omega$ resistance in series and two variable resistors ($0.1\,M\Omega$ and $1.0\,k\Omega$) parallel to one of the dummy strain gauges (R_2 in the shown circuit). To calibrate the bridge circuit a calibration resistance R_c is connected parallel to one of the active gauges (R_3 in the diagram) through a switch (K). The value of the calibration resistance is $47.0\,k\Omega$. The equations involving the calibration of the bridge circuit are as follows. For a balanced bridge circuit the output voltage (Δe) is given by

$$\frac{\Delta e}{E} = \frac{R_1 \cdot R_2}{(R_1+R_2)^2}\left(\frac{\Delta R_1}{R_1} - \frac{\Delta R_2}{R_2} + \frac{\Delta R_3}{R_3} - \frac{\Delta R_4}{R_4}\right) \qquad (3.23)$$

where E is the input voltage. It can be seen from the equation that similar (both positive or both negative) changes in resistance of opposite arms of the bridge circuit are added up and dissimilar (one positive and other negative) changes are cancelled out. Thus by having the active strain gauges at the opposite arms only compressive pulse is recorded and bending effect is neglected.

The relation between the strain in the strain gauge and corresponding change in its resistance is governed by the following equation

$$G.F. = \frac{\Delta R/R}{\Delta L/L}$$
$$\Delta L/L = \frac{\Delta R/R}{G.F.} \qquad (3.24)$$

where G.F. is the gauge factor and ΔL/L is the strain recorded by the strain gauge. The change in resistance of the arm CD after connecting R_c is given by

$$\Delta R_3 = R_3 - \left(\frac{R_3 . R_c}{R_3 + R_c} \right) \qquad (3.25)$$

leading to

$$\Delta R_3/R_3 = \frac{R_3}{R_3 + R_c} \qquad (3.26)$$

Corresponding to this change in resistance a voltage difference (Calibration Voltage, V_c) will occur between terminals A and C. Similar resistance change also occurs in R_3 when the load bar experiences the load pulses. From Eq. 3.24 and 3.26 the calibration voltage (V_c) corresponds to the strain

$$\varepsilon_c = \Delta L/L = \frac{R_3}{2 (R_3 + R_c)\ G.F.} \qquad (3.27)$$

Note that the factor of 1/2 is introduced to average out the strains recorded by the two strain gauges R_1 and R_3 which are at the opposite arms of the bridge circuit. By the linearity of the relation (Eq. 3.23 and Eq. 3.24) between voltage drop across AC and strain in the strain gauges bonded to the load bar, the strain in the load bar corresponding to a voltage V recorded on the oscilloscope can be given as

$$\varepsilon = \frac{\varepsilon_c}{V_c} . V \qquad (3.28)$$

In previous works BNC connectors were used in the bridge box. But available BNC

connectors were not of good quality. They did not provide reliable connections. These BNC connectors were replaced by specially designed cap and stud arrangement (Fig.3.23) to have press contact at the terminals. Four to six studs were screwed to a brass plate. They were provided with holes for the wires. The wires inserted in these holes were pressed against the plate by the cap. Fig. 3.23 shows the photograph of the cap and stud assembly. This figure also shows the photograph of the interior of the bridge box, showing bridge connections, dummy strain gauges and battery. Direct contact between brass plates and the bridge box is avoided using a wooden block.

3.3.5 OSCILLOSCOPE

A digital differential storage oscilloscope, model 1624 (Gould Inc., U.K.) was used. Its data can be stored in the 50 memory blocks and can be recalled. It has 12 bit resolution (i.e. 4096 points on the screen) in horizontal and 8 bit resolution (i.e. 256 points) in vertical direction. The maximum sensitivity in the vertical direction is 0.025 mV and that in the horizontal direction is 0.25 μs. This oscilloscope is provided with differential input facility.

3.3.6 CRACK VELOCITY

Crack velocity generally measured by placing standard propagation gauges ahead of the crack tip. But these gauges have polymeric backing material which requires considerable amount of the energy to tear it. The interlaminar fracture toughness of the bonded DCB specimen is estimated to be very low (of the order of 10 J/m^2) and hence conventional propagating gauges can not be used. Therefore, bonding of the strain gauges on the side face is preferred. Three strain gauges were bonded ahead of the crack tip. The first strain gauge was mounted close to the crack tip of precrack. As the crack advances and reach close to the strain gauge, the strain starts increasing to a maximum value due to singular stress field around the crack tip and then decreases as the crack passes underneath the strain gauge. If the times at which the strain gauges

record the maximum strain are known, then a curve can be drawn for the crack length as a function of time. The slope of this curve gives the crack velocity. The technique is discussed in detail in the subsequent section.

3.4 RESULTS AND DISCUSSION

As discussed earlier the input required for evaluation of $\hat{J}$-Integral from the finite element programs are:

(i) The deflection of cantilever end with time
(ii) The crack initiation time
(iii) The crack propagation history

The deflection of cantilever end with respect to time is obtained by analyzing incident and reflected pulse in the load bar as discussed in Sec. 3.3.3. The initiation of crack is monitored by the strain gauge bonded close to the crack tip on the side face of the specimen. As the crack approaches the strain gauge, the strain gauge records become maximum owing to singular stress field. When the crack further advances the second as well as the third strain gauge also records become maximum successively. The locations of strain gauges ahead of the crack tip are premeasured accurately and the time at which the peak appears on strain gauge record, can be obtained from the oscilloscope trace. A relation is thus obtained between the crack location and time. The crack initiation time is obtained by extrapolating the fitted curve to initial crack length. The slope of the curve gives crack velocity.

The deflection of the cantilever end with time was obtained from the incident and reflected pulse in the load bar, and becomes input to the finite element code. The FE program was executed for the stationary crack and a typical variation of $\hat{J}$-integral with time was obtained as shown in the Fig. 3.24. It is observed from the Fig. 3.24 that the $\hat{J}$-integral increases to a certain value and starts decreasing; it decreases to almost zero value and again increases later to a large value. This happens because the nature of the

loading pulse is reversed when it starts reflecting from the crack tip. This pulse again reflects from the loading end and the $\hat{J}$-integral starts increasing. If the $\hat{J}$-integral corresponding to the first peak is not sufficient to initiate the crack propagation, then the crack will open only after the $\hat{J}$-integral value shows increasing trend again and exceed the previous peak value, which is attained only after 100 μs. The probable time zones when the crack can start propagating is shown in Fig. 3.24. The intensity of variation of $\hat{J}$-integral with time depends upon the input deflection of cantilever end with time, which in turn depends on the magnitude of the load bar pulse as discussed in Sec. 3.3.3. Therefore, at *higher loads* with larger value of $\hat{J}$-integral the crack initiates in the first time zone, whereas for the *lower load* the crack initiates in the second time zone.

3.4.1 INTERLAMINAR INITIATION FRACTURE TOUGHNESS FOR HIGH LOAD

As discussed earlier, when the cantilever end is loaded, the flexural waves start propagating towards the crack tip. After sometime (depending upon the crack length), the stress intensity at the crack tip ($\hat{J}$-Integral) starts increasing as shown in the Fig. 3.24. When $\hat{J}$-Integral attains a certain value, the crack initiation occurs. The value of $\hat{J}$-Integral corresponding to this time is defined as initiation toughness. In this section, the experimental records, their subsequent analysis and the results from the finite element code are presented. Experimental measurements and subsequent finite element analysis for Expt. 1 are presented and discussed in detail and then results for other experiments are highlighted whenever necessary.

The details of the crack lengths and strain gauge locations for different experiments are given in Table 3.1.

Table 3.1 Length of precrack in the DCB specimen and strain gauge locations for Expt. 1 to 5.

Expt. No.	Crack Length (mm)	First* Strain Gauge Location (mm)	Second** Strain Gauge Location (mm)	Third*** Strain Gauge Location (mm)
1	40.9	2.3	5.0	5.1
2	40.8	1.0	5.1	4.5
3	42.1	2.3	5.1	5.2
4	41.1	1.3	4.9	5.0
5	39.3	1.5	4.9	5.1

* distance measured from the crack tip
** distance measured from the first strain gauge
*** distance measured from the second strain gauge

Experimental No. 1

The oscilloscope trace for Expt. 1 is shown in Fig 3.25. Channel 1 gives the record of incident and reflected pulses in the load bar. Channel 2, 3, and 4 give the records of the strain gauges mounted on the side face of the cantilever ahead of the crack tip of the specimen. The duration of the square incident pulse is nearly 130 μs. The velocity of the load bar end vs. time plots (Fig. 3.26(a)) were obtained from the incident and reflected pulses as described in Sec. 3.3.3. When the velocity of load bar end vs. time plot is integrated with respect to time, it gives the displacement of the load bar end face with time. This displacement is same as the deflection of cantilever end as shown in Fig. 3.26(b), because the load-bar-end is attached to the cantilever end as describes in Sec. 3.3.2. The loading of the cantilever starts at the time corresponding to midpoint of the head of the incident pulse and head of the reflected pulse. This is denoted as 'REFERENCE' in the Fig. 3.25.

The first strain gauge on the specimen is mounted 2.3 mm ahead of the crack. To

determine the initiation time, the response of all the three strain gauges are considered. A magnified view of the three strain gauges readings is shown in the Fig. 3.27. The crack length as a function of time is plotted in the Fig. 3.28(a). A second degree polynomial is fitted through three data points and extrapolated to the initial length of the crack (as shown in the Fig. 3.28(a) by dashed line). It provides the initiation time as 43.51 μs. The variation of crack velocity with respect to time (Fig. 3.28(b)) is obtained by differentiating crack length vs. time curve. The crack velocity decreases from a higher value of 1850 m/s at the initial crack tip to 1650 m/s at the third strain gauge location. It is to be noted here that the determination of initiation time by extrapolation is not expected to have much error because (i) crack velocity is extremely high, 1850 m/s at the initiation and (ii) the distance between the crack tip and the strain gauge is small. In fact it takes only 1.3 μs (approximately) for the crack tip to reach the first strain gauge. Furthermore, the peak corresponds to the crack tip location which is slightly before the strain gauge. In fact, in quasistatic study (Sec. 2.1.8), it was found that the peak strain value occurs when the crack tip is approximately 1 mm before the strain gauge location. Similar attempt was made to obtain the location of crack tip corresponding to the peak strain for the dynamic case through FE code. Owing to the oscillations in the strain field near the crack tip under dynamic loading, location of the crack tip relative to the first strain gauge could not be ascertained for the peak response.

The finite element code (Sec. 3.2) was executed using the displacement boundary conditions given by Fig. 3.26(a). The variation of $\hat{J}$-Integral with respect to time was obtained as shown in Fig. 3.29. The initiation toughness ($\hat{J}_{ini}$) was obtained corresponding to the initiation time as shown in the figure. The initiation toughness for Expt. 1 is 150 J/m^2.

Experiment Nos. 2-5

The details of initiation time and initiation toughness ($\hat{J}_{ini}$) is given in Table - 3.2 for Expt. 1 to 5.

Table 3.2 Crack lengths, time at different gauges, initiation time and initiation toughness for Expt. 1 to 5.

Exp No.	Crack Length (mm)	1st SG from C-tip (mm)	Time* of strain gauge peak (μs)			Init. Time# (μs)	J_{ini} (J/m^2)
			SG1	SG2	SG3		
1	40.9	2.3	44.8	47.6	50.6	43.51	150
2	40.8	1.0	43.4	47.0	49.8	42.64	90
3	42.1	2.3	46.5	50.0	54.0	45.20	160
4	41.1	1.3	45.0	48.5	52.7	44.32	200
5	39.3	1.5	44.3	49.6	55.6	42.76	125

SG1 - First Strain Gauge on the Specimen
SG2 - Second Strain Gauge
SG3 - Third Strain Gauge
C-tip - Crack Tip
Init. Time - Initiation time
* measured with respect to starting of loading of cantilever
# by extrapolation
J_{ini} = Initiation toughness

Similar to Expt. 1, the oscilloscope records and processed data of boundary conditions at the cantilever end and crack velocity variation are shown for Expt. 2 in Figs. 3.30 to 3.33. From the initiation time obtained through Fig. 3.32(a), the J_{ini} toughness is determined in Fig. 3.33 as 90 J/m^2. When the crack velocity of both the experiments are compared (Fig. 3.28(b) and Fig. 3.32(b)), the crack velocity in Expt. 2 increases with crack propagation whereas crack velocity in Expt. 1 decreases with advancement of crack tip. Only in Expt. 2, this anomalous behaviour is observed; the plausible causes will be discussed later after the presentation of the details of the five experiments.

Figures 3.34 to 3.37 provide the details of experimental records and processed data for Expt. 3. Fig. 3.36(b) shows that the crack velocity decrease with propagation, quite similar to the behaviour of Expt. 1 (Fig. 3.28(b)). Also the value of J_{ini}, 160 J/m^2 from Fig. 3.37 is very close to that of Expt. 1. The details of Expt. 4 are presented from Figs.

3.38 to 3.41, and those for Expt. 5 in Figs. 3.42 to 3.45.

The increase in crack velocity of Expt. 2 (Fig. 3.32(b)) might be due to nonuniform bonding or presence of very small void ahead of the crack tip. This reason looks more plausible because the J_{ini} is also comparatively low; only 90 J/m^2 (Table-3.2).

Sharp peaks were not observed for strain gauges SG2 and SG3. This is possibly due to the crack front deviating excessively from the direction normal to the length of the DCB specimen. Even in quasistatic experiments with DCB specimen, it is observed that crack on both sides of specimen do not propagate to the same distance. FE analysis of this work, for both quasistatic and dynamic studies is done under 2-D plane strain analysis under the assumption that the crack front remains normal to the direction of propagation. At high speeds of crack propagation of about 1500 m/s, even a small perturbation may cause the crack front to become inclined, so much so that superposition of stress waves no longer result into a peak.

The inclination of the crack front can be estimated by measuring crack tip history on both side faces of the specimen. On further studies, a criterion may be developed on the permissible limit of inclination of crack front for the reliability of the experiments. Also, it may be a worthwhile exercise to do complete 3-D FE analysis for the cases when the crack front of the precrack having an inclination, other than 90°. Moreover, the crack propagation velocities measured on both side of specimen will give more confidence to the result. At the same time, if more number of strain gauges are mounted in series ahead of the crack tip, a better variation of the crack velocity can be obtained. But due to unavailability of proper oscilloscope, it was not possible to use more strain gauges.

3.4.2 INTERLAMINARPROPAGATIONFRACTURETOUGHNESS FOR HIGH LOAD

The toughness of the interface decreases as soon as the crack starts propagating. The propagation toughness depends upon the crack propagation velocity. The crack propagates at varying speed along the interface depending upon the energy available.

As discussed in Sec. 3.4.1,the crack velocity is measured by peak response of the strain gauges bonded ahead of the crack tip on the side face of the specimen. Apart from the cantilever end deflection with time, the variation of crack length with time is also used as input to finite element code to calculate the propagation toughness. The crack propagation algorithm (Sec. 3.2.2) is called after the initiation time for the crack propagation analysis.

Experiment No. 1

Once the FE code is executed upto the time of crack initiation, the crack propagation module is called. The advancement of crack in each iteration is to be known so that an appropriate factor can be applied to the holding back force for modelling the crack propagation. The advancement of crack in each iteration is calculated, as discussed in Sec. 3.4.1,by the second degree polynomial fitted through the three data points of peak response of the strain gauges. With the load input and the crack propagation data, the dynamic FE analysis determine the stress/strain field in the specimen in successive time steps. Using this the variation of $\hat{J}$-integral with time is shown in Fig. 3.46. In the beginning the crack remain stationary and $\hat{J}$-integral increases. A stage is reached at the initiation time when the crack tip starts growing under the known dynamic displacement boundary conditions. The computer code provides the $\hat{J}$-integral for the measured crack velocity. The drop in $\hat{J}$-integral is sharp and substantial. In fact, Fig. 3.47 shows the magnified view of the $\hat{J}$-integral of the crack moving at high speed.

The fast drop in the $\hat{J}$-integral value as the crack starts moving, occurs because a large amount of energy is consumed to accelerate the crack. The faster the crack speed, the more is the radiated kinetic energy and the bigger the drop of $\hat{J}$-integral value. If the crack velocity is constant then the $\hat{J}$-integral starts increasing after initial drop because the energy input is increasing but the energy required to drive the crack is negligible. If the crack velocity keeps on increasing after initiation, more and more energy is required to accelerate the crack and the $\hat{J}$-integral will decrease further. On the other hand, with decreasing crack velocity the energy required to move the crack is less and hence the $\hat{J}$-integral is almost constant or increasing depending upon the energy input.

The $\hat{J}$-integral value for Expt. 1 is nearly constant in the period of observation.

The oscillatory behaviour of $\hat{J}$-integral is obtained during crack propagation owing to the following reasons:

(a) The free surfaces of DCB specimen are very close to the crack tip. In fact, propagation time for some stress waves to emanate from the crack tip and return to the tip are as small as 1-2 μs. The superpositions of the these waves and their effect on $\hat{J}$-integral will provide ripples.

(b) In the finite element modelling, the crack tip is moved from one point to other point in discrete steps by linearly decreasing holding back force may not be accurate and result in oscillatory stress/strain field near the crack tip and hence their effect on $\hat{J}$-integral.

Experiment Nos 2-5

The variation of $\hat{J}$-integral with time of Expt. 2 for stationary crack and propagating crack is shown in Fig. 3.48 and the propagation phase variation of $\hat{J}$-integral for the same experiment is separately shown in Fig. 3.49. In this case, it can be observed that the $\hat{J}$-integral drops sharply initially once the crack start propagating similar to the Expt. 1 and later slowly as the crack propagates further, unlike as in Expt. 1 where $\hat{J}$-integral remains nearly constant. This is explained owing to behaviour of increasing crack velocity in Expt. 2 and decreasing crack velocity in Expt. 1.

Time history of $\hat{J}$-integral for Expts. 3,4 and 5 are shown in Figs. 3.50 to 3.55. Their behaviour is similar to that of Expt. 1.

The average crack velocities between first and second gauge and second and third strain gauge, the initiation toughness and propagation toughness are given in Table 3.3 for all the five experiments.

Table 3.3 Crack velocity, initiation toughness ($\hat{J}_{ini}$) and propagation toughness ($\hat{J}_{prop}$) for Expt. 1 to 5.

Expt. No.	Length of pre-crack (mm)	Average Crack Velocity (m/s)		$\hat{J}_{ini}$ (J/m^2)	$\hat{J}_{prop}$ (J/m^2)
		$\dot{a}_1$*	$\dot{a}_2$#		
1.	40.9	1785	1700	150	3
2.	40.8	1416	1607	90	2
3.	42.1	1437	1300	160	3
4.	41.1	1400	1190	200	8
5.	39.3	925	850	140	13

* Average crack velocity between first and second strain gauge
# Average crack velocity between second and third strain gauge
J_{prop} Propagation toughness

At a relatively lower crack speed (850-1200 m/s), $\hat{J}_{prop}$ is much smaller than the initiation toughness but it is comparable to the quasistatic interlaminar toughness (12 J/m^2). At extremely high velocity, close to Rayleigh wave speed, $\hat{J}_{prop}$ is extremely small, of the order of 2-3 J/m^2.

The sharp drop in dynamic toughness of interlaminar crack should be noted. Based on the results of this work, it is now conjectured that interlaminar crack propagation in angle ply fibre reinforced plastic (FRP) laminates may show a similar behaviour. If that is so, it may explain why interlaminar cracks in FRP laminates show a large damage area even when the impacting mass is small with impact energy of the order of 5 J (Kumar and Rai, 1993). Also, it will explain the observation of high speed camera that the interlaminar crack initiated and propagated through impact move at very high speeds, of the order of 300-600 m/s (Takeda et al., 1982). It is to be noted that in the FRP material with much lower Rayleigh wave speed, the crack propagation velocity are comparable to high crack velocity obtained in this study with steel specimen.

3.4.3 INTERLAMINAR INITIATION FRACTURE TOUGHNESS FOR LOW LOAD

When a lower load is applied, the crack starts propagating at relatively late stage as discussed in the previous section. In two experiments of this study, it was observed that the crack initiates after 100 μs and the crack propagation speed was rather low (100 - 400 m/s). The details of crack length and the locations of strain gauges are given in Table - 3.4.

Table 3.4 Length of precrack in the DCB specimen and strain gauge location for Expt. 6 to 7.

Expt. No.	Crack Length (mm)	First* Strain Gauge Location (mm)	Second** Strain Gauge Location (mm)	Third*** Strain Gauge Location (mm)
6	40.2	1.3	4.9	4.7
7	40.9	1.8	4.8	5.3

* distance measured from the crack tip
** distance measured from the first strain gauge
*** distance measured from the second strain gauge

The oscilloscope trace of for Expt. 6 is shown in Fig. 3.56. The velocity of load bar end vs. time plot and cantilever end deflection vs. time plot are given in Fig. 3.57(a) and Fig. 3.57(b) respectively. The crack length as function of time is shown in Fig. 3.58(a) and the variation of crack velocity with time is shown in Fig. 3.58(b). The initiation time for Expt. 1 is obtained as 111.06 μs by extrapolation of curve in Fig. 3.58(a). The variation of $\hat{J}$-integral with time is shown in Fig. 3.59. At initiation time the $\hat{J}$-integral is 135 J/m^2. Similar plots were obtained for Expt. 7. The oscilloscope trace for Expt. 7 is shown in Fig. 3.60. The velocity input to load bar end vs time and cantilever end deflection with time plot are shown in Fig. 3.61(a) and Fig. 3.61(b) respectively. Variation of crack length and crack velocity with time are shown in Fig. 3.62(a) and Fig. 3.62(b) respectively. The initiation toughness was obtained as 230 J/m^2 as against the initiation time of 106.5 μs, as shown in Fig. 3.63. The details of crack length, initiation

time and J_{ini} for Expt 6 and 7 are given in Table 3.5.

Table 3.5 Crack lengths, time at different gauges, initiation time and initiation toughness for Expt. 6 to 7.

Exp No.	Crack Length (mm)	1st SG from C-tip (mm)	Time* of strain gauge peak (μs)			Init. Time# (μs)	J_{ini} (J/m^2)
			SG1	SG2	SG3		
6	40.2	1.3	114.0	130.0	201.0	111.06	135
7	40.9	1.8	109.6	120.9	156.9	106.50	230

SG1 - First Strain Gauge on the Specimen
SG2 - Second Strain Gauge
SG3 - Third Strain Gauge
C-tip - Crack Tip
Init. Time - Initiation time
* measured with respect to starting of loading of cantilever
# by extrapolation
J_{ini} Initiation toughness

3.4.4 INTERLAMINAR PROPAGATION FRACTURE TOUGHNESS FOR LOW LOAD

For low loads, $\hat{J}$-integral is evaluated for the displacement boundary conditions and the measured crack velocity. For Expt. 6 the variation of $\hat{J}$-integral during the period crack remains stationary and later when start propagating is shown in Fig. 3.64. The magnified view of variation of $\hat{J}$-integral with time for propagating crack is shown in Fig. 3.65. Sjmilar to Expt. 1 to 5, the $\hat{J}$-integral drops down, but to a relatively larger value because the crack velocity is not high. J_{prop} for Expt. 6 is obtained as 98 J/m^2 from Fig. 3.65. Similar curves were plotted for $\hat{J}$-integral variation for Expt. 7 in Figs. 3.66 and 3.67. The details of crack velocities, initiation toughness and propagation toughness for Expt. 6 and 7 given in Table 3.6.

Table 3.6 Crack velocity, initiation toughness and propagation toughness for Exp 6 to 7.

Expt. No.	Length of pre-crack (mm)	Average Crack Velocity (m/s)		$\hat{J}_{ini}$ (J/m^2)	$\hat{J}_{prop}$ (J/m^2)
		$\dot{a}_1$*	$\dot{a}_2$#		
6.	40.2	306	66	135	98
7.	40.9	424	147	235	85

* Average crack velocity between first and second strain gauge
\# Average crack velocity between second and third strain gauge
J_{prop} Propagation toughness

The finite element simulation agrees with experimental results, because the initiation time in all experiments is either in first zone or second zone (Fig. 3.24) and it was never between the first and second time zone. This observation validates the FE simulation.

Even though the initiation toughnesses are comparable, the crack velocities in Expts. 1 to 5 are much higher as compared to those of Expts. 6 and 7. This is because in Expt. 1 to 5 the crack opens early and there is sufficient energy available to move the crack, whereas in Expts. 6 and 7 the crack opens at a very late stage and not much energy available to move the crack (input load has a finite duration) late. This particular aspect needs further investigation to understand the mechanism of wave propagation and deflection patterns through FE analysis.

3.5 CLOSURE

The aim of this chapter was to develop a hybrid technique using experiment and finite element analysis to evaluate the initiation and propagation fracture toughness of the double cantilever beam specimen with slender cantilevers. A finite element analysis was developed which requires the displacement boundary conditions, initiation time and crack

propagation history as inputs. These data are determined through the experimental technique developed for the purpose.

With the aid of finite element code the variation of $\hat{J}$-integral was obtained for stationary and propagating crack. In a typical variation of $\hat{J}$-integral for stationary crack, the $\hat{J}$-integral remain nearly zero till the flexural wave reach the crack tip, then it start increasing. It increases to a maximum value at approximately 40 to 45 μs and then start decreasing, the value decreases to almost zero and then start increasing to a large value after approximately 100 μs. The magnitude of the peak value attained depends on the impact load applied to the specimen. Therefore, when higher load was applied, the crack initiated during the first peak phase. Whereas, for lower load, the first peak value of $\hat{J}$-integral was not high enough and crack started propagating only when the $\hat{J}$-integral exceeded the first peak value, which was attained only after 100 μs. In fact, out of seven experiments, in five experiments crack initiated between 40 to 45 μs and in two experiments crack initiated between 105 to 112 μs. This also validates the finite element simulation and predicts the experimental behaviour well. It was noted that the crack never initiated between 45 to 100 μs when the $\hat{J}$-integral had lower value.

The crack velocity was observed to vary between 100 and 1800 m/s. The initiation toughness ($\hat{J}_{ini}$) was found to vary between 90 to 230 J/m^2 and the propagation toughness ($\hat{J}_{prop}$) between 2 to 100 J/m^2 depending on the crack velocity. At higher crack velocity (close to Rayleigh wave speed), the crack propagates at very low toughness.

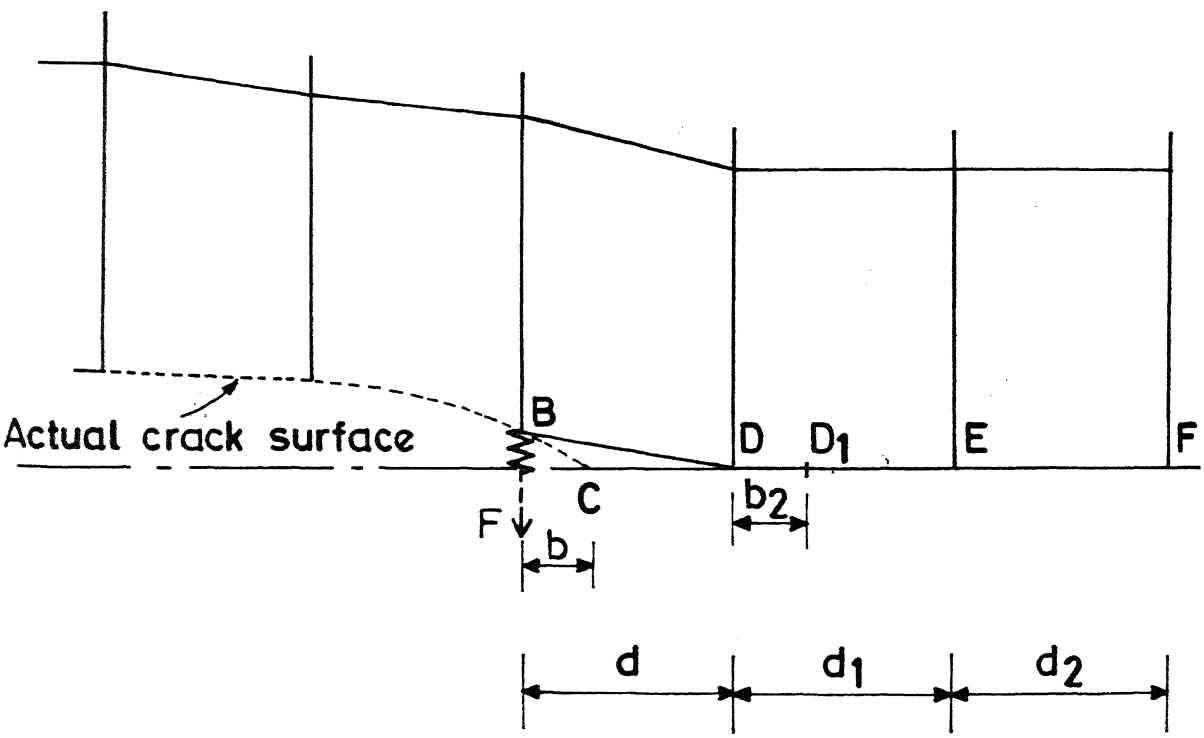

Fig. 3.1 Crack opening scheme

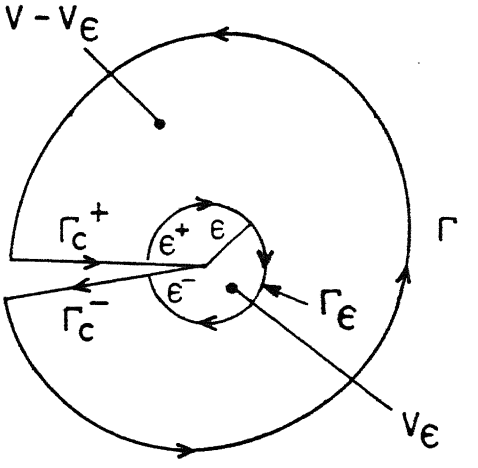

$$\Gamma_C = \Gamma_C^+ + \Gamma_C^-$$

$$\delta(V - V_\epsilon) = \Gamma + \Gamma_C - \Gamma_\epsilon$$

Fig. 3.2 Contour for $\hat{J}$-integral

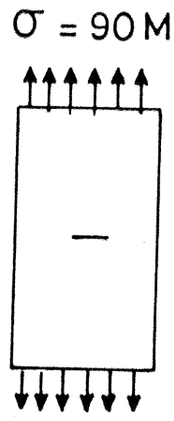

σ = 90 MPa

σ = 90 MPa
20 x 40 mm
2a = 4.8 mm
E = 200 GPa
ν = 0.3
f = 5000 Kg/m³

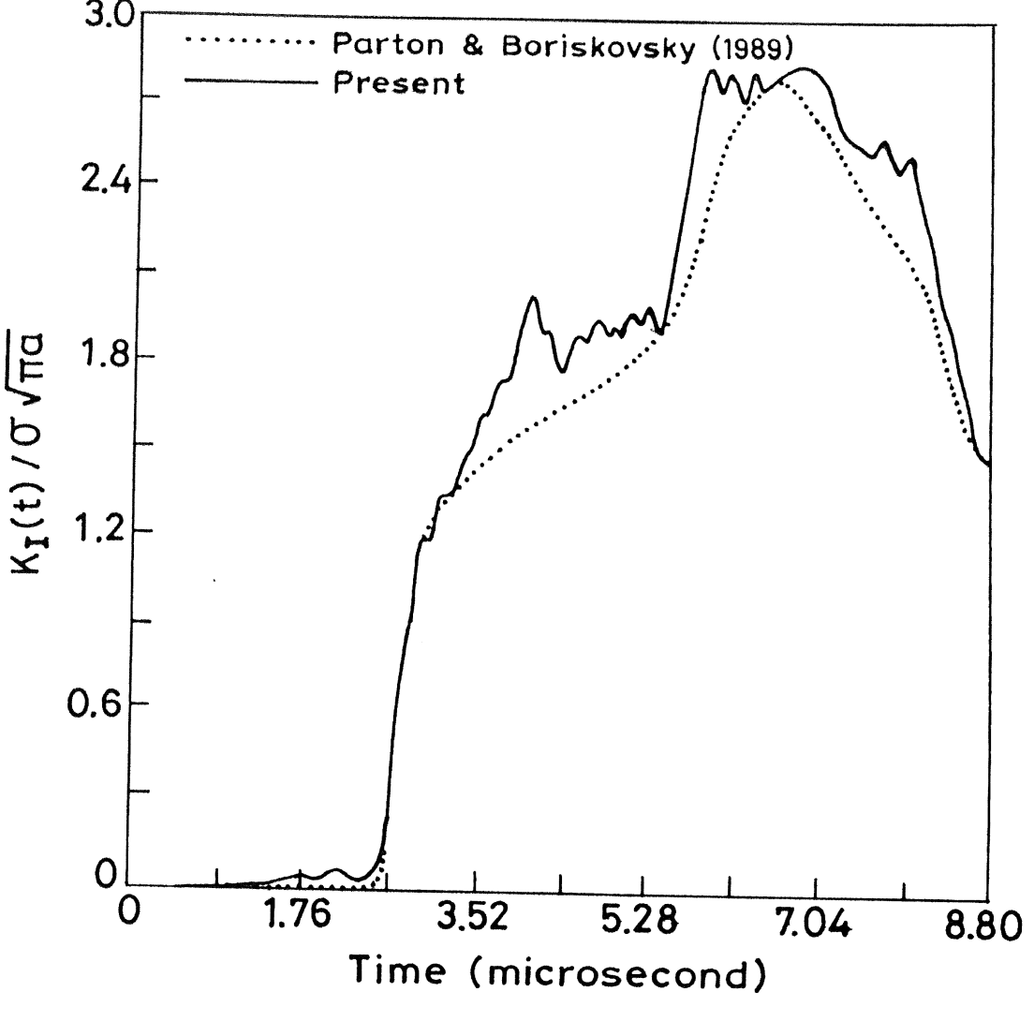

Fig. 3.3 Comparison of dynamic SIF variation with time (test problem)

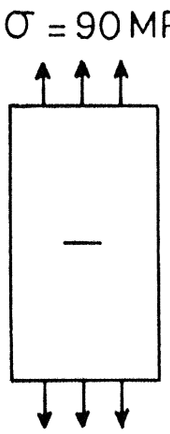

σ = 90 MPa

σ = 90 MPa
20 x 40 mm
2a = 4.8 mm
E = 200 GPa
ν = 0.3
f = 5000 Kg/m³

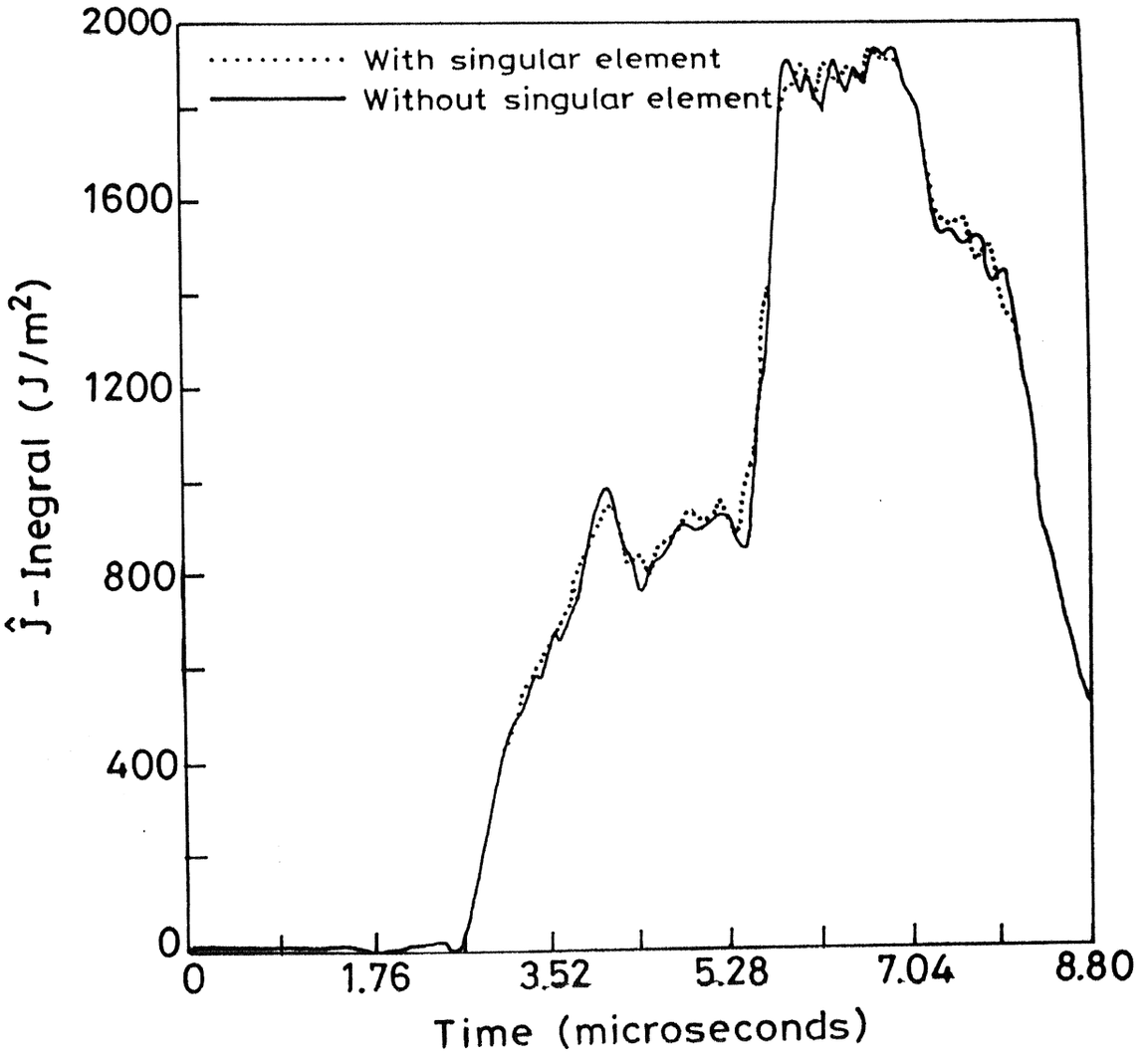

Fig. 3.4 Variation of $\hat{J}$-integral with time (with and without singular element around the crack tip)

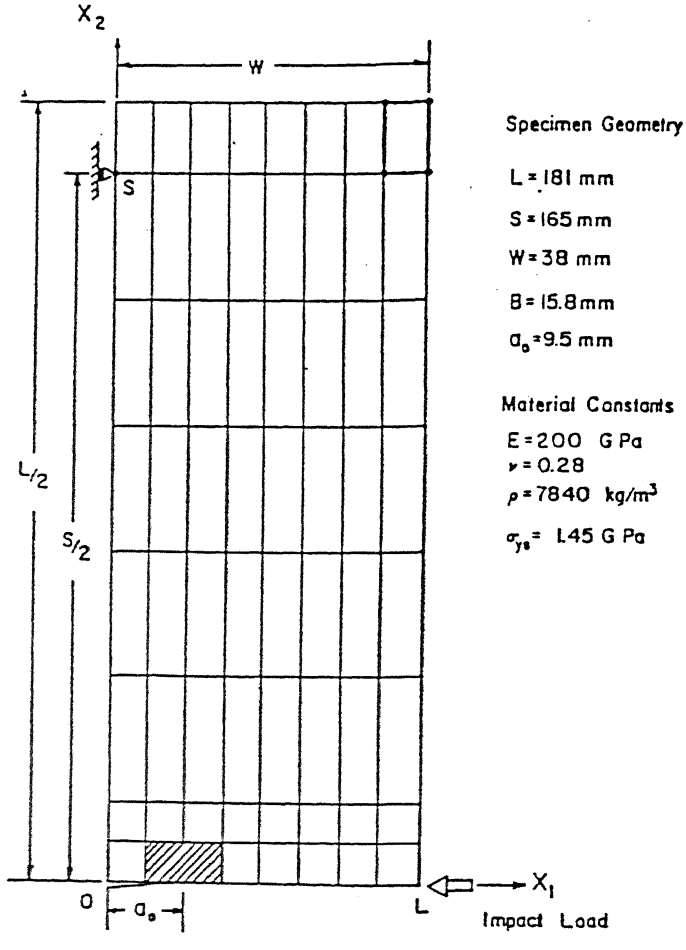

Fig. 3.5 3-point bend specimen (test problem)

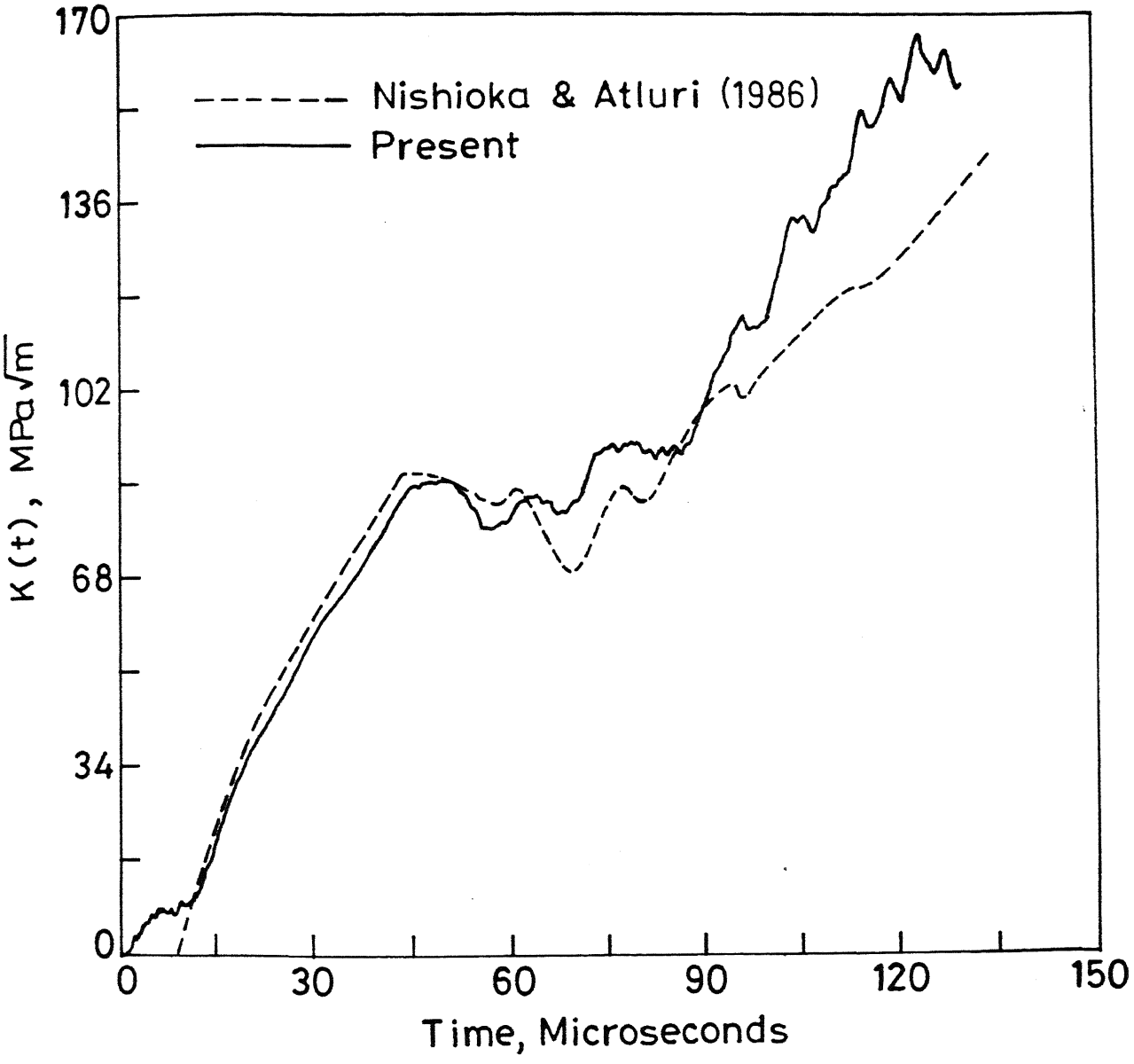

Fig. 3.6 Variation of dynamic SIF with time (test problem)

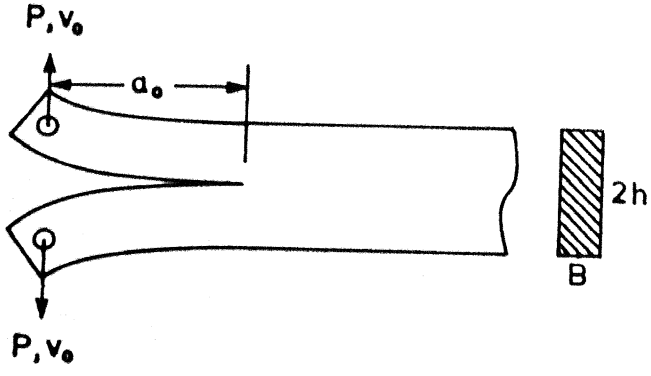

E = 1.5 GPa
ν = 0.33
ρ = 1500 kg/m³
h = 1.6 mm
L = 20 mm

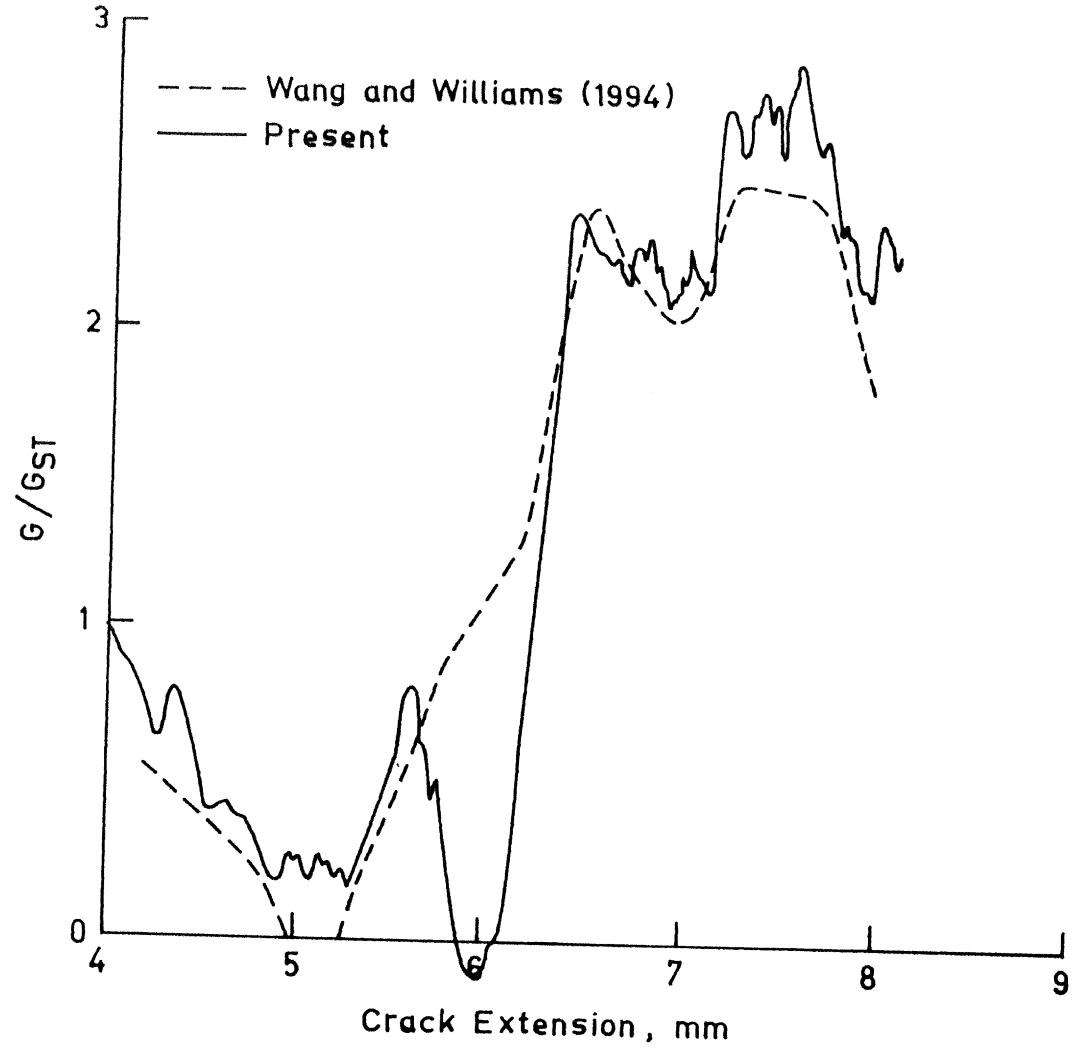

Fig. 3.7 Variation of normalised strain energy release rate with crack extension

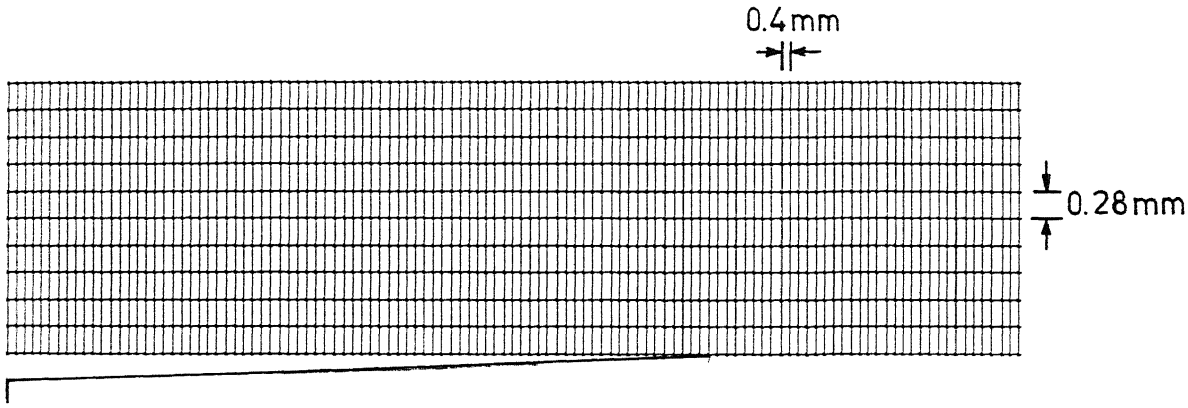

Fig. 3.8 Mesh for DCB specimen (one half)

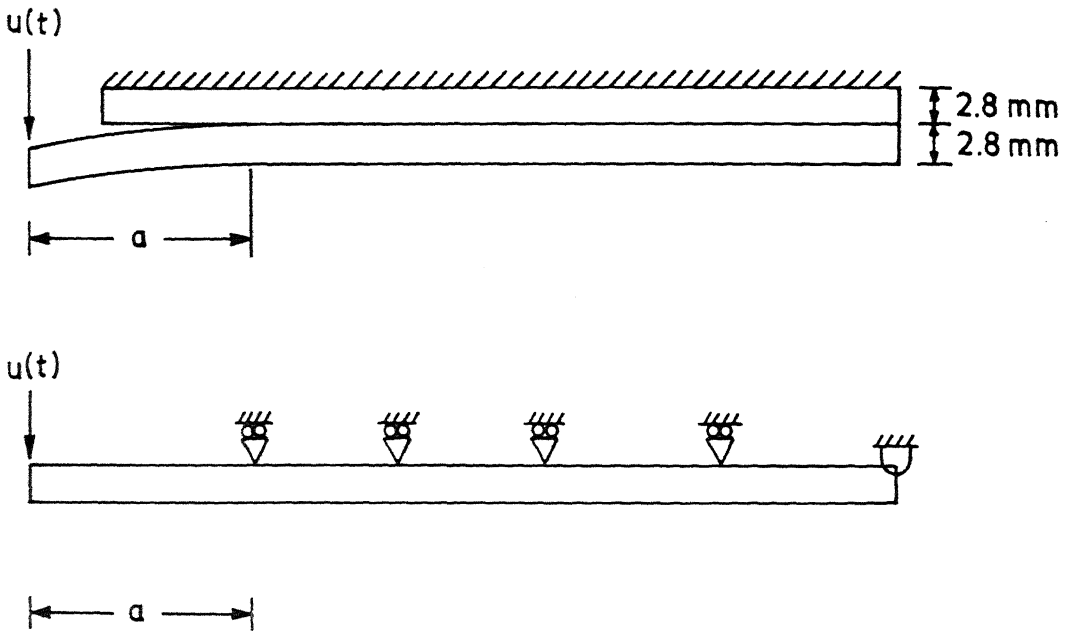

Fig. 3.9 Half and full DCB specimen configuration used for FE analysis

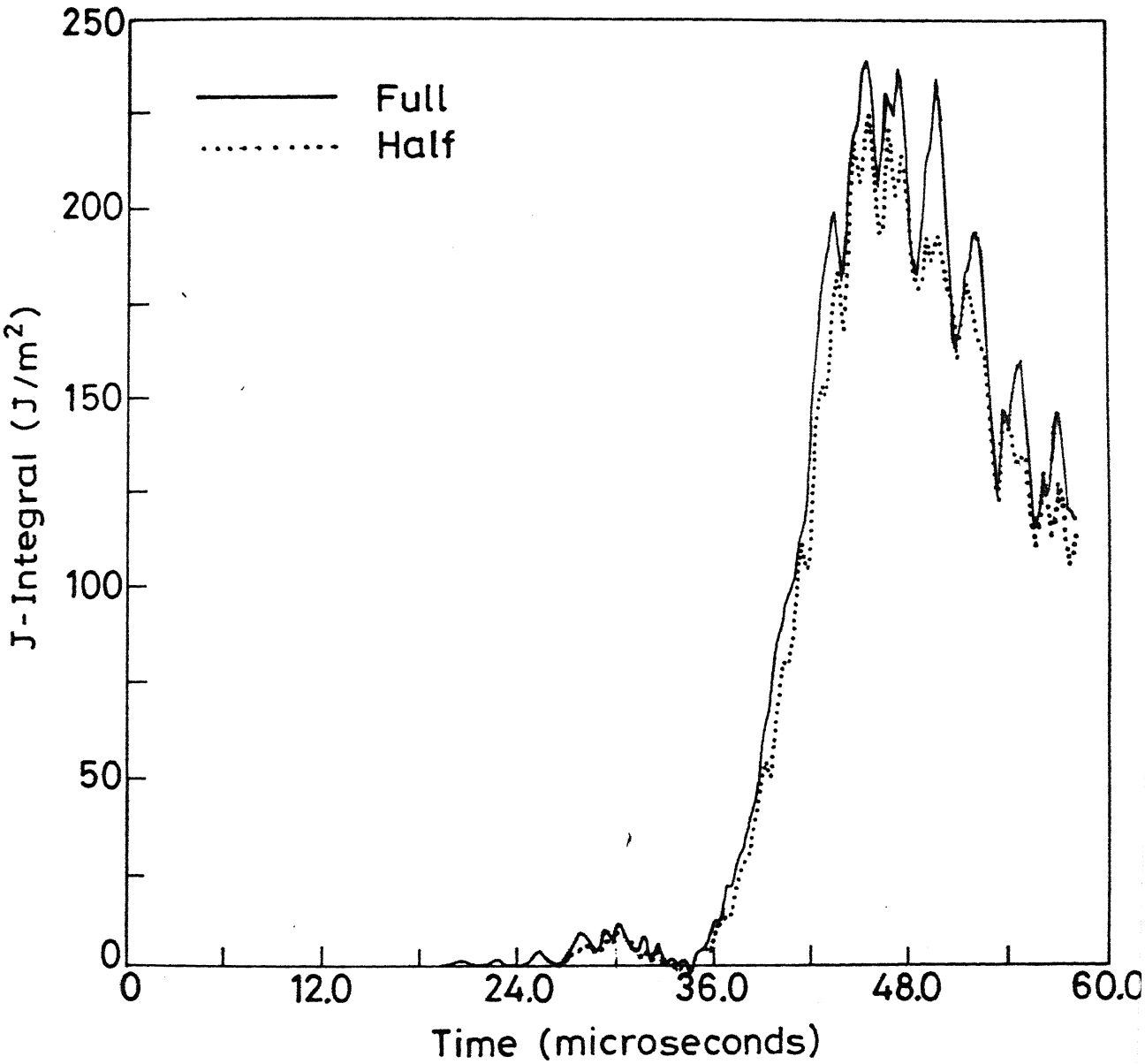

Fig. 3.10 Comparison on variation of $\hat{J}$-integral with time for half and full DCB configuration

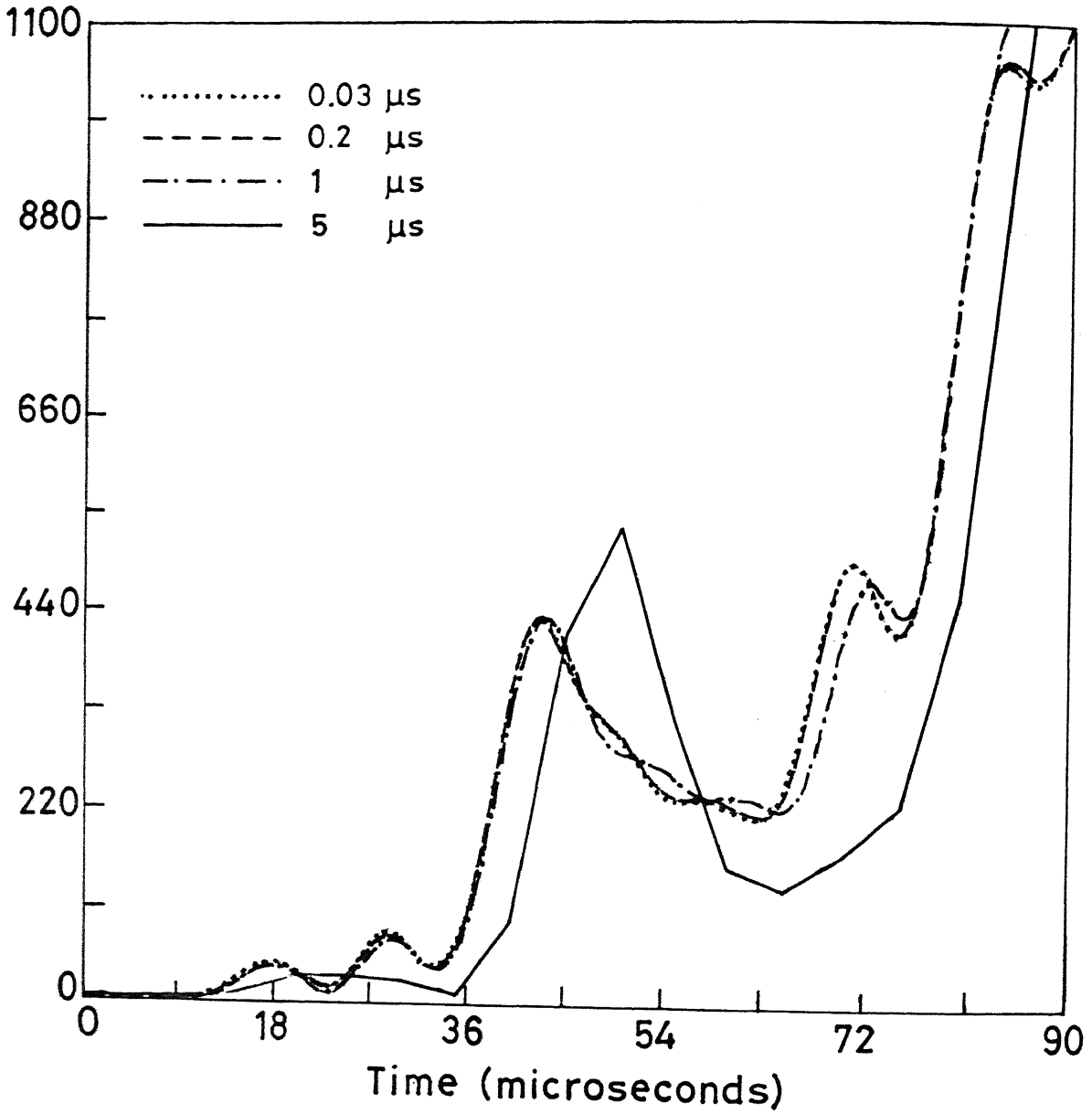

Fig. 3.11 Variation of $\hat{J}$-integral with time for different time step used in integration scheme

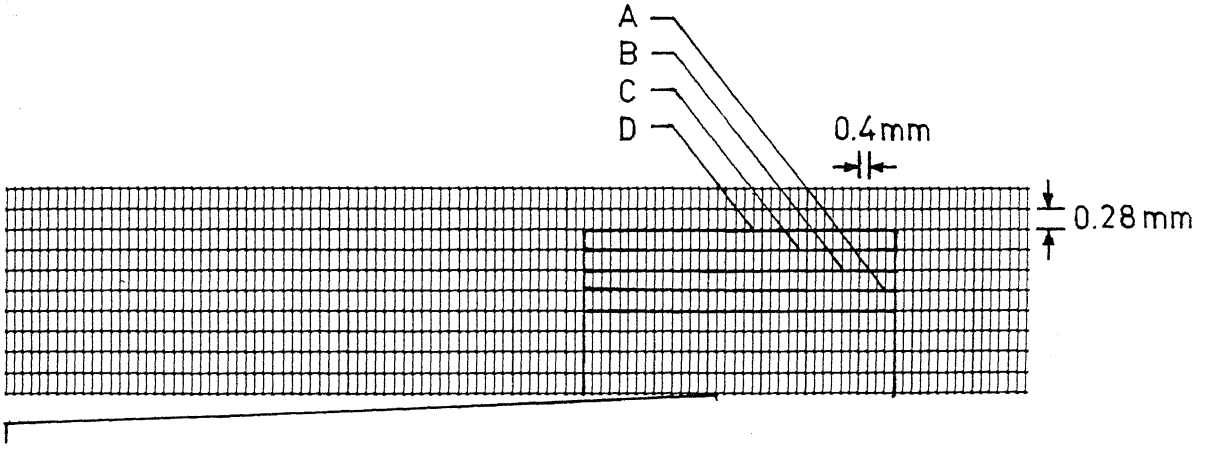

Fig. 3.12 Mesh showing different contours

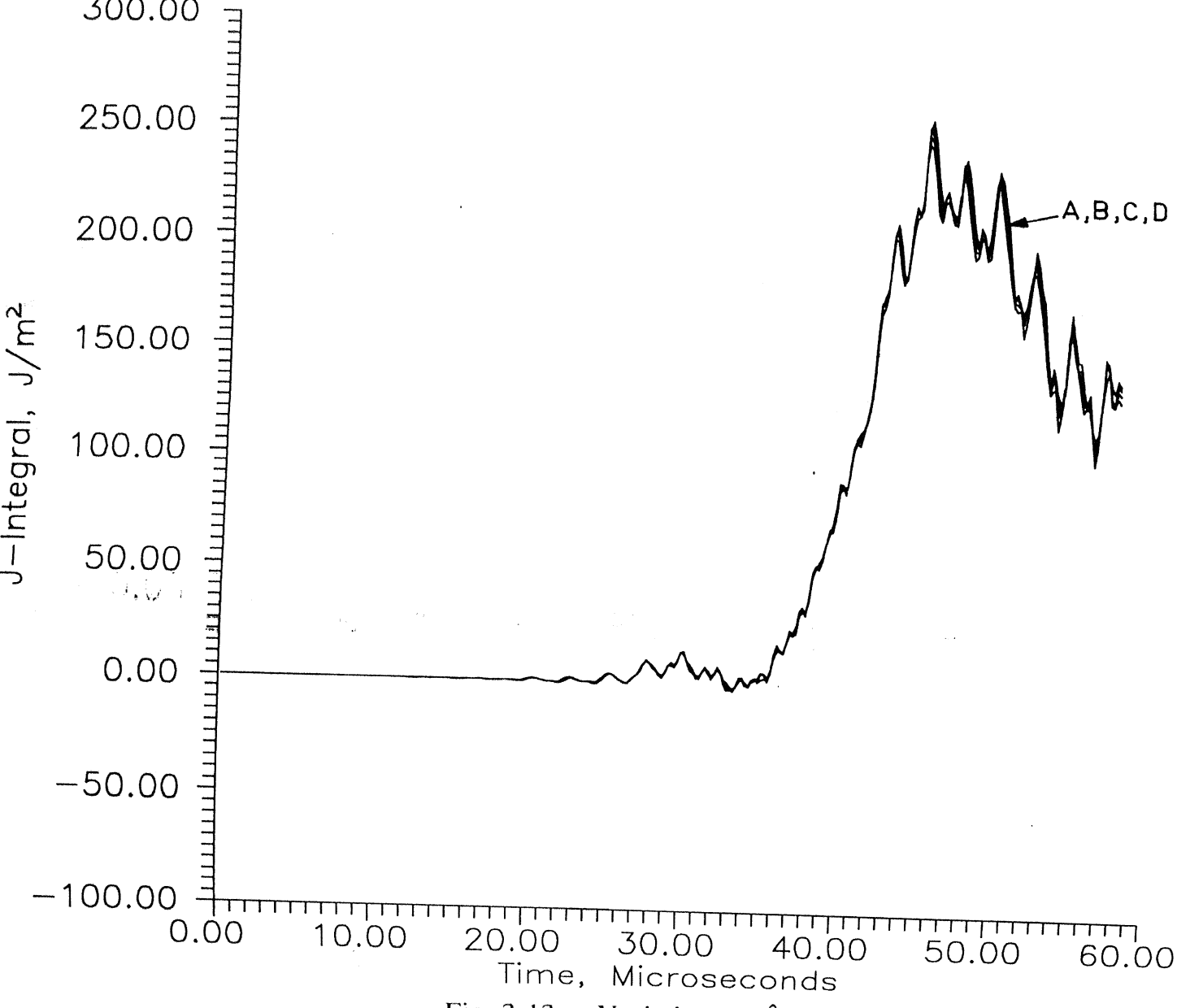

Fig. 3.13 Variation of $\hat{J}$-integral with time for different contours

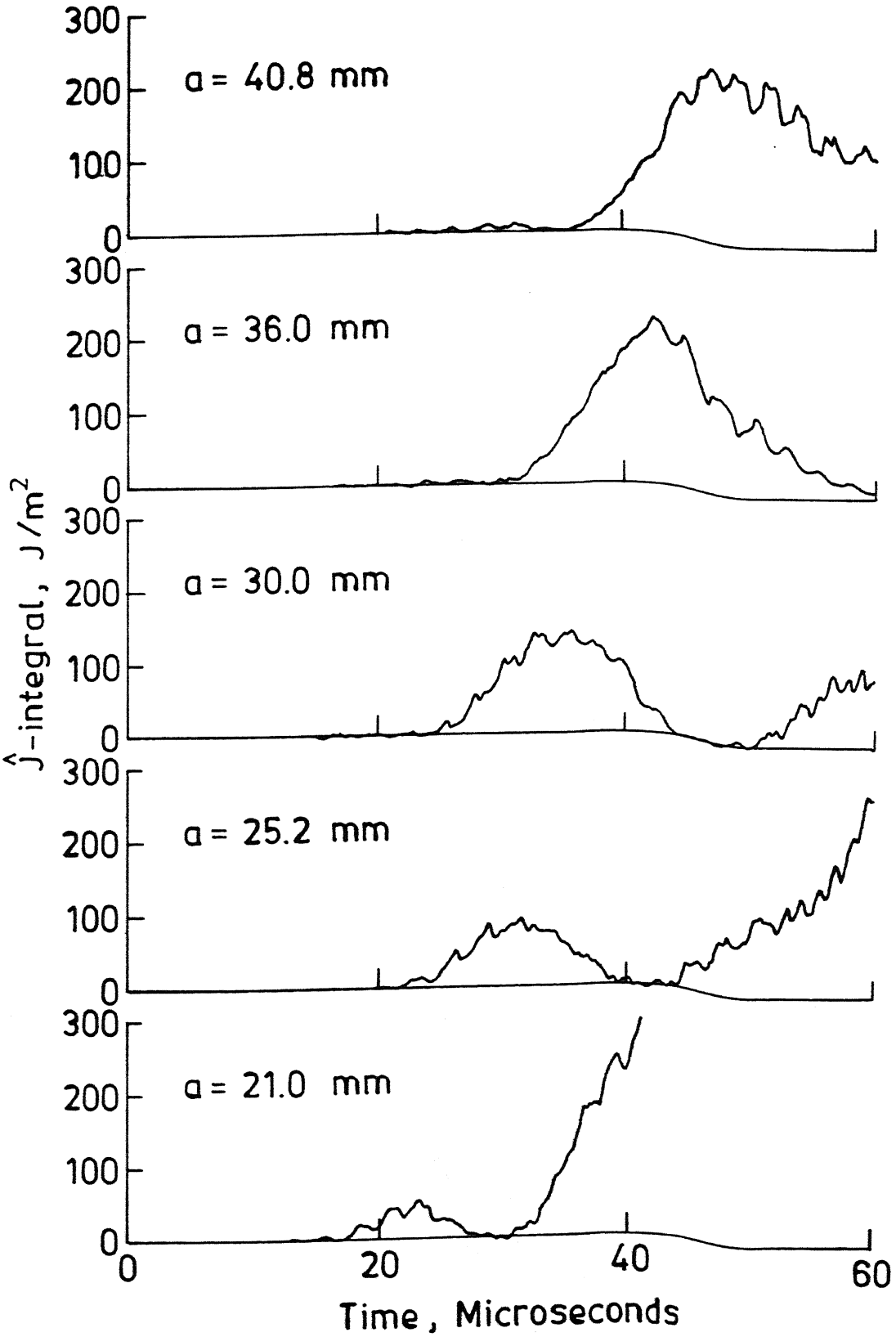

Fig. 3.14 Variation of $\hat{J}$-integral with time for different crack lengths

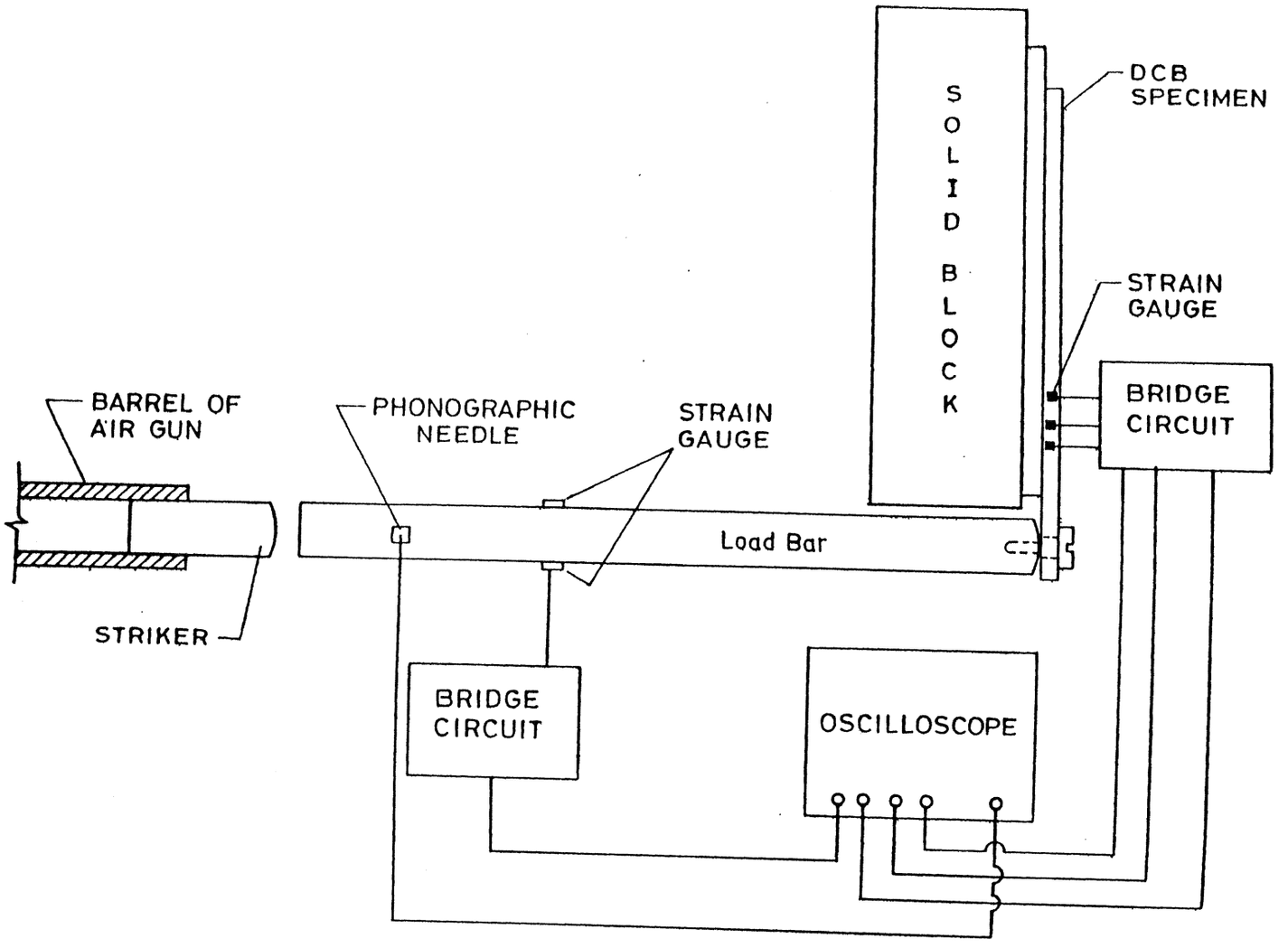

Fig. 3.15 Schematic diagram of the experimental setup

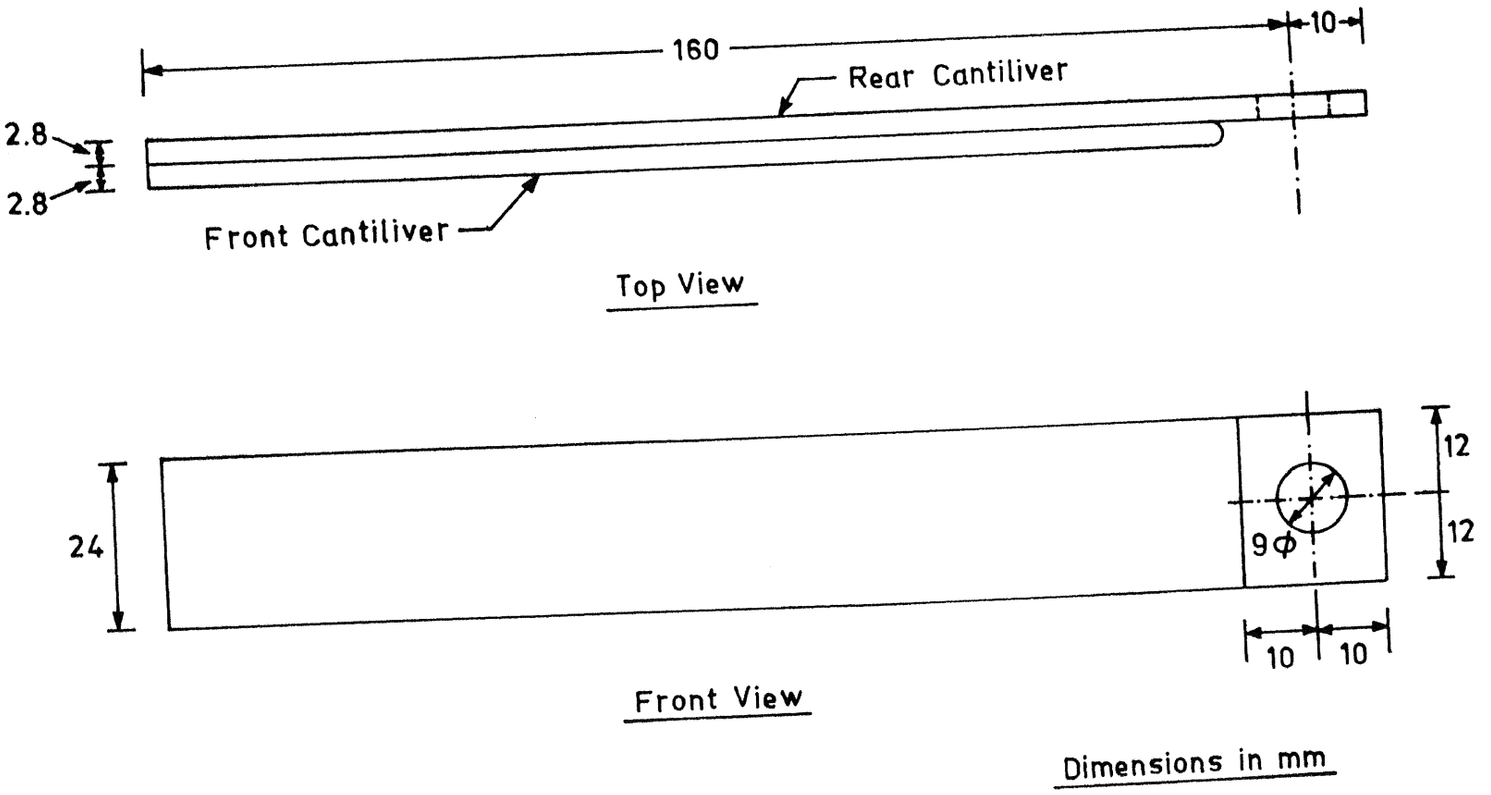

Fig. 3.16 DCB specimen

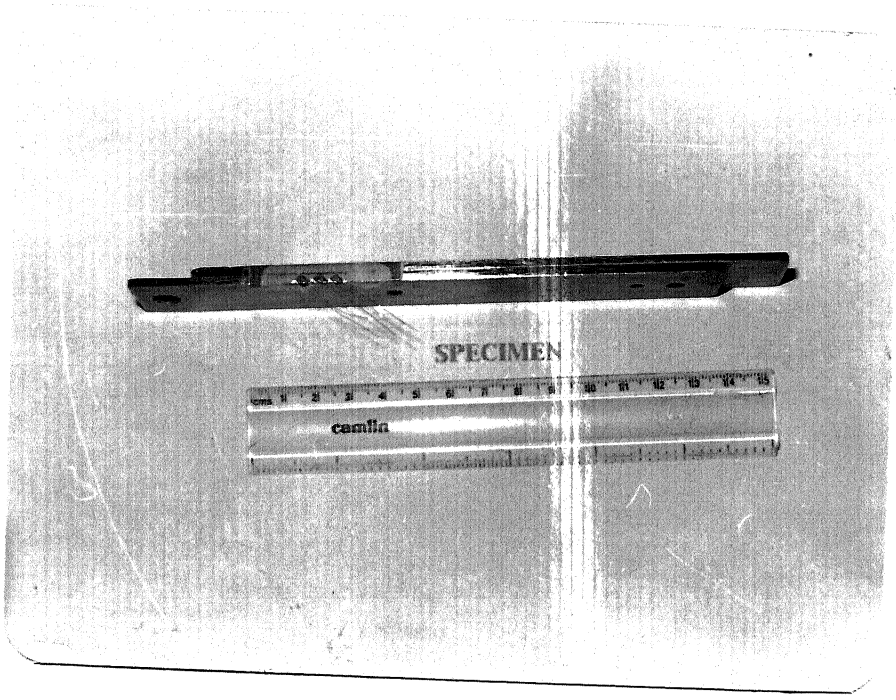

Fig. 3.17 Photograph of DCB specimen with strain gauge

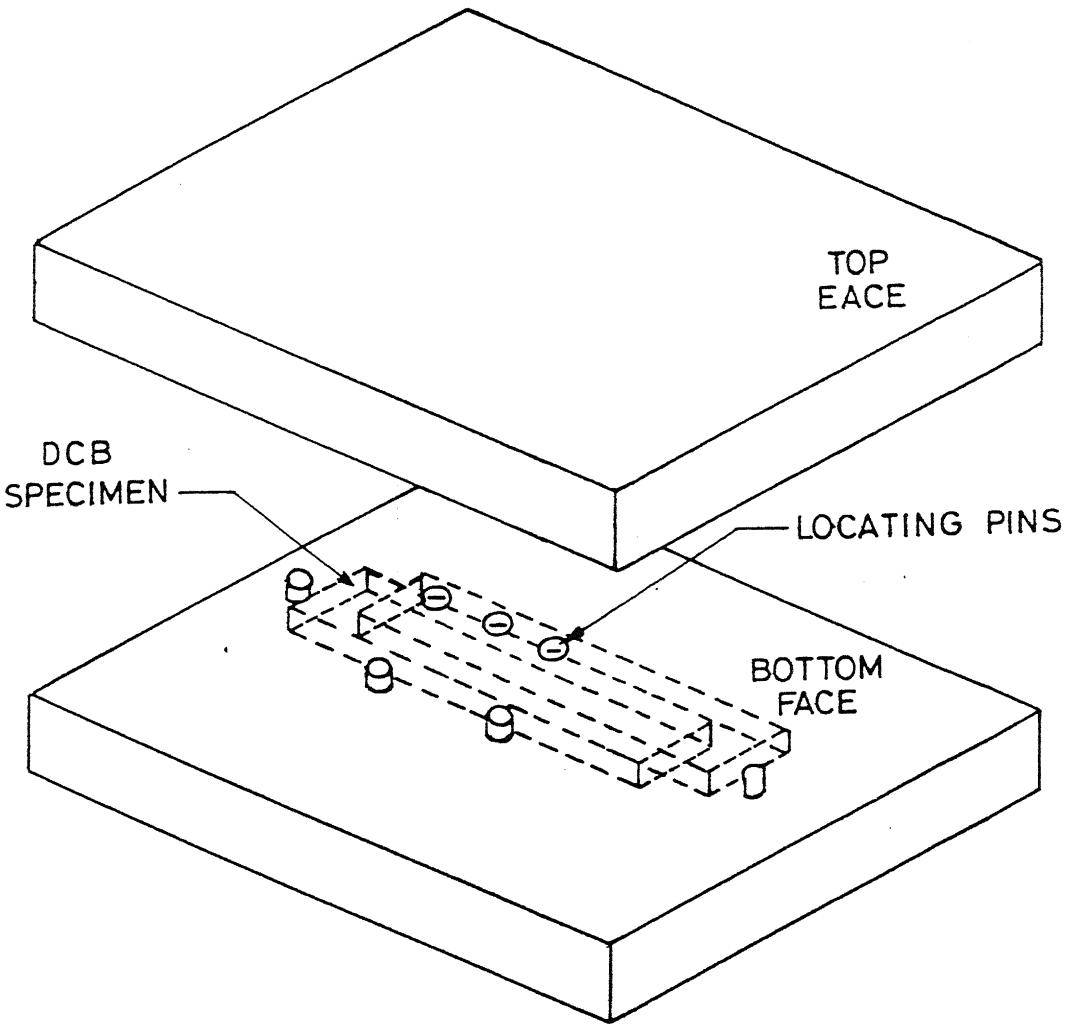

Fig. 3.18 Fixture for bonding the specimen

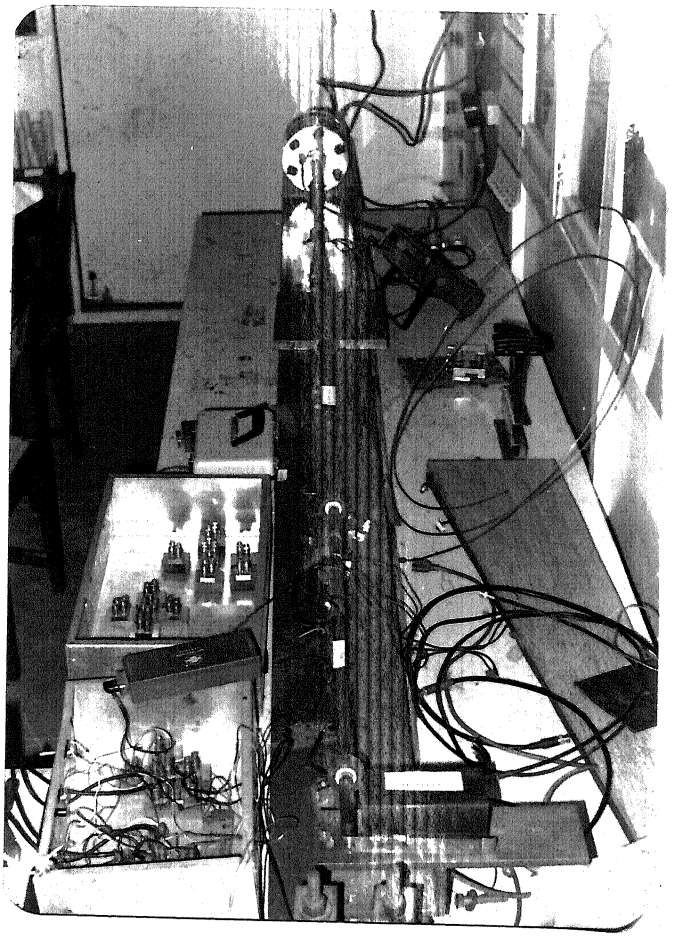

Fig. 3.19 Photograph of the experimental setup

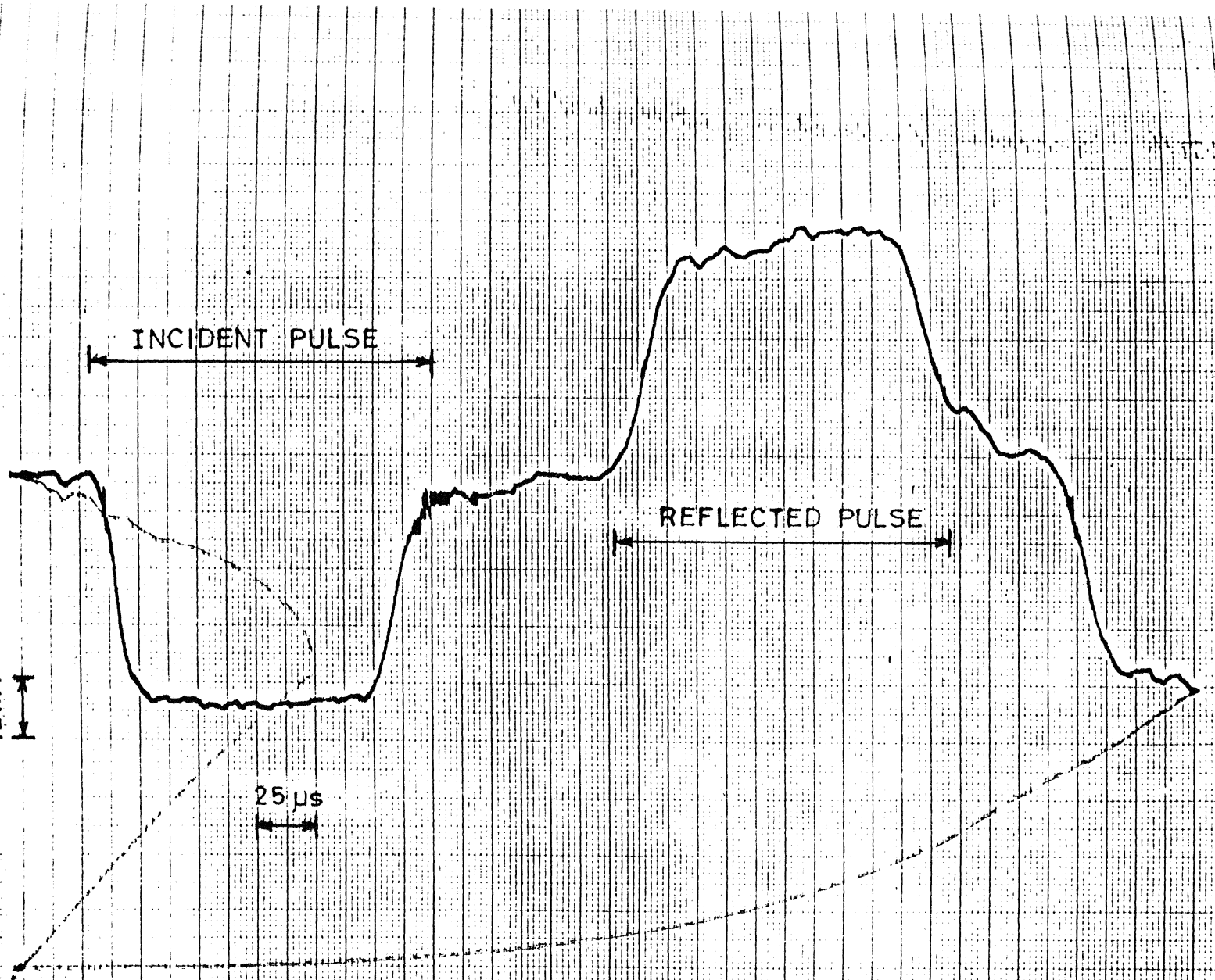

Fig. 3.20 A typical record of stress pulses in the load bar

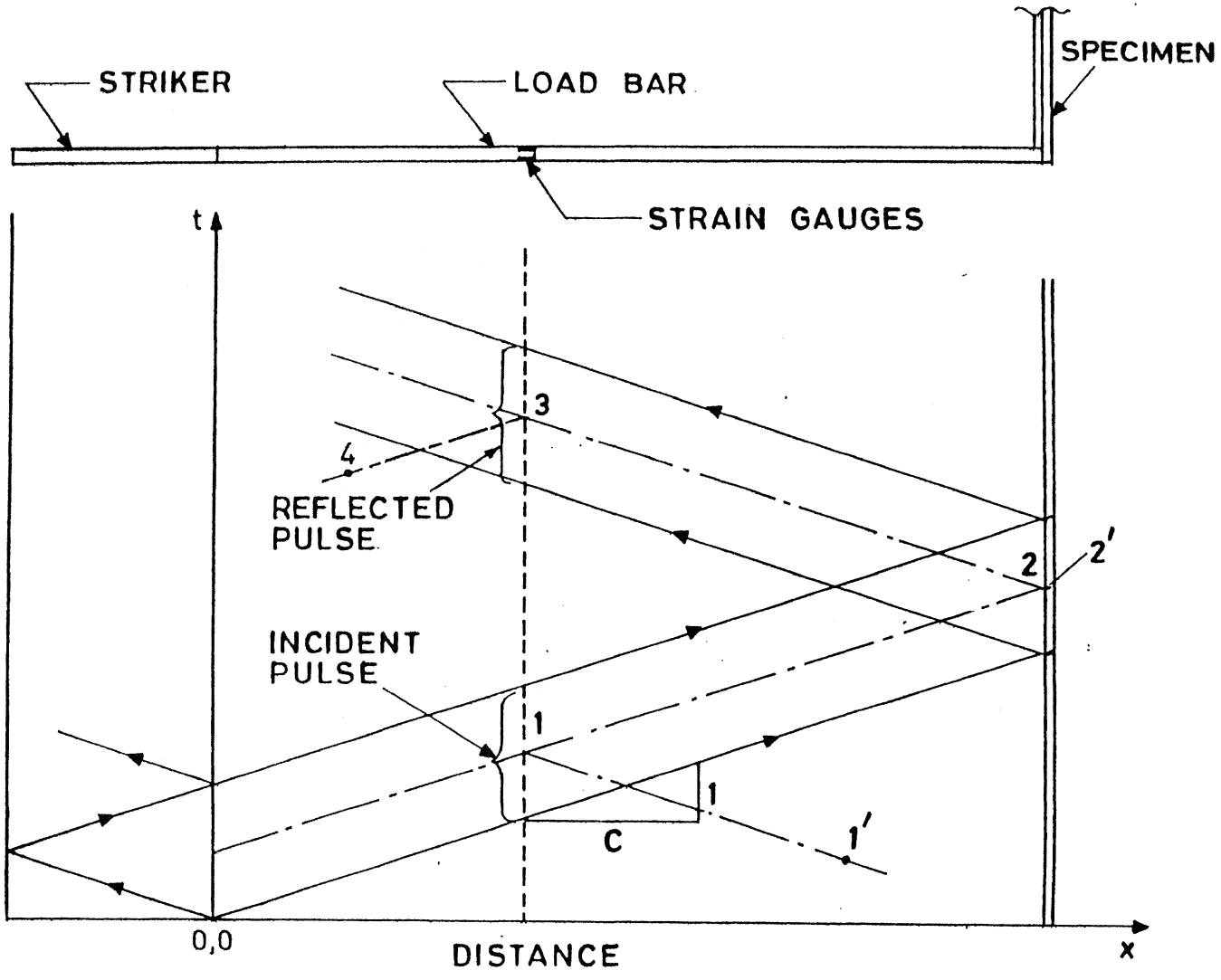

Fig. 3.21 Time-distance (t-x) diagram

R_1 , R_3 : ACTIVE GAUGES

R_2 , R_4 : DUMMY GAUGES

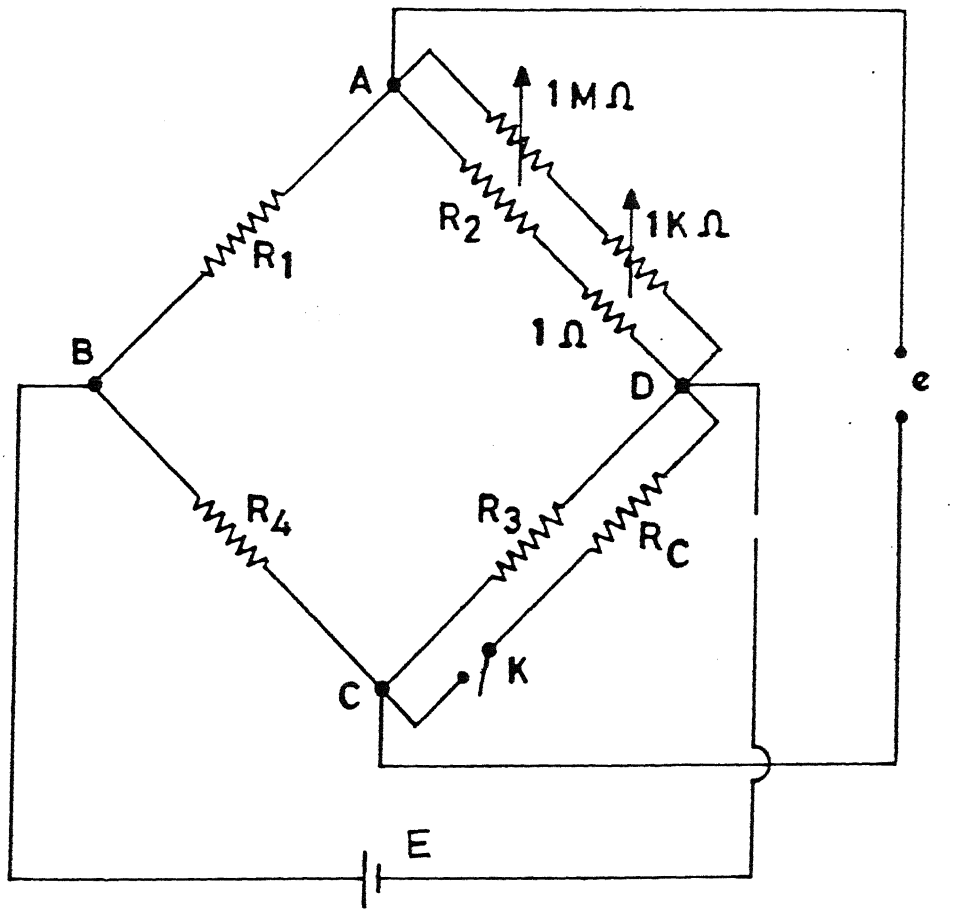

Fig. 3.22 Bridge circuit

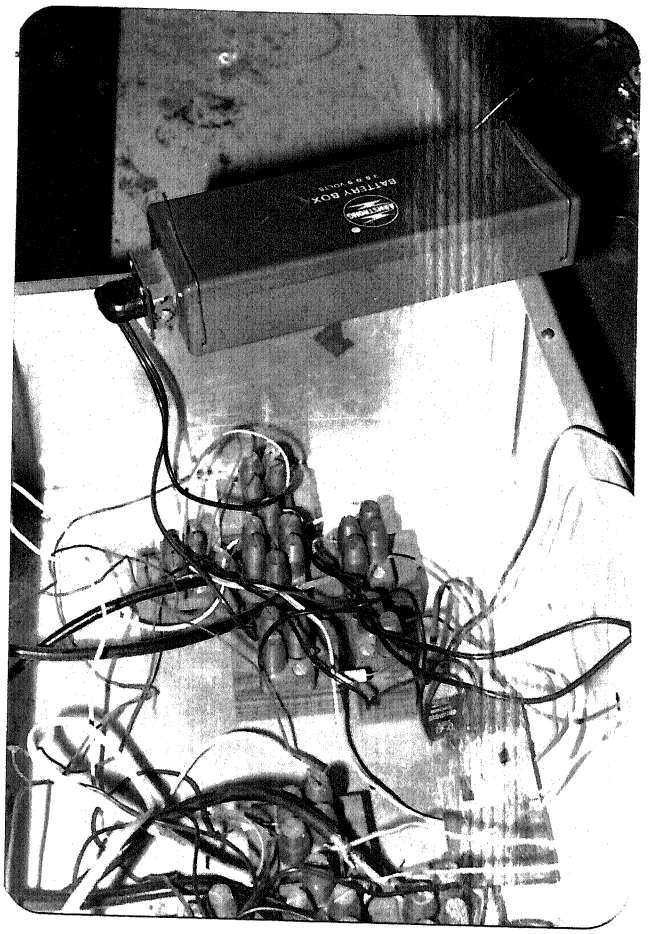

Fig. 3.23 Photograph of the bridge circuit

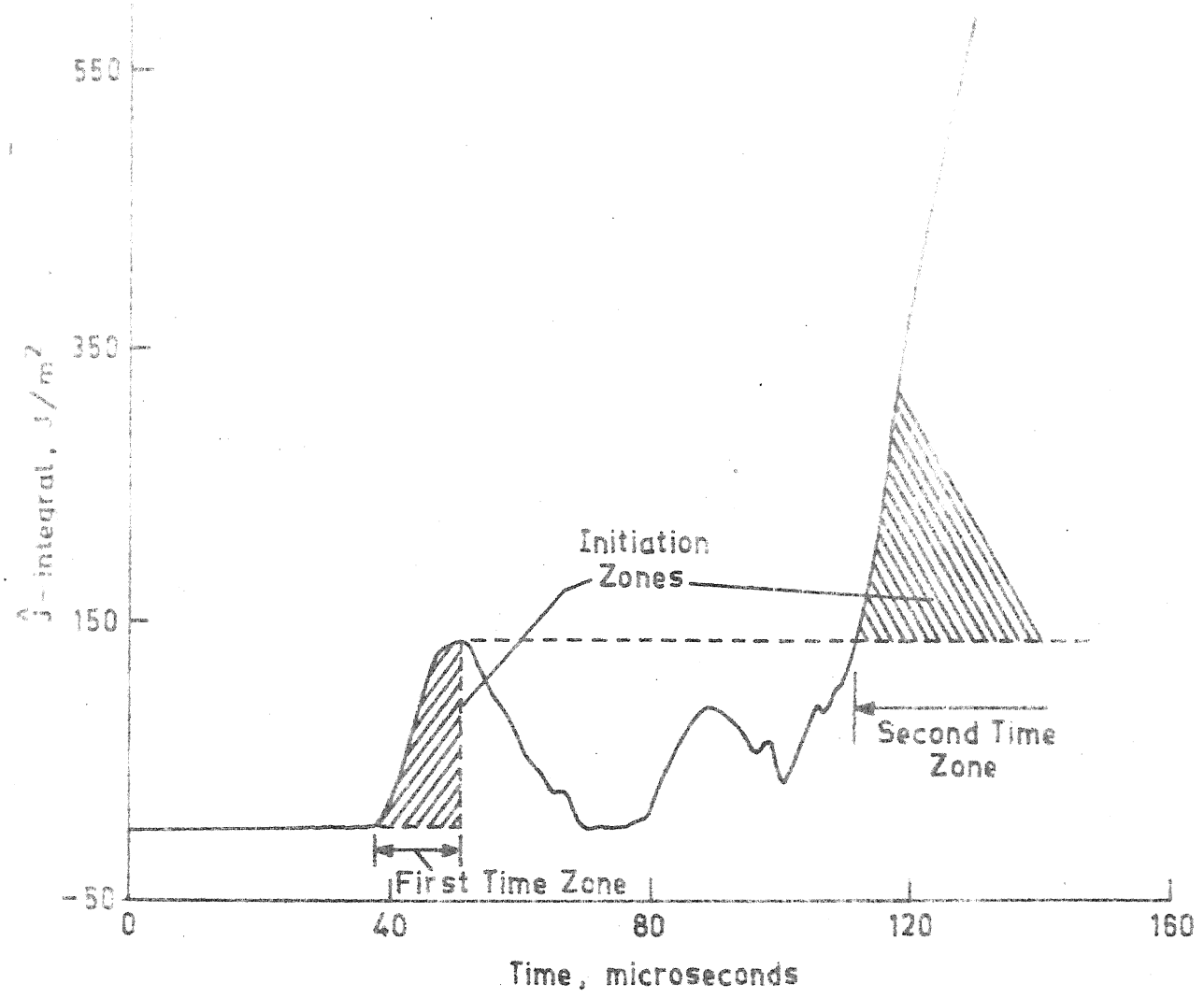

Fig. 3.24 A typical variation of J̇-integral with time for stationary crack

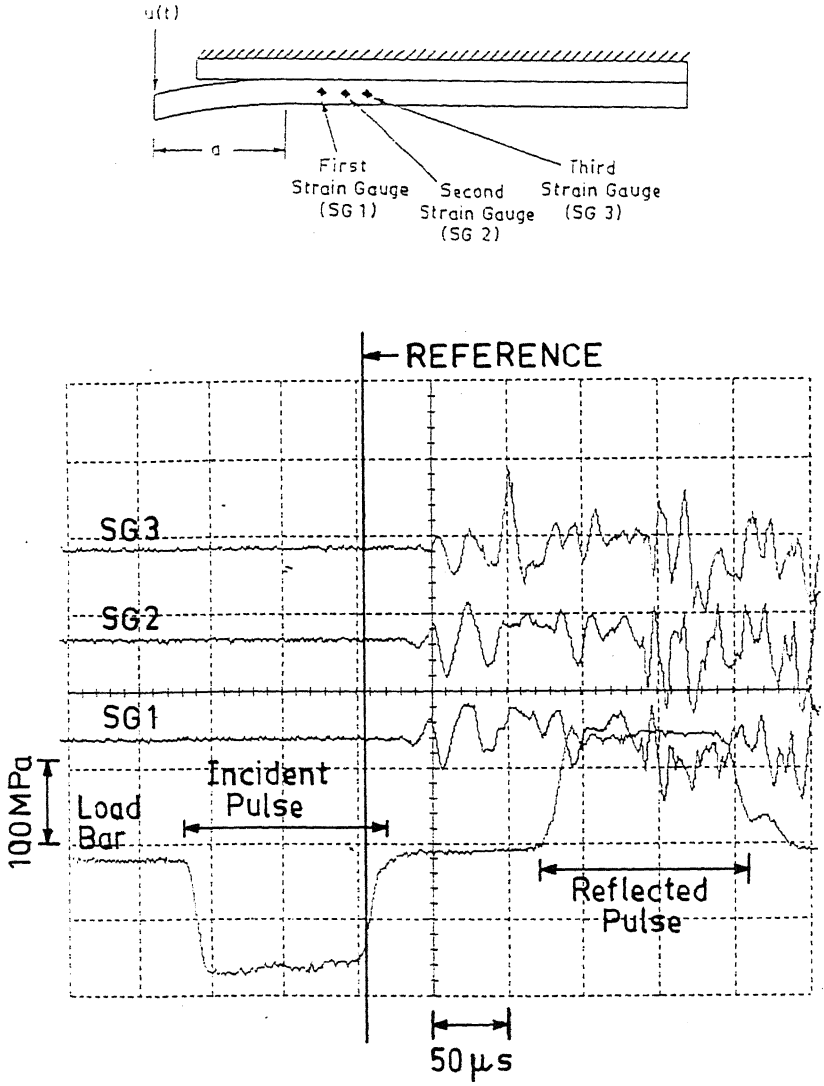

Fig. 3.25 Oscilloscope traces of Expt. 1

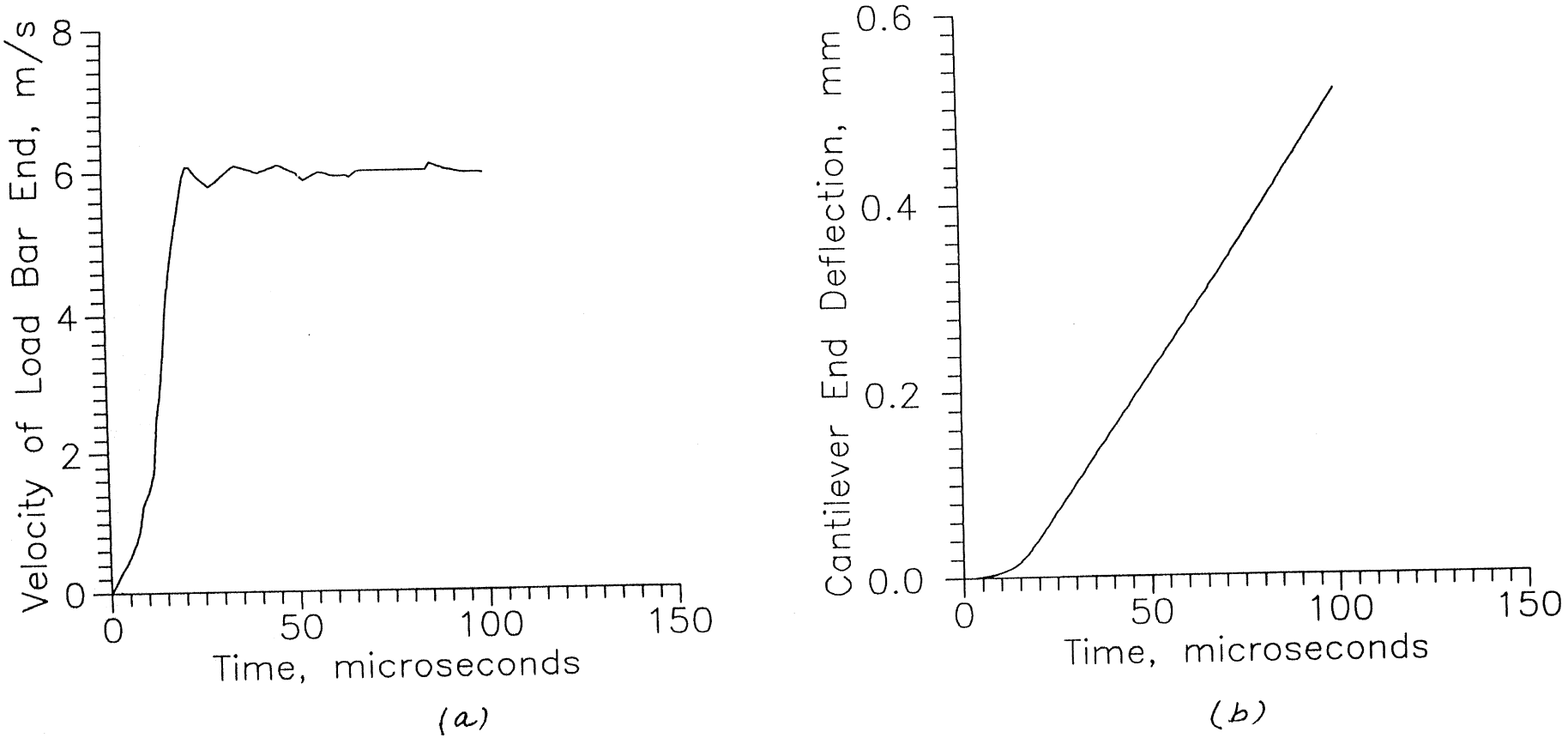

Fig. 3.26 (a) Velocity input at the cantilever end of the specimen obtained through incident and reflected Pulses of the load bar for Expt.–1

(b) Cantilever end deflection vs. time obtained by integrating the velocity input curve

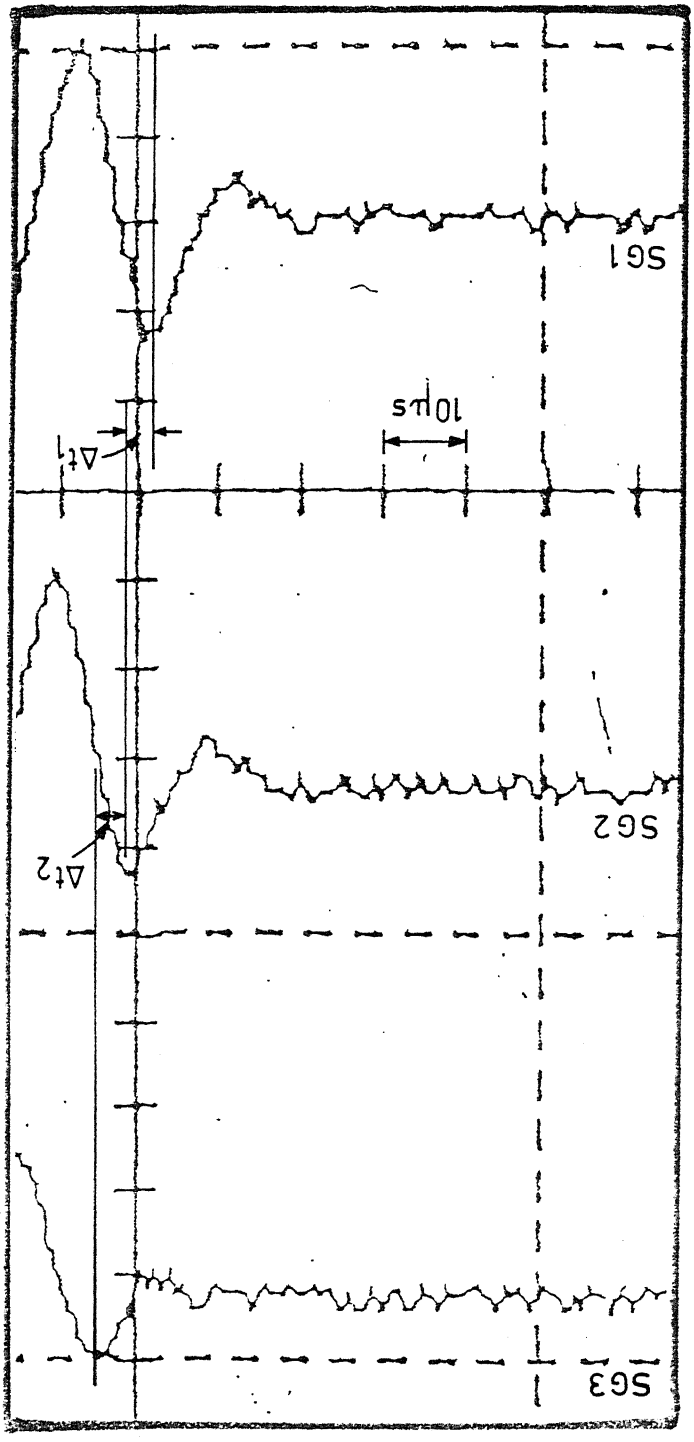

Fig. 3.27 Blown up view of the recorded peak responses of strain gauge bonded to the specimen of Expt. 1

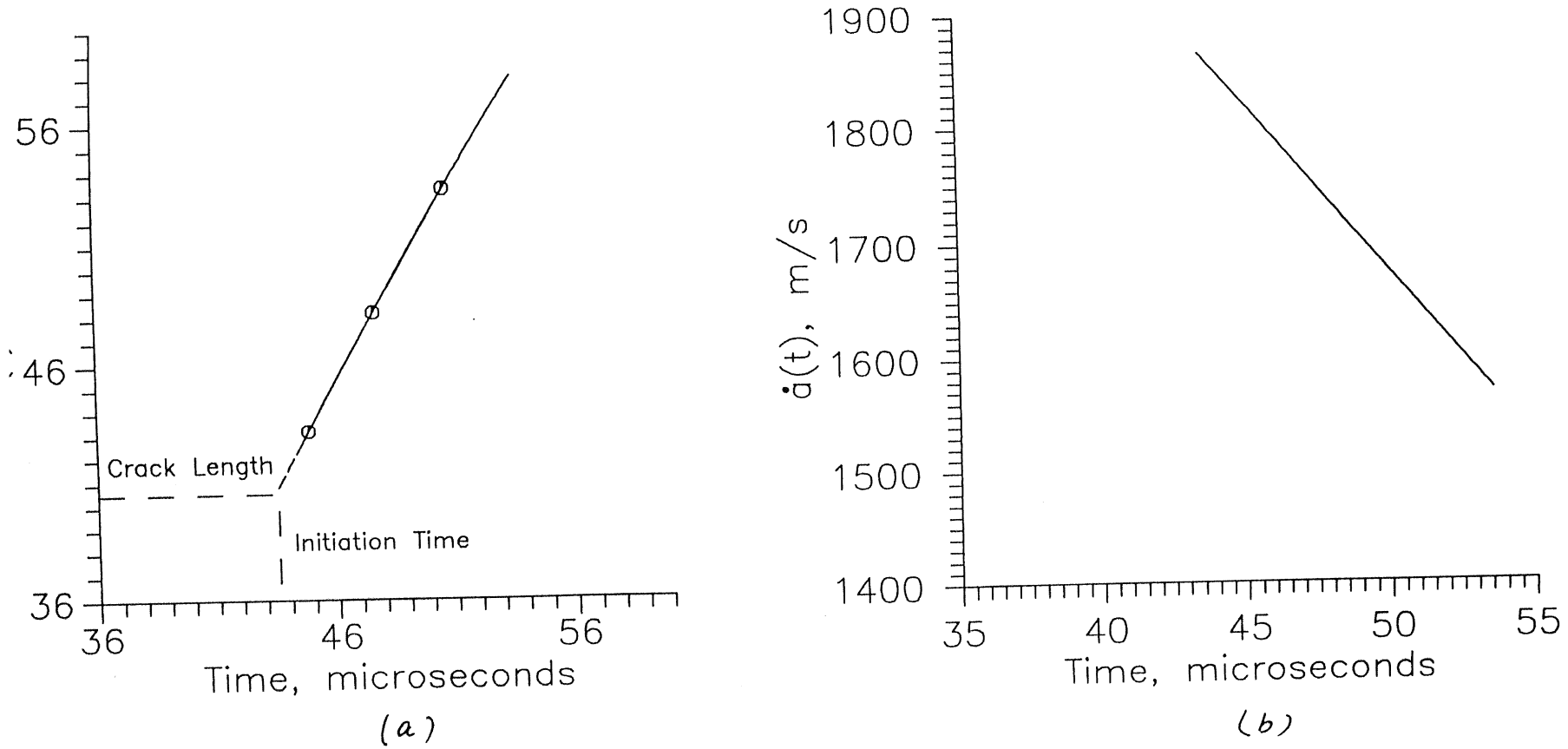

Fig. 3.28 (a) Variation of crack length with time of Expt.—1 shown with interpolation upto the length of precrack

(b) Variation of crack propagation speed with time obtained by differentiating the crack length vs time curve

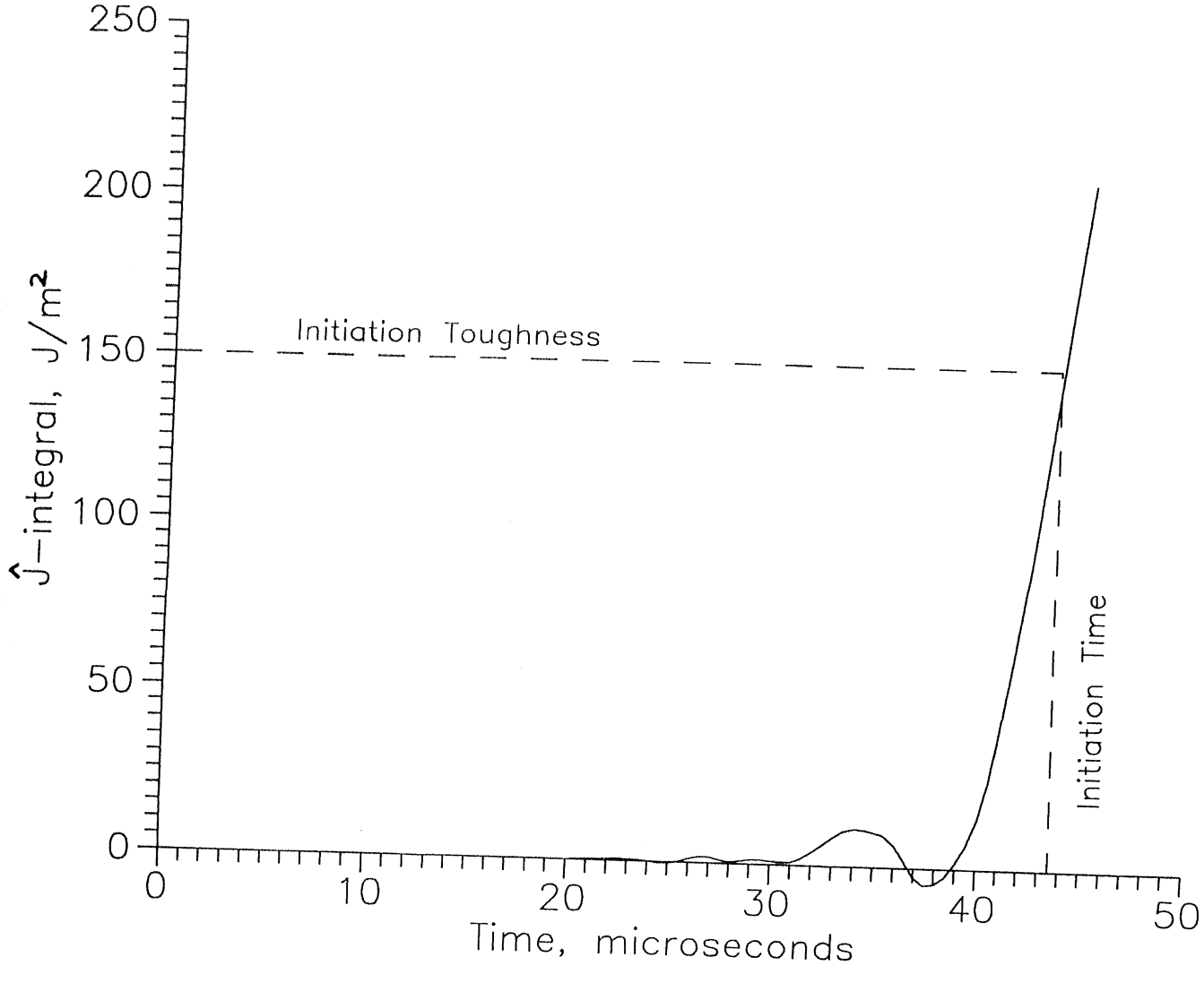

Fig. 3.29 Initiation toughness of Expt.–1

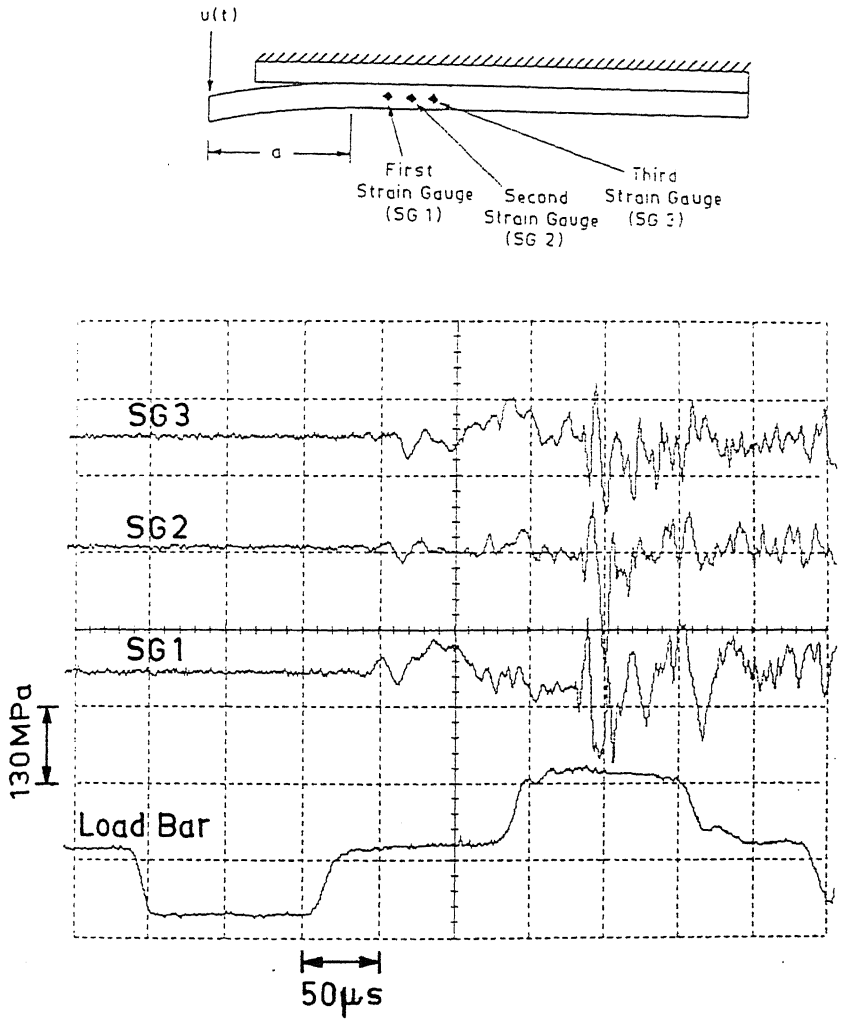

Fig. 3.30 Oscilloscope traces of Expt. 2

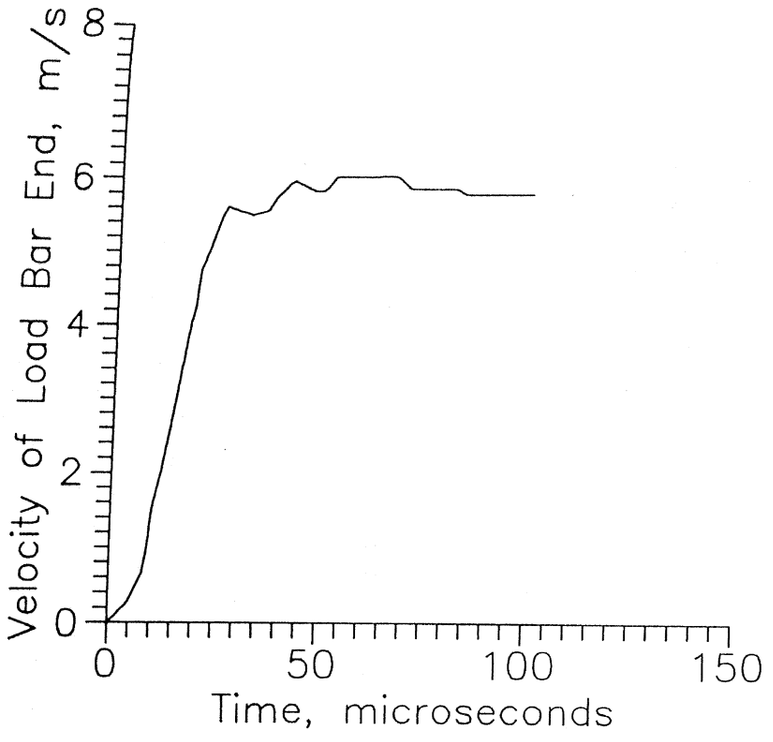

(a)

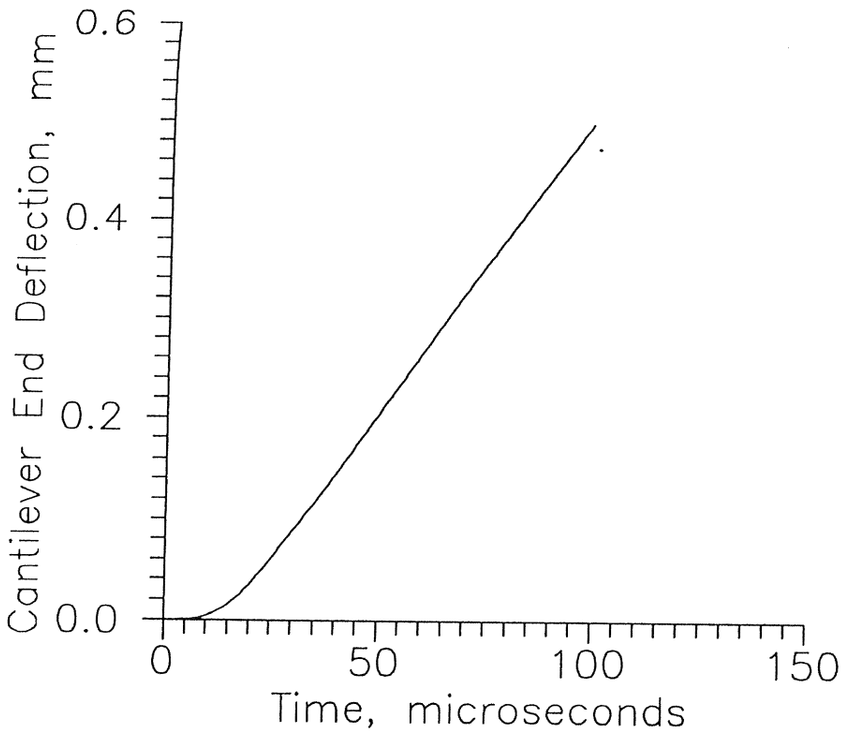

(b)

Fig. 3.31 (a) Velocity input at the cantilever end of the specimen obtained through incident and reflected Pulses of the load bar for Expt.–2

(b) Cantilever end deflection vs. time obtained by integrating the velocity input curve

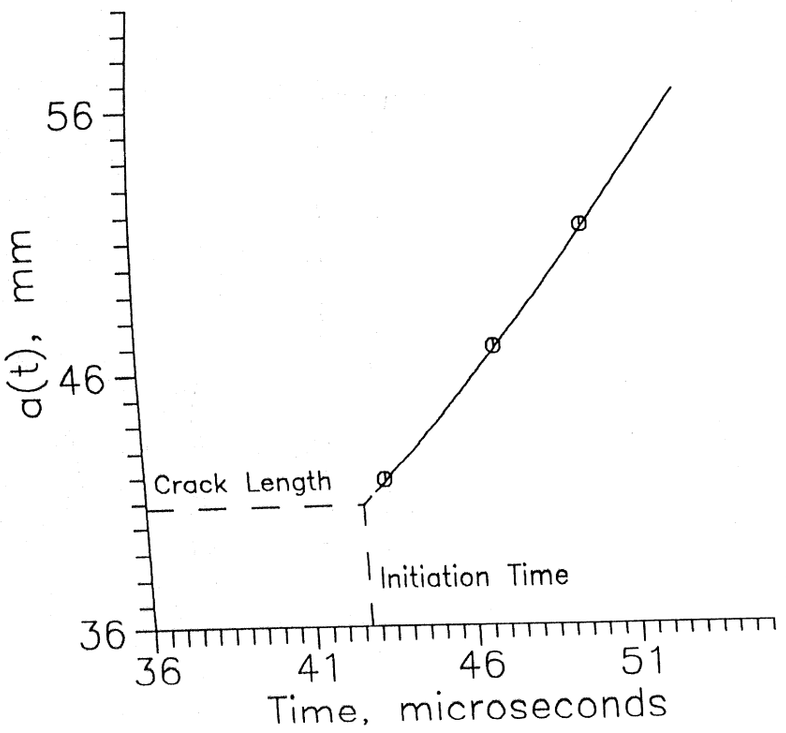

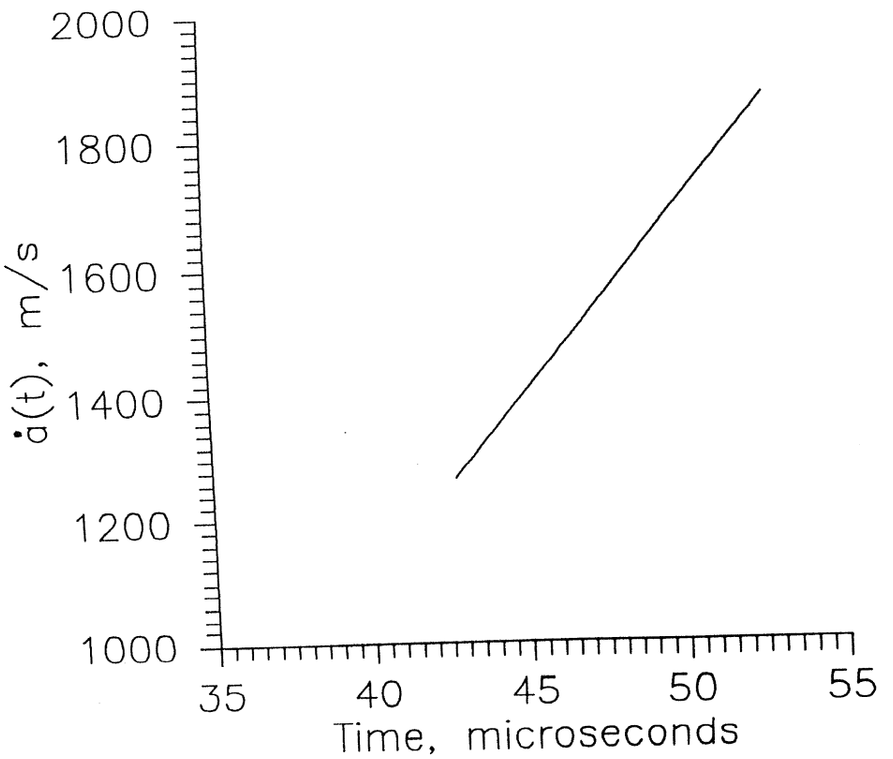

Fig. 3.32 (a) Variation of crack length with time of Expt.–2 shown with interpolation upto the length of precrack

(b) Variation of crack propagation speed with time obtained by differentiating the crack length vs time curve

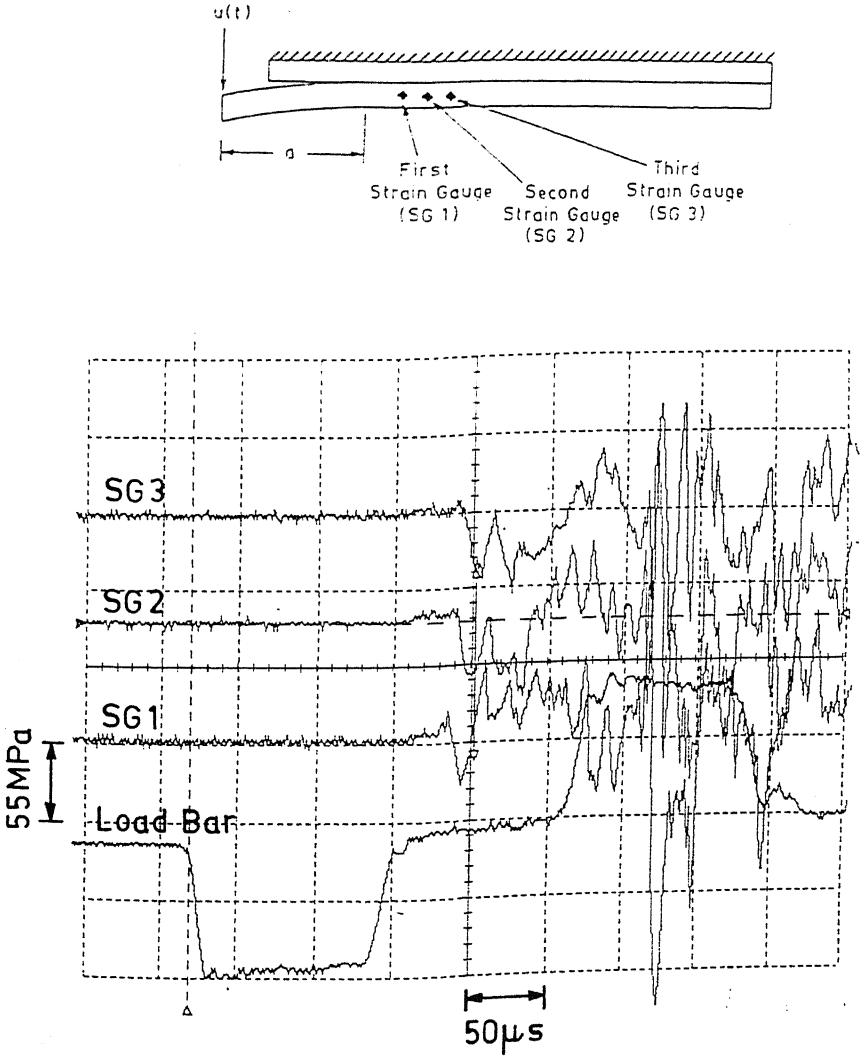

Fig. 3.34 Oscilloscope traces of Expt. 3

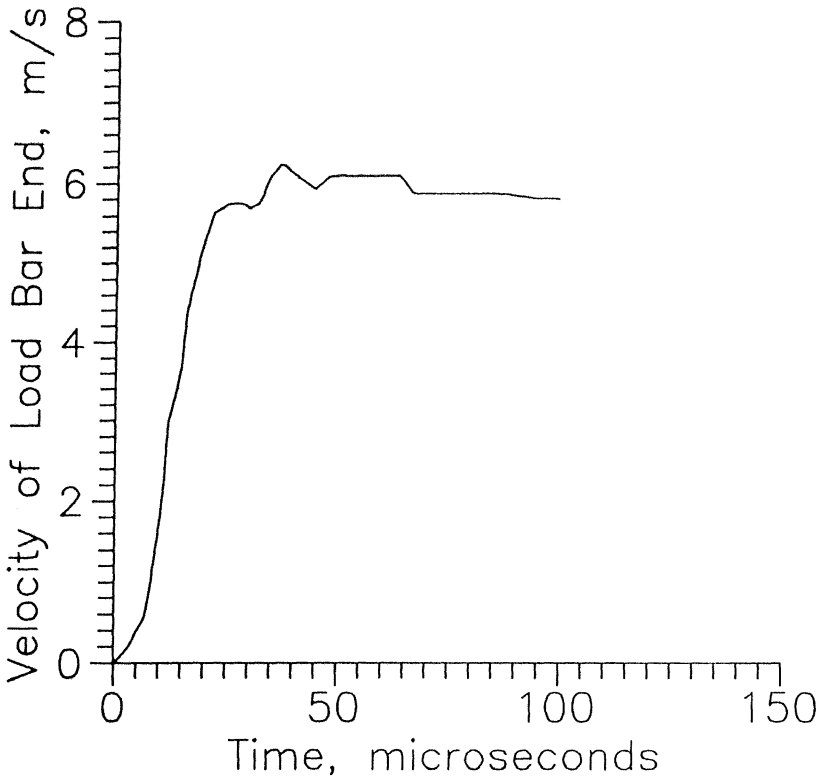

(a)

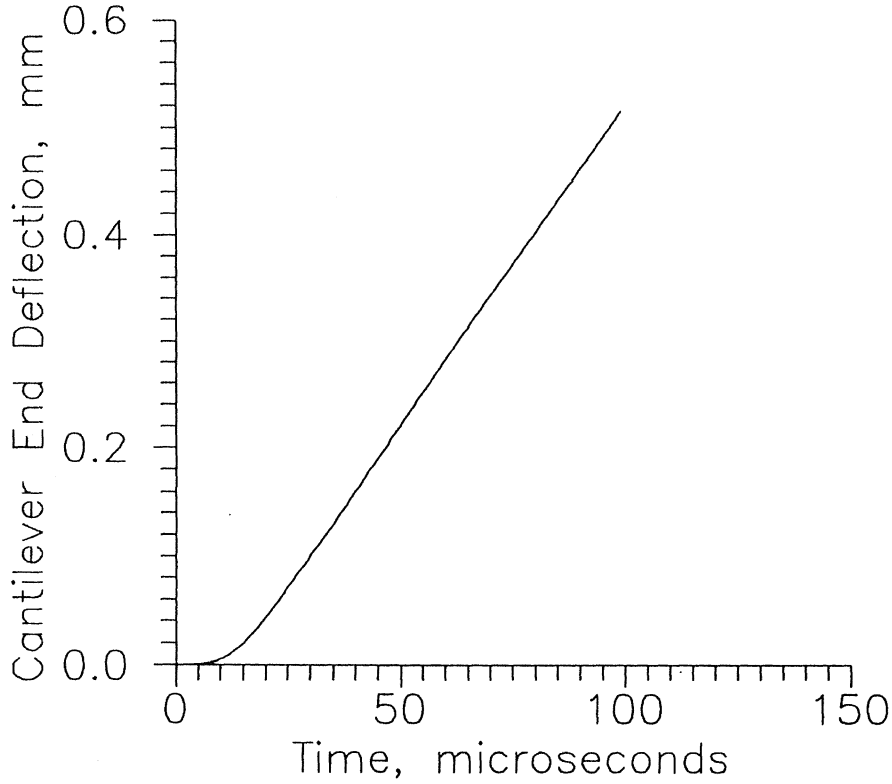

(b)

Fig. 3.35(a) Velocity input at the cantilever end of the specimen obtained through incident and reflected Pulses of the load bar for Expt.–3

(b) Cantilever end deflection vs. time obtained by integrating the velocity input curve

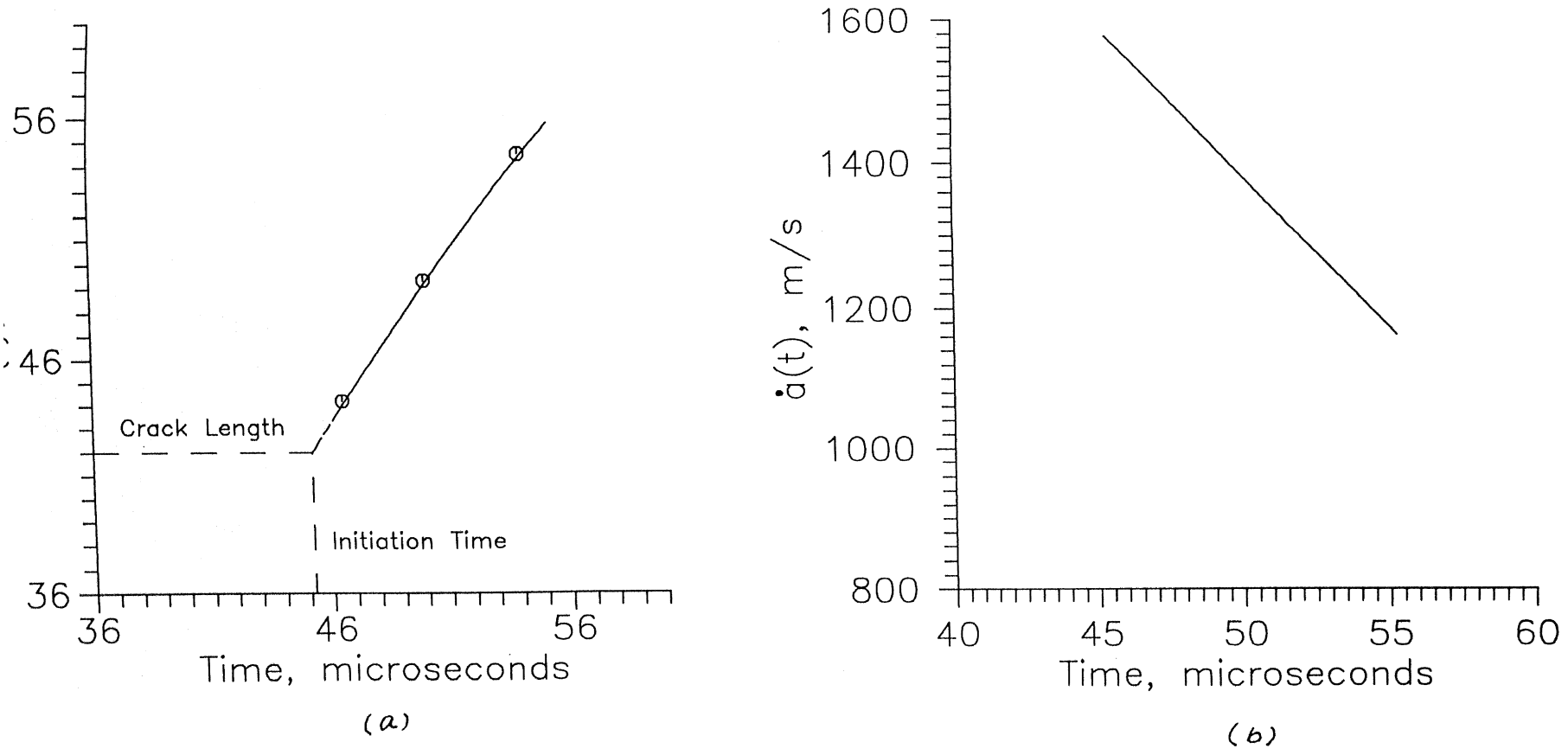

Fig. 3.36 (a) Variation of crack length with time of Expt.–3 shown with interpolation upto the length of precrack

(b) Variation of crack propagation speed with time obtained by differentiating the crack length vs time curve

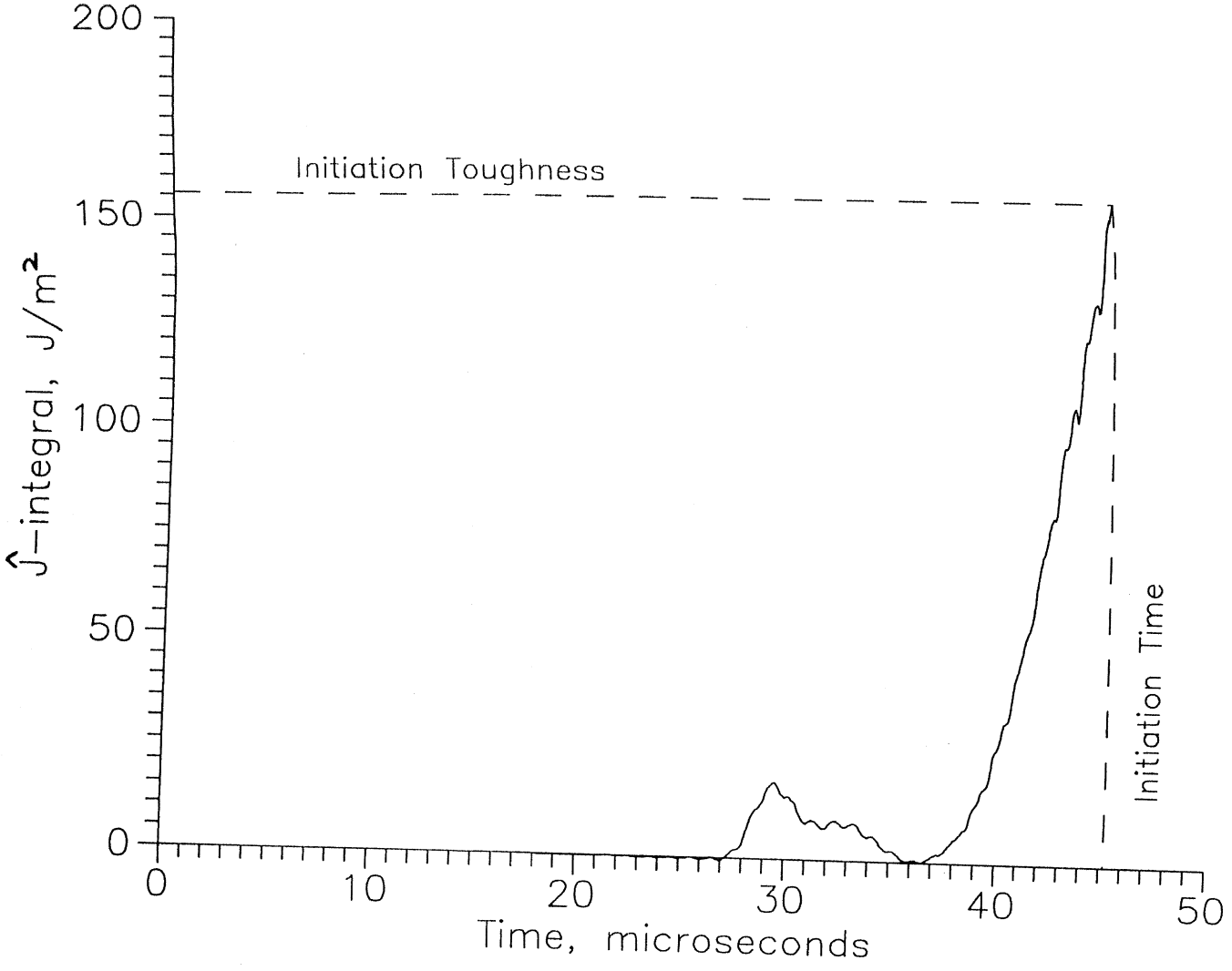

Fig. 3.37 Initiation toughness of Expt.–3

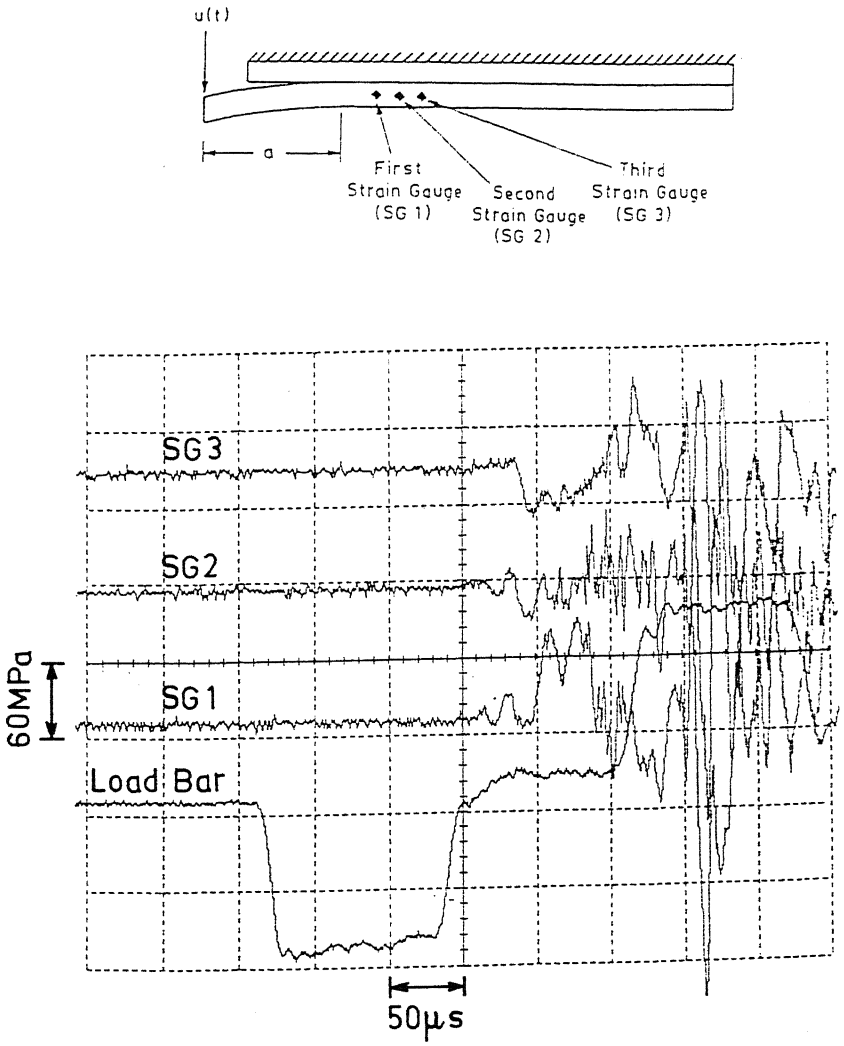

Fig. 3.38 Oscilloscope traces of Expt. 4

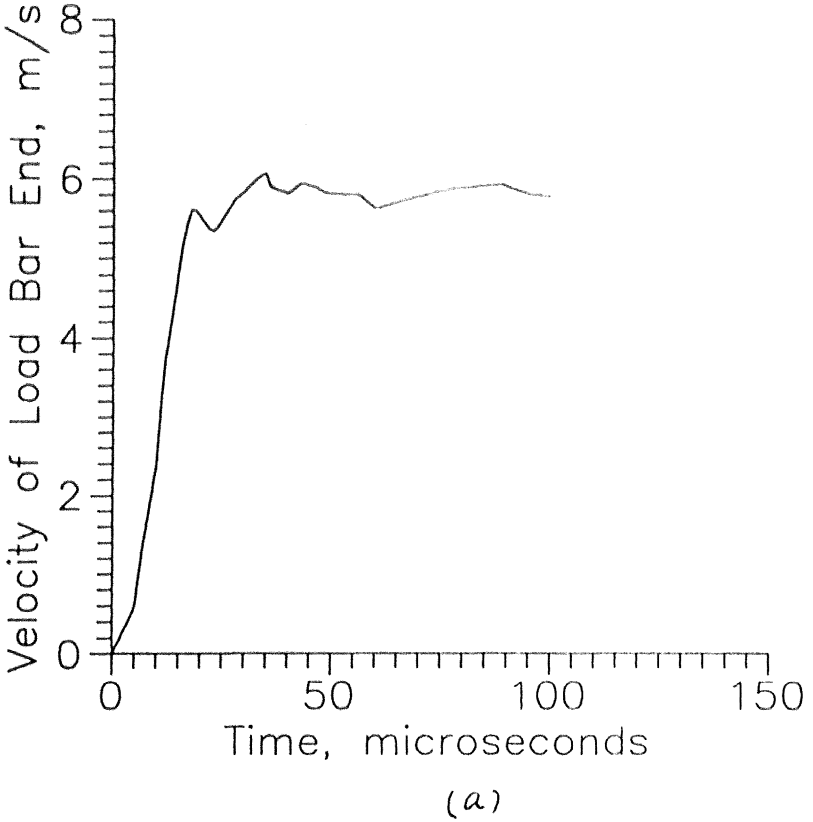

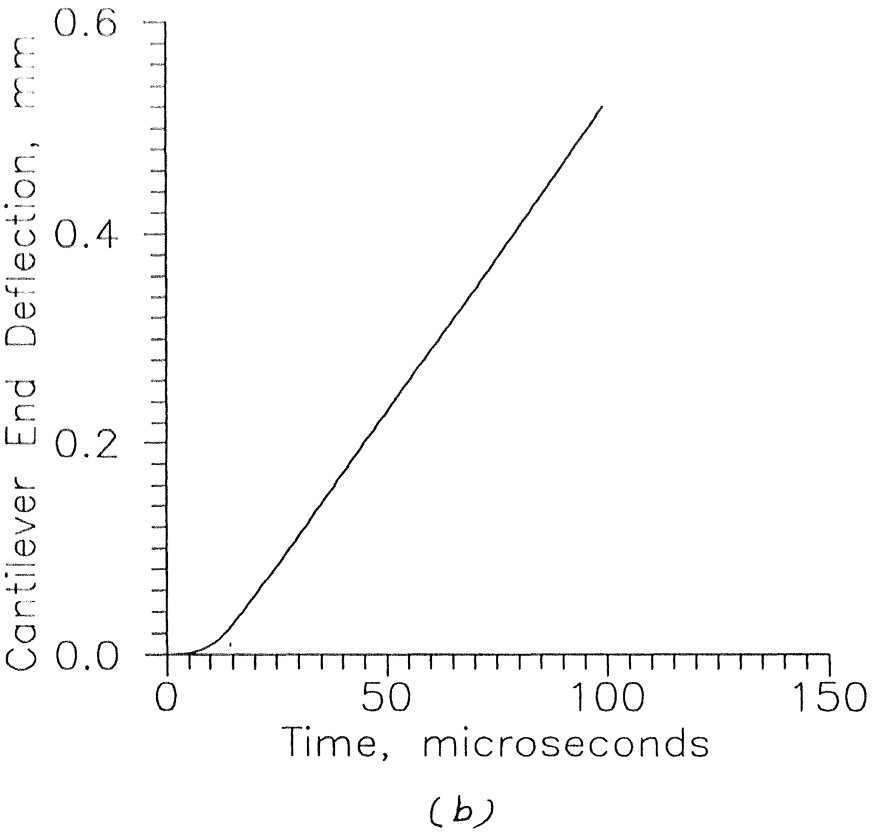

Fig. 3.39 (a) Velocity input at the cantilever end of the specimen obtained through incident and reflected Pulses of the load bar for Expt.–4

(b) Cantilever end deflection vs. time obtained by integrating the velocity input curve

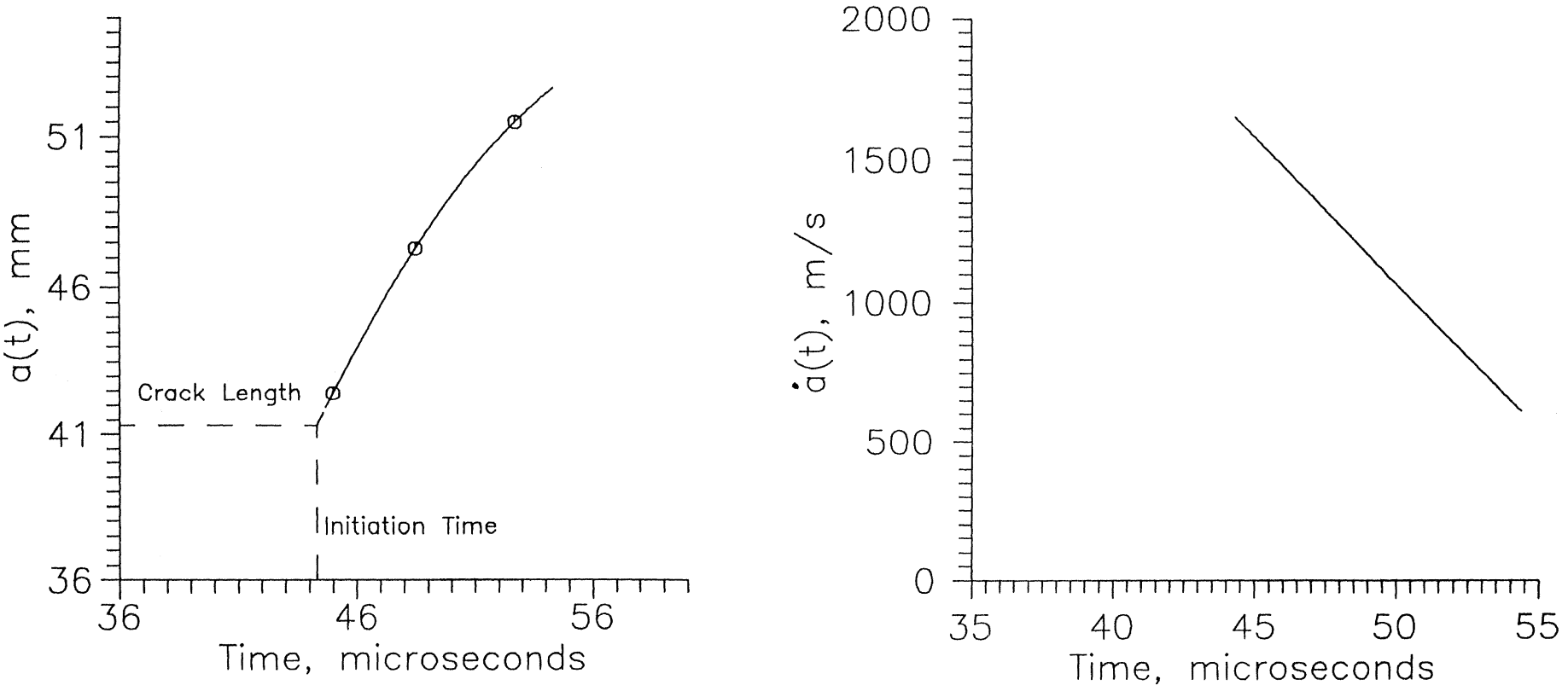

Fig. 3.40 (a) Variation of crack length with time of Expt.–4 shown with interpolation upto the length of precrack

(b) Variation of crack propagation speed with time obtained by differentiating the crack length vs time curve

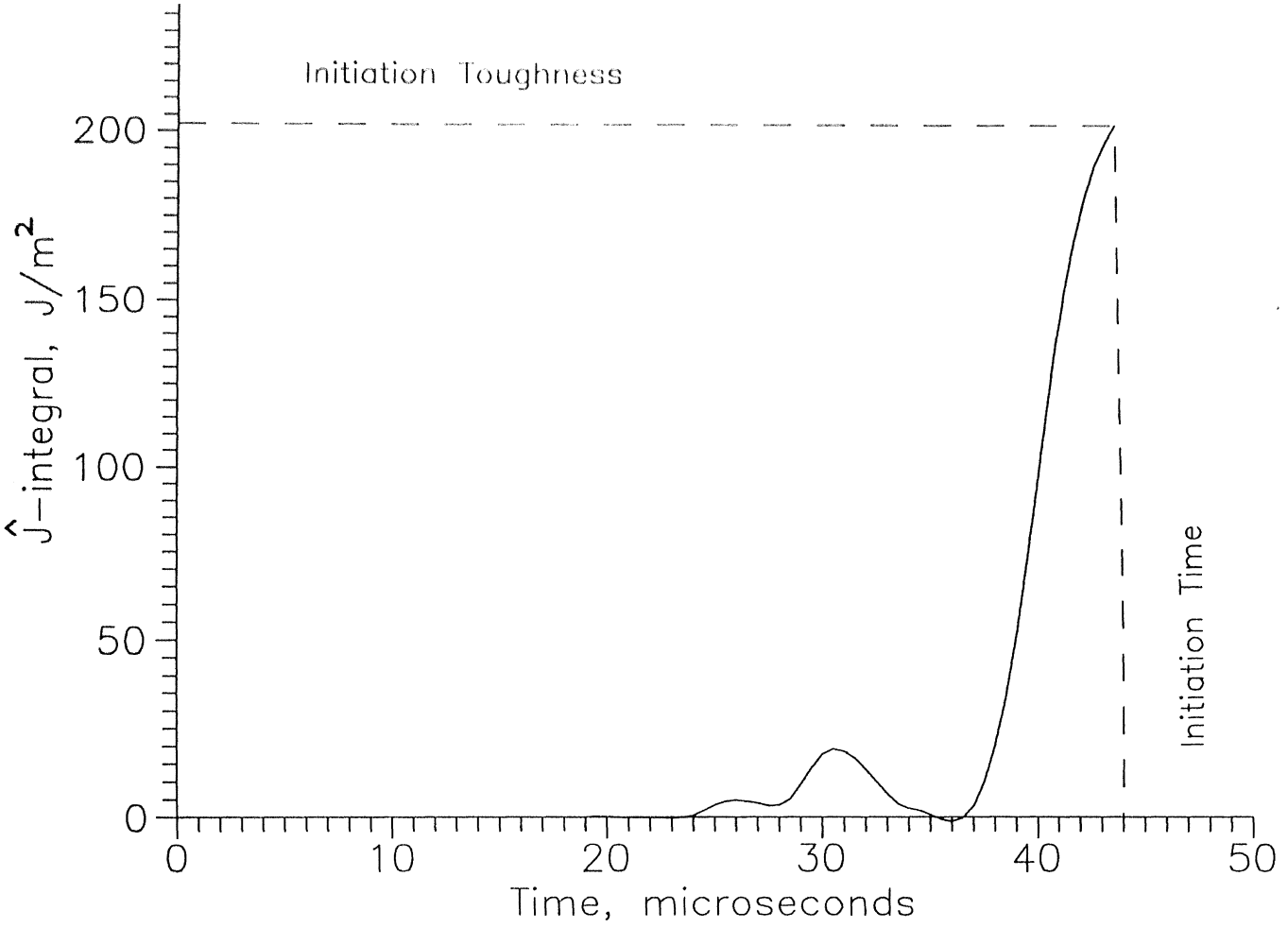

Fig. 3.41 Initiation toughness of Expt.–4

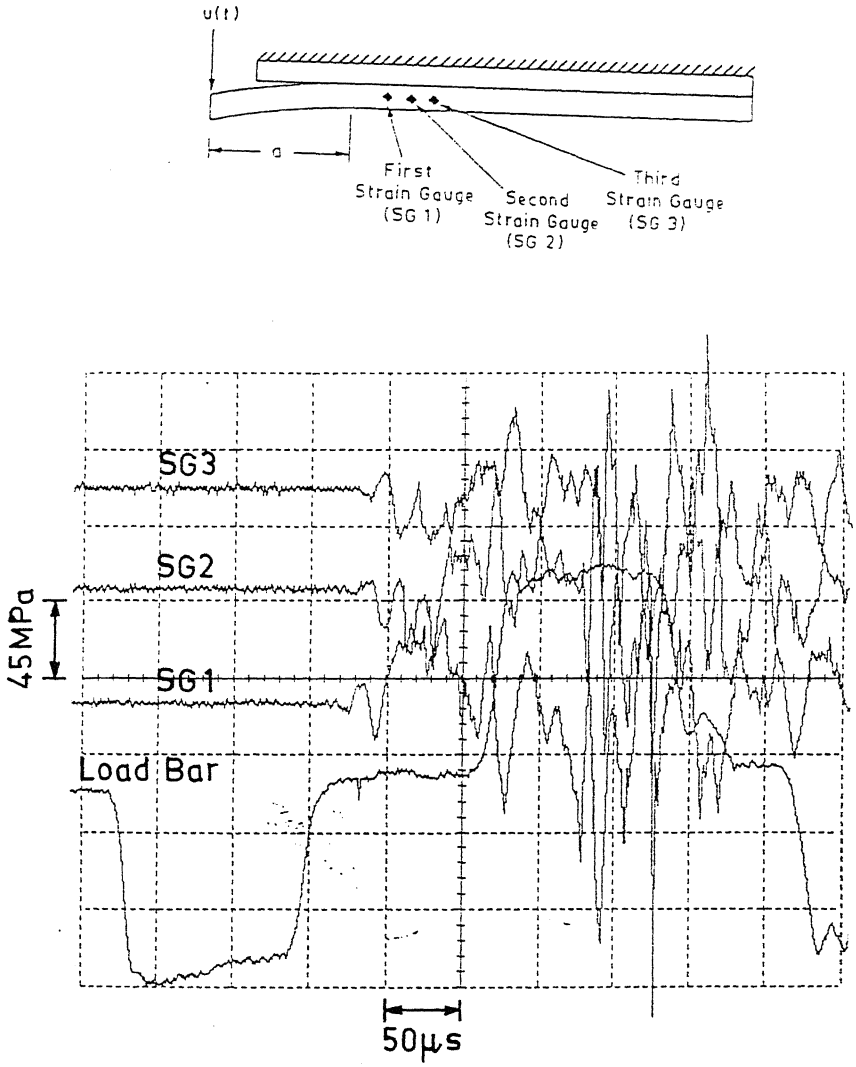

Fig. 3.42 Oscilloscope traces of Expt. 5

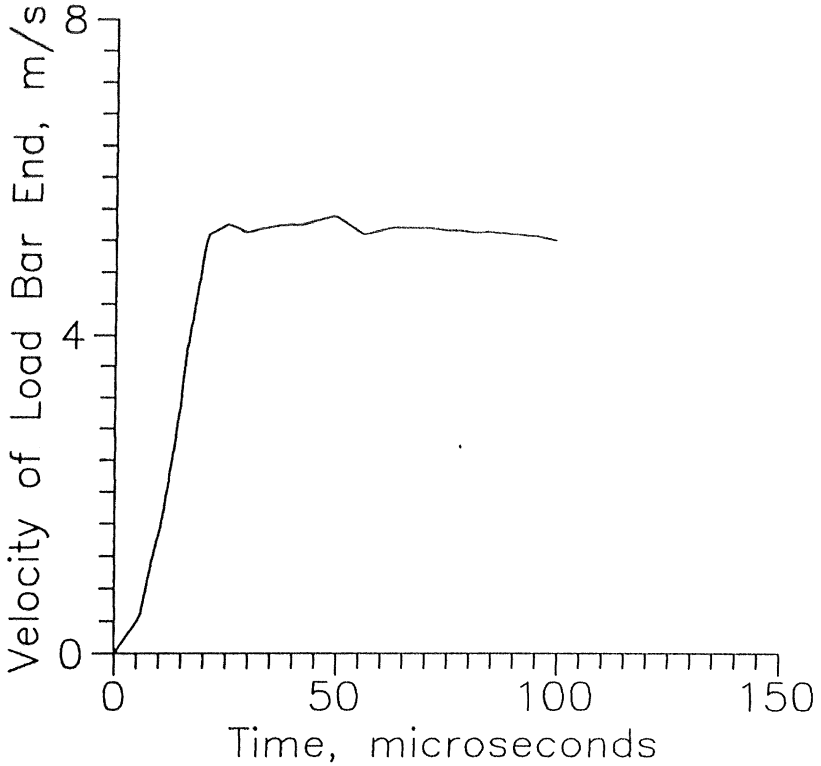

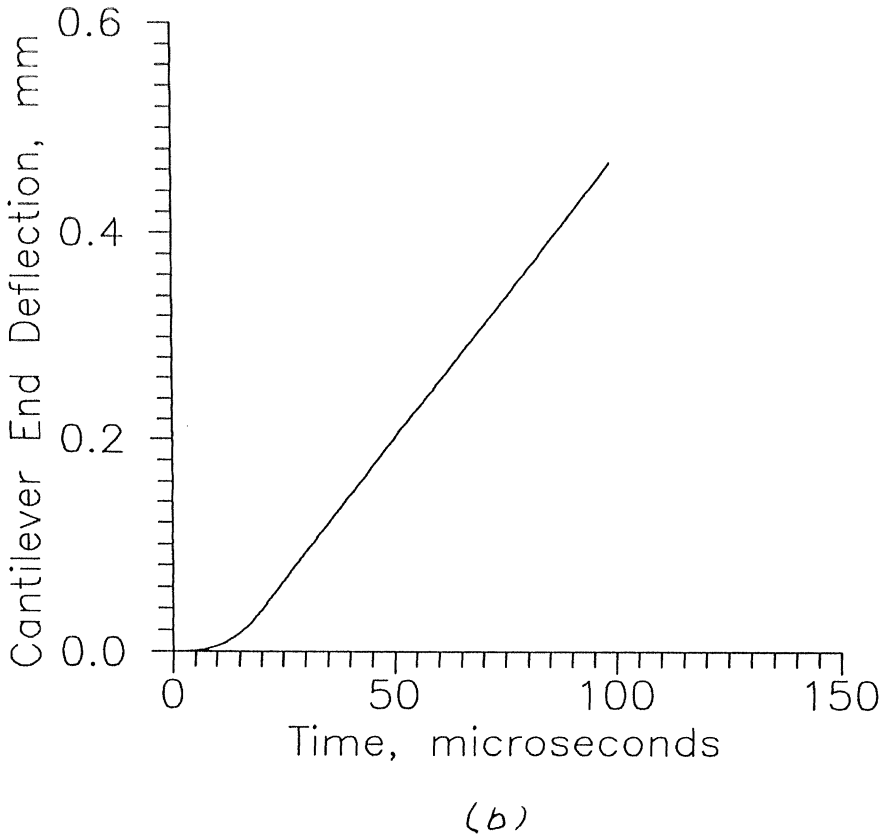

Fig. 3.43 (a) Velocity input at the cantilever end of the specimen obtained through incident and reflected Pulses of the load bar for Expt.–5

(b) Cantilever end deflection vs. time obtained by integrating the velocity input curve

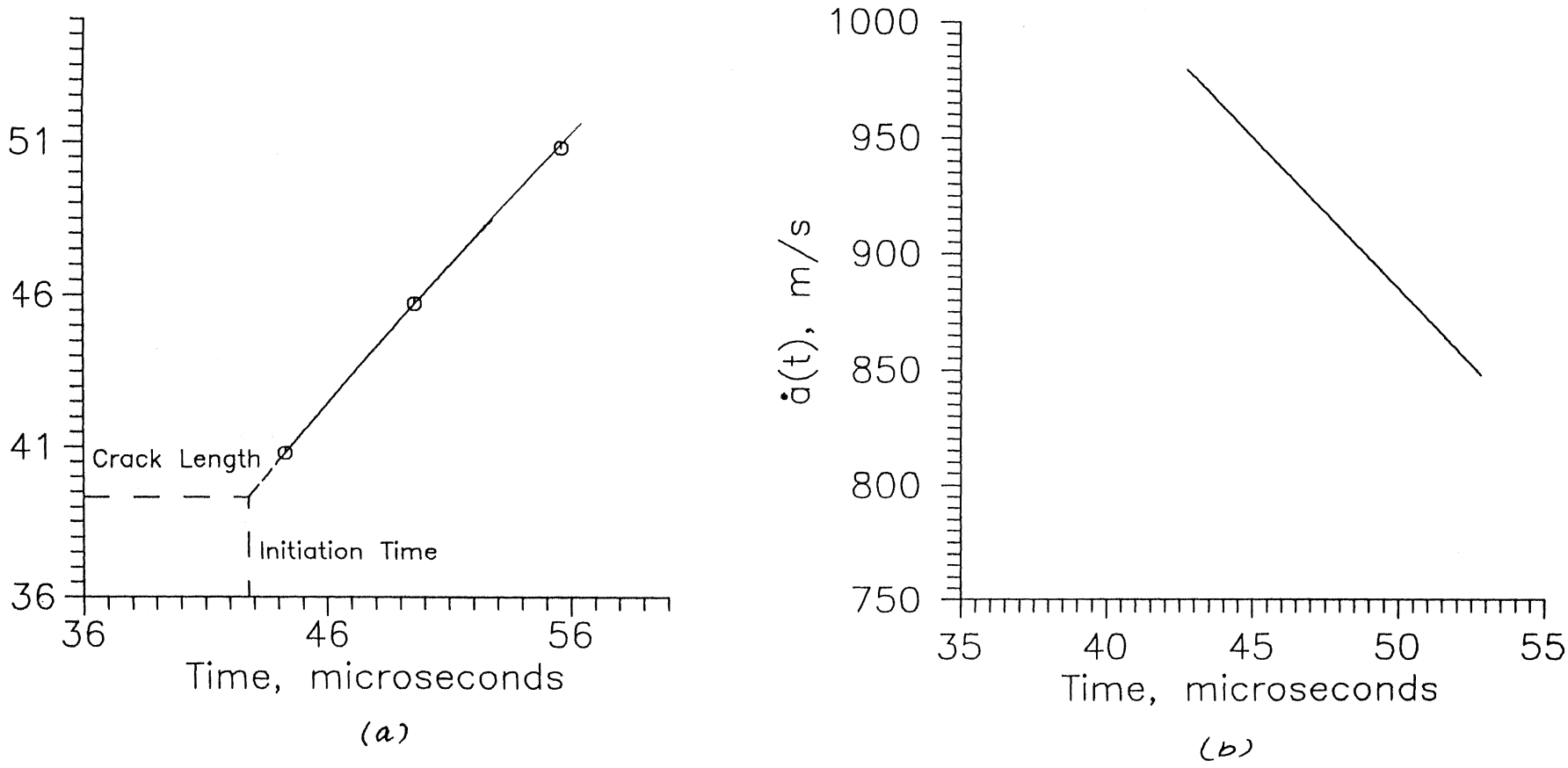

Fig. 3.44 (a) Variation of crack length with time of Expt.–5 shown with interpolation upto the length of precrack

(b) Variation of crack propagation speed with time obtained by differentiating the crack length vs time curve

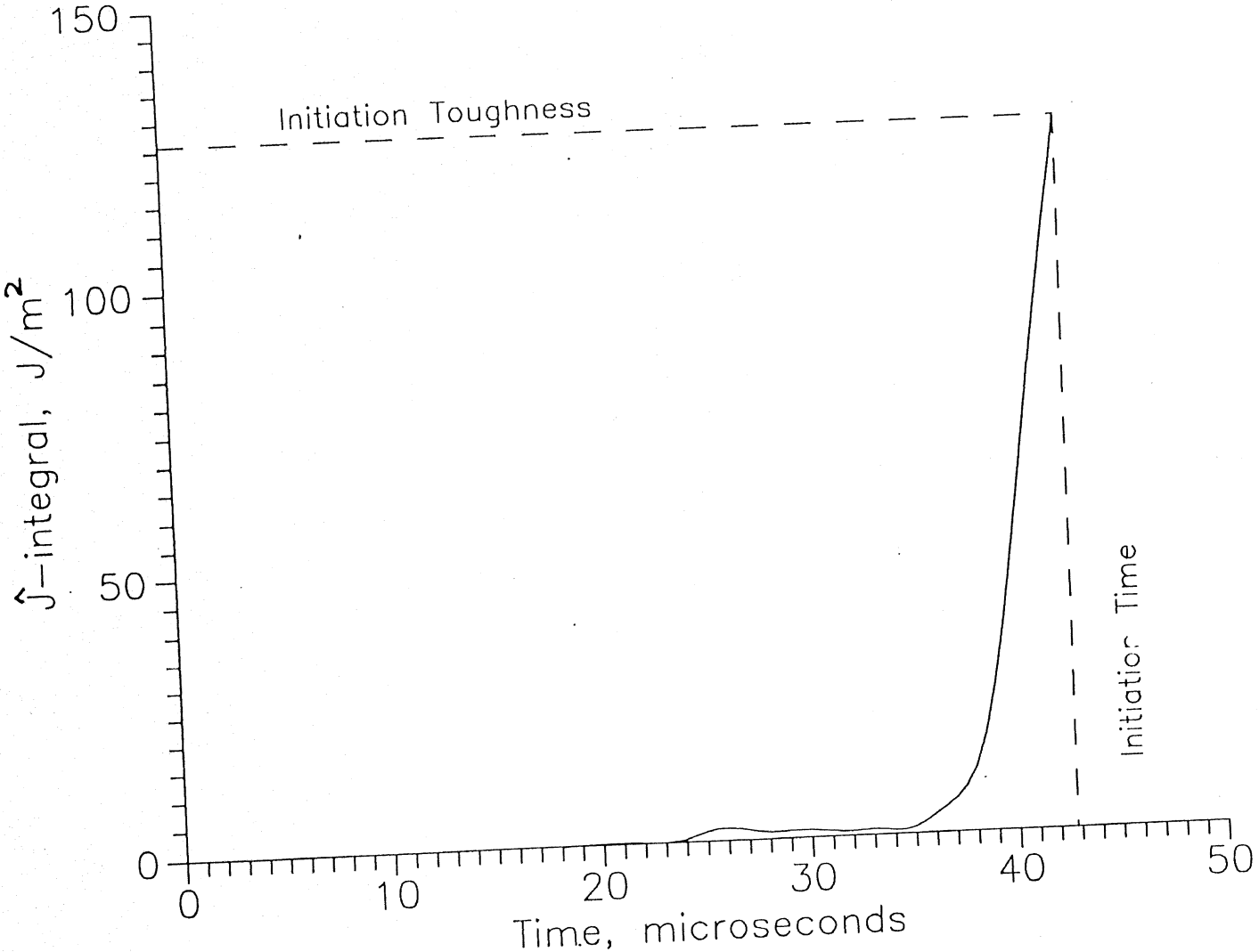

Fig. 3.45 Initiation toughness of Expt.–5

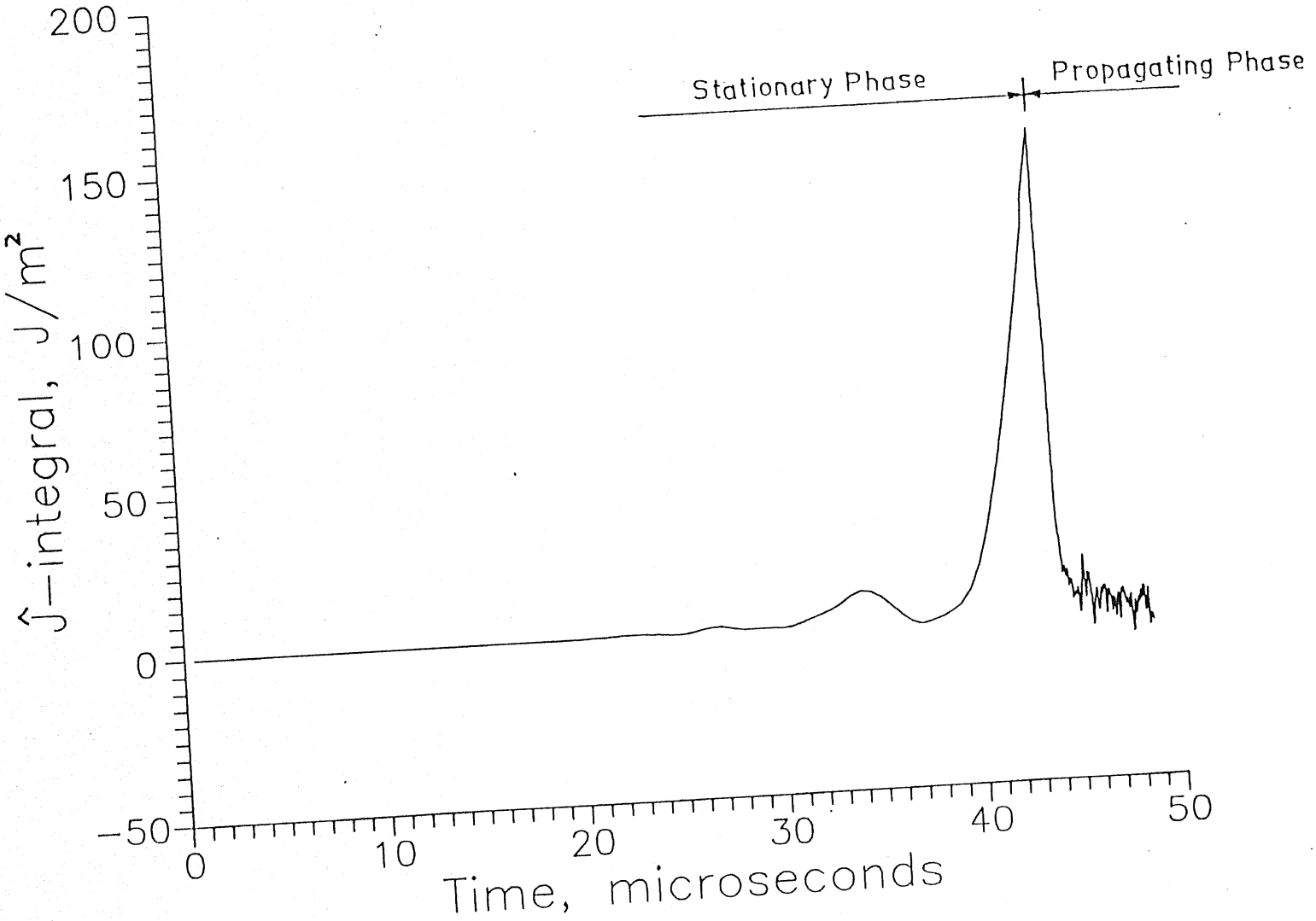

Fig. 3.46 Variation of $\hat{J}$−integral with time for stationary crack and propagating crack of Expt.−1

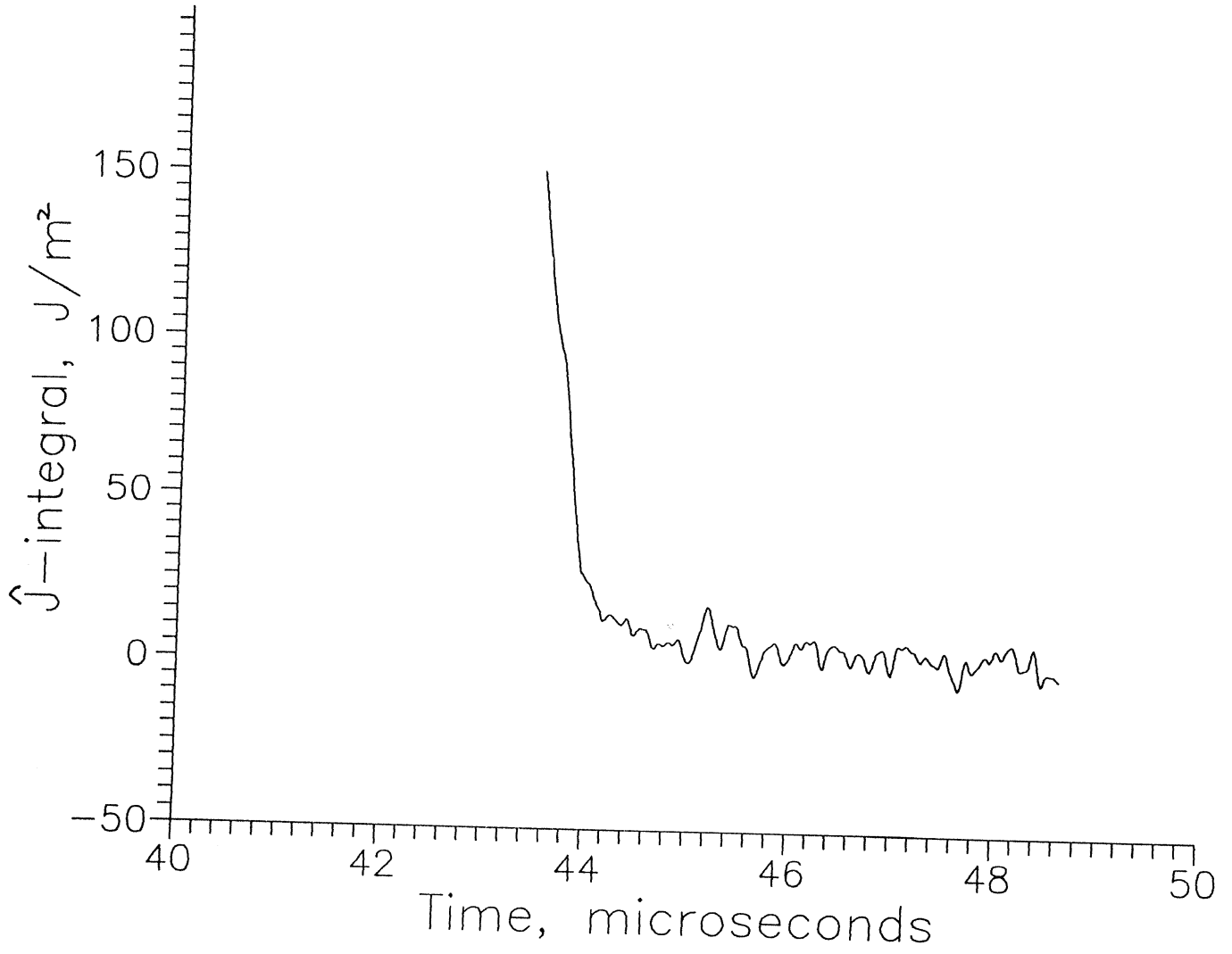

Fig. 3.47 Variation of $\hat{J}$−integral after the crack strat propagating for Expt.−1

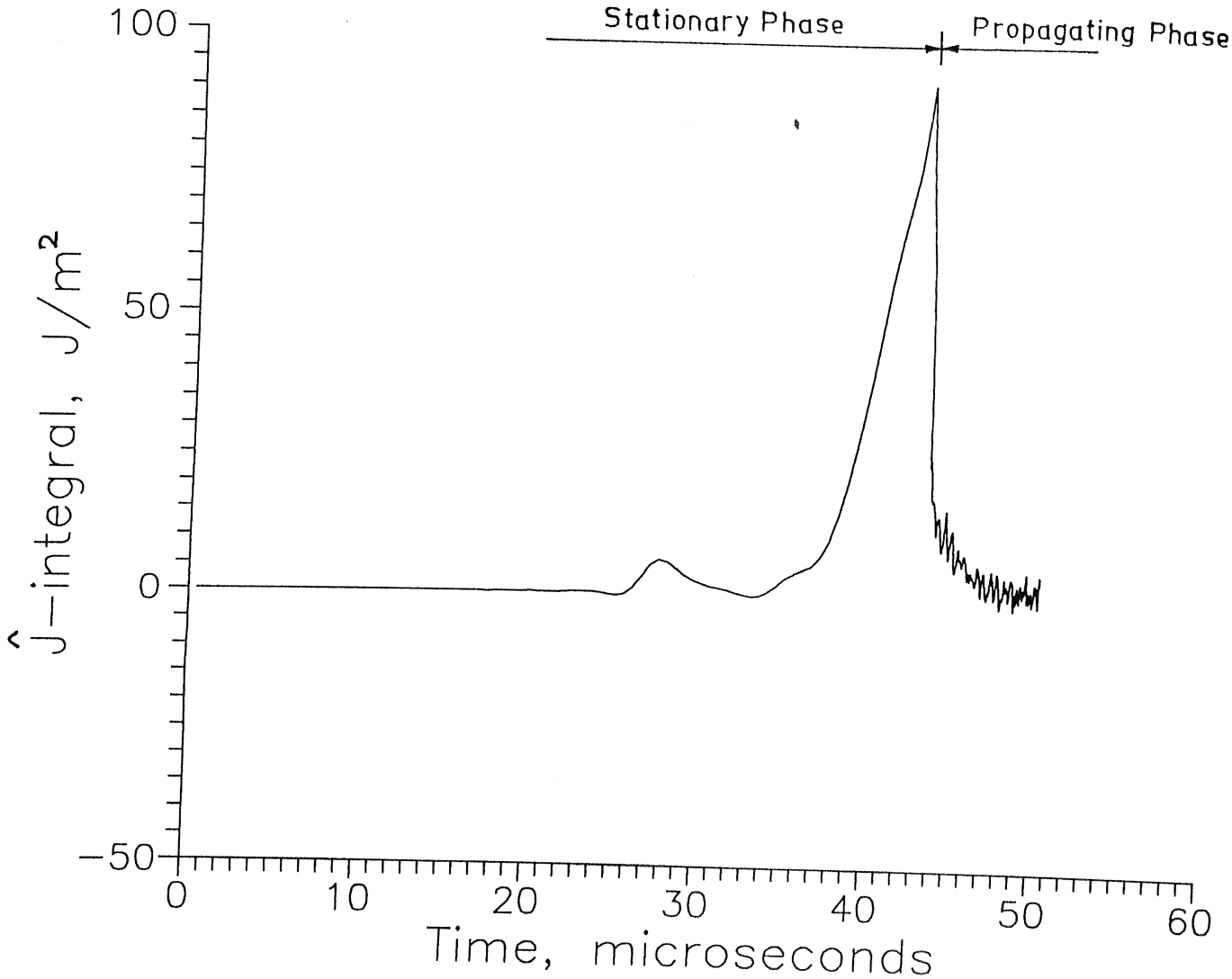

Fig. 3.48 Variation of $\hat{J}$−integral with time for stationary crack and propagating crack of Expt.−2

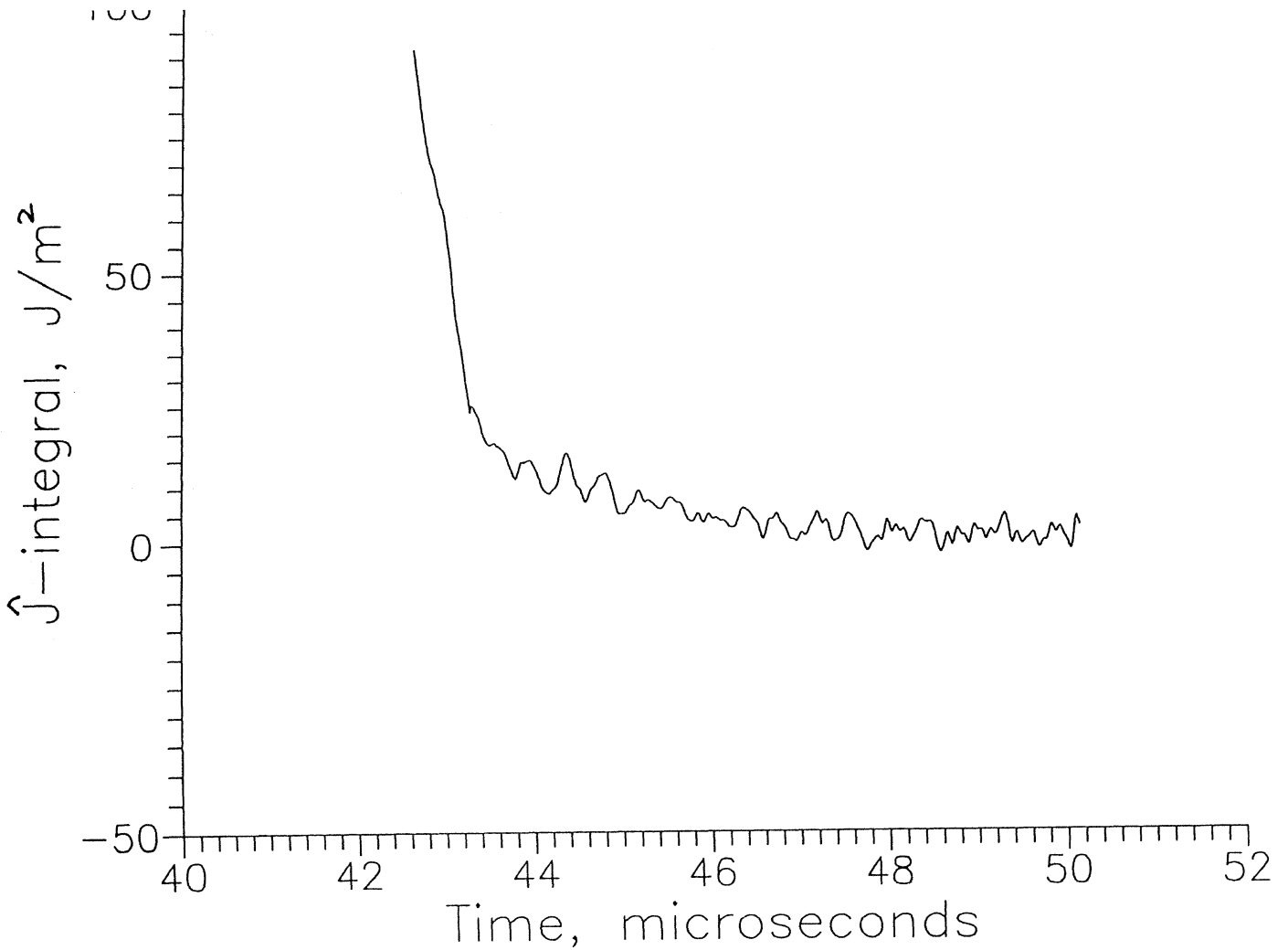

Fig. 3.49 Variation of $\hat{J}$−integral after the crack strat propagating for Expt.−2

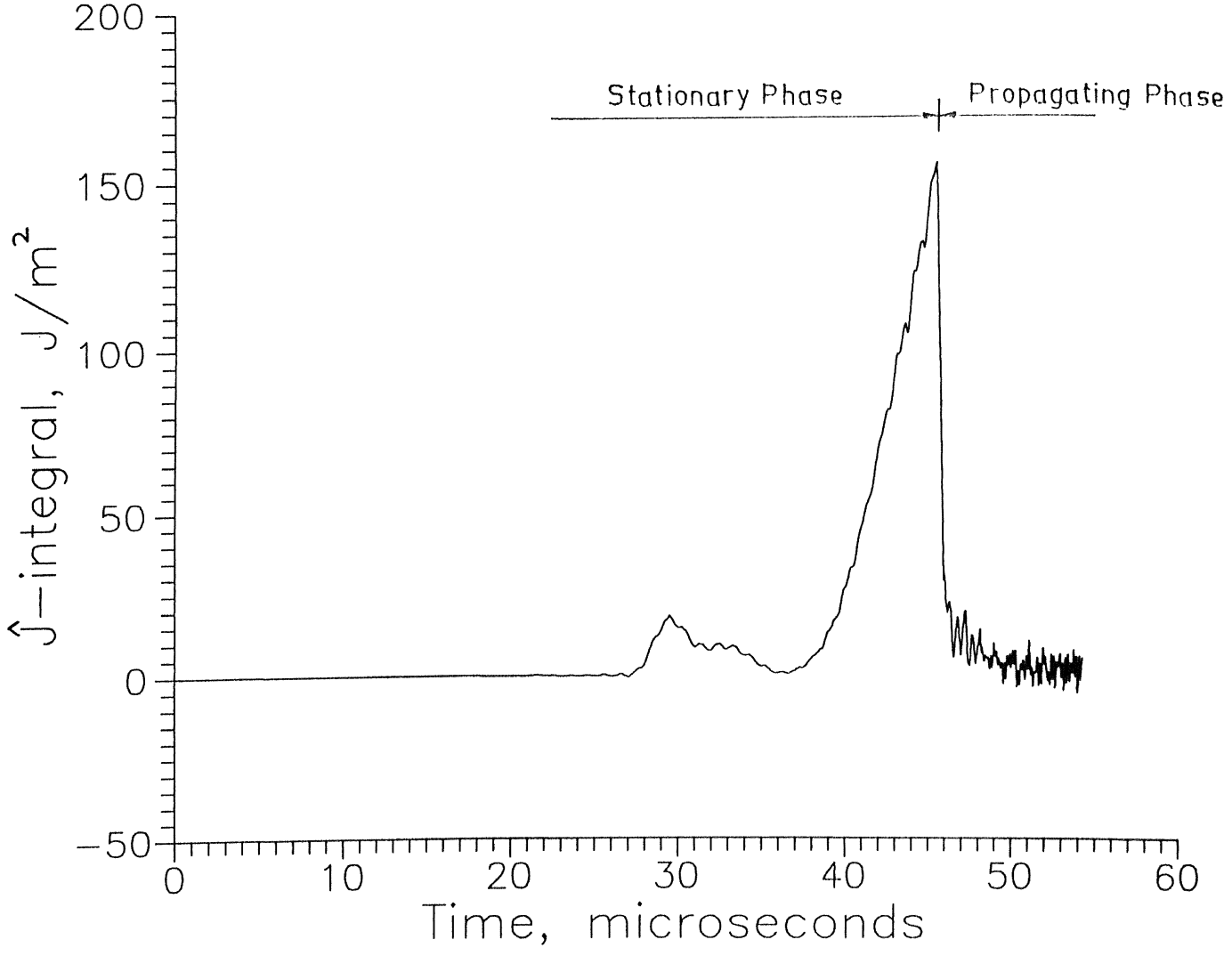

Fig. 3.50 Variation of $\hat{J}$−integral with time for stationary crack and propagating crack of Expt.−3

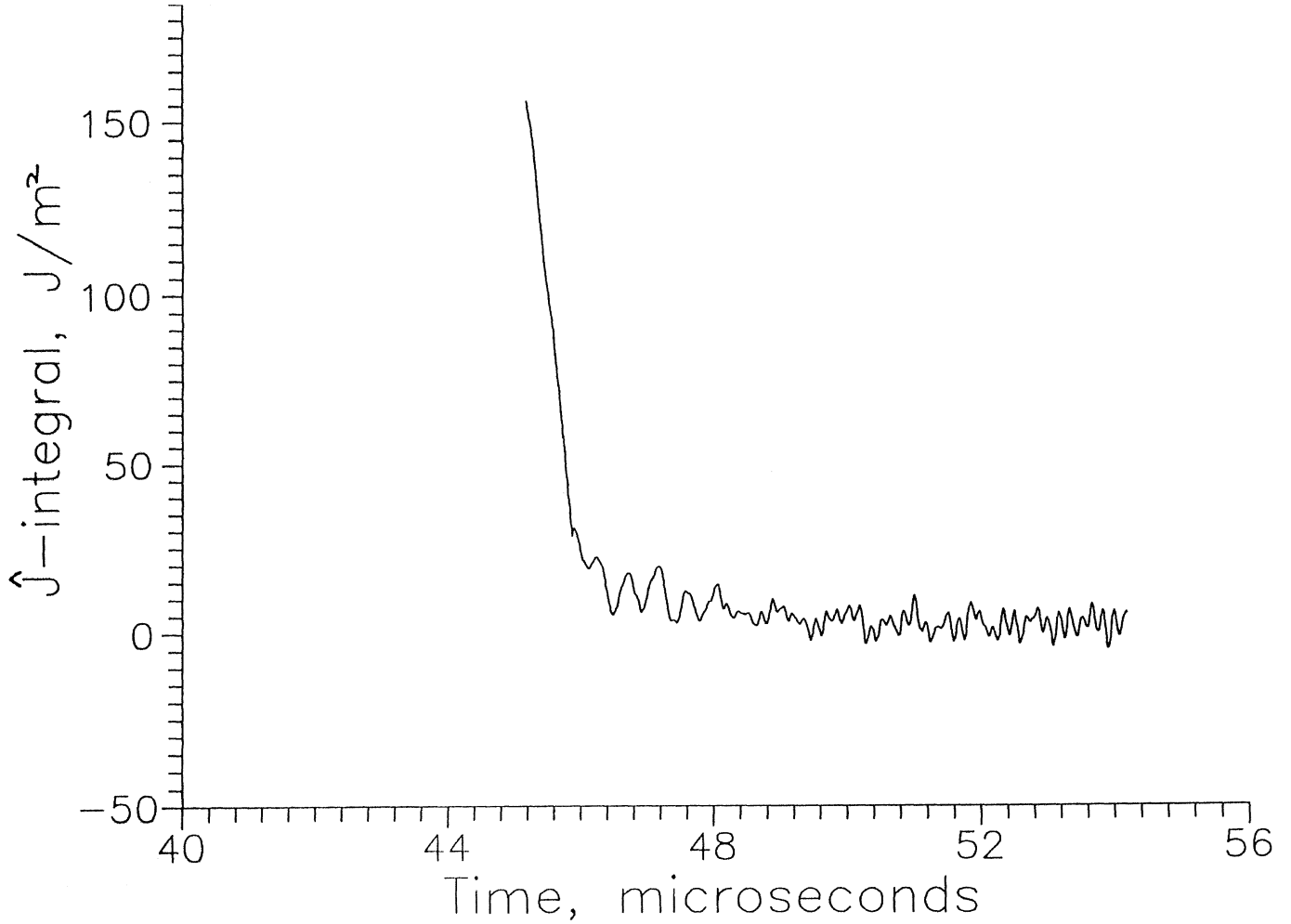

Fig. 3.51 Variation of Ĵ−integral after the crack strat propagating for Expt.−3

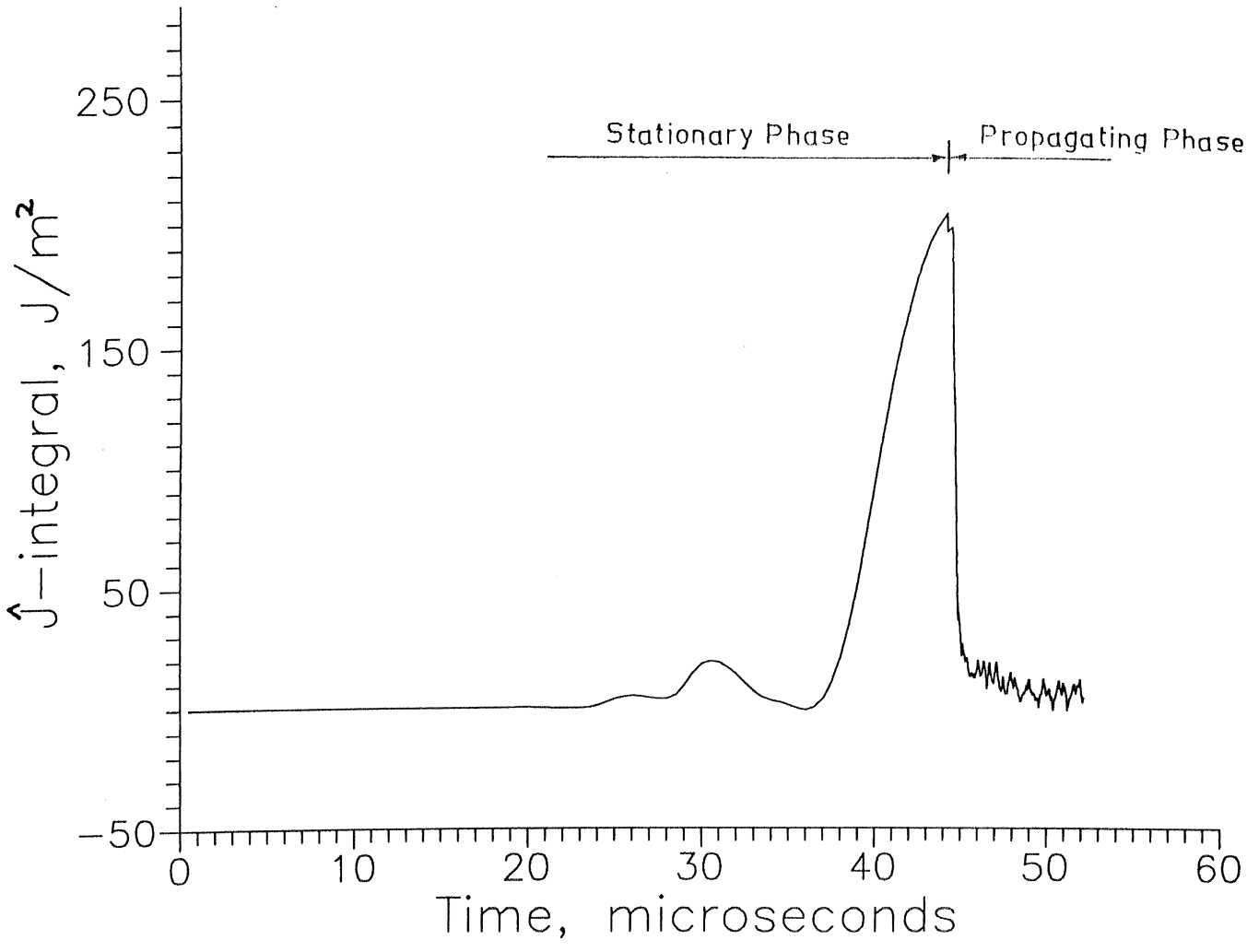

Fig. 3.52 Variation of $\hat{J}$–integral with time for stationary crack and propagating crack of Expt.–4

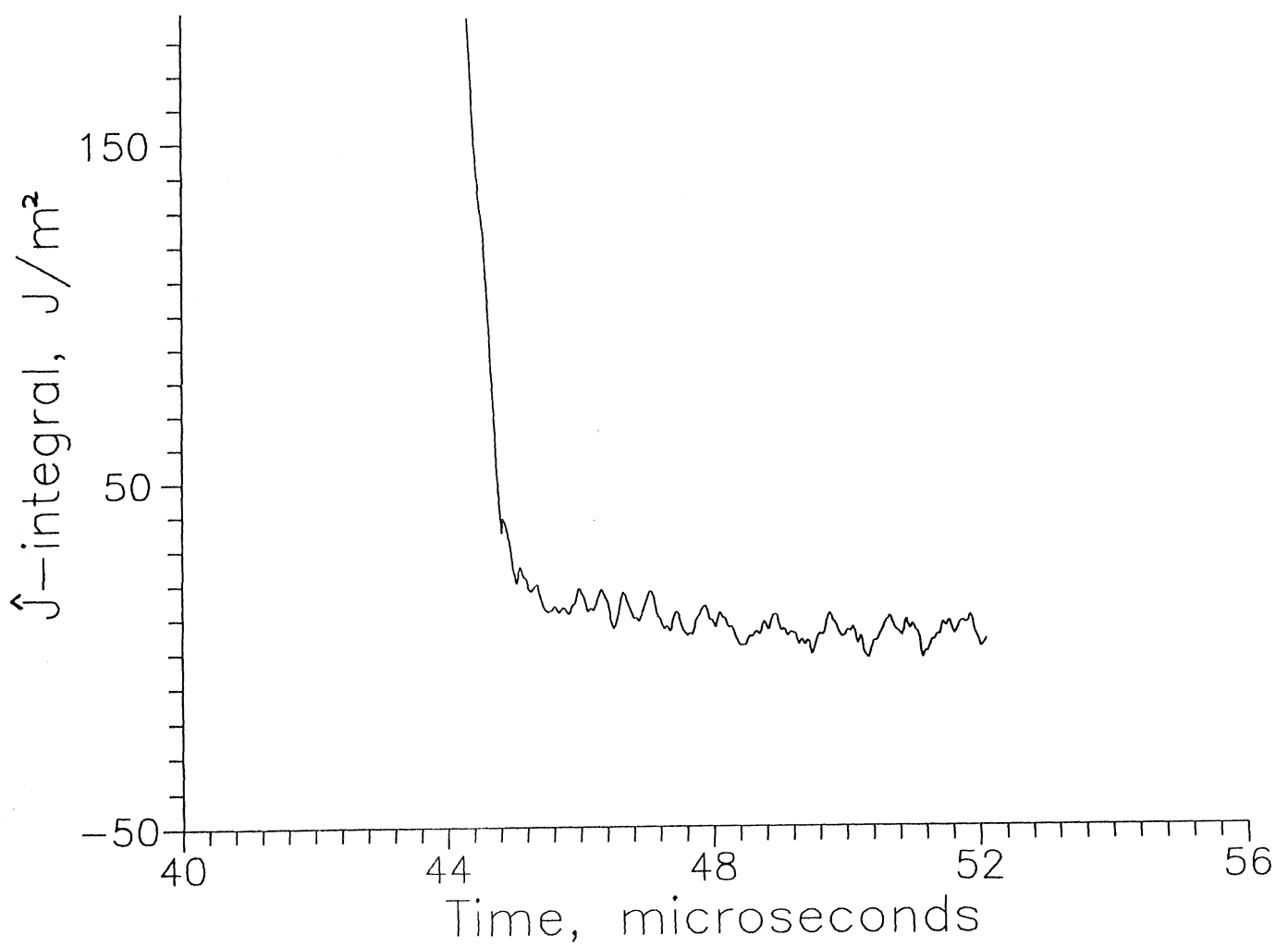

Fig. 3.53 Variation of $\hat{J}$−integral after the crack strat propagating for Expt.−4

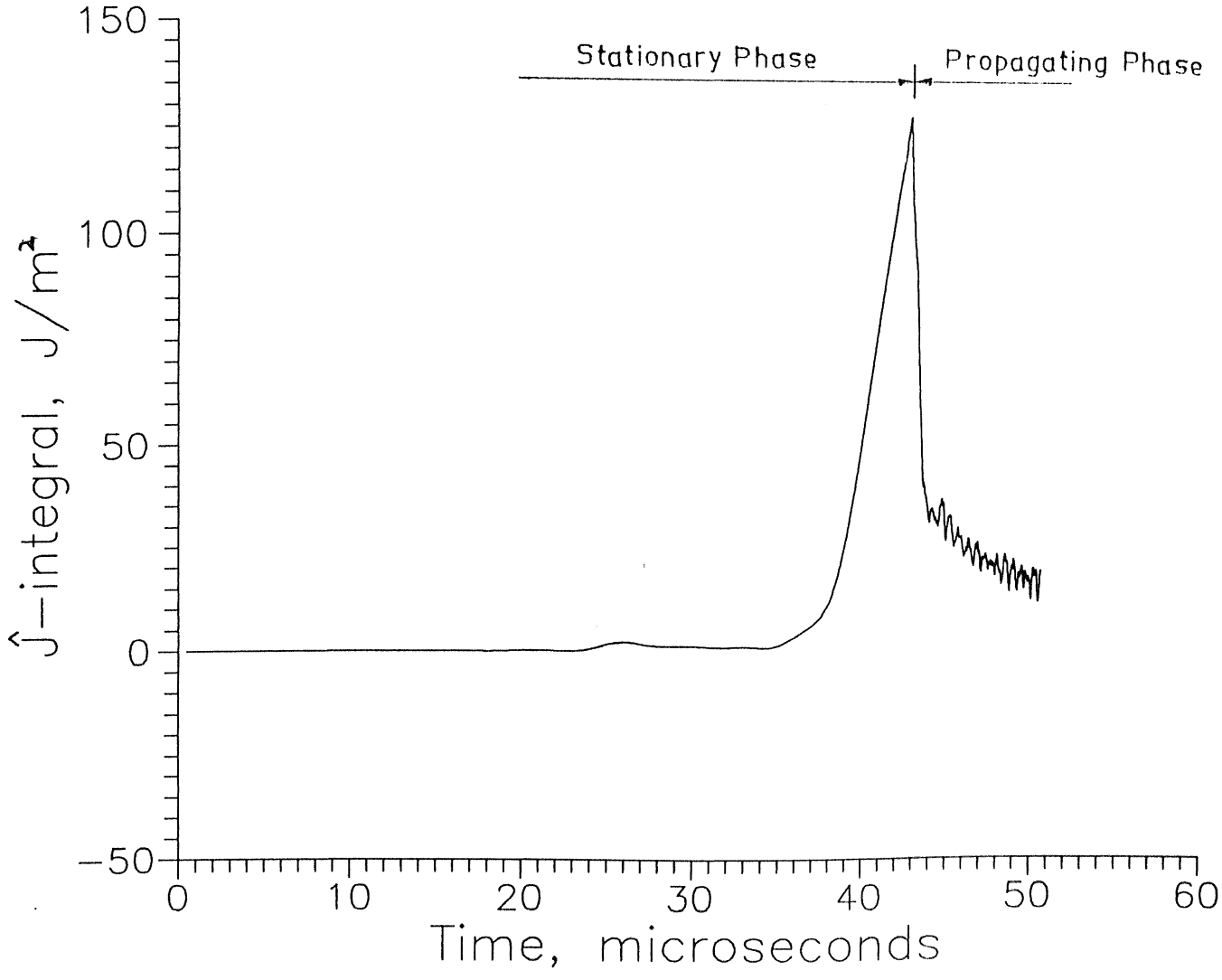

Fig. 3.54 Variation of Ĵ−integral with time for stationary crack and propagating crack of Expt.−5

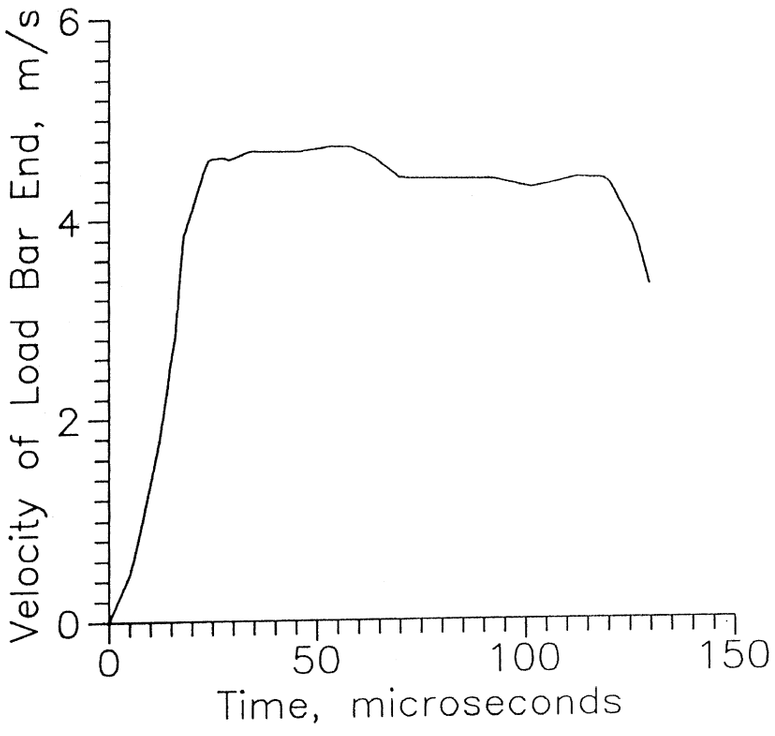

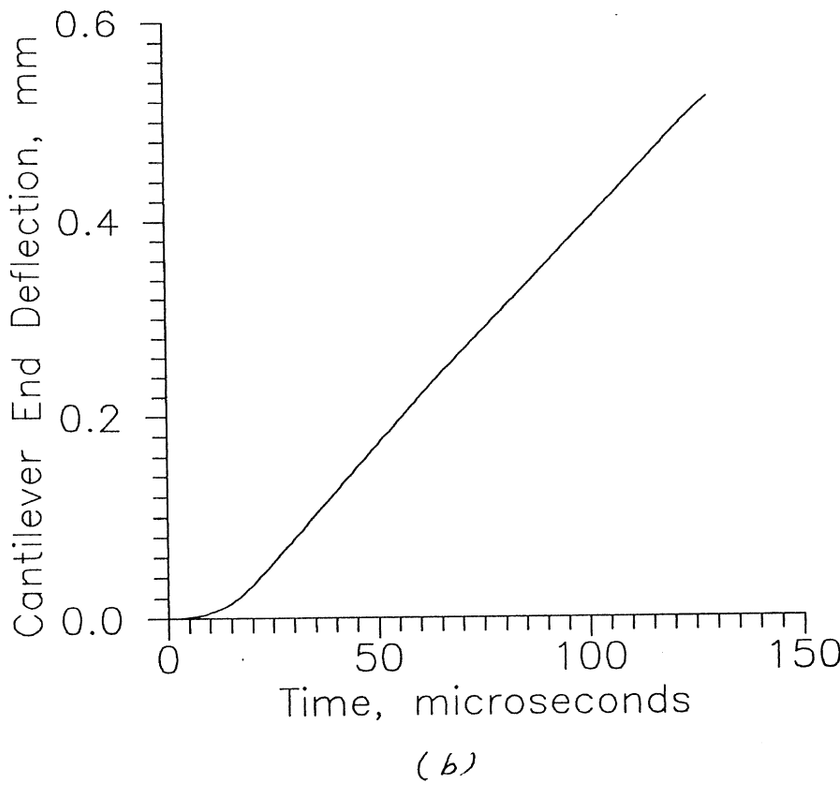

Fig. 3.57 (a) Velocity input at the cantilever end of the specimen obtained through incident and reflected Pulses of the load bar for Expt.–6

(b) Cantilever end deflection vs. time obtained by integrating the velocity input curve

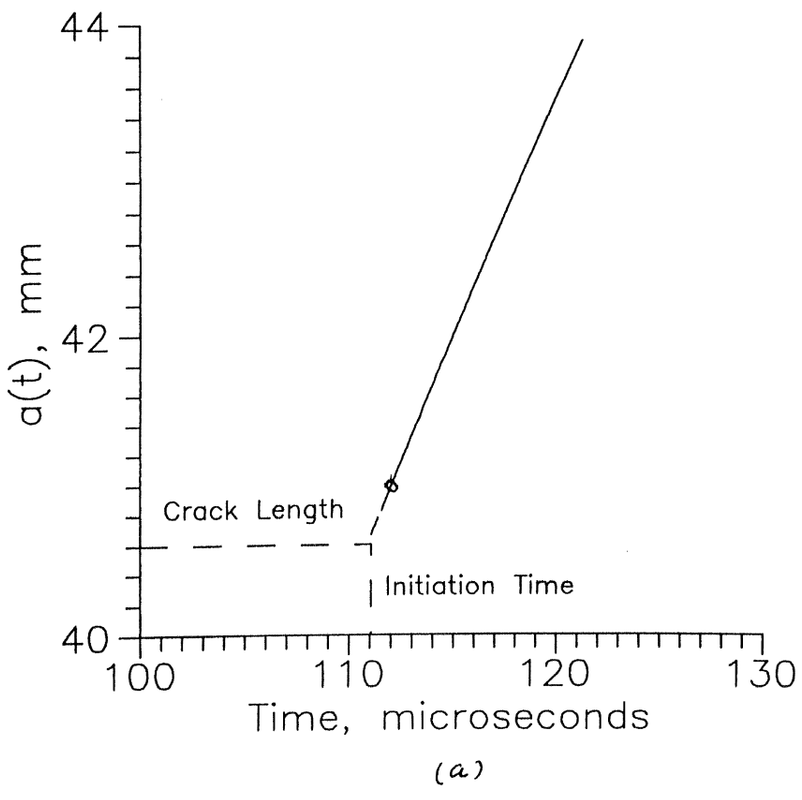

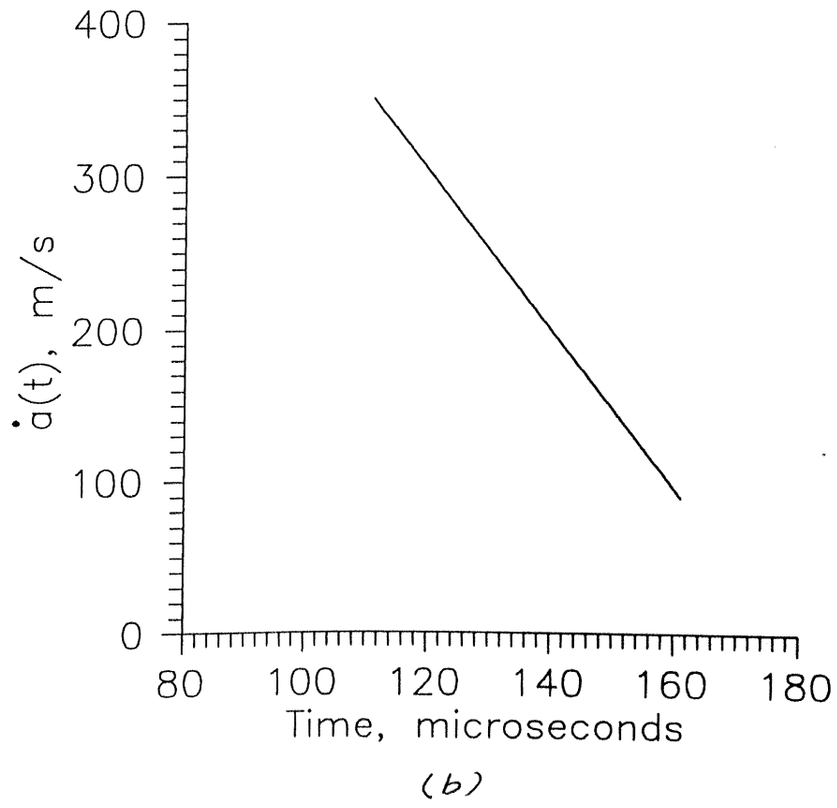

Fig. 3.58 (a) Variation of crack length with time of Expt.–6 shown with interpolation upto the length of precrack

(b) Variation of crack propagation speed with time obtained by differentiating the crack length vs time curve

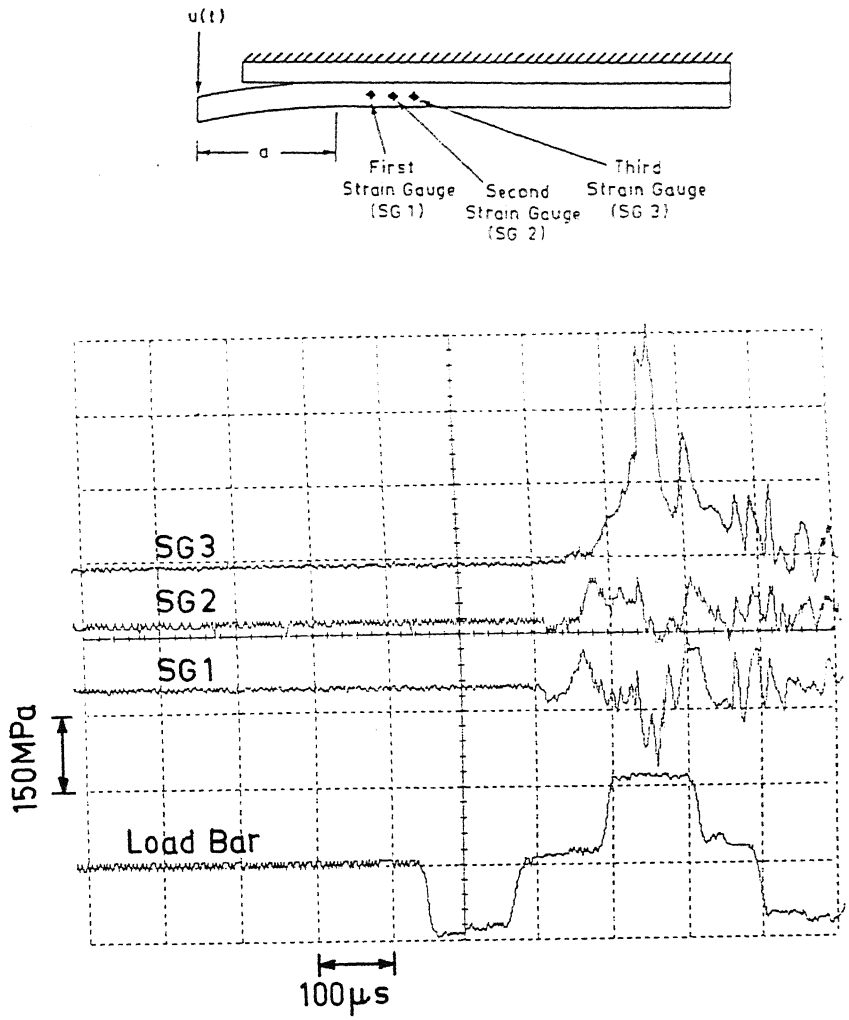

Fig. 3.56 Oscilloscope traces of Expt. 6

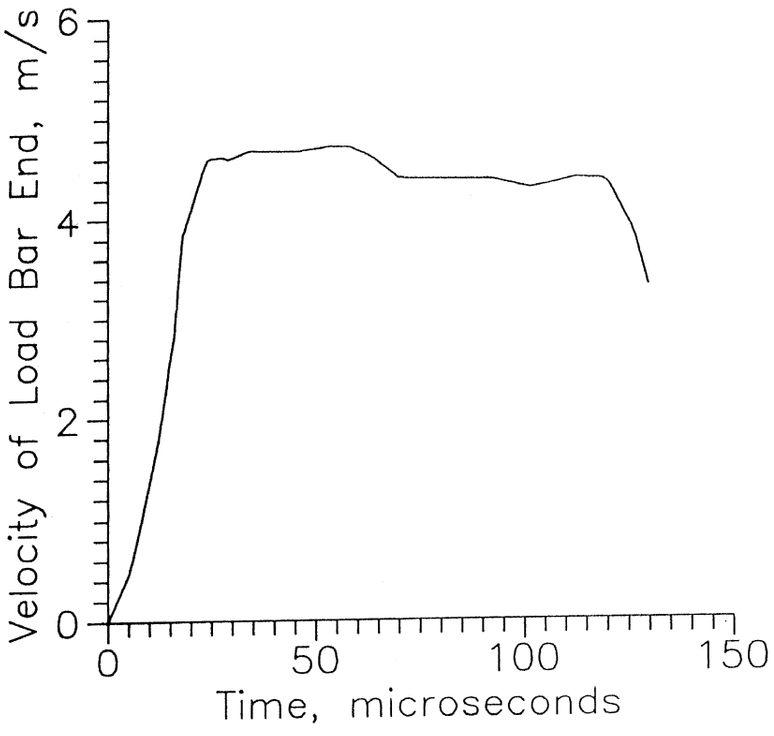

(a)

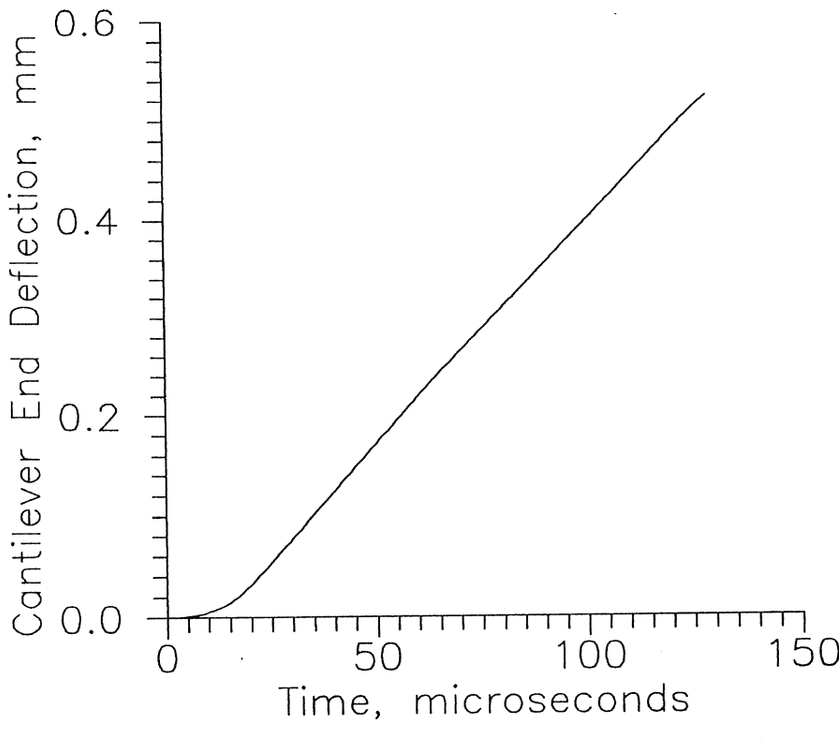

(b)

Fig. 3.57 (a) Velocity input at the cantilever end of the specimen obtained through incident and reflected Pulses of the load bar for Expt.–6

(b) Cantilever end deflection vs. time obtained by integrating the velocity input curve

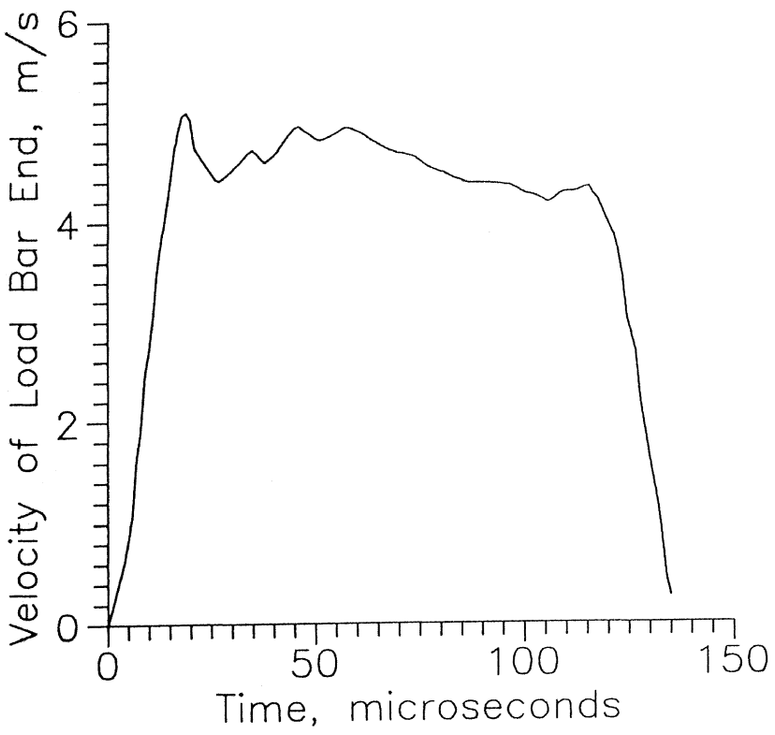

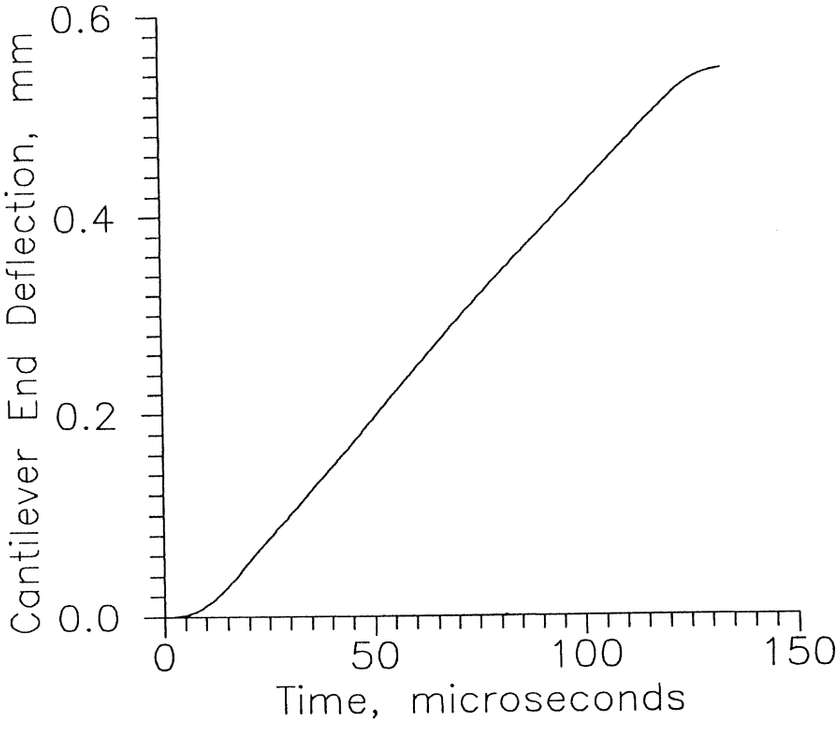

Fig. 3.61 (a) Velocity input at the cantilever end of the specimen obtained through incident and reflected Pulses of the load bar for Expt.–7

(b) Cantilever end deflection vs. time obtained by integrating the velocity input curve

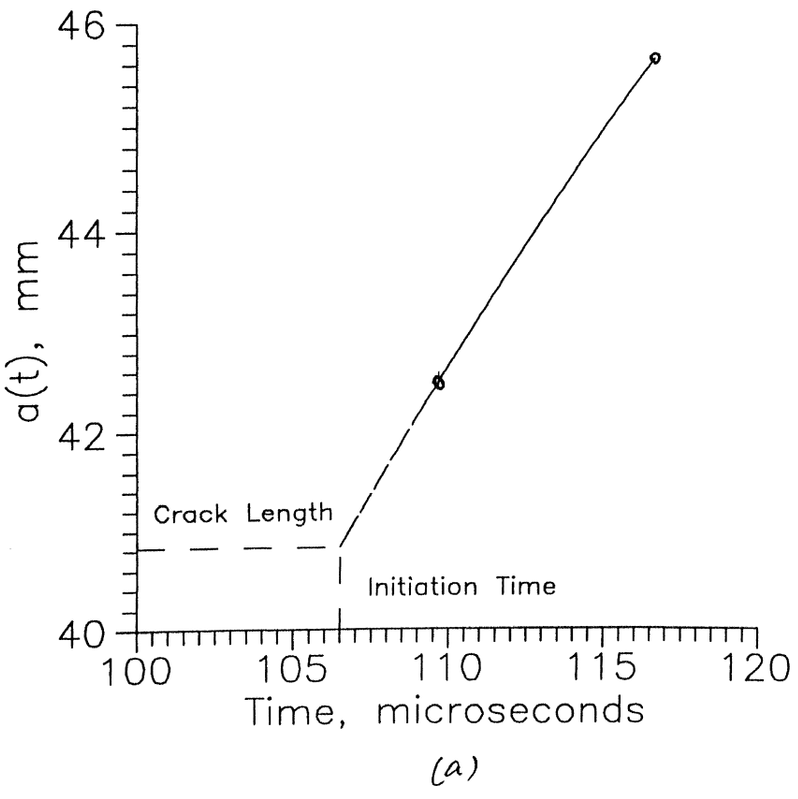

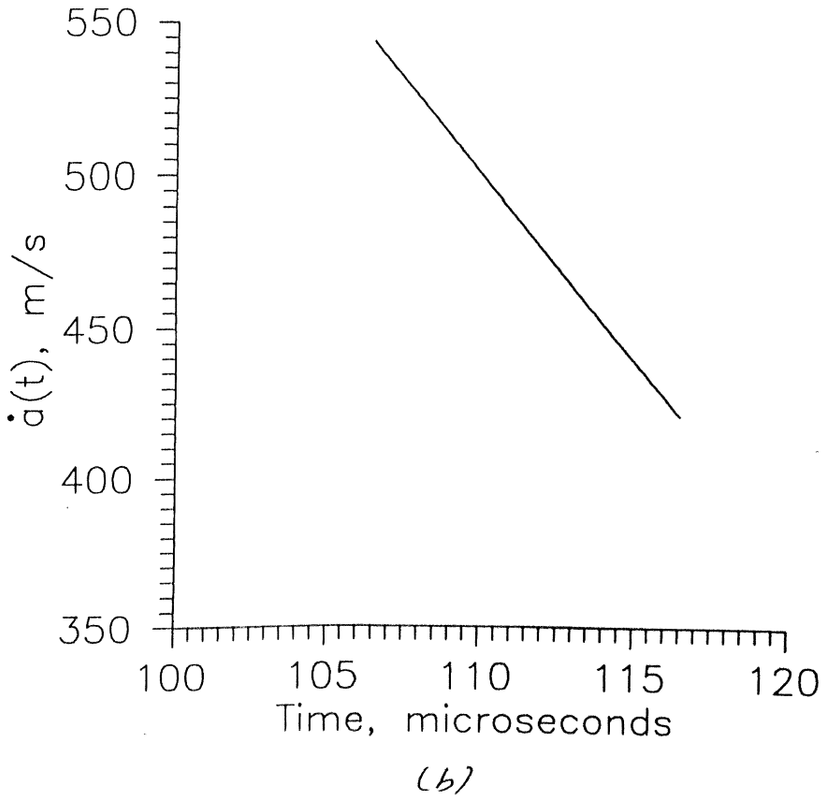

Fig. 3.62 (a) Variation of crack length with time of Expt.–7 shown with interpolation upto the length of precrack

(b) Variation of crack propagation speed with time obtained by differentiating the crack length vs time curve

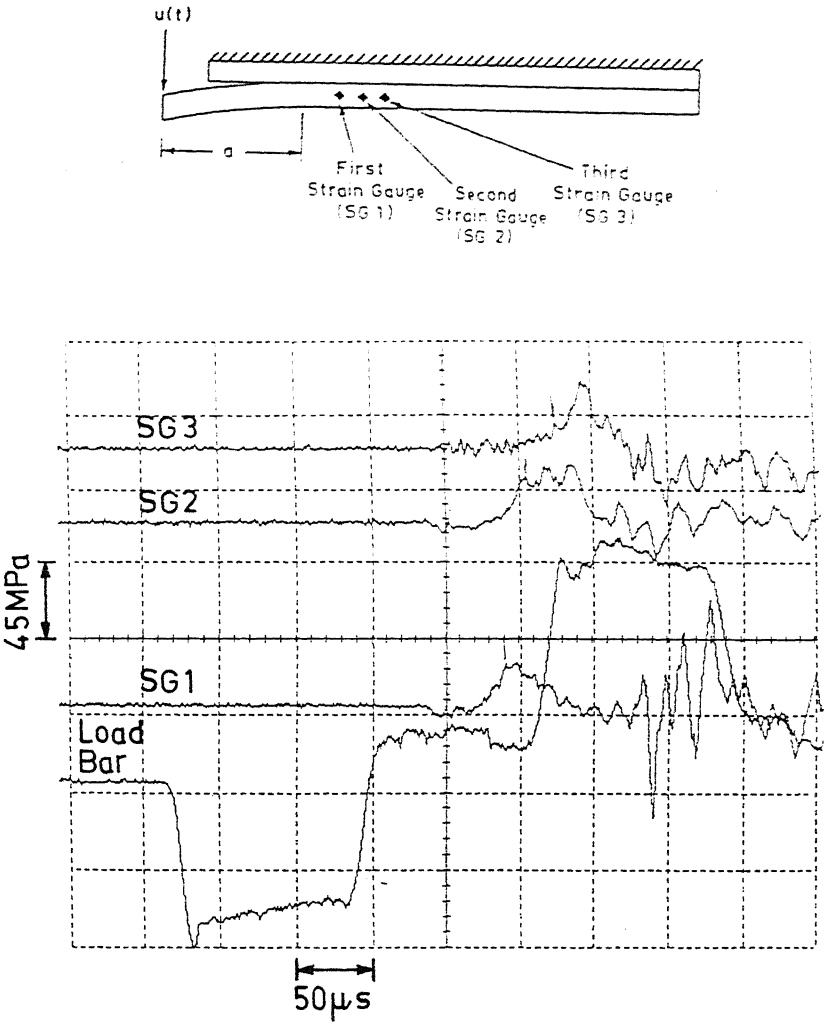

Fig. 3.60 Oscilloscope traces of Expt. 7

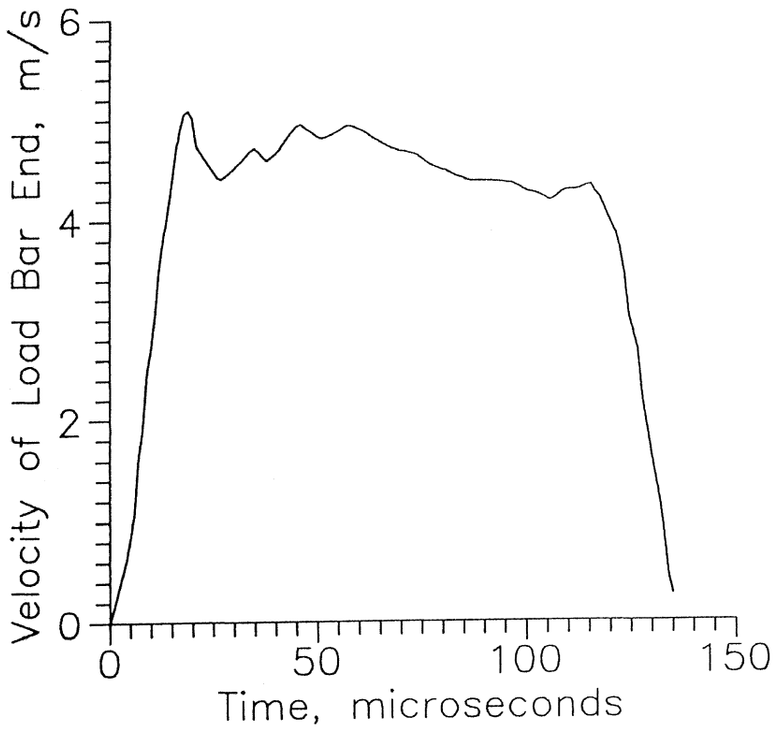

(a)

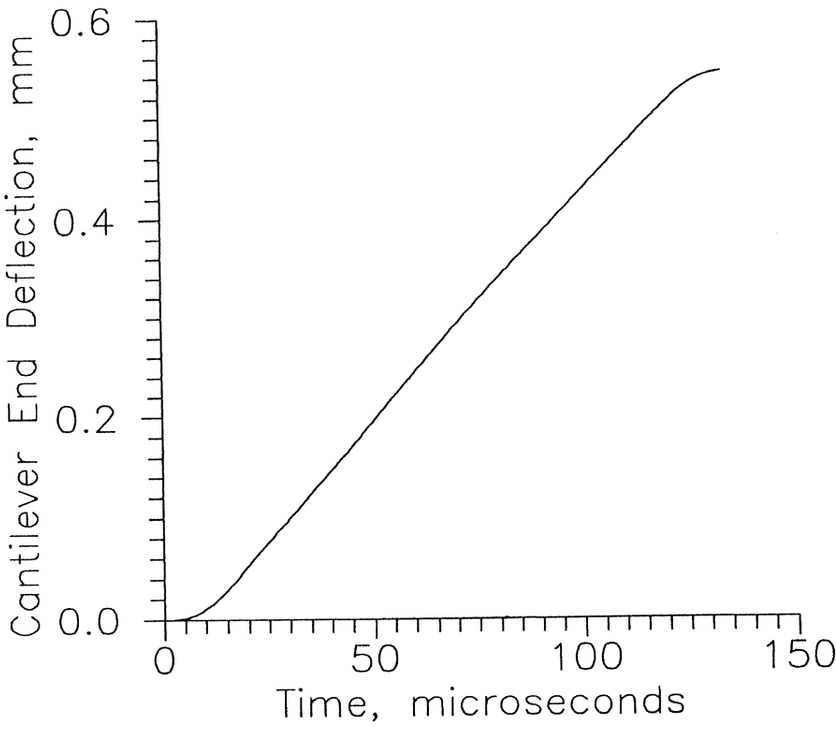

(b)

Fig. 3.61 (a) Velocity input at the cantilever end of the specimen obtained through incident and reflected Pulses of the load bar for Expt.–7

(b) Cantilever end deflection vs. time obtained by integrating the velocity input curve

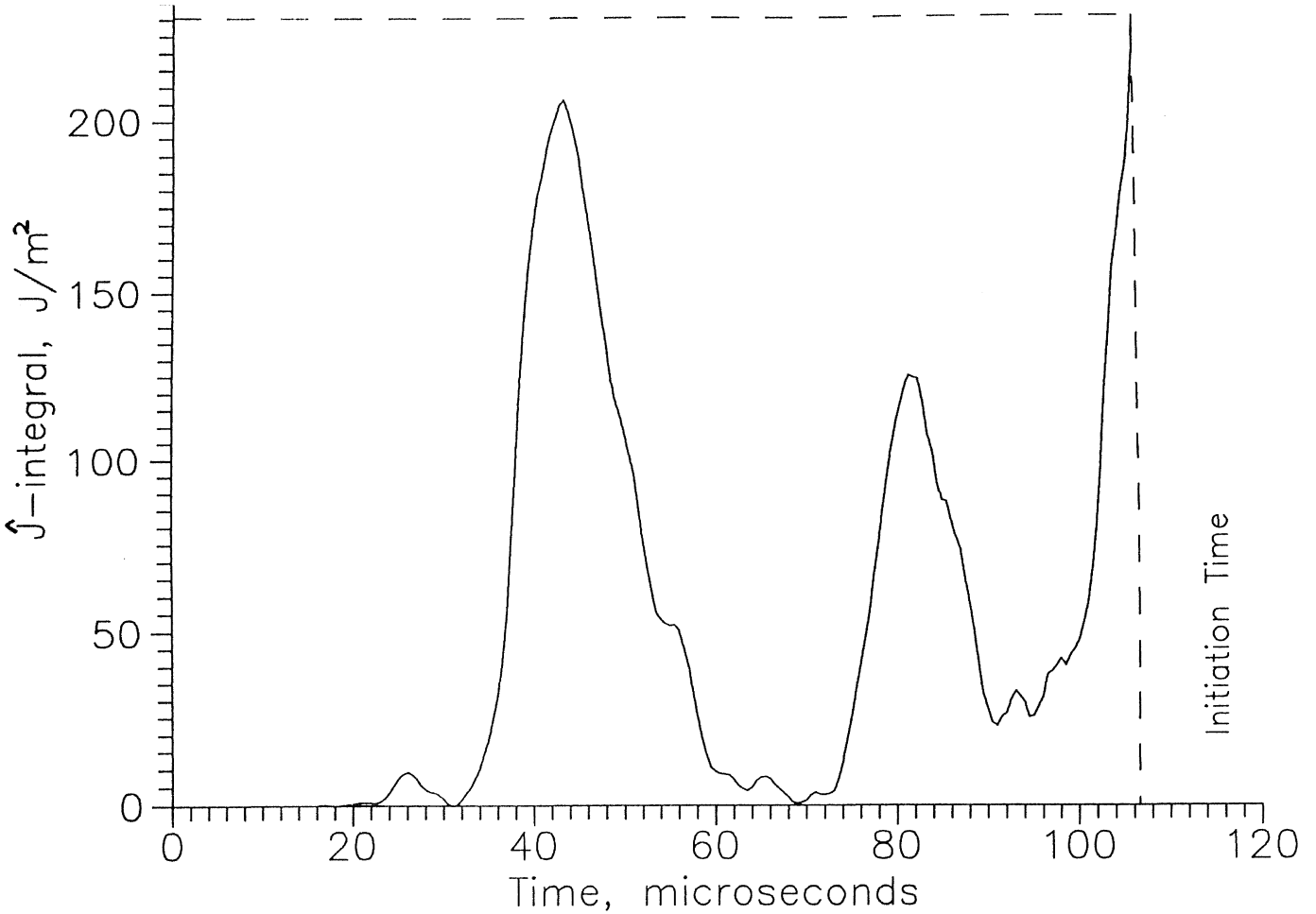

Fig. 3.63 Initiation toughness of Expt.–7

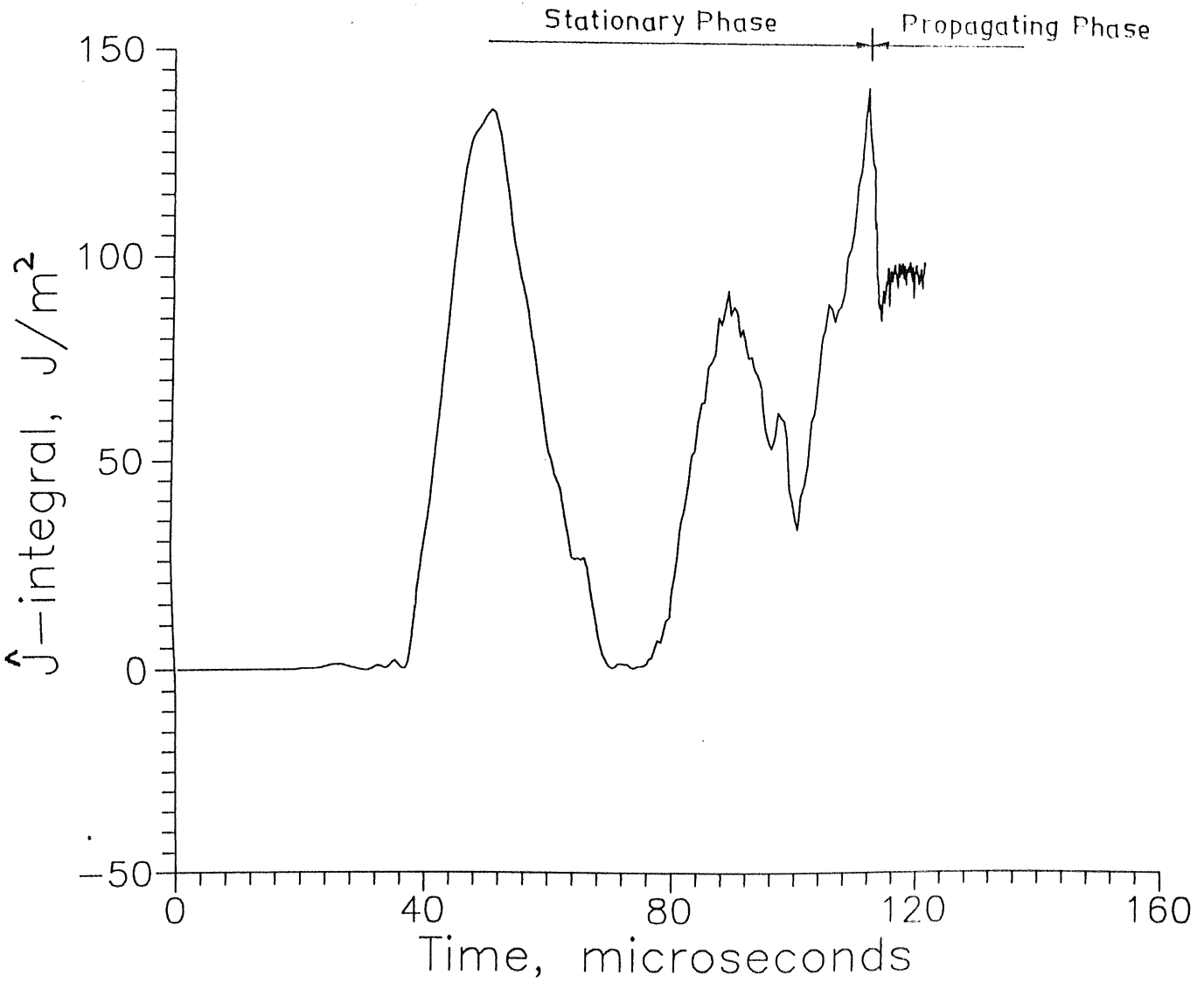

Fig. 3.64 Variation of $\hat{J}$−integral with time for stationary crack and propagating crack of Expt.−6

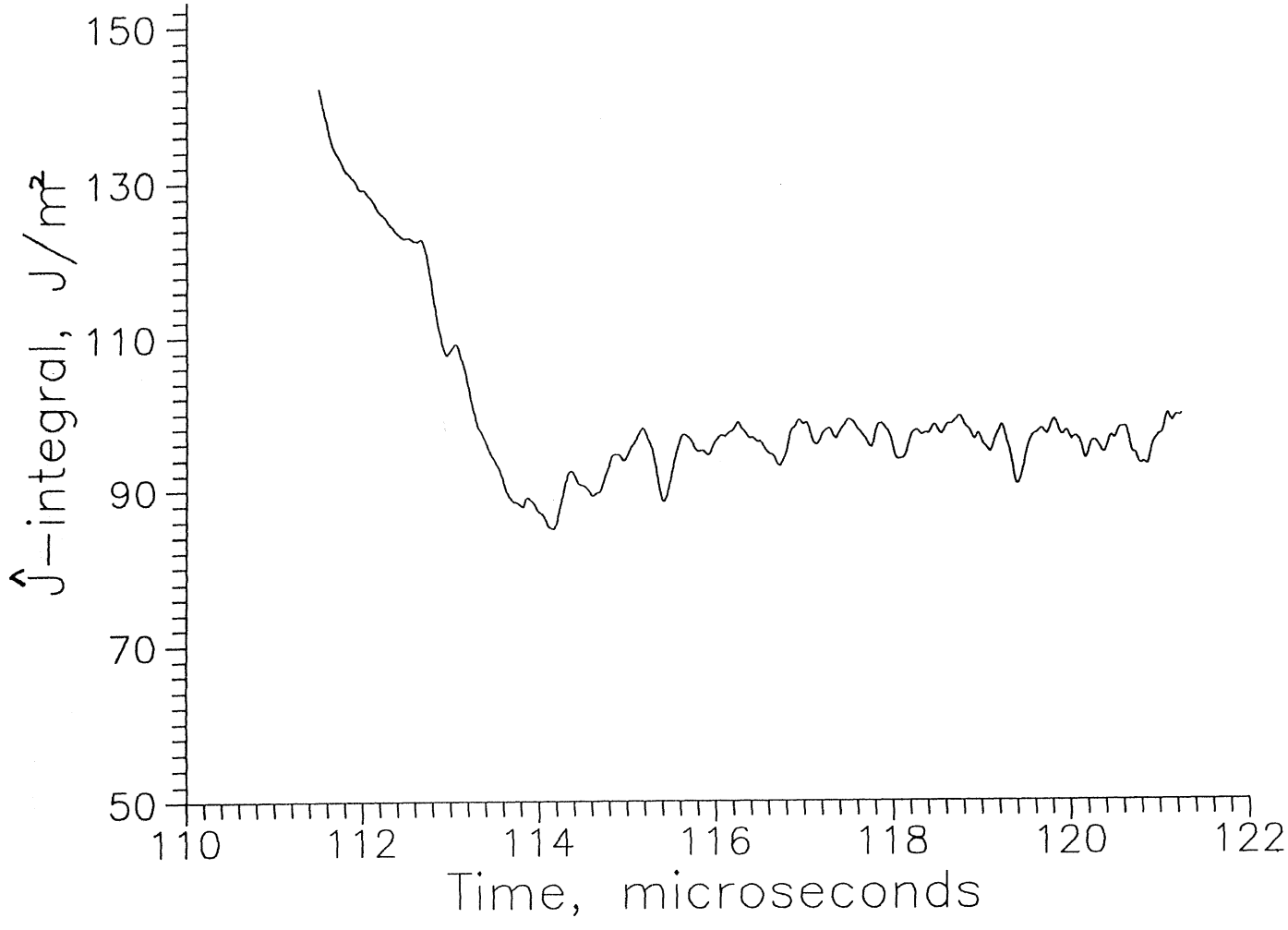

Fig. 3.65 Variation of $\hat{J}$–integral after the crack strat propagating for Expt.–6

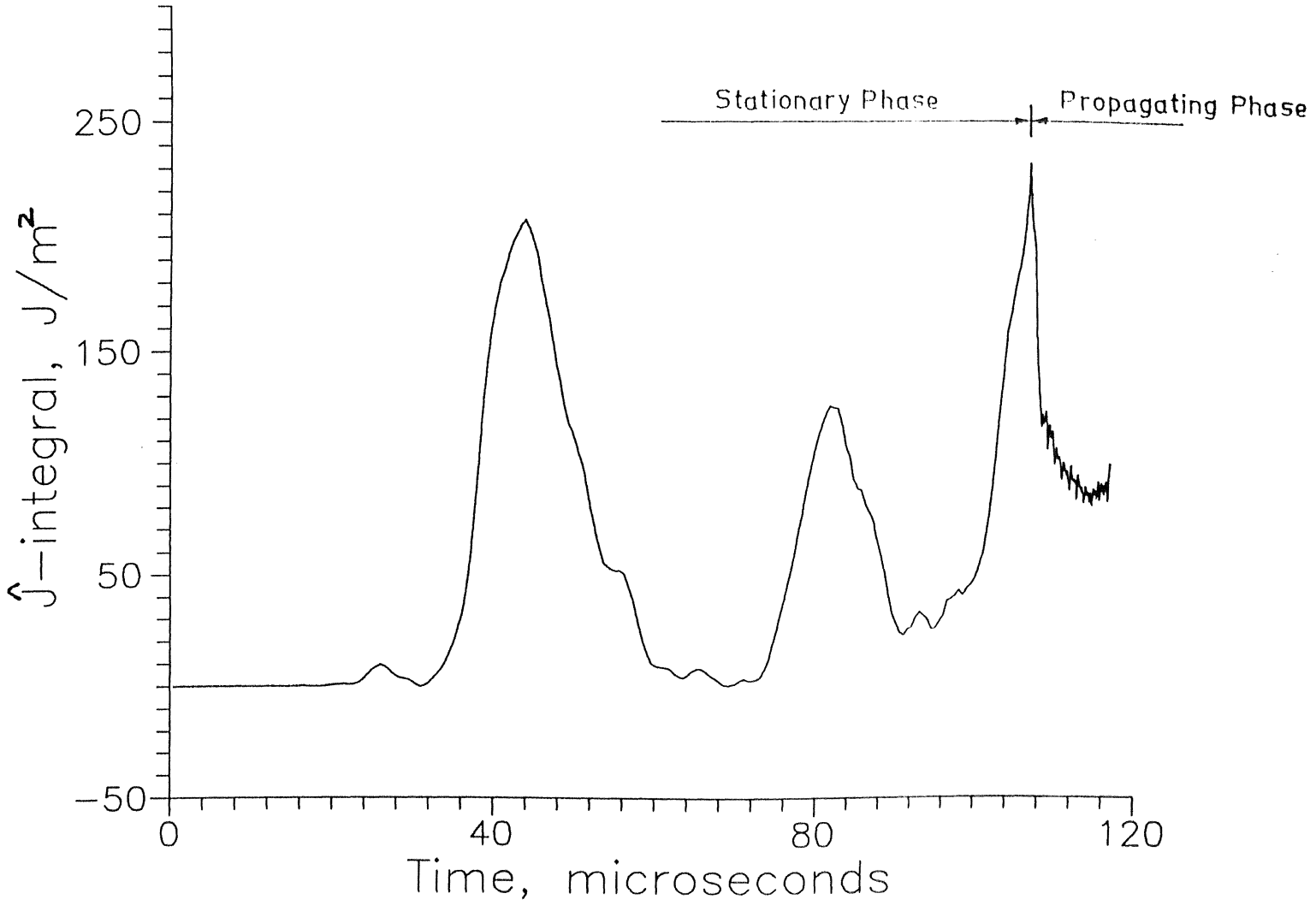

Fig. 3.66 Variation of $\hat{J}$−integral with time for stationary crack and propagating crack of Expt.−7

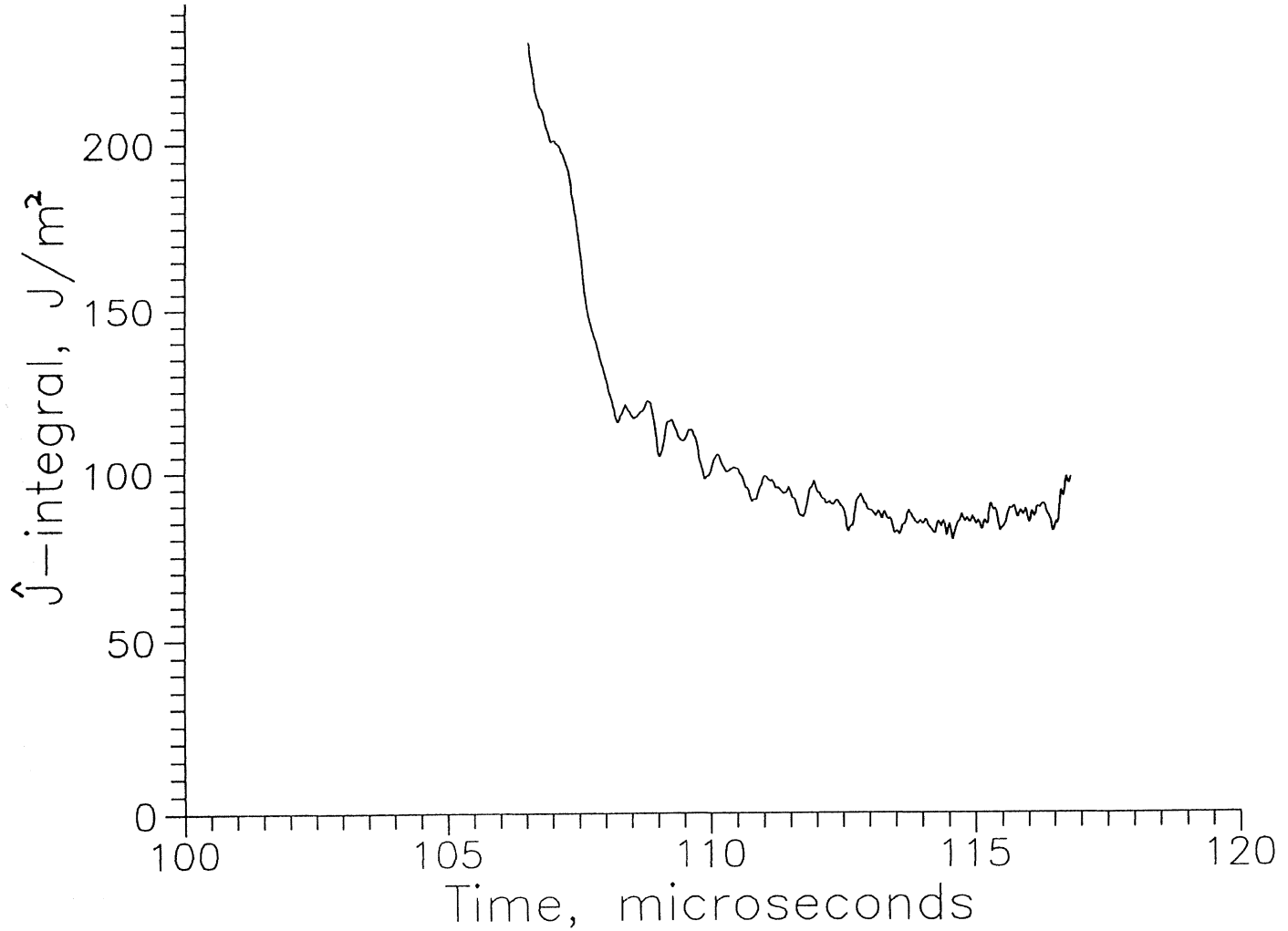

Fig. 3.67 Variation of $\hat{J}$–integral after the crack strat propagating for Expt.–7

CHAPTER - 4

CONCLUSIONS AND SCOPE FOR FUTURE WORK

4.1 CONCLUSIONS

Hybrid methods involving both experimental measurements and finite element analysis were developed separetly to determine interlaminar fracture toughness in a DCB specimen under quasistatic crack propagation and dynamic crack propagation.

The DCB specimen was made by bonding two slender strips of hardened alloy steel with epoxy. While bonding, a precrack was introduced by keeping a nonsticking polymeric sheet between the strips.

In the case of quasistatic crack propagation, a finite element code was developed to determine strain field and a relationship between the stress intensity factor and strain at an appropriate location and orientation. A strain gauge was bonded ahead of the crack tip and the specimen was loaded in mode I in an INSTRON machine in displacement controlled mode. When the crack start propagating very slowly and approaches the strain gauge, due to singular stress field around the crack tip, the strain gauge register a peak strain when the crack tip is 1 mm behind. The SIF was determined through measured peak strain and the relationship between peak strain and SIF developed through FE code. The SIF was also calculated through FE code for the load at which the peak strain was attained. The difference between these values were varying from 8 to 55 %.

A hybrid technique was also developed using experimental measurements and finite element analysis to determine the initiation and propagation toughness of DCB specimen. The FE code requires the displacement boundary conditions at the cantilever end, initiation time

and crack extension history as inputs. These data were measured through an experimental setup. in which one of the cantilevers of DCB specimen was glued to a rigid block and the other cantilever was loaded through a load bar. The load bar is impacted by a striker accelerated in an air gun. The displacement of the load bar end was calculated using one dimensional wave propagation analysis similar to one used in split Hopkinson bar technique. The crack velocity was measured by monitoring the strain response of the three strain gauges bonded in series ahead of the crack tip.

Two sets of initiation time were observed. One between 40 to 45 μs and other between 105 to 112 μs. The initiation toughness ($\hat{J}_{ini}$) was found to vary between 90 and 230 J/m^2. The propagation toughness ($\hat{J}_{prop}$) was found to vary between 2 and 100 J/m^2 depending on the crack velocity which was varying in the range 100 - 1800 m/s. The proagation toughness was observed to be very low at higher crack velocity (close to Rayleigh wave).

4.2 SUGGESTIONS FOR FUTURE WORK

In dynamic crack propagation, the crack front was assumed normal to the direction of crack propagation, which may not be true. Therefore, the strain gauges can be bonded on both side of the specimen and the computer code can be modified to account for inclined wave front through 3-D analysis.

To have a better distribution of crack velocity more number of strain gauges can be bonded ahead of the crack tip or a suitable propagation gauge can be designed that gives continuous variation of crack tip velocity.

The technique can be extended to determine dynamic behaviour of interlaminar crack propagating in the FRP laminates and bimaterial composites.

High speed photography may be used to measure the crack velocity.

REFERENCES

Abdelaziz M. Nait, Neviere R. and Pluvinage, 1987, Experimental Method for J_{Ic} Computation on Fracture of Solid Propellants Under Dynamic Loading Conditions, Engineering Fracture Mechnaics, Vol. 28, pp. 425-434.

Aminpour M.A. and Holsapple K.A., 1991, Finite Element Solutions for Propagating Interface Crack with Singularity Elements, Enginering Fracture Mechanics, Vol. 39, No. 3, pp. 451-468.

Andrews D.J., 1976, Rupture Velocity of Plane Strain Shear Cracks, Journal of Geophysical Research, Vol. 81, No. 32, pp. 5679-5687.

Atkinson C., December 1977, On Stress Singularities and Interfaces in Linear Fracture Mechnics, International Journal of Fracture, Vol. 13, No. 6, pp. 807-820.

Atluri Satya N., 1982, Path-Independent Integrals in Finite Elasticity and Inelasticity, with Body Forces, Inertia and Arbitrary Crack-Face Conditions, Engineering Fracture Mechanics, Vol. 16, No. 3, pp. 341-364.

Barsowm R.S., 1976, On the Use of Isoparametric Finite Element in Linear Fracture Mechanics, International Journal of Numerical Methods in Engineering, Vol. 10, pp. 25-37.

Bathe Klauss-jurgen, 1990, Finite Element Procedure in Engineering Analysis, Prentice Hall of India.

Berger J.R. and Dally J.W., June 1988, An Overdeterministic Approach for Measuring K_I Using Strain Gages, Experimental Mechanics, pp. 142-145.

Berger J.R. and Dally J.W., 1990a, A Spatially Overdetermined Analysis for Propagation Toughness using Strain Gages, Mechanics Research Communications, Vol. 17(2), pp. 93-99.

Berger J.R., Dally J.W. and Sanford R.J., 1990b, Determining the Dynamic Strees Intensity Factor with Strain Gages using a Crack tip Location Algorithm, Engineering Fracture Mechanics, Vol. 36, No. 1, pp. 145-156.

Brickstad Bjorn, 1983, A FEM Analysis of Crack Arrest Experiments, International Journal of Fracture, Vol. 21, pp. 177-194.

Broek D., 1984, Elementary Engineering Fracture Mechanics, Martinus Nijhoff Publishers, The Hague.

Burridge Robert, 1973, Admissible speeds for plane strain self-similar shear cracks with friction but lacking cohesion, Geophysical Journal of the Royal Astronomy Society, Vol. 35, pp. 439-455.

Cantwell W.J., Stoll D., Kausch H.H., July 1989, Crack Velocity Measurements in Fibre Reinforced Composites, Composites, Vol. 20, No. 4, pp. 389-391.

Chiang C. R., 1990, Determination of the Dynamic Stress Intensity Factor of a Moving Crack by Numerical Method, International Journal of Fracture, Vol. 45, pp. 123-130.

Comninou Maria, 1990, An Overview of Interface Cracks, Engineering Fracture Mechanics, Vol. 37, No. 1, pp. 197-208.

Cook Robert D., Malkus David S. and Plesha Micheal E., 1989, Concept and Applications of Finite Element Analysis, 3rd edition, John Wiley and Sons, Newyork.

Crouch B.A. and Williams J.G., 1987, Application of Dynamic Solution to High Speed Fracture Experiments - I. Analysis of Experimental Geometries, Engineering Fracture Mechanics, Vol. 26, No. 4, pp. 541-551.

Dattaguru B., Venkatesha K.S., Ramamurthy T.S. and Buchholz F.G., 1994, Finite Element Estimates of Strain Energy Release Rate Componenets at the Tip of an Interface Crack Under Mode I Loading, Engineering Fracture Mechanics, Vol. 49, No. 3, pp. 451-463.

Dally J.W. and Barker D.B., Sept. 1988, Dynamic Mesurements of Initiation Toughness at High Loading Rates, Experimental Mechanics, pp. 298-303.

Dally J.W. and Sanford R.J., Dec. 1987, Strain Gage Methods for Measuring the Opening Mode Stress Intensity Factor, KI, Experimental Mechanics, pp. 381-388.

Davies P., Moulin C., Kausch H.H. and Fischer M., 1990, Measurements of G_{Ic} and G_{IIc} in Carbon/Epoxy Composites, Composite Science and Technology, Vol. 39, pp. 193-205.

Dexter R.J., 1987, Source of Error in Finite Element Computations of the Stress Intensity Factor for Running Cracks, Numerical Method in Fracture Mechanics, Eds. A.R. Luxmoore, D.R.J. Owen, Y.P.S. Rajapakse and M.F. Kanninen, pp. 153-172.

Epstein Jonathan S., 1993, Experimental Technique in Fracture, VCH Publishers, Newyark.

Freund L.B., 1990, Dynamic Fracture Mechanics, Cambridge University Press, Newyork.

Hwu chyabin and Hu Jian S., 1992, Sress Intensity Factor and Strain energy Release Rates of Delaminations in Composite Laminates, Engineering Fracture Mechanics, Vol. 42, No. 6, pp. 977-988.

Jensen Henrik Myhre, 1991, The Blister Test for Interface Toughness Measurement, Engineering Fracture Mechanics, Vol. 40, No. 3, pp. 475-486.

Kalthoff J.F., 1985, On the Measurement of Dynamic Fracture Toughness - A Review of Recent Work, International Fracture Mechanics, Vol. 27, pp. 277-298.

Kennedy T.C. and Kim J.B., 1993, Dynamic Analysis of Cracks in Micropolar Elastic Materials, Engineering Fracture Mechanics, Vol. 44, No. 2, pp. 207-216.

Kishimoto K., Aoki S. and Sakata M., 1980, On the Path Independent Integral - J, Engineering Fracture Mechanics, Vol. 13, pp. 841-850.

Kobayasi A.S., Mall S., Urabe Y. and Emery A.F., 1978, A Numerical Dynamic Fracture Analysis of Three Wedge Load DCB Specimen, Numerical Methods in Fracture Mechanics, eds. A.R. Luxmoore and D.R.J. Owen, Univ. College, Swesna, pp. 673-684.

Kumar Prashnat and Rai Badri, 1993, Delaminations of Barely Visible Impact Damage in CFRP Laminates, Composite Structure, Vol. 23, pp. 313-318.

Manoharan M.G. and Sun C.T., 1990, Strain Energy Release Rates of an Interfacial Crack Between Two Anisotropic Solids Under Uniform Axial Strain, Composite Science and Technology, Vol. 39, pp. 99-116.

Malluck J.F. and King W.W., 1978, Fast Fracture Simulated by Finite Element Analysis which Accounts for Crack tip Energy Dissipation, Numerical Methods in Fracture Mechanics, eds. A.R. Luxmoore and D.R.J. Owen, Univ. College, Swesna, pp. 648-659.

Manogg P., 1966, Investigations of the Rupture of a Plexiglass Plate by Means of an Optical Method Involving High Speed Filming of Shadow Originating Around Holes Drilled in Plate, International Journal of Fracture, vol.2, pp. 604-613.

Marom G., Roamn I., Harel H., Rosensaft M., Kenig S. and Moshonov M., 1987, The Characterization of Mode I and Mode II Delamination Failure in Fabric Reinforced Laminates, Proceedings of ICCM -VI and ECCM-2, edited by F.L. Mathew, N.C.R. Buskell, J.M. Hodgkinson and J. Morton, Elsevier Applied Science, London, pp. 3265-3273.

Narayan M.D., 1988, Energy Release Rates in Delamination of Glass Fabric Reinforced Composite Laminates, M.Tech thesis, Indian Institute of Technology, Kanpur, India.

Nishioka T. and Atluri S.N., 1982a, Numerical Analysis of Dynamic Crack Propagation : Generation and Prediction Studies, Engineering Fracture Mechanics, Vol. 16, No. 3, pp. 303-332.

Nishioka T. and Atluri S.N., 1982b, Finite Element Simulation of Fast Fracture in Steel DCB Specimen, Engineering Fracture Mechanics, Vol. 16, No. 2, pp. 157-175.

Iishioka T. and Atluri S.N., 1983, Path Independent Integrals, Energy Release Rate and Ieneral Solution of Near-tip Fields in Mixed Mode Dynamic Fracture Mechanics, ngineering Fracture Mechanics, Vol. 18, No. 1, pp. 1-22.

Iishioka T. and Atluri Satya N., 1986, Computational Methods in Mechanics of Fracture, d. S.N. Atluri, Elsevier Science Publisher, Newyork.

Iishioka Toshihisa, Murakami Tatsuyuki, Uchiyama Hidetoshi, Sakakura Keigo and Cittaka Hiroyuki, 1991, Specimen Size Effecs on Dynamic Crack Propagation and rrest in DCB Specimens, Engineering Fracture Mechanics, Vol. 39, No. 4, pp. 57-767.

)zdil F. and Carlsson L.A., 1992, Finite Element Analysis of Interleaved DCB Specimen, ngineering Fracture mechanics, Vol. 41, No. 4, pp. 475-485.

)wen D.R.J. and Shantaram D., December 1977, Numerical study of Dynamic Crack rowth by the Finite Element Method, International Journal of Fracture, Vol. 13, No. , pp. 821-837.

'arton V.Z. and Boriskovsky V.G., 1989, Dynamic Fracture Mechanics, Vol. 1, Iemisphere Publishing Corporation, Newyork, pp. 203-204.

'opadopoulos George A., 1993, Fracture Mechanics : The Experimental Method of austics and The Det.-criterion of Fracture, Springer-Verlag, London.

amesh K., 1991, Dept. of Mechanical Engineering, IIT Kanpur.

avichandran G. and Clifton R.J., 1989, Dynamic Fracture Under Plane Wave Loading, nternational Journal of Fracture, Vol. 40, pp. 157-201.

avi Chandar K. and Knauss W.G., 1982, Dynamic Crack tip Stresses Under Stress Wave Loading - A Comparison of Theory and Experiment, International Journal of racture, Vol. 20, pp. 202-222.

avi Chandar K. and Knauss W.G., 1984a, An Experimental Investigation into)ynamic Fracture: I. Crack Initiation and Arrest, International Journal of racture, Vol. 25, pp. 247-262.

avi Chandar K. and Knauss W.G., 1984b, An Experimental Investigation into)ynamic fracture: II. Microstructural Aspects, International Journal of Fracture, Vol. 6, pp. 65-80.

avi Chandar K. and Knauss W.G., 1984c, An Experimental Investigation into Dynamic racture: III. On Steady-state Crack Propagation and Crack Branching, International ournal of Fracture, Vol. 26, pp. 141-154.

Ravi Chandar K. and Knauss W.G., 1984d, An Experimental Investigation into Dynamic fracture: IV. On Interaction of Stress Waves with Propagating Cracks, International Journal of Fracture, Vol. 26, pp. 189-200.

Renard Jacques and Roudolff Florence, 1991, Analytical and Numerical Calculation of Strain Energy Release Rate During Delamination Growth in a Carbon Epoxy Laminate, Composite Science and Technology, Vol. 42, pp. 305-316.

Rice J.R. , June 1968, A path Independent Integral and Approximate Analysis of Strain Concentration by Notches and Cracks, Journal of Applied Mechanics, Transactions of ASME, Vol. 85, p. 379.

Rosakis A.J., Duffy J. and Freund L.B., 1984, The Determination of Dynamic Fracture Toughness of AISI 4340 Steel by the Shadow Spot Method, Journal of Mechanical Physics and Solids, No. 4, pp. 443-460.

Rybicki E.F. and Kanninen M.F., 1977, A Finite Element Calculation of Stress Intensity Factors by a Modified Crack Closure Integrals, Engineering Fracture Mechanics, Vol. 9, pp. 931-938.

Rydhom G., Fredriksson B. and Nilsson F., 1978, Numerical Investigation of Rapid Crack Propagation, Numerical Methods in Fracture Mechanics, eds. A.R. Luxmoore and D.R.J. Owen, Univ. College, Swesna, pp. 660-672.

Sarkar P.K. and Maiti S.K., 1991, Prediction of Mode I Fracture toughness of a Laminated Fibre Composite from Matrix Fracture Toughness of the Basic Layer, Engineering Fracture Mechanics, Vol. 38, No. 1, pp. 71-82.

Seron F.J., Sang F.J., Kindelan M. and Badal J.I., 1990, Finite Element Method for Elastic Wave Propagation, Communications in Applied Numerical Methods, Vol. 6, pp. 359-368.

Schardin H., 1959, Velocity Effect in Fracture, in Fracture, ed. B.L. Averbach, Cambridge MA, MIT press, pp. 297-350.

Shanbag M.R., Eshwaran K. and Maiti S.K., 1993, Mesuremant of Fracture Toughness of Bimaterial Interfaces and a Stress Based Approach to Their Fracture, Engineering Fracture mechanics, Vol. 44, No. 1, pp. 75-89.

Shukla A., 1983, Comparision of Static and Dynamic Energy Release Rates for Different Fracture Specimens, Engineering Fracture Mechanics, Vol. 18, No. 3, pp. 725-730.

Shukla A., Agarwal B.D. and Bharat Bhusan, 1989, Determination of Stress Intensity Factor in Orthotropic Composite Materials Using Strain Gages, Engineering Fracture Mechanics, Vol. 32, No. 3, pp. 469-477.

Shukla A., Agarwal R.K. and Nigam H., 1988, Dynamic Fracture Studies on 7075-T6 Aluminium and 4340 Steel Using Strain Gages and Photoelastic Coatings, Engineering Fracture Mechanics, Vol. 31, No. 3, pp. 501-515.

Sun C.T. and Lih C.J., 1987, On Strain Energy Release Rate For Interfacial Cracks in Bi-material Media, Engineering Fracture Mechanics, Vol. 28, No. 1, pp. 13-20.

Sun C.T. and Grady J.E., 1988, Dynamic Delamination Fracture Toughness of a Graphite/Epoxy Laminate Under Impact, Composite Science and Technology, Vol. 31, pp. 55-72.

Suo Zhigang and Hutchinson John W., 1989, Sandwich Test for Measuring Interface Crack Toughness, Material Science and Engineering, A107, pp. 135-143.

Suo Zhigang and Hutchinson John W., 1990, Interface Crack Between Two Elastic Layers, International Journal of Fracture, Vol. 43, pp. 1-18.

Takahashi K. and Arakawa K., June 1987, Dependence of Crack Acceleration on the Dynamic Stress Intensity Factors in Polymers, Experimental Mechanics, pp. 195-200.

Takeda N., Sierakowski R.L., Ross C.A. and Malvern L.E., 1982, Delaminaiton Crack Propagation in Ballistically Impact Glass/Epoxy Composite Laminates, Experimental Mechanics, Vol. 22, pp. 19-25

Thesken J.C. and Gudmundson Peter, 1991, Application of a Moving Variable Order Singular Element to Dynamic Fracture Mechanics, Internation Journal of Fracture, Vol. 52, pp. 47-65.

Theocaris P.S., 1970, Local Yielding around a Crack Tip in Plexiglass, Journal of Applied Mechanics, 37, pp. 409-415.

Wada Hitoshi, 1992, Determination of Dynamic Fracture Toughness for PMMA, Engineering Fracture Mechanics, Vol. 41, No. 6, pp. 821-831.

Wang Y. and Williams J.G., 1994, A Numerical Study of Dynamic Crack Growth in Isotropic DCB Specimens, Composites, Vol. 25, No. 5, pp.323-331.

Williams J.G. and Ivankovic A., 1991, Limiting Crack Speed in Dynamic Fracture Tests, International Journal of Fracture, Vol. 51, pp. 319-330.

Williams M.R., April 1959, The Stress Around a Fault or Crack in Dissimilar Media, Bulletin of Seismological Society of America, Vol. 49, No. 2, pp. 199-204.

Wilson M.L., Hawley R.H. and Duffy J., 1980, The Effect of Loading Rate and Temperature on Fracture Initiation in 1020 Hot-Rolled Steel, Engineering Fracture Mechanics, Vol. 13, pp. 371-385.

Yoon S.H. and Hong C.S., Sept. 1993, Interlaminar Fracture Toughness of

Graphite/Epoxy Composite Under Mixed Mode Deformation, Experimental Mechanics, pp. 234-239.

Yuechuan Li, 1991, The Application of Gurtin Variational Principle in the Computation of Dynamic Stress Intensity Factors, Engineering Fracture Mechanics, Vol. 39, No. 3, pp. 469-476.

Zehnder Alant T. and Rosakis Ares J., 1990, Dynamic Fracture Initiation and Propagation in 4340 Steel Under Impact Loading, International Journal of Fracture, Vol. 43, pp. 271-285.

APPENDIX - A

BASICS OF FINITE ELEMENT METHOD

In the DCB specimen the width of the plate along Z-direction of Fig. 2.1 is relatively large, thus making it suitable for modelling it as a plane strain problem. The FE technique involves the discretization of the domain into a number of finite elements, assume a displacement interpolation function in each element, construct the potential energy Φ and minimize Φ of the whole body. The potential energy is defined as

$$\phi = U - W_{ext} \tag{A.1}$$

where U represents the strain energy and W_{ext}, the work done by external forces. External forces include boundary forces and body forces. In the present analysis, body forces have been neglected. For a linear elastic material, the strain energy per unit volume is given as

$$U = \int_0^{\varepsilon_{ij}} \sigma_{ij}\, d\varepsilon_{ij} = \frac{1}{2}\sigma_{ij}\varepsilon_{ij} \tag{A.2}$$

where σ_{ij} and ε_{ij} are stress and strain components at a point within the element.

Using the matrix notations for stress and strain components,

$$\phi = \frac{1}{2}\int \sigma_{ij}\varepsilon_{ij}dV = \frac{1}{2}\int [\sigma_{xx}\varepsilon_{xx}+\sigma_{yy}\varepsilon_{yy}+\tau_{xy}\gamma_{xy}]dV \qquad (A.3)$$

$$\{\sigma\} = \begin{Bmatrix} \sigma_{xx} \\ \sigma_{yy} \\ \tau_{xy} \end{Bmatrix} \qquad (A.4)$$

$$\{\varepsilon\} = \begin{Bmatrix} \varepsilon_{xx} \\ \varepsilon_{yy} \\ \gamma_{xy} \end{Bmatrix} \qquad (A.5)$$

The strain energy can be expressed in the form,

$$\{\phi\} = \frac{1}{2}\int_v \{\varepsilon\}^T \{\sigma\}\, dV \qquad (A.6)$$

and W_{ext} as

$$W_{ext} = \int_s F_i\, u_i\, ds \qquad (A.7)$$

where u_i is the displacement vector, F_i is the surface traction and s is the surface on which F_i acts. For an 8-noded isoparametric element chosen (Fig. 2.2), the displacements components u^x and u^y are expressed in term of displacements of nodes, given by the expressions,

$$u^x = \sum_1^8 u_i^x\, N_i(\xi,\eta) \qquad (A.8)$$

$$u^y = \sum_1^8 u_i^y\, N_i(\xi,\eta) \qquad (A.9)$$

where N_i are shape functions expressed in terms of (ζ, η). The geometrical mapping is given by

$$x = \Sigma N_i \, x_i$$
$$y = \Sigma N_i \, y_i \qquad \text{(A.10)}$$

where x_i, y_i are the coordinates of i^{th} point.

Putting Eq.(A.10) and (A.11) in the form of matrix, we get

$$\begin{Bmatrix} u^x \\ u^y \end{Bmatrix} = \begin{bmatrix} N_1 & 0 & N_2 & 0 & \cdots & N_8 & 0 \\ 0 & N_1 & 0 & N_2 & \cdots & 0 & N_8 \end{bmatrix} \begin{Bmatrix} u_1^x \\ u_1^y \\ u_2^x \\ u_2^y \\ \cdot \\ \cdot \\ \cdot \\ u_8^x \\ u_8^y \end{Bmatrix} \qquad \text{(A.11)}$$

Alternatively,

$$\begin{Bmatrix} u^x \\ u^y \end{Bmatrix} = [N]\{u\} \qquad \text{(A.12)}$$

The strain can be obtained by differentiating the displacements using the expressions to yield,

$$\begin{Bmatrix} \varepsilon_{xx} \\ \varepsilon_{yy} \\ \gamma_{xy} \end{Bmatrix} = \begin{Bmatrix} \dfrac{\partial u^x}{\partial x} \\ \dfrac{\partial u^y}{\partial y} \\ \dfrac{\partial u^x}{\partial y} + \dfrac{\partial u^y}{\partial x} \end{Bmatrix} \tag{A.13}$$

$$\begin{Bmatrix} \varepsilon_{xx} \\ \varepsilon_{yy} \\ \gamma_{xy} \end{Bmatrix} = \begin{bmatrix} \dfrac{\partial N_1}{\partial x} & 0 & \dfrac{\partial N_2}{\partial x} & 0 & \cdots & 0 \\ 0 & \dfrac{\partial N_1}{\partial y} & 0 & \dfrac{\partial N_2}{\partial y} & \cdots & \dfrac{\partial N_8}{\partial y} \\ \dfrac{\partial N_1}{\partial y} & \dfrac{\partial N_1}{\partial x} & \dfrac{\partial N_2}{\partial y} & \dfrac{\partial N_2}{\partial x} & \cdots & \dfrac{\partial N_8}{\partial x} \end{bmatrix} \begin{Bmatrix} u_1{}^x \\ u_1{}^y \\ u_2{}^x \\ u_2{}^y \\ \cdot \\ \cdot \\ \cdot \\ u_8{}^y \end{Bmatrix} \tag{A.14}$$

which can be further expressed as,

$$\{\varepsilon\} = [B]\{u\} \tag{A.15}$$

The stress strain relation is represented as

$$\{\sigma\} = [D]\{\varepsilon\} \tag{A.16}$$

where [D] is the material property matrix defined as

$$[D]=\frac{E}{(1+\nu)(1-2\nu)}\begin{bmatrix}1-\nu & \nu & 0\\ \nu & 1-\nu & 0\\ 0 & 0 & \frac{1-2\nu}{2}\end{bmatrix} \qquad \text{(A.17)}$$

for plane strain. In the above matrix, ν is the Poisson's ration and E is the Young's modulus. The expression for strain energy of an element can be rewritten in the form,

$$U = \frac{1}{2}\int_v \{\varepsilon\}^T[\sigma]dV = \frac{1}{2}\int_A \{u\}^T[B]^T[D][B]\{u\}t\ dxdy \qquad \text{(A.18)}$$

where t is the thickness of the element. Transforming into natural coordinates ξ and η,

$$U = \frac{1}{2}\int_A \{u\}^T[B]^T[D][B]\{u\}t|J|d\xi d\eta \qquad \text{(A.19)}$$

where $|J|$ is the Jacobian. Substituting in Eq. A.1, for potential energy of an element, ϕ^e, is

$$\phi^e = \frac{1}{2}\int_A \{u\}^T[B]^T[D][B]\{u\}t|J|d\xi d\eta - \int_S F.u\ dS \qquad \text{(A.20)}$$

This equation can be written as,

$$\phi^e = \frac{1}{2}\{u\}^T[K^e]\{u\} - \{u\}^T\{F^e\} \qquad \text{(A.21)}$$

where

$$[K]^e = \int_A [B]^T[D][B]\ |J|\ d\xi d\eta \qquad (A.22)$$

$$\{F\}^e = \int_s F\ ds$$

The total potential energy of the system can be obtained by summation of the elemental potential energies as

$$\phi = \sum_{e=1}^{N} \phi^e = \sum_{e=1}^{N} \{u\}^T[K^e]\{u\} - \sum_{e=1}^{N} \{u\}^T\{F^e\} \qquad (A.23)$$

which is expressed in the matrix form as

$$\phi = \{u^G\}^T[K^G]\{u^G\} - \{u^G\}^T\{F^G\} \qquad (A.24)$$

where the superscript G denotes the global domain. It is to be noted here that summation represents assembly. The nodal displacement {u} which minimizes ϕ;i.e. $\partial\phi/\partial\{u\}$ is equated to zero. From equation A.1

$$\frac{\partial\phi}{\partial\{u\}} = [K^G]\{u^G\} - \{F^G\} = 0 \qquad (A.25)$$

yielding,

$$[K^G]\{u^G\} = \{F^G\} \qquad (A.26)$$

The set of simultaneous equations [K]{u} = {F} has been solved using a sky-line solution algorithm.

APPENDIX - B

ANALYTICAL FRACTURE TOUGHNESS EQUATION

quation used in calculating K_I through G_I has been derived in this appendix. G can e calculated by the formula,

$$G = \frac{P^2}{2B}\frac{\partial C}{\partial a} \qquad \text{(B.1)}$$

/here B is the thickness, a is the crack length and C is the compliance of the specimen nd P is the applied load. C is defined as C = u/P where u is the displacement of the oint loads.

For a cantilever with length L, moment of inertia I and Young's modulus E under the ction of a force P, displacement u is expressed as,

$$u = \frac{P L^3}{3EI}$$

n the case of a DCB specimen, the length of each of the cantilevers is equal to the crack length and since there are two cantilevers, the compliance of the specimen is given by,

$$C = \frac{2u}{P} = \frac{2 a^3}{3EI} \qquad \text{(B.2)}$$

Substituting Eq. B.2 in B.1, the expression for G is obtained as

$$G_I = \frac{12P^2\, a^2}{EB^2h^3} \tag{B.3}$$

Using the relation

$$G_I = \frac{K_I^2}{E}(1 - \nu^2)$$

for plane strain, the equation yields

$$K_I = \frac{2\sqrt{3}\; P\; a}{B\; h^{3/2}(1-\nu^2)} \tag{B.4}$$